

AD-A080 961

VARIAN ASSOCIATES INC PALO ALTO CA PALO ALTO MICROWA--ETC F/G 9/1
EFFICIENCY IMPROVEMENTS IN COUPLED CAVITY TRAVELING WAVE TUBES.(U)

OCT 79 W R AYERS, F R WALKER

F30602-78-C-0117

UNCLASSIFIED

RADC-TR-79-264

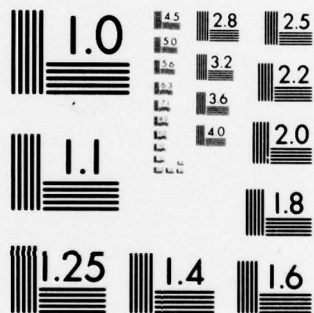
NL

1 OF 3

AD-

A080961





MICROCOPY RESOLUTION TEST CHART
NATIONAL BUREAU OF STANDARDS-1963-A

LEVEL

12

RADC-TR-79-264
Final Technical Report
October 1979

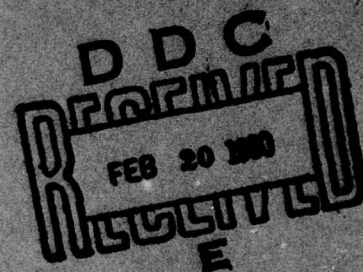


AD A 0 80961

EFFICIENCY IMPROVEMENT IN COUPLED CAVITY TRAVELING WAVE TUBES

Varian Associates, Inc.

W. R. Ayers
F. Ruth Walker



DDC FILE COPY

APPROVED FOR PUBLIC RELEASE; DISTRIBUTION UNLIMITED

ROME AIR DEVELOPMENT CENTER
Air Force Systems Command
Griffiss Air Force Base, New York 13441

80 2 19 214

This report has been reviewed by the RADC Public Affairs Office (PA) and is releasable to the National Technical Information Service (NTIS). At NTIS it will be releasable to the general public, including foreign nations.

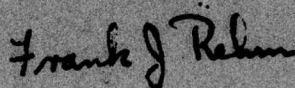
RADC-TR-79-264 has been reviewed and is approved for publication.

APPROVED:



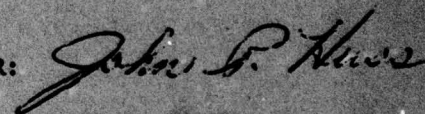
JOSEPH J. POLNIASZEK
Project Engineer

APPROVED:



FRANK J. REHM
Technical Director
Surveillance Division

FOR THE COMMANDER:



JOHN P. HUSS
Acting Chief, Plans Office

If your address has changed or if you wish to be removed from the RADC mailing list, or if the addressee is no longer employed by your organization, please notify RADC (OCTP), Griffiss AFB NY 13441. This will assist us in maintaining a current mailing list.

Do not return this copy. Retain or destroy.

UNCLASSIFIED

SECURITY CLASSIFICATION OF THIS PAGE (When Data Entered)

(19) REPORT DOCUMENTATION PAGE		READ INSTRUCTIONS BEFORE COMPLETING FORM
1. REPORT NUMBER 18) RADC-TR-79-264	2. GOVT ACCESSION NO.	3. RECIPIENT'S CATALOG NUMBER
4. TITLE (and Subtitle) 6) EFFICIENCY IMPROVEMENT IN COUPLED CAVITY TRAVELING WAVE TUBES	5. TYPE OF REPORT & PERIOD COVERED 9) Final Technical Report 10 Mar 78 - 10 Jun 79	6. PERFORMING ORG. REPORT NUMBER N/A
7. AUTHOR(s) 10) W. R. Ayers F. Ruth Walker	8. CONTRACT OR GRANT NUMBER(s) 15) F30602-78-C-01174v	
9. PERFORMING ORGANIZATION NAME AND ADDRESS Varian Associates, Inc. 611 Hansen Way Palo Alto CA 94303 PE62702F	10. PROGRAM ELEMENT, PROJECT, TASK AREA & WORK UNIT NUMBERS 16) 45061220 17) 12	
11. CONTROLLING OFFICE NAME AND ADDRESS Rome Air Development Center (OCTP) Griffiss AFB NY 13441	12. REPORT DATE 11) Oct 1979	13. NUMBER OF PAGES 264
14. MONITORING AGENCY NAME & ADDRESS (if different from Controlling Office) Same 12) 253C	15. SECURITY CLASS. (of this report) UNCLASSIFIED	15a. DECLASSIFICATION/DOWNGRADING SCHEDULE N/A
16. DISTRIBUTION STATEMENT (of this Report) Approved for public release; distribution unlimited. 364100		
17. DISTRIBUTION STATEMENT (of the abstract entered in Block 20, if different from Report) Same		
18. SUPPLEMENTARY NOTES RADC Project Engineer: Joseph Polniaszek (OCTP)		
19. KEY WORDS (Continue on reverse side if necessary and identify by block number) Traveling Wave Tubes Phase Focusing High Efficiency Circuit Tapering Coupled-Cavity Large Signal Theory		
20. ABSTRACT (Continue on reverse side if necessary and identify by block number) This report describes an analytical study of schemes for maximizing the conversion efficiency in high power coupled-cavity traveling-wave tubes. The procedures developed in this study were used to design a 100 KW, S-band coupled-cavity TWT with a predicted 40 percent conversion efficiency.		

DD FORM 1 JAN 73 1473

UNCLASSIFIED

SECURITY CLASSIFICATION OF THIS PAGE (When Data Entered)

406552

set

PREFACE

The work described herein was done by Varian Associates, Inc., Palo Alto Microwave Tube Division under RADC Contract F30602-78-C-0117 with Dr. W. R. Ayers as principal investigator. Others contributing to the project included Ms. Ruth Walker, Mr. Erling Lien, Dr. Arthur Karp, Mr. John Fenwick and Mr. Fred Friedlander. Mr. Joseph Polniaszek, Rome Air Development Center, was Project Manager.

Accession For	
NTIC - GMAI	<input checked="checked" type="checkbox"/>
DDC TAB	<input type="checkbox"/>
Unannounced	<input type="checkbox"/>
Justification	<input type="checkbox"/>
By _____	
Distribution/	
Availability Codes	
Dist	Avail and/or special
A	

TABLE OF CONTENTS

<u>Section</u>	<u>Page No.</u>
1.0 INTRODUCTION	1
2.0 REVIEW OF RELATED WORK	3
3.0 ANALYTIC METHODS	11
3.1 The Varian Small-Signal Program for Coupled-Cavity TWTs ...	11
3.2 The Varian Large-Signal Program for Coupled-Cavity TWTs ...	19
4.0 THE BUNCHING PROCESS	25
5.0 OPTIMIZING THE OUTPUT CIRCUIT SECTION	67
5.1 Introduction	67
5.2 Circuits Which Do Not Support a Backward Wave	67
5.3 Backward-Wave Effects in the Output Circuit Section	95
5.4 Analysis of Pretaper	113
5.5 Variation of Beam Current	132
5.6 Optimization of Low Current TWT	137
5.7 Optimization with Frequency as a Parameter	180
6.0 FINAL DESIGN	211
7.0 CONCLUSIONS	229
8.0 REFERENCE LIST	233

LIST OF ILLUSTRATIONS

<u>Figure No.</u>		<u>Page No.</u>
3.1	CIRCUIT MODEL USED FOR REPRESENTING EACH CAVITY OF THE COUPLED-CAVITY TWT	15
3.2	MATRIX MULTIPLICATION FOR OBTAINING THE SMALL-SIGNAL CHARACTERISTICS OF THE COUPLED-CAVITY TWT	17
3.3	FORCE FIELDS OF VARIOUS DISK MODELS	20
3.4	STEPS USED IN CARRYING OUT THE LARGE-SIGNAL, COUPLED-CAVITY COMPUTATIONS	22
4.1	PEAK VELOCITY SPREAD AT MAXIMUM RF BEAM CURRENT VS THE RELATIVE EXCITATION OF THE FAST AND SLOW SPACE-CHARGE WAVES	27
4.2	BRILLOUIN DIAGRAM FOR VTS-5753	28
4.3	PEAK POWER VS FREQUENCY FOR VTS-5753 S/N 117.....	30
4.4	PLOTTING FORMAT FOR LARGE-SIGNAL COMPUTER PROGRAM	31
4.5	PLOTTING FORMAT FOR LARGE-SIGNAL COMPUTER PROGRAM	32
4.6	COMPUTED RF BEAM CURRENTS AND GAP VOLTAGES VS DISTANCE IN SIMULATED COUPLED-CAVITY TWT WITH NINE CAVITIES IN EACH SECTION	36
4.7	COMPUTED RELATIVE PHASES OF ELECTRON DISKS VS DISTANCE IN SIMULATED COUPLED-CAVITY TWT WITH NINE CAVITIES IN EACH SECTION	37
4.8	COMPUTED RF BEAM CURRENTS AND GAP VOLTAGES VS DISTANCE IN SIMULATED COUPLED-CAVITY TWT WITH NINE CAVITIES IN EACH SECTION	39
4.9	COMPUTED RELATIVE PHASES OF ELECTRON DISKS VS DISTANCE IN SIMULATED COUPLED-CAVITY TWT WITH NINE CAVITIES IN EACH SECTION	40
4.10	COMPUTED RF BEAM CURRENTS AND GAP VOLTAGES VS DISTANCE IN SIMULATED COUPLED-CAVITY TWT WITH NINE CAVITIES IN EACH SECTION	41
4.11	COMPUTED RELATIVE PHASES OF ELECTRON DISKS VS DISTANCE IN SIMULATED COUPLED-CAVITY TWT WITH NINE CAVITIES IN EACH SECTION	42

Figure No.Page No.

4.12	COMPUTED RF BEAM CURRENTS AND GAP VOLTAGES VS DISTANCE IN SIMULATED COUPLED-CAVITY TWT WITH NINE CAVITIES IN EACH SECTION	43
4.13	COMPUTED RELATIVE PHASES OF ELECTRON DISKS VS DISTANCE IN SIMULATED COUPLED-CAVITY TWT WITH NINE CAVITIES IN EACH SECTION	44
4.14	COMPUTED RF BEAM CURRENTS AND GAP VOLTAGES VS DISTANCE IN SIMULATED COUPLED-CAVITY TWT WITH NINE CAVITIES IN EACH SECTION	46
4.15	COMPUTED RELATIVE PHASES OF ELECTRON DISKS VS DISTANCE IN SIMULATED COUPLED-CAVITY TWT WITH NINE CAVITIES IN EACH SECTION	47
4.16	COMPUTED RF BEAM CURRENTS AND GAP VOLTAGES VS DISTANCE IN SIMULATED NINE CAVITY DRIVER SECTION	49
4.17	COMPUTED RELATIVE PHASES OF ELECTRON DISKS VS DISTANCE IN SIMULATED NINE CAVITY DRIVER SECTION	50
4.18	COMPUTED VELOCITY SPECTRUM AND PHASES OF ELECTRON DISKS IN SIMULATED NINE CAVITY DRIVER SECTION	51
4.19	COMPUTED RF BEAM CURRENTS AND GAP VOLTAGES VS DISTANCE IN SIMULATED NINE CAVITY DRIVER SECTION	53
4.20	COMPUTED RELATIVE PHASES OF ELECTRON DISKS VS DISTANCE IN SIMULATED NINE CAVITY DRIVER SECTION	54
4.21	COMPUTED VELOCITY SPECTRUM AND PHASES OF ELECTRON DISKS IN SIMULATED NINE CAVITY DRIVER SECTION	55
4.22	COMPUTED RF BEAM CURRENTS AND GAP VOLTAGES VS DISTANCE IN SIMULATED NINE INCH DRIFT SPACE BEYOND DRIVER SECTION	57
4.23	COMPUTED RELATIVE PHASES OF ELECTRON DISKS VS DISTANCE IN SIMULATED NINE INCH DRIFT SPACE BEYOND DRIVER SECTION	58
4.24	COMPUTED RF BEAM CURRENTS AND GAP VOLTAGES VS DISTANCE IN SIMULATED NINE INCH DRIFT SPACE BEYOND DRIVER SECTION	59
4.25	COMPUTED RELATIVE PHASES OF ELECTRON DISKS VS DISTANCE IN SIMULATED NINE INCH DRIFT SPACE BEYOND DRIVER SECTION	60
4.26	COMPUTED VELOCITY SPECTRUM AND BUNCHED DENSITY OF ELECTRON DISKS ONE INCH INTO SEVER	62

4.27	COMPUTED VELOCITY SPECTRUM AND BUNCHED DENSITY OF ELECTRON DISKS ONE INCH INTO SEVER	63
4.28	COMPUTED RF BEAM CURRENTS AND GAP VOLTAGES VS DISTANCE IN SIMULATED COUPLED-CAVITY TWT WITH SEVER	64
4.29	COMPUTED RF BEAM CURRENTS AND GAP VOLTAGES VS DISTANCE IN SIMULATED COUPLED-CAVITY TWT WITHOUT SEVER	65
5.1	COMPUTED RELATIVE PHASES OF ELECTRON DISKS VS DISTANCE IN SIMULATED COUPLED-CAVITY TWT WITH UNIFORM PERIODS	68
5.2	COMPUTED RELATIVE PHASES OF ELECTRON DISKS VS DISTANCE IN SIMULATED COUPLED-CAVITY TWT WITH TAPERED PERIODS	69
5.3	COMPUTED RF BEAM CURRENTS AND GAP VOLTAGES VS DISTANCE IN SIMULATED COUPLED-CAVITY TWT WITH UNIFORM PERIODS	71
5.4	COMPUTED RF BEAM CURRENTS AND GAP VOLTAGES VS DISTANCE IN SIMULATED COUPLED-CAVITY TWT WITH POSITIVE TAPERED OUTPUT PERIODS	73
5.5	COMPUTED RELATIVE PHASES OF ELECTRON DISKS VS DISTANCE IN SIMULATED COUPLED-CAVITY TWT WITH POSITIVE TAPERED OUTPUT PERIODS	74
5.6	COMPUTED RF BEAM CURRENTS AND GAP VOLTAGES VS DISTANCE IN SIMULATED COUPLED-CAVITY TWT WITH NEGATIVE TAPERED OUTPUT CIRCUIT	76
5.7	COMPUTED RELATIVE PHASES OF ELECTRON DISKS VS DISTANCE IN SIMULATED COUPLED-CAVITY TWT WITH NEGATIVE TAPERED OUTPUT CIRCUIT	77
5.8	COMPUTED RF BEAM CURRENTS AND GAP VOLTAGES VS DISTANCE IN SIMULATED COUPLED-CAVITY TWT WITH FOUR LOSSLESS OUTPUT CAVITIES	78
5.9	COMPUTED RELATIVE PHASES OF ELECTRON DISKS VS DISTANCE IN SIMULATED COUPLED-CAVITY TWT WITH FOUR LOSSLESS OUTPUT CAVITIES	79
5.10	COMPUTED RF BEAM CURRENTS AND GAP VOLTAGES VS DISTANCE IN SIMULATED COUPLED-CAVITY TWT WITH FOUR LOSSLESS OUTPUT CAVITIES	81

5.11	COMPUTED RELATIVE PHASES OF ELECTRON DISKS VS DISTANCE IN SIMULATED COUPLED-CAVITY TWT WITH FOUR LOSSLESS OUTPUT CAVITIES	82
5.12	COMPUTED RF BEAM CURRENTS AND GAP VOLTAGES VS DISTANCE IN SIMULATED COUPLED-CAVITY TWT WITH FOUR LOSSLESS OUTPUT CAVITIES	83
5.13	COMPUTED RELATIVE PHASES OF ELECTRON DISKS VS DISTANCE IN SIMULATED COUPLED-CAVITY TWT WITH FOUR LOSSLESS OUTPUT CAVITIES	84
5.14	POWER GAIN AND CONVERSION EFFICIENCY VS INPUT POWER IN SIMULATED COUPLED-CAVITY TWT WITH FOUR LOSSLESS OUTPUT CAVITIES AND FINAL TWO CAVITIES WITH DECREASED PERIODS	85
5.15	COMPUTED RF BEAM CURRENTS AND GAP VOLTAGES VS DISTANCE IN SIMULATED COUPLED-CAVITY TWT WITH FOUR LOSSLESS OUTPUT CAVITIES, POSITIVE PRETAPERED OUTPUT CIRCUIT, AND FINAL TWO CAVITIES WITH DECREASED PERIODS	87
5.16	COMPUTED RELATIVE PHASES OF ELECTRON DISKS VS DISTANCE IN SIMULATED COUPLED-CAVITY TWT WITH FOUR LOSSLESS OUTPUT CAVITIES, POSITIVE PRETAPERED OUTPUT CIRCUIT, AND FINAL TWO CAVITIES WITH DECREASED PERIODS	88
5.17	COMPUTED RF BEAM CURRENTS AND GAP VOLTAGES VS DISTANCE IN SIMULATED COUPLED-CAVITY TWT WITH FOUR LOSSLESS OUTPUT CAVITIES, NEGATIVE PRETAPERED OUTPUT CIRCUIT, AND FINAL TWO CAVITIES WITH DECREASED PERIODS	89
5.18	COMPUTED RELATIVE PHASES OF ELECTRON DISKS VS DISTANCE IN SIMULATED COUPLED-CAVITY TWT WITH FOUR LOSSLESS OUTPUT CAVITIES, NEGATIVE PRETAPERED OUTPUT CIRCUIT, AND FINAL TWO CAVITIES WITH DECREASED PERIODS	90
5.19	COMPUTED RF BEAM CURRENTS AND GAP VOLTAGES VS DISTANCE IN SIMULATED COUPLED-CAVITY TWT WITH FOUR LOSSLESS OUTPUT CAVITIES, NEGATIVE PRETAPERED OUTPUT CIRCUIT, AND FINAL TWO CAVITIES WITH DECREASED PERIODS	91
5.20	COMPUTED RELATIVE PHASES OF ELECTRON DISKS VS DISTANCE IN SIMULATED COUPLED-CAVITY TWT WITH FOUR LOSSLESS OUTPUT CAVITIES, NEGATIVE PRETAPERED OUTPUT CIRCUIT, AND FINAL TWO CAVITIES WITH DECREASED PERIODS	92

Figure No.Page No.

5.21	COMPUTED RF BEAM CURRENTS AND GAP VOLTAGES VS DISTANCE IN SIMULATED COUPLED-CAVITY TWT WITH FOUR LOSSLESS OUTPUT CAVITIES, NEGATIVE PRETAPERED OUTPUT CIRCUIT, AND FINAL TWO CAVITIES WITH DECREASED PERIODS	93
5.22	COMPUTED RELATIVE PHASES OF ELECTRON DISKS VS DISTANCE IN SIMULATED COUPLED-CAVITY TWT WITH FOUR LOSSLESS OUTPUT CAVITIES, NEGATIVE PRETAPERED OUTPUT CIRCUIT, AND FINAL TWO CAVITIES WITH DECREASED PERIODS	94
5.23	COMPUTED RF BEAM CURRENTS AND GAP VOLTAGES VS DISTANCE IN SIMULATED COUPLED-CAVITY TWT WITH FOUR LOSSLESS OUTPUT CAVITIES	96
5.24	COMPUTED RELATIVE PHASES OF ELECTRON DISKS VS DISTANCE IN SIMULATED COUPLED-CAVITY TWT WITH FOUR LOSSLESS OUTPUT CAVITIES	97
5.25	COMPUTED RF BEAM CURRENTS AND GAP VOLTAGES VS DISTANCE IN SIMULATED COUPLED-CAVITY TWT WITH UNIFORM PERIODS	98
5.26	COMPUTED RELATIVE PHASES OF ELECTRON DISKS VS DISTANCE IN SIMULATED COUPLED-CAVITY TWT WITH UNIFORM PERIODS	99
5.27	COMPUTED RF BEAM CURRENTS AND GAP VOLTAGES VS DISTANCE IN SIMULATED COUPLED-CAVITY TWT WITH A TWO CAVITY PERIOD MODIFICATION	100
5.28	COMPUTED RELATIVE PHASES OF ELECTRON DISKS VS DISTANCE IN SIMULATED COUPLED-CAVITY TWT WITH A TWO CAVITY PERIOD MODIFICATION	101
5.29	COMPUTED RF BEAM CURRENTS AND GAP VOLTAGES VS DISTANCE IN SIMULATED COUPLED-CAVITY TWT WITH A TWO CAVITY PERIOD MODIFICATION	102
5.30	COMPUTED RELATIVE PHASES OF ELECTRON DISKS VS DISTANCE IN SIMULATED COUPLED-CAVITY TWT WITH A TWO CAVITY PERIOD MODIFICATION	103
5.31	COMPUTED RF BEAM CURRENTS AND GAP VOLTAGES VS DISTANCE IN SIMULATED COUPLED-CAVITY TWT WITH MODIFIED OUTPUT PERIODS	105
5.32	COMPUTED RELATIVE PHASES OF ELECTRON DISKS VS DISTANCE IN SIMULATED COUPLED-CAVITY TWT WITH MODIFIED OUTPUT PERIODS	106

Figure No.Page No.

5.33	COMPUTED RF BEAM CURRENTS AND GAP VOLTAGES VS DISTANCE IN SIMULATED COUPLED-CAVITY TWT WITH FOUR LOSSLESS OUTPUT CAVITIES, POSITIVE PRETAPERED OUTPUT CIRCUIT AND FINAL TWO CAVITIES WITH DECREASED PERIODS	107
5.34	COMPUTED RELATIVE PHASES OF ELECTRON DISKS VS DISTANCE IN SIMULATED COUPLED-CAVITY TWT WITH FOUR LOSSLESS OUTPUT CAVITIES, POSITIVE PRETAPERED OUTPUT CIRCUIT AND FINAL TWO CAVITIES	108
5.35	COMPUTED RF BEAM CURRENTS AND GAP VOLTAGES VS DISTANCE IN SIMULATED COUPLED-CAVITY TWT WITH FOUR LOSSLESS OUTPUT CAVITIES, POSITIVE PRETAPERED OUTPUT CIRCUIT AND FINAL TWO CAVITIES	109
5.36	COMPUTED RELATIVE PHASES OF ELECTRON DISKS VS DISTANCE IN SIMULATED COUPLED-CAVITY TWT WITH FOUR LOSSLESS OUTPUT CAVITIES, POSITIVE PRETAPERED OUTPUT CIRCUIT AND FINAL TWO CAVITIES	110
5.37	COMPUTED RF BEAM CURRENTS AND GAP VOLTAGES VS DISTANCE IN SIMULATED COUPLED-CAVITY TWT WITH FOUR LOSSLESS OUTPUT CAVITIES, POSITIVE PRETAPERED OUTPUT CIRCUIT AND FINAL TWO CAVITIES	111
5.38	COMPUTED RELATIVE PHASES OF ELECTRON DISKS VS DISTANCE IN SIMULATED COUPLED-CAVITY TWT WITH FOUR LOSSLESS OUTPUT CAVITIES, POSITIVE PRETAPERED OUTPUT CIRCUIT AND FINAL TWO CAVITIES	112
5.39	COMPUTED RF BEAM CURRENTS AND GAP VOLTAGES VS DISTANCE IN SIMULATED COUPLED-CAVITY TWT WITH FOUR LOSSLESS OUTPUT CAVITIES, NEGATIVE PRETAPERED OUTPUT CIRCUIT, AND FINAL TWO CAVITIES WITH DECREASED PERIODS	114
5.40	COMPUTED RELATIVE PHASES OF ELECTRON DISKS VS DISTANCE IN SIMULATED COUPLED-CAVITY TWT WITH FOUR LOSSLESS OUTPUT CAVITIES, NEGATIVE PRETAPERED OUTPUT CIRCUIT, AND FINAL TWO CAVITIES WITH DECREASED PERIODS	115
5.41	COMPUTED RF BEAM CURRENTS AND GAP VOLTAGES VS DISTANCE IN SIMULATED COUPLED-CAVITY TWT WITH FOUR LOSSLESS OUTPUT CAVITIES, NEGATIVE PRETAPERED OUTPUT CIRCUIT, AND FINAL TWO CAVITIES WITH DECREASED PERIODS	116

5.42	COMPUTED RELATIVE PHASES OF ELECTRON DISKS VS DISTANCE IN SIMULATED COUPLED-CAVITY TWT WITH FOUR LOSSLESS OUTPUT CAVITIES, NEGATIVE PRETAPERED OUTPUT CIRCUIT, AND FINAL TWO CAVITIES WITH DECREASED PERIODS	117
5.43	COMPUTED RF BEAM CURRENTS AND GAP VOLTAGES VS DISTANCE IN SIMULATED COUPLED-CAVITY TWT WITH FOUR LOSSLESS OUTPUT CAVITIES, NEGATIVE PRETAPERED OUTPUT CIRCUIT, AND FINAL TWO CAVITIES WITH DECREASED PERIODS	118
5.44	COMPUTED RELATIVE PHASES OF ELECTRON DISKS VS DISTANCE IN SIMULATED COUPLED-CAVITY TWT WITH FOUR LOSSLESS OUTPUT CAVITIES, NEGATIVE PRETAPERED OUTPUT CIRCUIT, AND FINAL TWO CAVITIES WITH DECREASED PERIODS	119
5.45	COMPUTED RF BEAM CURRENTS AND GAP VOLTAGES VS DISTANCE IN SIMULATED COUPLED-CAVITY TWT WITH FOUR LOSSLESS OUTPUT CAVITIES, NEGATIVE PRETAPERED OUTPUT CIRCUIT, AND FINAL TWO CAVITIES WITH DECREASED PERIODS	120
5.46	COMPUTED RELATIVE PHASES OF ELECTRON DISKS VS DISTANCE IN SIMULATED COUPLED-CAVITY TWT WITH FOUR LOSSLESS OUTPUT CAVITIES, NEGATIVE PRETAPERED OUTPUT CIRCUIT, AND FINAL TWO CAVITIES WITH DECREASED PERIODS	121
5.47	POWER GAIN AND CONVERSION EFFICIENCY IN SIMULATED COUPLED- CAVITY TWT WITH FOUR LOSSLESS OUTPUT CAVITIES, FINAL TWO CAVITIES WITH DECREASED PERIODS, AND NEGATIVE PRETAPERED OUTPUT CIRCUIT	122
5.48	COMPUTED RF BEAM CURRENTS AND GAP VOLTAGES VS DISTANCE IN SIMULATED COUPLED-CAVITY TWT WITH FOUR LOSSLESS OUTPUT CAVITIES AND FINAL TWO CAVITIES WITH DECREASED PERIODS	123
5.49	COMPUTED RELATIVE PHASES OF ELECTRON DISKS VS DISTANCE IN SIMULATED COUPLED-CAVITY TWT WITH FOUR LOSSLESS OUTPUT CAVITIES AND FINAL TWO CAVITIES WITH DECREASED PERIODS	124
5.50	COMPUTED RF BEAM CURRENTS AND GAP VOLTAGES VS DISTANCE IN SIMULATED COUPLED-CAVITY TWT WITH FOUR LOSSLESS OUTPUT CAVITIES AND FINAL TWO CAVITIES WITH DECREASED PERIODS	126
5.51	COMPUTED RELATIVE PHASES OF ELECTRON DISKS VS DISTANCE IN SIMULATED COUPLED-CAVITY TWT WITH FOUR LOSSLESS OUTPUT CAVITIES AND FINAL TWO CAVITIES WITH DECREASED PERIODS	127

5.52	COMPUTED RF BEAM CURRENTS AND GAP VOLTAGES VS DISTANCE IN SIMULATED COUPLED-CAVITY TWT WITH FOUR LOSSLESS OUTPUT CAVITIES, POSITIVE PRETAPERED OUTPUT CIRCUIT AND FINAL TWO CAVITIES WITH DECREASED PERIODS	128
5.53	COMPUTED RELATIVE PHASES OF ELECTRON DISKS VS DISTANCE IN SIMULATED COUPLED-CAVITY TWT WITH FOUR LOSSLESS OUTPUT CAVITIES, POSITIVE PRETAPERED OUTPUT CIRCUIT AND FINAL TWO CAVITIES WITH DECREASED PERIODS	129
5.54	COMPUTED RF BEAM CURRENTS AND GAP VOLTAGES VS DISTANCE IN SIMULATED COUPLED-CAVITY TWT WITH FOUR LOSSLESS OUTPUT CAVITIES, NEGATIVE PRETAPERED OUTPUT CIRCUIT AND FINAL TWO CAVITIES WITH DECREASED PERIODS	130
5.55	COMPUTED RELATIVE PHASES OF ELECTRON DISKS VS DISTANCE IN SIMULATED COUPLED-CAVITY TWT WITH FOUR LOSSLESS OUTPUT CAVITIES, NEGATIVE PRETAPERED OUTPUT CIRCUIT AND FINAL TWO CAVITIES WITH DECREASED PERIODS	131
5.56	COMPUTED RF BEAM CURRENTS AND GAP VOLTAGES VS DISTANCE IN SIMULATED COUPLED-CAVITY TWT WITH SIX LOSSLESS OUTPUT CAVITIES AND FINAL THREE CAVITIES WITH DECREASED PERIODS	135
5.57	COMPUTED RELATIVE PHASES OF ELECTRON DISKS VS DISTANCE IN SIMULATED COUPLED-CAVITY TWT WITH SIX LOSSLESS OUTPUT CAVITIES AND FINAL THREE CAVITIES WITH DECREASED PERIODS	136
5.58	COMPUTED RF BEAM CURRENTS AND GAP VOLTAGES VS DISTANCE IN SIMULATED COUPLED-CAVITY TWT WITH SIX LOSSLESS OUTPUT CAVITIES AND FINAL THREE CAVITIES WITH DECREASED PERIODS	139
5.59	COMPUTED RELATIVE PHASES OF ELECTRON DISKS VS DISTANCE IN SIMULATED COUPLED-CAVITY TWT WITH SIX LOSSLESS OUTPUT CAVITIES AND FINAL THREE CAVITIES WITH DECREASED PERIODS	140
5.60	COMPUTED RELATIVE PHASES OF ELECTRON DISKS VS DISTANCE IN SIMULATED COUPLED-CAVITY TWT WITH SIX LOSSLESS OUTPUT CAVITIES AND FINAL THREE CAVITIES WITH DECREASED PERIODS	141
5.61	COMPUTED RELATIVE PHASES OF ELECTRON DISKS VS DISTANCE IN SIMULATED COUPLED-CAVITY TWT WITH SIX LOSSLESS OUTPUT CAVITIES AND FINAL THREE CAVITIES WITH DECREASED PERIODS	142
5.62	COMPUTED RF BEAM CURRENTS AND GAP VOLTAGES VS DISTANCE IN SIMULATED COUPLED-CAVITY TWT WITH SIX LOSSLESS OUTPUT CAVITIES, NEGATIVE PRETAPERED OUTPUT CIRCUIT AND FINAL THREE CAVITIES WITH DECREASED PERIODS	143

Figure No.Page No.

5.63	COMPUTED RELATIVE PHASES OF ELECTRON DISKS VS DISTANCE IN SIMULATED COUPLED-CAVITY TWT WITH SIX LOSSLESS OUTPUT CAVITIES, NEGATIVE PRETAPERED OUTPUT CIRCUIT AND FINAL THREE CAVITIES WITH DECREASED PERIODS	144
5.64	COMPUTED RF BEAM CURRENTS AND GAP VOLTAGES VS DISTANCE IN SIMULATED COUPLED-CAVITY TWT WITH SIX LOSSLESS OUTPUT CAVITIES, NEGATIVE PRETAPERED OUTPUT CIRCUIT AND FINAL THREE CAVITIES WITH DECREASED PERIODS	145
5.65	COMPUTED RELATIVE PHASES OF ELECTRON DISKS VS DISTANCE IN SIMULATED COUPLED-CAVITY TWT WITH SIX LOSSLESS OUTPUT CAVITIES, NEGATIVE PRETAPERED OUTPUT CIRCUIT AND FINAL THREE CAVITIES WITH DECREASED PERIODS	146
5.66	COMPUTED RF BEAM CURRENTS AND GAP VOLTAGES VS DISTANCE IN SIMULATED COUPLED-CAVITY TWT WITH SIX LOSSLESS OUTPUT CAVITIES, NEGATIVE PRETAPERED OUTPUT CIRCUIT AND FINAL THREE CAVITIES WITH DECREASED PERIODS	147
5.67	COMPUTED RELATIVE PHASES OF ELECTRON DISKS VS DISTANCE IN SIMULATED COUPLED-CAVITY TWT WITH SIX LOSSLESS OUTPUT CAVITIES, NEGATIVE PRETAPERED OUTPUT CIRCUIT AND FINAL THREE CAVITIES WITH DECREASED PERIODS	148
5.68	COMPUTED RF BEAM CURRENTS AND GAP VOLTAGES VS DISTANCE IN SIMULATED COUPLED-CAVITY TWT WITH SIX LOSSLESS OUTPUT CAVITIES, POSITIVE PRETAPERED OUTPUT CIRCUIT AND FINAL THREE CAVITIES WITH DECREASED PERIODS	150
5.69	COMPUTED RELATIVE PHASES OF ELECTRON DISKS VS DISTANCE IN SIMULATED COUPLED-CAVITY TWT WITH SIX LOSSLESS OUTPUT CAVITIES, POSITIVE PRETAPERED OUTPUT CIRCUIT AND FINAL THREE CAVITIES WITH DECREASED PERIODS	151
5.70	COMPUTED RF BEAM CURRENTS AND GAP VOLTAGES VS DISTANCE IN SIMULATED COUPLED-CAVITY TWT WITH SIX LOSSLESS OUTPUT CAVITIES, POSITIVE PRETAPERED OUTPUT CIRCUIT AND FINAL THREE CAVITIES WITH DECREASED PERIODS	152
5.71	COMPUTED RELATIVE PHASES OF ELECTRON DISKS VS DISTANCE IN SIMULATED COUPLED-CAVITY TWT WITH SIX LOSSLESS OUTPUT CAVITIES, POSITIVE PRETAPERED OUTPUT CIRCUIT AND FINAL THREE CAVITIES WITH DECREASED PERIODS	153

<u>Figure No.</u>		<u>Page No.</u>
5.72	COMPUTED RF BEAM CURRENTS AND GAP VOLTAGES VS DISTANCE IN SIMULATED COUPLED-CAVITY TWT WITH SIX LOSSLESS OUTPUT CAVITIES, POSITIVE PRETAPERED OUTPUT CIRCUIT AND FINAL THREE CAVITIES WITH DECREASED PERIODS	154
5.73	COMPUTED RELATIVE PHASES OF ELECTRON DISKS VS DISTANCE IN SIMULATED COUPLED-CAVITY TWT WITH SIX LOSSLESS OUTPUT CAVITIES, POSITIVE PRETAPERED OUTPUT CIRCUIT AND FINAL THREE CAVITIES WITH DECREASED PERIODS	155
5.74	COMPUTED RF BEAM CURRENTS AND GAP VOLTAGES VS DISTANCE IN SIMULATED COUPLED-CAVITY TWT WITH SIX LOSSLESS OUTPUT CAVITIES, POSITIVE PRETAPERED OUTPUT CIRCUIT AND FINAL TWO CAVITIES WITH DECREASED PERIODS	156
5.75	COMPUTED RELATIVE PHASES OF ELECTRON DISKS VS DISTANCE IN SIMULATED COUPLED-CAVITY TWT WITH SIX LOSSLESS OUTPUT CAVITIES, POSITIVE PRETAPERED OUTPUT CIRCUIT AND FINAL TWO CAVITIES WITH DECREASED PERIODS	157
5.76	COMPUTED RF BEAM CURRENTS AND GAP VOLTAGES VS DISTANCE IN SIMULATED COUPLED-CAVITY TWT WITH SIX LOSSLESS OUTPUT CAVITIES, POSITIVE PRETAPERED OUTPUT CIRCUIT AND FINAL TWO CAVITIES WITH DECREASED PERIODS	158
5.77	COMPUTED RELATIVE PHASES OF ELECTRON DISKS VS DISTANCE IN SIMULATED COUPLED-CAVITY TWT WITH SIX LOSSLESS OUTPUT CAVITIES, POSITIVE PRETAPERED OUTPUT CIRCUIT AND FINAL TWO CAVITIES WITH DECREASED PERIODS	159
5.78	COMPUTED RF BEAM CURRENTS AND GAP VOLTAGES VS DISTANCE IN SIMULATED COUPLED-CAVITY TWT WITH SIX LOSSLESS OUTPUT CAVITIES, POSITIVE PRETAPERED OUTPUT CIRCUIT AND FINAL TWO CAVITIES WITH DECREASED PERIODS	160
5.79	COMPUTED RELATIVE PHASES OF ELECTRON DISKS VS DISTANCE IN SIMULATED COUPLED-CAVITY TWT WITH SIX LOSSLESS OUTPUT CAVITIES, POSITIVE PRETAPERED OUTPUT CIRCUIT AND FINAL TWO CAVITIES WITH DECREASED PERIODS	161
5.80	COMPUTED RF BEAM CURRENTS AND GAP VOLTAGES VS DISTANCE IN SIMULATED COUPLED-CAVITY TWT WITH SIX LOSSLESS OUTPUT CAVITIES, LARGE GAPS IN OUTPUT SECTION, AND FINAL THREE CAVITIES WITH DECREASED PERIODS	163

<u>Figure No.</u>		<u>Page No.</u>
5.81	COMPUTED RELATIVE PHASES OF ELECTRON DISKS VS DISTANCE IN SIMULATED COUPLED-CAVITY TWT WITH SIX LOSSLESS OUTPUT CAVITIES, LARGE GAPS IN OUTPUT SECTION, AND FINAL THREE CAVITIES WITH DECREASED PERIODS	164
5.82	COMPUTED RF BEAM CURRENTS AND GAP VOLTAGES VS DISTANCE IN SIMULATED COUPLED-CAVITY TWT WITH SIX LOSSLESS OUTPUT CAVITIES, LARGE GAPS IN OUTPUT SECTION, AND FINAL THREE CAVITIES WITH DECREASED PERIODS	165
5.83	COMPUTED RELATIVE PHASES OF ELECTRON DISKS VS DISTANCE IN SIMULATED COUPLED-CAVITY TWT WITH SIX LOSSLESS OUTPUT CAVITIES, LARGE GAPS IN OUTPUT SECTION, AND FINAL THREE CAVITIES WITH DECREASED PERIODS	166
5.84	COMPUTED RF BEAM CURRENTS AND GAP VOLTAGES VS DISTANCE IN SIMULATED COUPLED-CAVITY TWT WITH SIX LOSSLESS OUTPUT CAVITIES, POSITIVE PRETAPERED OUTPUT CIRCUIT, AND FINAL THREE CAVITIES WITH DECREASED PERIODS	167
5.85	COMPUTED RELATIVE PHASES OF ELECTRON DISKS VS DISTANCE IN SIMULATED COUPLED-CAVITY TWT WITH SIX LOSSLESS OUTPUT CAVITIES, POSITIVE PRETAPERED OUTPUT CIRCUIT, AND FINAL THREE CAVITIES WITH DECREASED PERIODS	168
5.86	COMPUTED RF BEAM CURRENTS AND GAP VOLTAGES VS DISTANCE IN SIMULATED COUPLED-CAVITY TWT WITH SIX LOSSLESS OUTPUT CAVITIES, POSITIVE PRETAPERED OUTPUT CIRCUIT, AND FINAL THREE CAVITIES WITH DECREASED PERIODS	169
5.87	COMPUTED RELATIVE PHASES OF ELECTRON DISKS VS DISTANCE IN SIMULATED COUPLED-CAVITY TWT WITH SIX LOSSLESS OUTPUT CAVITIES, POSITIVE PRETAPERED OUTPUT CIRCUIT, AND FINAL THREE CAVITIES WITH DECREASED PERIODS	170
5.88	COMPUTED RF BEAM CURRENTS AND GAP VOLTAGES VS DISTANCE IN SIMULATED COUPLED-CAVITY TWT WITH SIX LOSSLESS OUTPUT CAVITIES, FASTER VELOCITY OUTPUT CIRCUIT, AND FINAL THREE CAVITIES WITH DECREASED PERIODS	172
5.89	COMPUTED RF BEAM CURRENTS AND GAP VOLTAGES VS DISTANCE IN SIMULATED COUPLED-CAVITY TWT WITH SIX LOSSLESS OUTPUT CAVITIES, FASTER VELOCITY OUTPUT CIRCUIT, AND FINAL THREE CAVITIES WITH DECREASED PERIODS	173

Figure No.Page No.

5.90	COMPUTED RF BEAM CURRENTS AND GAP VOLTAGES VS DISTANCE IN SIMULATED COUPLED-CAVITY TWT WITH SIX LOSSLESS OUTPUT CAVITIES, FASTER VELOCITY OUTPUT CIRCUIT, AND FINAL THREE CAVITIES WITH DECREASED PERIODS	174
5.91	COMPUTED RELATIVE PHASES OF ELECTRON DISKS VS DISTANCE IN SIMULATED COUPLED-CAVITY TWT WITH SIX LOSSLESS OUTPUT CAVITIES, FASTER VELOCITY OUTPUT CIRCUIT, AND FINAL THREE CAVITIES WITH DECREASED PERIODS	175
5.92	COMPUTED RF BEAM CURRENTS AND GAP VOLTAGES VS DISTANCE IN SIMULATED COUPLED-CAVITY TWT WITH SIX LOSSLESS OUTPUT CAVITIES, FASTER VELOCITY OUTPUT CIRCUIT, AND FINAL THREE CAVITIES WITH DECREASED PERIODS	176
5.93	COMPUTED RELATIVE PHASES OF ELECTRON DISKS VS DISTANCE IN SIMULATED COUPLED-CAVITY TWT WITH SIX LOSSLESS OUTPUT CAVITIES, FASTER VELOCITY OUTPUT CIRCUIT, AND FINAL THREE CAVITIES WITH DECREASED PERIODS	177
5.94	COMPUTED RF BEAM CURRENTS AND GAP VOLTAGES VS DISTANCE IN SIMULATED COUPLED-CAVITY TWT WITH SIX LOSSLESS OUTPUT CAVITIES, FASTER VELOCITY OUTPUT CIRCUIT, AND FINAL THREE CAVITIES WITH DECREASED PERIODS	178
5.95	COMPUTED RELATIVE PHASES OF ELECTRON DISKS VS DISTANCE IN SIMULATED COUPLED-CAVITY TWT WITH SIX LOSSLESS OUTPUT CAVITIES, FASTER VELOCITY OUTPUT CIRCUIT, AND FINAL THREE CAVITIES WITH DECREASED PERIODS	179
5.96	COMPUTED RF BEAM CURRENTS AND GAP VOLTAGES VS DISTANCE IN SIMULATED COUPLED-CAVITY TWT WITH SIX LOSSLESS OUTPUT CAVITIES, FASTER VELOCITY OUTPUT CIRCUIT, AND FINAL THREE CAVITIES WITH DECREASED PERIODS	181
5.97	COMPUTED RELATIVE PHASES OF ELECTRON DISKS VS DISTANCE IN SIMULATED COUPLED-CAVITY TWT WITH SIX LOSSLESS OUTPUT CAVITIES, FASTER VELOCITY OUTPUT CIRCUIT, AND FINAL THREE CAVITIES WITH DECREASED PERIODS	182
5.98	COMPUTED RF BEAM CURRENTS AND GAP VOLTAGES VS DISTANCE IN SIMULATED COUPLED-CAVITY TWT HOTMATCHED AT OUTPUT WITH SIX LOSSLESS OUTPUT CAVITIES, AND FINAL THREE CAVITIES WITH DECREASED PERIODS	183

<u>Figure No.</u>		<u>Page No.</u>
5.99	COMPUTED RELATIVE PHASES OF ELECTRON DISKS VS DISTANCE IN SIMULATED COUPLED-CAVITY TWT HOTMATCHED AT OUTPUT WITH SIX LOSSLESS OUTPUT CAVITIES, AND FINAL THREE CAVITIES WITH DECREASED PERIODS	184
5.100	COMPUTED RF BEAM CURRENTS AND GAP VOLTAGES VS DISTANCE IN SIMULATED COUPLED-CAVITY TWT WITH TWELVE CAVITY OUTPUT SECTION AND SIX LOSSLESS OUTPUT CAVITIES AT A FREQUENCY OF 3.1 GHz	185
5.101	COMPUTED RELATIVE PHASES OF ELECTRON DISKS VS DISTANCE IN SIMULATED COUPLED-CAVITY TWT WITH TWELVE CAVITY OUTPUT SECTION AND SIX LOSSLESS OUTPUT CAVITIES AT A FREQUENCY OF 3.1 GHz	186
5.102	COMPUTED RF BEAM CURRENTS AND GAP VOLTAGES VS DISTANCE IN SIMULATED COUPLED-CAVITY TWT WITH TWELVE CAVITY OUTPUT SECTION AND SIX LOSSLESS OUTPUT CAVITIES AT A FREQUENCY OF 3.6 GHz	187
5.103	COMPUTED RELATIVE PHASES OF ELECTRON DISKS VS DISTANCE IN SIMULATED COUPLED-CAVITY TWT WITH TWELVE CAVITY OUTPUT SECTION AND SIX LOSSLESS OUTPUT CAVITIES AT A FREQUENCY OF 3.6 GHz	188
5.104	COMPUTED RF BEAM CURRENTS AND GAP VOLTAGES VS DISTANCE IN SIMULATED COUPLED-CAVITY TWT WITH TWELVE CAVITY OUTPUT SECTION AND SIX LOSSLESS OUTPUT CAVITIES AT A FREQUENCY OF 3.5 GHz	189
5.105	COMPUTED RELATIVE PHASES OF ELECTRON DISKS VS DISTANCE IN SIMULATED COUPLED-CAVITY TWT WITH TWELVE CAVITY OUTPUT SECTION AND SIX LOSSLESS OUTPUT CAVITIES AT A FREQUENCY OF 3.5 GHz	190
5.106	SATURATION GAIN AND EFFICIENCY VS FREQUENCY IN SIMULATED COUPLED-CAVITY TWT WITH THIRTEEN CAVITY OUTPUT SECTION AND SIX LOSSLESS OUTPUT CAVITIES	193
5.107	LOSS PER CAVITY VS FREQUENCY FOR COUPLED-CAVITY DESIGNS E, F AND H	199
5.108	COMPUTED RF BEAM CURRENTS AND GAP VOLTAGES VS DISTANCE IN SIMULATED COUPLED-CAVITY TWT WITH TWELVE CAVITY OUTPUT SECTION AND FIVE LOSSLESS OUTPUT CAVITIES AT A FREQUENCY OF 3.6 GHz	201

<u>Figure No.</u>		<u>Page No.</u>
5.109	COMPUTED RELATIVE PHASES OF ELECTRON DISKS VS DISTANCE IN SIMULATED COUPLED-CAVITY TWT WITH TWELVE CAVITY OUTPUT SECTION AND FIVE LOSSLESS OUTPUT CAVITIES AT A FREQUENCY OF 3.6 GHz	202
5.110	BRILLOUIN DIAGRAM FOR VTS-5753 AND HIGH FREQUENCY CIRCUIT	203
5.111	COMPUTED START OSCILLATION CURRENT VS BEAM VOLTAGE FOR SIMULATED N-2 DESIGN COUPLED-CAVITY TWT WITH TWELVE CAVITY OUTPUT SECTION AND FIVE LOSSLESS OUTPUT CAVITIES	204
5.112	COMPUTED START OSCILLATION CURRENT VS BEAM VOLTAGE FOR SIMULATED 2-N-2 DESIGN COUPLED-CAVITY TWT WITH 1.08 INCH OUTPUT PERIODS	206
5.113	BRILLOUIN DIAGRAM FOR VTS-5753 AND ULTRA-HIGH FREQUENCY CIRCUIT	207
5.114	COMPUTED START OSCILLATION CURRENT VS BEAM VOLTAGE FOR SIMULATED 2-N-2 DESIGN COUPLED-CAVITY TWT WITH TWELVE CAVITY OUTPUT SECTION AND FIVE LOSSLESS OUTPUT CAVITIES	209
6.1	SCHEMATIC FOR 100 KW S-BAND COUPLED-CAVITY TWT (FINAL DESIGN)	212
6.2	LOSS PER CAVITY VS FREQUENCY FOR FINAL DESIGN	214
6.3	COMPUTED SMALL-SIGNAL GAIN FOR FINAL DESIGN	215
6.4	COMPUTED SATURATED OUTPUT POWER AND GAIN VS FREQUENCY FOR FINAL DESIGN	216
6.5	COMPUTED RF BEAM CURRENTS AND GAP VOLTAGES VS DISTANCE IN SIMULATED COUPLED-CAVITY TWT WITH TWELVE CAVITY OUTPUT SECTION AND FIVE LOSSLESS OUTPUT CAVITIES AT A FREQUENCY OF 3.10 GHz	217
6.6	COMPUTED RELATIVE PHASES OF ELECTRON DISKS VS DISTANCE IN SIMULATED COUPLED-CAVITY TWT WITH TWELVE CAVITY OUTPUT SECTION AND FIVE LOSSLESS OUTPUT CAVITIES AT A FREQUENCY OF 3.10 GHz	218
6.7	COMPUTED RF BEAM CURRENTS AND GAP VOLTAGES VS DISTANCE IN SIMULATED COUPLED-CAVITY TWT WITH TWELVE CAVITY OUTPUT SECTION AND FIVE LOSSLESS OUTPUT CAVITIES AT A FREQUENCY OF 3.20 GHz	219

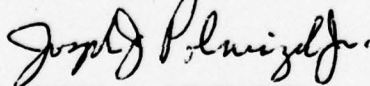
Figure No.Page No.

6.8	COMPUTED RELATIVE PHASES OF ELECTRON DISKS VS DISTANCE IN SIMULATED COUPLED-CAVITY TWT WITH TWELVE CAVITY OUTPUT SECTION AND FIVE LOSSLESS OUTPUT CAVITIES AT A FREQUENCY OF 3.20 GHz	220
6.9	COMPUTED RF BEAM CURRENTS AND GAP VOLTAGES VS DISTANCE IN SIMULATED COUPLED-CAVITY TWT WITH TWELVE CAVITY OUTPUT SECTION AND FIVE LOSSLESS OUTPUT CAVITIES AT A FREQUENCY OF 3.35 GHz	221
6.10	COMPUTED RELATIVE PHASES OF ELECTRON DISKS VS DISTANCE IN SIMULATED COUPLED-CAVITY TWT WITH TWELVE CAVITY OUTPUT SECTION AND FIVE LOSSLESS OUTPUT CAVITIES AT A FREQUENCY OF 3.35 GHz	222
6.11	COMPUTED RF BEAM CURRENTS AND GAP VOLTAGES VS DISTANCE IN SIMULATED COUPLED-CAVITY TWT WITH TWELVE CAVITY OUTPUT SECTION AND FIVE LOSSLESS OUTPUT CAVITIES AT A FREQUENCY OF 3.50 GHz	223
6.12	COMPUTED RELATIVE PHASES OF ELECTRON DISKS VS DISTANCE IN SIMULATED COUPLED-CAVITY TWT WITH TWELVE CAVITY OUTPUT SECTION AND FIVE LOSSLESS OUTPUT CAVITIES AT A FREQUENCY OF 3.50 GHz	224
6.13	COMPUTED RF BEAM CURRENTS AND GAP VOLTAGES VS DISTANCE IN SIMULATED COUPLED-CAVITY TWT WITH TWELVE CAVITY OUTPUT SECTION AND FIVE LOSSLESS OUTPUT CAVITIES AT A FREQUENCY OF 3.60 GHz	225
6.14	COMPUTED RELATIVE PHASES OF ELECTRON DISKS VS DISTANCE IN SIMULATED COUPLED-CAVITY TWT WITH TWELVE CAVITY OUTPUT SECTION AND FIVE LOSSLESS OUTPUT CAVITIES AT A FREQUENCY OF 3.60 GHz	226

EVALUATION

This program was aimed at improving the basic or conversion efficiency in coupled cavity traveling wave tubes while maintaining the wide bandwidth that is typical of present day tubes. The program directed attention at the physics of the bunching process and attempted to better understand the physics involved so that a goal of 40% conversion efficiency could be realized. The results of the study have been for the most part successful in that only a slight decrease in bandwidth resulted.

In order to satisfy tactical needs with respect to transmitter efficiency, overall efficiency of the device must also be of concern. So, although this program has resulted in significant energy savings in tactical transmitters other techniques such as multiple stage collector depression must also be addressed in conjunction with the results of this program. In this way, it may be feasible to attain a 60% overall efficiency in a coupled cavity traveling wave tube amplifier. Presently, a program of this type is anticipated.



JOSEPH J. POLNIASZEK
Project Engineer

1.0 INTRODUCTION

The inherent efficiency of the O-type traveling-wave amplifier has been the subject of much investigation, both experimental and theoretical. The basic parameters determining the efficiency of a uniform TWT were ascertained early in its history. Since then, optimization of these parameters has proceeded with mixed success.

Immediately obvious collector-depression schemes have been successfully implemented and interest in multistage depressed collectors for helix TWTs is running high. Nevertheless, complex collectors increase the cost, weight and complexity of microwave amplifier systems and reduce their reliability. One is tantalized by the fact that klystrons have been built with conversion efficiencies approaching 80 percent, which is greater than the overall efficiency that all but the most optimistic collector designers ever hope to achieve.

The high conversion efficiency of some klystrons naturally leads one to speculate on whether a coupled-cavity TWT, a device employing klystron-like cavities, can be made to achieve comparable conversion efficiencies. This report concerns itself with a study of that question.

This investigation is specifically aimed at the design of a coupled-cavity traveling wave tube of the following parameter goals:

Frequency Band	3.1 to 3.6 GHz
Electronic Bandwidth	500 MHz
Peak Power	>100 kW
Average Power	10 KW
Duty Factor	10% min
Pulse Width	10 to 300 μ sec
Gain	40 dB min
Conversion Efficiency	40% minimum across the band

Section 2 of this report contains a review of previous work done in this area. In Section 3, analytic procedures are described which form the basis for analysis and synthesis of new techniques.

The approach chosen for this investigation is to discover the most effective way to bunch the beam, then to maximize power extraction by phase focusing. Section 4 contains an analysis of various schemes for enhanced bunching. Section 5 deals with velocity resynchronization and the particular problems encountered in attempting to phase focus a TWT with a relatively dispersive circuit.

In Section 6, the results of this investigation are employed to synthesize a paper design for a coupled-cavity TWT specifically aimed at achieving the design goals cited above. Section 7 offers concluding remarks regarding this program and some other ideas which are suggested by this work.

2.0 REVIEW OF RELATED WORK

Nordsieck [19] was one of the earliest to treat the large-signal problem. His paper was written in 1947. He assumed, initially, a one-dimensional beam with zero space-charge and very small C (Pierce coupling parameter). His predicted efficiency is unrealistically high. Even when he introduced finite C he estimated, for example, a conversion efficiency of 52 percent for a TWT with $C = 0.1$ and b (Pierce velocity parameter) $= 1.5$. Although Nordsieck's results are optimistic, his method established a firm foundation for later workers. Nordsieck made no attempt to recommend ways to increase efficiency.

Cutler and Brangaccio [7] were the first to show how efficiency is affected by the amount of attenuation and the profile of the attenuator of a helix TWT. They conducted a series of experiments using an external probe on a helix TWT with a glass barrel. From these measurements they were able to construct a number of graphs which provide empirical guidance for the design of an efficient TWT. Their curves show that one needs about 15 to 30 dB of small-signal gain beyond the attenuator, depending on the nature of the attenuator. Their work shows that more gain beyond the sever is required as the space-charge parameter is increased.

Poulter [23] examined the large-signal behavior of TWTs including space-charge, finite C , and circuit loss. The space-charge model employed was quasi-static, involving the solution of Poisson's equation in the beam but permitting no transverse variation of fields. The inclusion of loss was an important extension since loss is a necessary evil in all TWTs. Poulter did not properly evaluate the backward-wave.

Tien et al. [36] built on Nordsieck's beginnings by adding a space-charge model. They retained Nordsieck's other assumptions: one dimensional beam, small C , and most important, a single forward-wave on the circuit. This analysis probably fits the helix TWT rather well, but cannot be expected to

give meaningful results for TWTs with bandpass circuits. The space-charge model is one which employs charged disks. It is a straightforward matter to calculate the force exerted by one such disk on another at a given distance. The space-charge force is found by integrating over the z -distribution of electrons. This procedure has a shortcoming shared by all so-called distance-stepping procedures: to find the space-charge force at a point, it is necessary to know the positions of electrons further downstream from this point. These electron positions have not yet been computed. It is therefore necessary to assume that the spacial distribution can be adequately predicted from the known temporal distribution at a given position.

These authors exhibit some computed typical examples for cases with parameters one would expect to encounter in helix TWTs. They employ a modified Appligate Diagram to show how electrons are bunched and trapped in the circuit waves. They compare performance of TWTs with differing velocity parameters, space-charge parameters, and space-charge range parameters. They propose a means for increasing efficiency by introducing a sudden phase-shift to the circuit wave near saturation level such that the bunch may be moved inside the decelerating region.

Rowe's work [26] is similar to that of Poulter [23]. Rowe assumed finite C and finite circuit loss. His space-charge model assumed that the distribution of charge along the axis of the beam was equivalent to the distribution of charge in time at a particular point along the axis. From this equivalence he was able to compute the space-charge forces. Rowe's results are in reasonable agreement with those of Tien, Walker and Wolontis. Rowe's method obscures the role of the backward-wave thereby preventing the easy extension of his method to cases in which there are internal or external reflections of the circuit wave.

Tien [35] improved on Tien, Walker and Wolontis by taking into account finite C , finite circuit to beam coupling, and rf space-charge effects, but neglected circuit loss. Tien's analysis explicitly included the backward-wave,

a feature which is particularly significant in coupled-cavity TWT analysis although, in this paper, he assumed that the circuit was a helix. Tien concluded that efficiency increases very slowly with C , decreases with QC and is not much affected by b (over the range of values normally encountered). He computed an efficiency of 42 percent, with $C = 0.2$, $QC = 0.1$ and $b = 0.72$, and an efficiency of 25 percent, with $C = 0.1$, $QC = 0.4$ and $b = 1.38$. In both of these cases, b is chosen to maximize the small-signal gain.

In his paper, Cutler [6] gathered the results of a number of experimental efficiency measurements and attempted to plot contours of constant η/C on a b vs QC plot. He superimposed the computed results of Tien, Walter and Wolontis. The resultant showed the measured contours to be virtually orthogonal to the computed contours. Cutler perhaps tried too hard to correlate experimental data which was anything but consistent. As he pointed out himself in an earlier paper, reported experimental efficiencies were widely varying and apparently inconsistent.

Hess [12] introduced an analysis of the voltage taper, that is, the acceleration of the beam in place of, or in addition to, the deceleration of the circuit wave. While voltage taper might be expected to achieve slightly higher conversion efficiency, it has not achieved commercial success because it does not appear to justify the additional cost and risk involved in using a more complex structure.

Ruetz et al. [31] measured the efficiency of a high power coupled-cavity TWT with four different velocity tapers. They concluded that the conversion efficiency could be significantly increased at the low frequency end of the passband with a slight reduction in efficiency at the upper end. This appears to be the first reported example demonstrating an increase in efficiency bandwidth in a dispersive TWT.

Clarke [4] computed some cases employing a helix with velocity taper. He assumed zero loss and zero space-charge. He concluded that the maximum

achievable conversion efficiency could not be improved by velocity tapering because saturation is due to a combination of asynchronism of the bunches combined with bunch spread, and the taper can only work against the first effect. Clarke suggested that a voltage jump might provide a higher efficiency by reducing velocity spread.

Meeker and Rowe [17] used Rowe's analysis to compute the conversion efficiency of a tapered helix TWT. They also used the computer to choose an optimum taper profile. In addition, they built and tested a TWT to show experimentally the difference in performance between a tapered and an untapered TWT. Their experimental results show that the efficiency enhancement is greatest near the bottom of the frequency band where the efficiency is highest in the untapered TWT (only results with optimized beam voltage are presented). At the high end of the frequency band, where the efficiency is lowest, the taper provides very little improvement. The experimental results agree qualitatively with the large-signal theory, however the computed efficiencies were approximately 50 percent higher than those measured. This discrepancy is unexplained except for suggesting that it might be associated with shortcomings of their one-dimensional beam model.

Bates and Scott [1] used a Pierce-type analysis to show how the wave will grow beyond the sever in tapered and untapered circuits. They concluded that a taper could help to achieve approximately constant efficiency over a range of velocity parameters from $b = 0.0$ to $b = 1.5$. They pointed out that the ability to achieve near maximum efficiency over such a range of velocity parameters was the critical factor in achieving power-bandwidth in dispersive TWTs. They reported on a taper experiment which qualitatively confirmed their calculations but which fell short of the predicted efficiency by almost 40 percent. They explained that the experimental tube had a lesser taper than was employed in the computation, that there was insufficient gain beyond the sever and that perhaps the one-dimensional beam model was inadequate.

Ruetz, Kino, Hiramatsu and Bates [32] began the Varian large-signal and small-signal computer programs in 1963. These programs were to be used for design and diagnostic purposes on both TWTs and klystrons. The microwave structures of interest to these investigators were:

1. Terminated helix circuits used in TWTs
2. Conventional signal gap reentrant cavities for use in klystrons
3. Terminated coupled-cavity circuits used in TWTs
4. Resonant slow wave structures used in extended interaction klystrons
5. Combinations of the above for broadband klystrons and hybrid tubes

In addition to modeling such a complete array of O-type tubes, it was decided to incorporate the following:

1. Space-charge effects
2. Large values of C
3. Arbitrary loss distribution
4. Severs of arbitrary length
5. Interaction impedance and circuit phase velocity variable along the circuit
6. Space-charge potential depression
7. Total gap field analysis in coupled-cavity circuits with backward-wave exactly taken into account
8. Internal and external rf mismatches taken into account in coupled-cavity circuits

The Varian coupled-cavity TWT programs secured, for the first time, the ability to analyze and understand coupled-cavity TWTs, and to include practical design features, such as imperfect rf matches, which had not previously been available, even in helix TWT analyses. These programs have been improved upon over a period of years and now include virtually every feature that could be usefully incorporated; they lack only a two-dimensional beam model and harmonic interaction. The latter feature is of little value to the present work since

coupled-cavity tubes are usually designed to avoid harmonic interaction. The one-dimensional beam model could doubtless be improved on. However, the good agreement between computed and measured performance [32] [14] in klystrons and TWTs at about 40 percent efficiency would seem to imply that the extra expense of a two dimensional beam model is not warranted. There is some evidence that the use of a time stepping computer model with one-dimensional beam might be more accurate in the 40-60 percent efficiency range than a distance stepping program with a two-dimensional beam model.

Nichlas and Gerchberg [18] reported on an experimental helix TWT which possessed both a voltage jump and a circuit wave phase jump. They indicate a maximum efficiency of 43.5 percent; however, the conversion efficiency is defined in such a way that this result should be compared with similar results for TWTs with single-stage depressed collectors. This is a very complex TWT with narrow-band performance which has never been commercially exploited.

Rowe and Brackett [30] estimated the ideal velocity taper based on a simplified model which assumes that the charge is concentrated at a single point in each rf cycle (Hard Kernal Bunch or HKB approximation). They reported on experimental results from a number of TWTs with identical uniform sections but differing taper sections. They achieved their best results with a 50 percent HKB taper, second best was a two-step 50 percent taper and worst was a single step 50 percent taper. A 70 percent HKB taper and a 40 percent linear taper were computed for comparison.

The TWT with the 50 percent taper displayed improved efficiency over the entire one-octave band with maximum net efficiency of 37 percent which, when corrected for coupler loss, yielded a gross efficiency of 47 percent. This latter value is in good agreement with theory. The efficiency enhancement was found not to be too critical with respect to taper profile; only the one-step taper had an obviously deleterious effect.

It was found possible to further increase the overall efficiency by use of a single-stage depressed collector. The lower efficiency untapered TWTs showed more improvement from collector depression than did the tapered TWTs; however, the tapered and depressed TWTs scored the best overall efficiency.

Pond and Twiggs [22] were able to increase the conversion efficiency of a coupled-cavity TWT by approximately 17 percent by means of period tapering. These researchers showed a relatively flat efficiency vs frequency for the untapered case and a domed curve for the tapered case, the exact opposite of the results obtained by Bates and Scott. Perhaps Pond and Twiggs were using a less dispersive circuit than Bates and Scott.

Gerchberg and Niclas [18] reported on an experimental helix TWT with positive taper. They measured conversion efficiency as high as 40.6 percent; however, the band over which the tube had high efficiency was narrow and there is no reason to believe that equivalent or better results could not have been obtained in a more conventional way.

3.0 ANALYTIC METHODS

The analytic design procedure employed in the present work is based on a number of Varian computer programs which model the rf interaction process in a coupled-cavity traveling wave tube. The synthesis of a new design is accomplished by analyzing an initial design, chosen usually by extrapolation of existing designs, then systematically modifying parameters and recomputing performance until the design is optimized. This section contains a brief description of the two major computer programs employed in the present work.

3.1 The Varian Small-Signal Program for Coupled-Cavity TWTs

The small-signal program is a valuable tool for adjusting a preliminary design to ensure that it has sufficient gain in the output section to assure reasonable conversion efficiency or to adjust the sever match to obtain minimum gain ripple. Sometimes the small-signal program is used to determine how many circuit sections will be needed to provide adequate overall gain. Of all the features possessed by the small-signal program, none is more important than its ability to predict the onset of electronic instability. This feature of the program is provided by means of a search routine which systematically searches in the beam voltage, beam current, drive frequency, three-space for a pole of gain. It is then possible to plot a curve of start oscillation current vs beam voltage, the frequency of oscillation being of secondary interest, and thereby to determine whether the nominal operating point is inside or outside the stable region. Of interest in the design of cathode pulsed tubes is the requirement that a curve representing the current vs voltage for the intended beam perveance must entirely avoid the instability region in order to achieve stable operation and avoid "rabbit ear" oscillations, i.e., oscillations on the rising and falling edges of the beam pulse.

The Varian small-signal program for coupled-cavity TWTs was begun by Ruetz et al [32] in 1963. It has been modified in many ways since that time but has maintained from the beginning the form developed by Kino [14] to extend the work of Pierce [21] to adequately take account of the fields which exist in a coupled-cavity slow-wave circuit. In this analysis, it is assumed that the beam interacts with the actual circuit gap fields rather than with sinusoidal traveling components, that interaction is with the total gap field including all space-harmonic components and that the beam simultaneously interacts with the fields of both forward and backward traveling circuit waves. Further, it is required that the parameters defining the model be completely defined at each frequency in terms of measurable circuit parameters. Since the coupled-cavity circuit consists of a chain of connected cavities, the basic model need only represent the single-cavity unit. The model chosen to represent each cavity cell is shown in Figure 3.1. It comprises a general three-port linear network with two sets of terminals representing the coupling to other cavities in the chain and a third set representing coupling to the electron beam. The impedance matrix representation of the cavity model is also shown in Figure 3.1. From symmetry and reciprocity, the impedance matrix elements must satisfy certain relationships also indicated in the figure. Note that the sign relating Z_{ib} to Z_{ob} depends upon symmetry considerations; it is positive for cloverleaf or fundamental circuits and negative for a folded or space-harmonic type circuit.

In order to calculate the coupled-cavity TWT behavior, the impedance elements of the circuit model must be identified with the actual cavity parameters. By setting $I_b = 0$ it can be shown that

$$\cos \theta_c = \frac{Z_{ii}}{Z_{io}} \quad (1)$$

where θ_c is the cold circuit phase angle. Likewise, it can be shown that

$$K = -2j \frac{Z_{ib} Z_{ib}^*}{Z_{io}} \left(\tan \theta_c / 2 \right)^{\pm 1} \quad (2)$$

where K is the beam interaction impedance defined by

$$K = \frac{V_b V_b^*}{2P} \quad (3)$$

The upper and lower signs in Eq. (2) correspond to the positive and negative symmetry between Z_{ib} and Z_{ob} .

An additional impedance term needing identification with the actual circuit is the Z_{bb} term. This would normally be found from an open circuit impedance measurement made at the cavity gap terminals. Since this measurement would be difficult to make in practice an alternative is to determine Z_{bb} from a short circuit measurement made at the cavity resonant frequency. By assuming that the shorted cavity can be adequately represented by a simple lumped parallel tuned circuit, the element Z_{bb} can then be expressed at all frequencies by

$$Z_{bb} = \frac{R_{sh}/Q}{1/Q + j \frac{\omega}{\omega_0} - \frac{\omega_0}{\omega}} = \mp j \frac{K}{\sin \theta_c} \quad (4)$$

where R_{sh}/Q is the value obtained for a single resonant cavity as defined by

$$\frac{R_{sh}}{Q} = \frac{V_b V_b^*}{2U\omega_0} \quad (5)$$

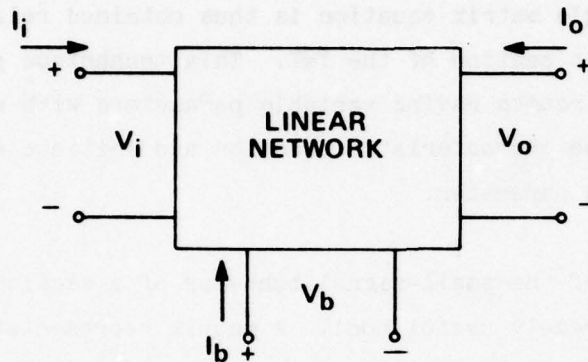
In the above, U is the total stored energy in the shorted cavity at resonance and ω_0 is the angular resonant frequency of the cavity.

The impedance term Z_{bb} is a new element involving quantities which do not appear in the Pierce analysis. It is interesting to observe the variation of this term with frequency. For both the cloverleaf circuit and the space-harmonic, coupled-cavity circuit it is found that Z_{bb} is capacitive over the entire pass band. For the lossless case the term Z_{bb} approaches infinity at the lower cut-off frequency due to the influence of K but always remains finite at the upper cut-off frequency.

Curnow [5] has derived a lumped element equivalent circuit for the generalized coupled-cavity which is capable of representing the characteristics of these circuits with considerable accuracy. Although an equivalent circuit is not required by the analysis, a Curnow circuit is normally employed because it is relatively simple to determine the element values from cold-test measurements and because this representation is valid both in the pass band and in the stop-bands, the latter feature being crucial for calculating band edge stability. Use of the Curnow circuit permits a complete specification with about ten real numbers, whereas the direct specification would require the generation of the impedance matrix of Figure 3.1 at each frequency at which the gain is to be computed. Within the circuit pass-band this latter description would be cumbersome, at the band-edge and in the stop-band most difficult, and, when searching for electronic instability, quite impossible. In this report, Curnow equivalent circuits are used to model the actual slow-wave circuit.

The small-signal gain in a signal cavity cell is computed by combining the above circuit model with a one dimensional beam equation [3]. The interaction field used with the beam equation is the total axial field existing within each of the cavity boundaries. Either measured or theoretically calculated field shapes may be used. The beam coupling factors and induced cavity currents are obtained by integration over the length of the cavity of the gap fields averaged over the beam cross-section.

The small-signal coupled-cavity analysis results in a set of four linear equations relating the output or downstream values of the system variables to the input or upstream values of the same variables. The variables used could be any set of four independent variables such as voltage and current, etc., or the normal mode variables of Pierce [21]. The variables chosen here are the normalized forward-wave and backward-wave voltage on the circuit and the velocity and current modulation on the beam. These appear to be the most



$$\begin{bmatrix} V_i \\ V_o \\ V_b \end{bmatrix} = \begin{bmatrix} Z_{ii} & Z_{io} & Z_{ib} \\ Z_{oi} & Z_{oo} & Z_{ob} \\ Z_{bi} & Z_{bo} & Z_{bb} \end{bmatrix} \times \begin{bmatrix} I_i \\ I_o \\ I_b \end{bmatrix}$$

$$\text{RECIPROCITY: } Z_{io} = Z_{oi} \quad Z_{ib} = Z_{bi} \quad Z_{ob} = Z_{bo}$$

$$\text{SYMMETRY: } Z_{ii} = Z_{oo} \quad Z_{ib} = \pm Z_{ob}$$

FIGURE 3.1 CIRCUIT MODEL USED FOR REPRESENTING EACH CAVITY OF THE COUPLED-CAVITY TWT.

natural variables to employ since the beam variables are known to be zero at the input (unmodulated beam) and the circuit variables are well chosen for matching end conditions and for modeling internal mismatches which may exist in real circuits.

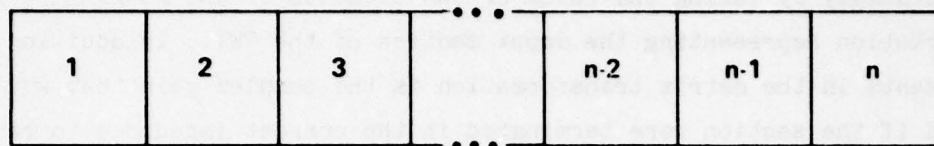
Small-signal calculations are performed by the multiplication of cavity matrices as indicated in Figure 3.2. Each cavity is represented by a four-by-four matrix which transforms circuit and beam parameters from the input to the output of the cavity. A single matrix equation is thus obtained relating input and output parameters for each section of the TWT. This technique permits calculations to be made on circuits having variable parameters with distance without having to re-solve the characteristic equation and initiate new wave amplitudes for each change in parameter.

The matrix formulation of the small-signal behavior of a section of a coupled-cavity TWT is an extremely useful tool. A matrix representation of the sever section can be derived which operates on the beam parameters in the sever section and sets the forward circuit wave to zero insofar as the upstream circuit wave is completely terminated. The assumed mismatches at the input and output ends of each circuit section can also be written in matrix form. By multiplying together, in the correct order, all the section matrices, the mismatch matrices and the sever matrices one obtains a single matrix for the entire TWT. One term in this overall matrix relates the forward-wave at the output (the wave incident on the load) to the forward-wave at the input (drive signal). This ratio is defined to be the small-signal gain. This analysis differs from many similar analyses in that it makes no simplifying assumption regarding the backward-wave; all ramifications of the backward-wave, its generation, its interaction with the electron beam and its coupling to the forward-wave via circuit and load mismatches are included.

Another virtue of the matrix form of the solution is the ease with which certain other tube characteristics may be computed. If, for example, one wishes to obtain a perfect hot match at the input to the TWT, this result can

INPUT

OUTPUT



COUPLED CAVITY TWT

$$X_{out} = A_n \cdot A_{n-1} \cdot \dots \cdot A_3 \cdot A_2 \cdot A_1 \cdot X_{in} = A \cdot X_{in}$$

$$X = \begin{bmatrix} x_1 \\ x_2 \\ x_3 \\ x_4 \end{bmatrix}$$

$$A = \begin{bmatrix} a_{11} & a_{12} & a_{13} & a_{14} \\ a_{21} & a_{22} & a_{23} & a_{24} \\ a_{31} & a_{32} & a_{33} & a_{34} \\ a_{41} & a_{42} & a_{43} & a_{44} \end{bmatrix}$$

- x_1 = FORWARD CIRCUIT VOLTAGE
- x_2 = BACKWARD CIRCUIT VOLTAGE
- x_3 = a-c BEAM CURRENT
- x_4 = a-c BEAM VELOCITY

FIGURE 3.2. MATRIX MULTIPLICATION FOR OBTAINING THE SMALL-SIGNAL CHARACTERISTICS OF THE COUPLED-CAVITY TWT.

be accomplished by providing, at the sever load, a mismatch which can be computed simply by taking the ratio of two elements of the matrix transformation representing the input section of the TWT. In addition, one of the elements in the matrix transformation is the complex gain that would be obtained if the section were terminated in the correct impedance to cause a hot match at the input. The gain of a hot matched section is typically ripple free. In principle, one can design an internally equalized TWT. Unfortunately, the impedance functions required for internal compenstion are usually too complex to contemplate synthesizing within the limited space available inside the TWT.

The computation of start oscillation current for various electronic instability modes is achieved by running the small-signal program in a search mode. The instability mode with the lowest starting current, in a space harmonic coupled-cavity TWT, is usually that mode for which all cavities are excited in phase, i.e., a 2π mode. With the beam voltage adjusted so that the beam is synchronous with the circuit wave at the upper band edge, oscillation will occur at a frequency very near the upper band edge frequency and the start oscillation current for this condition will be near the absolute minimum start oscillation current. As the beam voltage is increased toward the nominal operating value, the start oscillation current is found invariably to increase as does also the frequency of oscillation. If the frequency has increased above the band edge value, it will not be possible to compute this case unless the circuit parameters are available at frequencies within the stopband. Additionally, it will not be possible to operate in the search mode unless the circuit parameters are available at every frequency chosen by the search algorithm. The use of an equivalent circuit such as the Curnow circuit is therefore essential to the computation of electronic instability.

3.2 The Varian Large-Signal Program for Coupled-Cavity TWTs

The methodology for the large-signal program follows closely that of the small-signal program. Interaction inside a single-cavity cell is analyzed first, then the cells are joined together into circuit sections, and finally into an entire TWT. Both large and small-signal programs share a common generalized three-port circuit. For the large-signal program the beam, which is the only non-linear component of the system, is modeled with a disk model similar to that employed by Tien [35]. Consideration has been given to models proposed by Kino and others which reduce the rather high force that is obtained in the Tien model when two electrons approach each other. It is apparent that a force of this type between two rather large "lumped" charges is not truly representative of the forces that exist in a beam when it contains a very large number of electrons, each having a very small charge. One solution is to employ a "thick" electron disk model with a linearly varying force that passes through zero as the two electrons pass through each other. The electron thickness in this model approaches zero as the total number of electrons is increased. A model has also been implemented, that was proposed by S. Wallender, in which the space-charge fields are obtained by summing the field contributions from the various harmonics which make up the total beam current. Since it takes $2N$ electron disks to accurately represent N beam harmonics, Wallender sums only the N lowest beam harmonics to achieve a more consistent force relationship between the electron disks when a finite number of disks are used. The effect of limiting the number of harmonics is to round off the discontinuity in the force curve, as illustrated in Figure 3.3.

If one considers the charged disks to represent sampling points on the beam, one need not assume that the space-charge force on an electron is the sum of all interactions between a given disk and all other disks (Tien model); rather, it is equally valid to compute the force on a point charge due to all the disks. If one analyzes the force between a point charge and a charged disk, one obtains a force function similar to the Wallender model, neither like the Tien model nor the thick disk model.

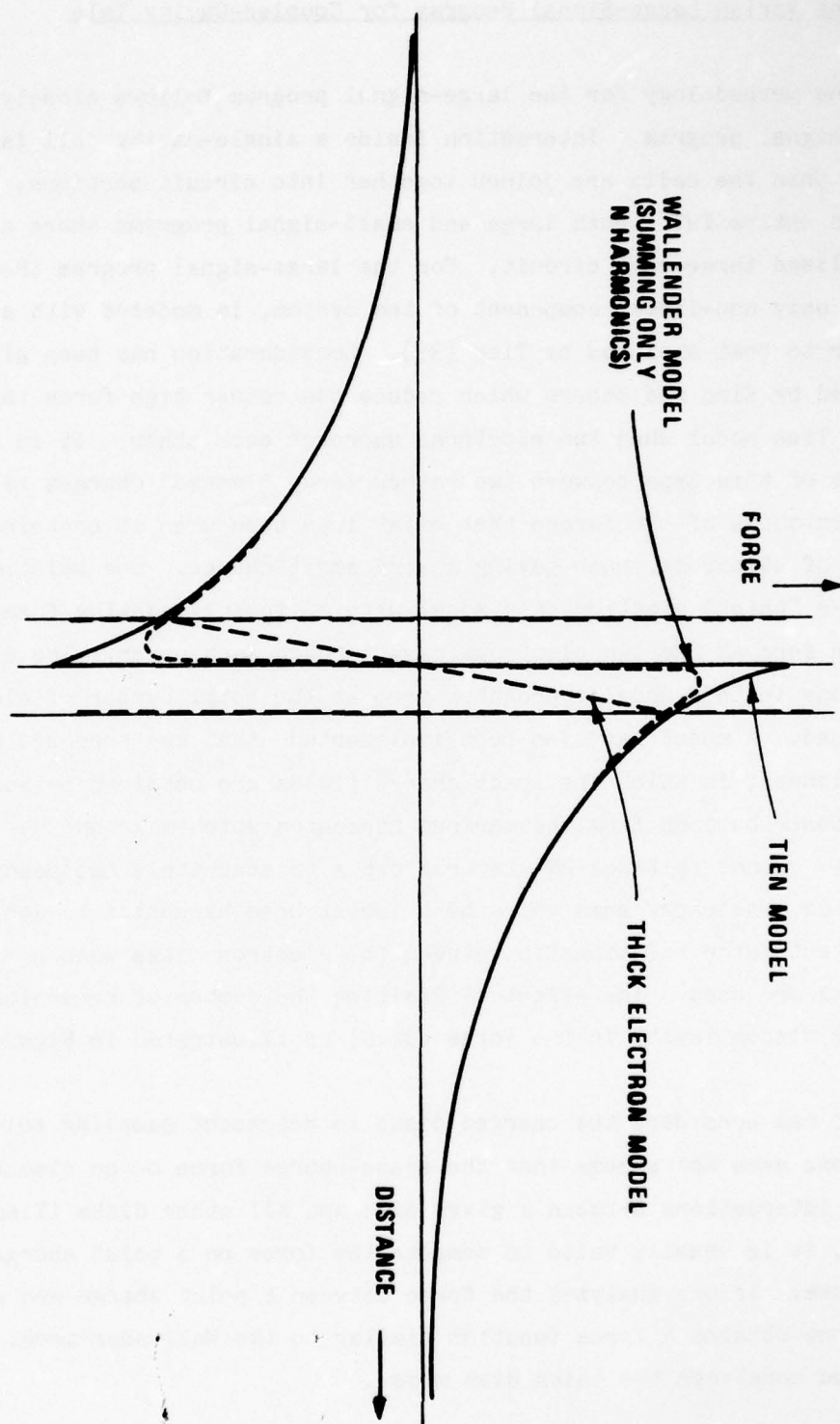


FIGURE 3.3 FORCE FIELDS OF VARIOUS DISC MODELS

The large-signal calculations carried out in the present investigation have employed the Wallender space-charge model. In this formalism, the space-charged field components are derived from the Fourier components of the rf convection current which relates to the time of arrival of the disks at a given location. Since the beam convection current at a point is a periodic function of time, there is no explicit limit imposed by this formalism on the number of rf cycles of disks employed. In the previously used thick disk model, three rf cycles of disks were employed.

Figure 3.4 illustrates the various steps required to perform the large-signal calculation. Firstly, the single cavity cell is analyzed. Assuming that one starts at the first cavity in the TWT, the input conditions are, the assumed input forward-wave, an initially assumed zero backward-wave (or some non-zero estimate if one is known) and the beam represented by electron disks with equi-spaced times of arrival. A first forward integration through the cell results in the calculation of two induced waves on this circuit. In order to satisfy the input condition (no backward-wave), a backward circuit wave must be assumed at the output which is just sufficient to cancel the induced backward-wave at the input. With this new set of initial conditions the forward integration through the first cell is repeated. The computed induced backward-wave must once more be cancelled by assuming a backward-wave at the output just sufficient to do so. After a small number of iterations, it will be found that negligible adjustment is required to satisfy the assumed zero backward-wave at the input. The solution is then said to be converged. The next cell can then be analyzed. The forward-wave and backward-wave at the input to this cell are known as is the condition of the beam at the entrance to this cell, the trajectories of the electron disks having been computed during the forward integration in the previous cell. A repetition of the computation procedure described above results in a converged solution for the second cavity. This procedure is repeated until the end of the circuit section.

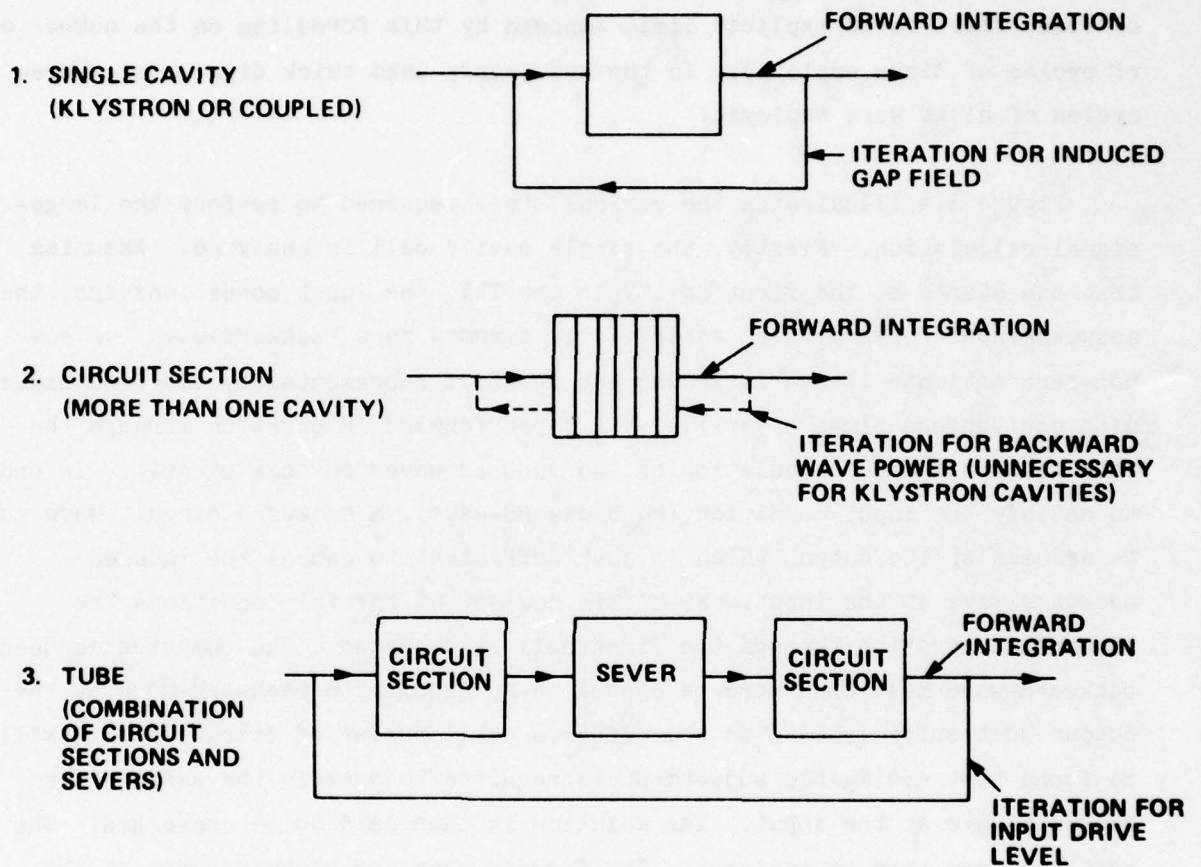


FIGURE 3.4. STEPS USED IN CARRYING OUT THE LARGE-SIGNAL, COUPLED-CAVITY COMPUTATIONS.

The first forward integration through a section results in a solution which has assumed zero backward-wave at the input and a computed forward-wave and backward-wave at the output. Application of the boundary condition at the output (sewer load reflection coefficient) provides a relationship between the forward-wave and backward-wave which must be satisfied. If, for example, the sewer load is perfectly matched, then a zero backward-wave must exist at the output of the section. To achieve this, a backward integration is performed beginning with zero at the output and adding all the induced backward-waves from the previous forward integration resulting in a new non-zero backward-wave estimate at the input. Repetition of the forward integration through the section will then produce an output backward-wave closer to the required value (zero). By continuing this procedure until there is a negligible change in the section iteration, one obtains a so-called converged section. The converged solution gives a fully consistent set of output values (backward-wave at the input, forward-wave at the sewer and velocity and phases of electron disks) for the given input wave and circuit match conditions.

Integration of the drifting beam through the sewer region provides the necessary input conditions for computation of the next circuit section. The circuit wave on a section which is driven by the beam is initially assumed to have zero forward-wave and zero backward-wave at the input end. A self-consistent solution for each section can be obtained in the same manner as was accomplished in the input section. Finally, the total large-signal solution is complete. Typically, it is necessary to compute the performance at a number of input drive levels in order to get a complete picture of tube performance from small-signal through saturation and into the overdriven region.

4.0 THE BUNCHING PROCESS

It seems intuitively obvious that, if the maximum energy is to be extracted from the beam, it must be bunched, as nearly as possible, into one single simple uniform tight bunch per rf cycle with the electrons in the bunch all travelling at, or near, the same velocity. This bunch must be either maintained during the slow extraction of power or one must contrive to quickly reduce the bunch velocity at the point of optimum bunching. In a coupled-cavity TWT, the gap impedance is typically not high enough to permit generation of gap fields strong enough to extract all the power in one gap, hence it is necessary to attempt to maintain the bunch so that the power may be extracted over a number of cavities. However, the quasi-static or adiabatic extraction of power is hampered by other phenomena which limit, in a relatively broad band device, the ability to simultaneously maintain all the necessary conditions to extract power from the bunch without destroying the very bunch characteristics required to be maintained. In any case, it is important to bear in mind we are interested only in solutions which have validity over a bandwidth of more than 10 percent.

In a slow space-charge wave, the bunch travels more slowly than the average velocity of the electrons. Interbunch electrons travel at relatively high speeds until they overtake the bunch and are slowed by space-charge forces. Electrons on the front of the bunch are expelled by space-charge forces and accelerate to become high speed interbunch electrons. Electrons are decelerated as they enter the bunch and accelerated as they leave; therefore, the velocity spread in the bunch is large. In a fast space-charge wave the bunch travels more rapidly than the average velocity of the electrons. The slow interbunch electrons are gathered up by the speeding bunch as electrons on the back of the bunch are expelled by space-charge forces. The slow space-charge wave tends to predominate in TWTs because it is this wave which grows as the beam gives up power to the circuit.

The electron velocity spread in beams with predominant excitation of the slow space-charge wave is large by the very nature of this beam wave. For the slow space-charge wave, the electrons at the highest density modulation (or rf beam current) have the lowest velocity. A high rf beam current therefore cannot be achieved without severe electron overtaking. As mentioned earlier, the velocity spread can be reduced by a simultaneous excitation of the fast space-charge wave. This is illustrated in Figure 4.1, where the peak velocity deviation at positions of maximum rf beam current in a modulated beam is plotted vs the ratio of amplitude of the fast and slow space-charge waves. The result shown in the figure is derived from small-signal space-charge wave theory. As shown in Figure 4.1, the velocity spread drops rapidly with the partial excitation of the fast space-charge wave, and is reduced by, for example, a factor of 4 for a ratio of A_F/A_S of 0.6.

The plan for this research was to begin by investigating means for producing well formed bunches or at least to attempt to begin the bunching process with minimum velocity spread so as to provide the best possible bunches for optimum power extraction.

The Varian VTS-5753 coupled cavity TWT is the basis for computer emulation carried in this research. This TWT satisfies all the requirements of the present program except for the conversion efficiency specification. In addition, the VTS-5753 exceeds the power requirement of the present study with the promise that significant reduction of the beam current might be possible without major modification of circuit parameters, thereby providing a vehicle for comparing results as a function of beam perveance over a wide range of perveances.

Figure 4.2 is the brillouin diagram for the circuit employed in the VTS-5753. The Curnow equivalent circuit is shown in the inset. It is this equivalent circuit, derived from cold-test measurements, which is used in the small-signal and large-signal computer programs throughout most of this report.

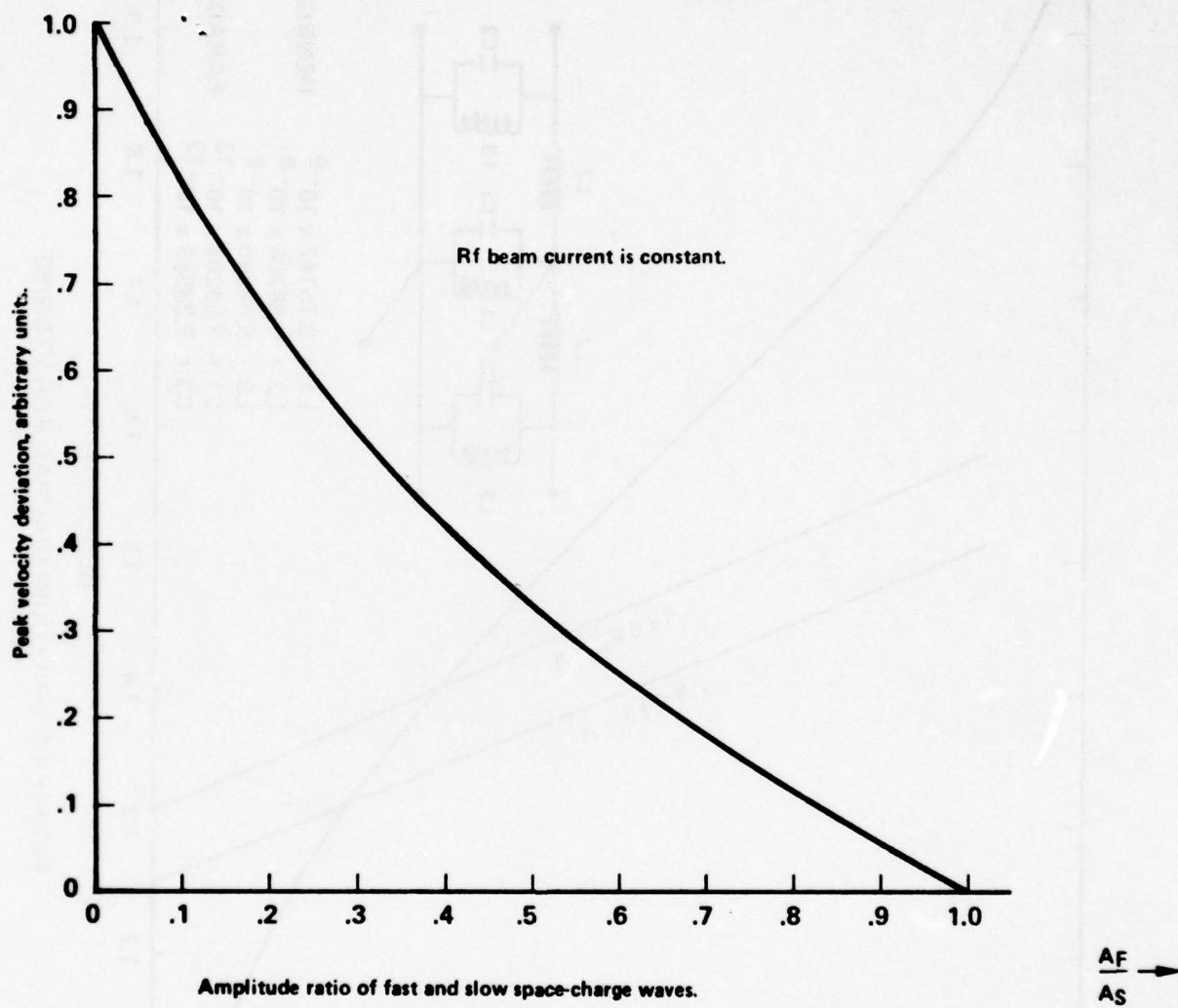


Figure 4.1 Peak velocity spread at maximum rf beam current vs the relative excitation of the fast and slow space-charge waves.

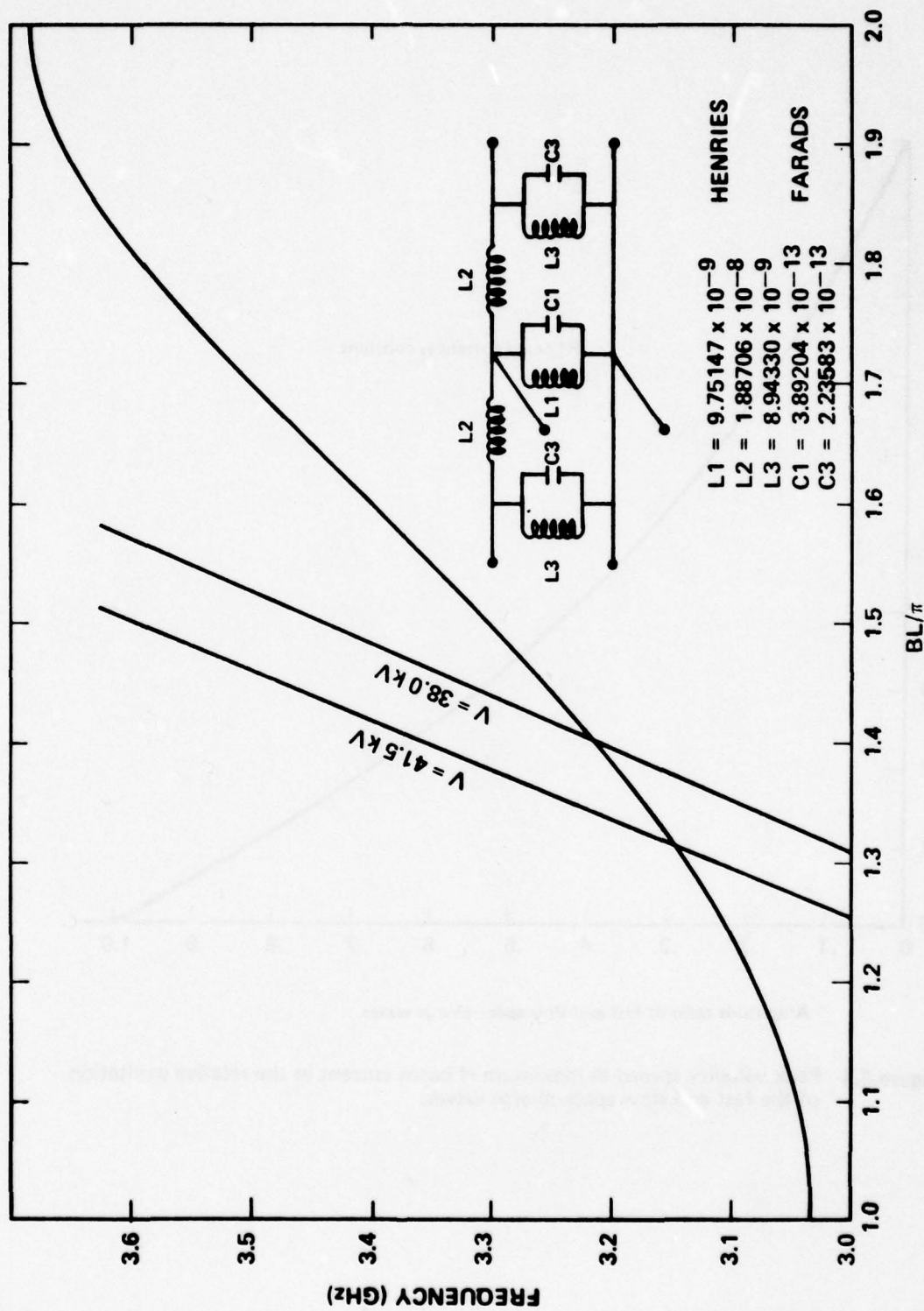


FIGURE 4.2 BRILLOUIN DIAGRAM FOR VTS-5753

Test data for a typical VTS-5753 are shown in Figure 4.3. The heavy curve shows the output power at a constant drive power of one watt. The three lighter curves correspond to successive drive reductions of 1 dB each. No data are presented for frequencies above 3.5 GHz because of the presence of a "ghost mode" in the output window. Other versions of this window have been built, however, which can be operated over the full 3.1 to 3.6 GHz band. The maximum conversion efficiency exhibited by this TWT with these operating parameters is 26 percent.

Figures 4.4 and 4.5 illustrate the formats employed for plotting some of the important parameters output by the large-signal computer program.

Figure 4.4 shows the rf beam current and cavity gap voltages as a function of distance along the circuit. The figure in this particular example covers the last 13 cavities of the circuit -- the portion in which most of the interesting behavior occurs. The lower-most (stepped) curve shows gap voltage normalized to the beam voltage. The length of each step is equal to the length of the cavity. The fact that the steps do not increase monotonically illustrates the significant contribution of the backward-wave in coupled-cavity TWTs. The upper two curves represent normalized fundamental and second-harmonic components of rf convection current in the beam. The rf current is normalized with respect to the dc beam current. In this example, saturation is occurring, as evidenced by the leveling off of the convection currents. Throughout the present report these figures will be referred to as amplitude charts.

Figure 4.5 is a modified Applegate diagram; a plot of normalized electron phase vs distance. In the large-signal analysis of a TWT, the electron beam is modeled as a set of charged disks -- in this case, 32 disks per rf cycle -- which are injected into the tube at $Z = 0$, equispaced in time. The ordinate in Figure 4.5 can be thought of as showing the normalized time of arrival of the electron disks at each position along the circuit. This figure differs from an Applegate diagram in that an unperturbed disk, traveling at the dc beam

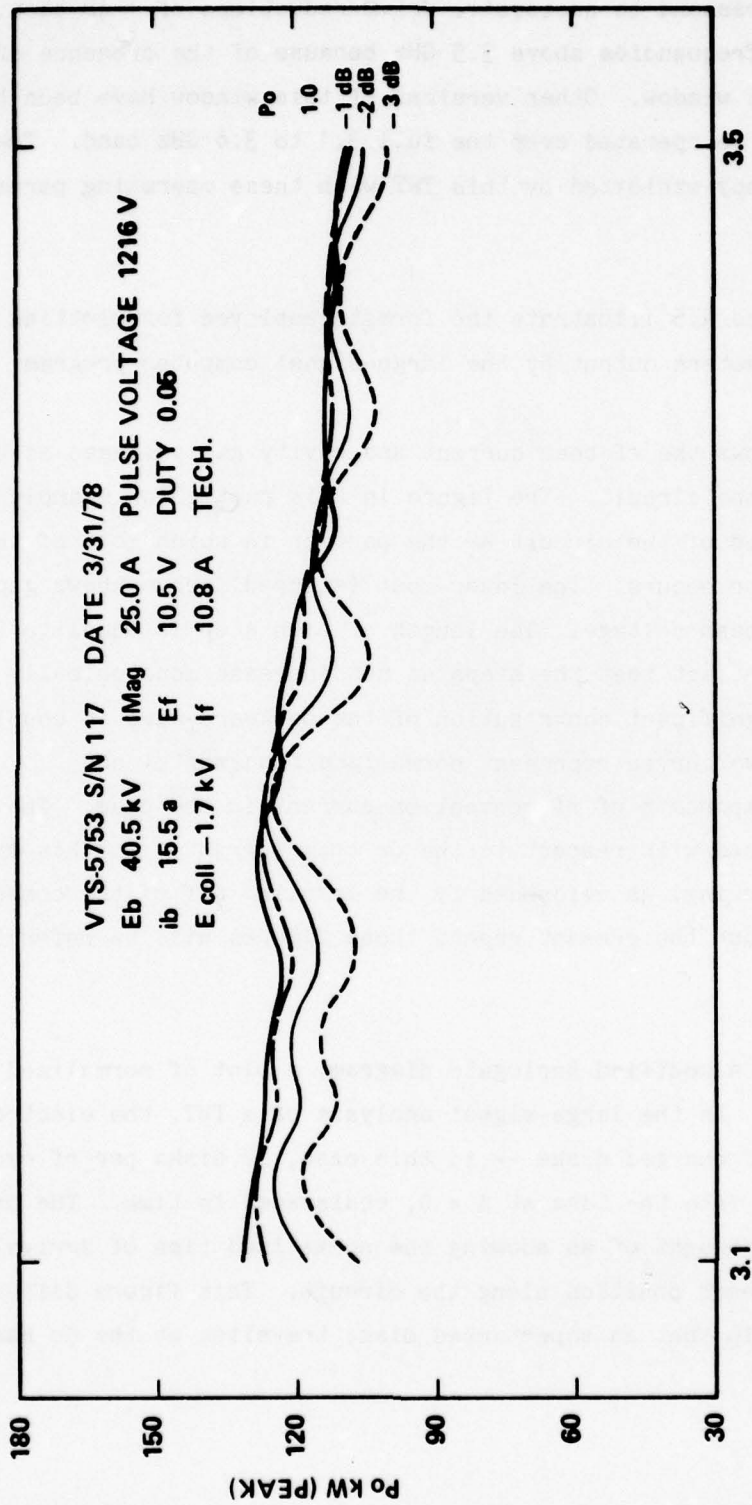


FIGURE 4.3 PEAK POWER VS FREQUENCY FOR VTS-5753 S/N 117

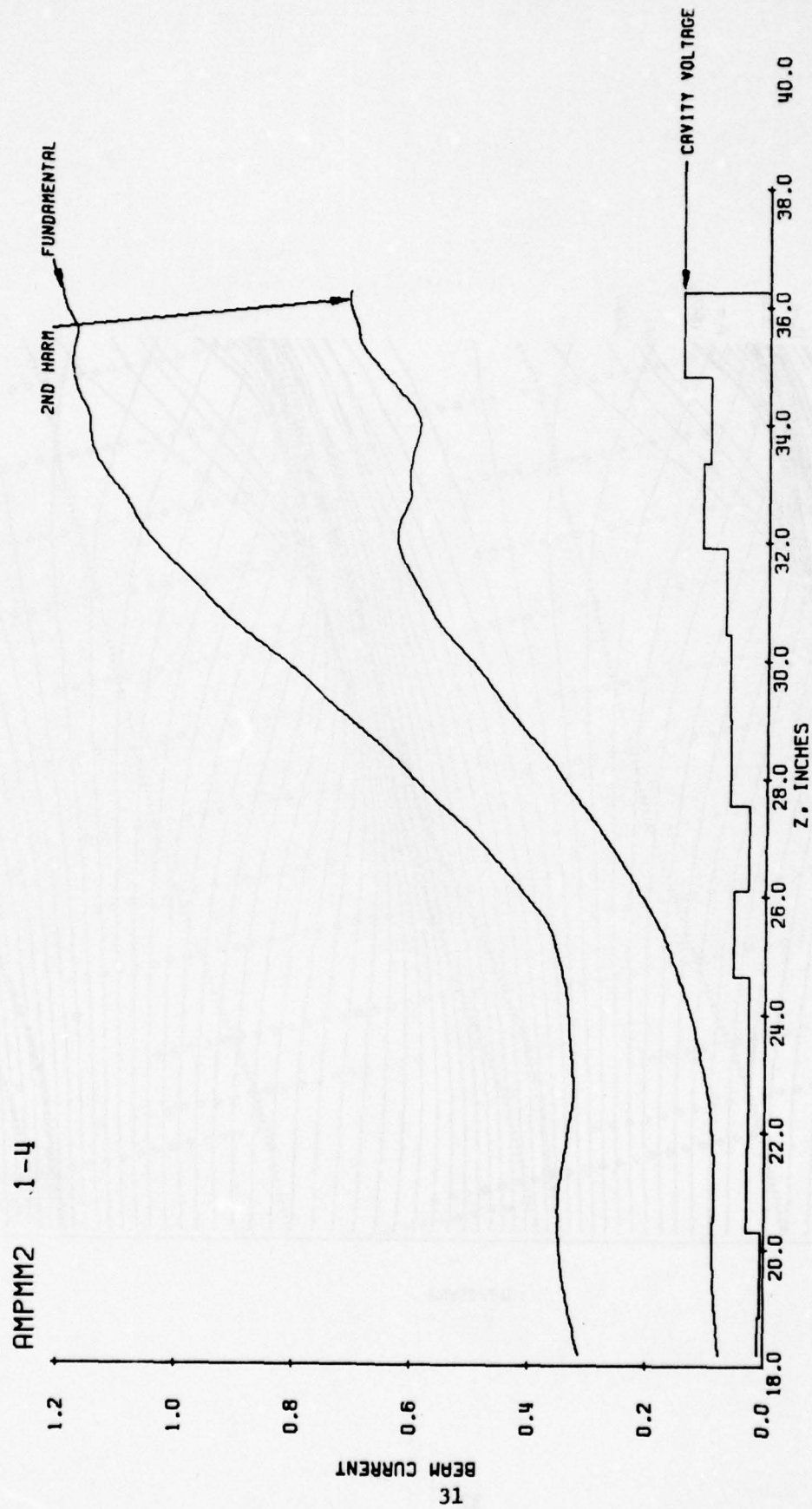


FIGURE 4.4 PLOTTING FORMAT FOR LARGE-SIGNAL COMPUTER PROGRAM

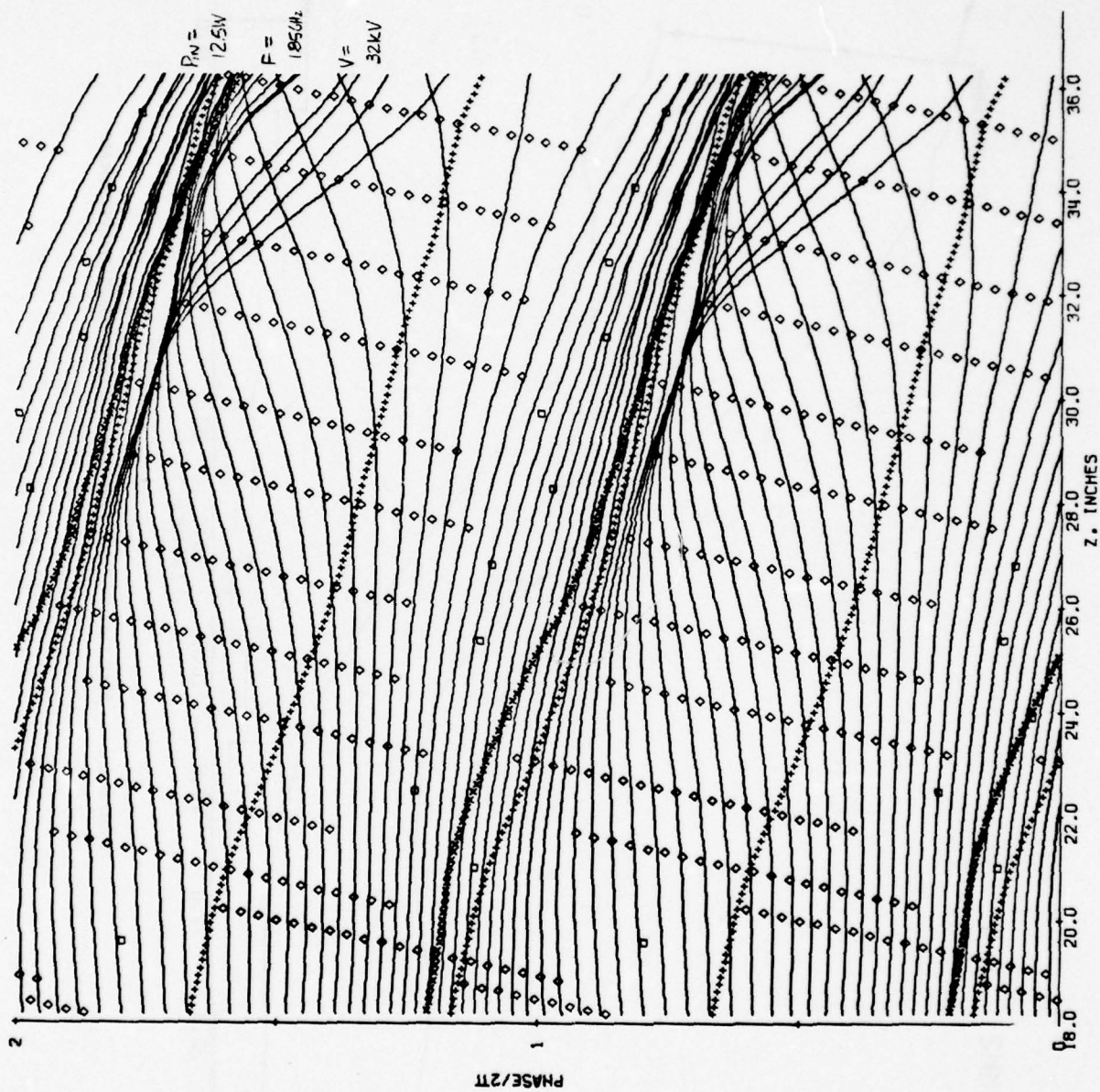


FIGURE 4.5 PLOTTING FORMAT FOR LARGE-SIGNAL COMPUTER PROGRAM

velocity, moves along a horizontal trajectory rather than an oblique one; that is, the ordinate here represents the entry time of the electron disk plus or minus the difference in time of flight relative to an unmodulated disk traveling at the dc beam velocity. This diagram differs further from an Applegate diagram in that the ordinate represents time of arrival with time increasing downward. An electron moving slower than the dc beam velocity will have a downward sloping trajectory while fast electrons are represented by upward sloping trajectories. Finally, the pattern is repeated (vertically) over two rf cycles to improve its readability. These plots will be referred to as phase diagrams.

The following comments are presented as a guide to interpreting the phase diagram: the solid curves, which are approximately equispaced and horizontal at the left side of the diagram, represent the thirty-two electron disks which, in this example, model the beam. The pattern is repeated twice vertically, i.e., there are 64 electron disks over two rf cycles. The curves traced by "X" symbols indicate the phase of the fundamental component of rf convection current in the beam. Phase is defined so that "X" corresponds to the maximum of electron current, or the center of the electron bunch. The doubly numerous curves traced by the "+" symbols indicate the phase of the second-harmonic component of rf convection current. In ideally symmetrical bunching, alternate curves marked by "+" would be coincident with an "X" curve and the remaining "+" curves would lie exactly midway between the zero-phase curves for the fundamental component.

The oblique rows of diamond symbols indicate the phase of the rf circuit fields within the cavities. For each integration step in Z, a diamond is printed at the ordinate corresponding to the maximum accelerating phase. The slope of a line joining such points corresponds to infinite electron velocity, i.e., an electron moving at infinite velocity would sample rf fields of constant phase in any cavity.

The small square is used to indicate the maximum decelerating rf cavity field at the center of each gap. This helps in visualizing the axial positions of the cavities and keep track of those electron disks which are giving up energy to the rf fields.

Since time is increasing downward, the front of the bunch is located just above an "X" and the rear of the bunch just below. The bunch develops because the electrons at the front of the bunch encounter a retarding field while those behind the bunch encounter accelerating fields. To obtain good bunching, it is desirable to have the rf fields in phase quadrature with the bunch phase, i.e., the small square should be approximately midway between the curve traced by "X" symbols and the curve above it traced by "+" symbols.

Analysis of bunching performance has been carried out by computer simulation of an S-band TWT composed of two identical sections of nine cavities, each separated by a sever drift-space equal to the length of one cavity. The sever matches, as well as the input and output matches, are assumed to be perfect cold matches. All cavities are assumed to be identical, having the same impedance, loss and physical dimensions. This buncher design is purposely primitive in order to facilitate the study of the effect of the controllable tube parameters on bunching.

Figure 4.2 is the brillouin diagram for the coupled-cavity slow-wave circuit which is simulated in the experiments reported here. Velocity lines corresponding to the two different beam voltages employed are plotted, and the operating frequency, 3.350 GHz, is marked.

The controllable parameters investigated are beam voltage, circuit loss, ratio of beam to tunnel radius (B/A), and ratio of magnetic focusing field to brillouin field strength (B/BBR).

Figures 4.6 and 4.7 show the computed currents and gap field voltages and the electron phase trajectories respectively for a simulated TWT buncher operating with all parameters at their nominal or par values. This simulation will be used as a standard against which other buncher designs may be measured. Figure 4.6 shows the fundamental and second harmonic components of rf convection current plotted vs distance in inches. The step-like curve represents the rf gap voltages; these are labeled with the appropriate cavity numbers. The first seven cavities are omitted because the very small-signal behavior is of little interest. The space between cavities 9 and 10 represents the sever. The drive level has been chosen to produce the onset of electron overtaking at or near the output cavity, since in general the quality of the bunch can be expected to deteriorate once significant overtaking has occurred. Two factors stand out in this figure:

1. The fundamental current dips significantly just beyond the sever and reaches a minimum in cavity 12.
2. The gap fields do not increase monotonically with gap number. This behavior implies that the backward-wave is relatively strong and it is interfering destructively with the forward-wave, particularly in cavities 12 and 14. The bunching process can hardly be aided by having gaps with low voltages. Consideration must be given to correcting this defect.

Figure 4.7 shows the computed electron trajectories for the same case as illustrated in Figure 4.6. The bumps on the curves which show the phases of the fundamental ("X") and harmonic ("+") current correspond to the dip in magnitude of fundamental current which occurs after the sever in the previous figure. Both the phase of the bunch and the magnitude of the fundamental current are adversely affected, apparently by the sever. The small square boxes mark the phase at which the gap field retardation is maximum. Optimum bunching occurs when the electrons on the front of the bunch are decelerated and the electrons behind the bunch are accelerated. This condition is

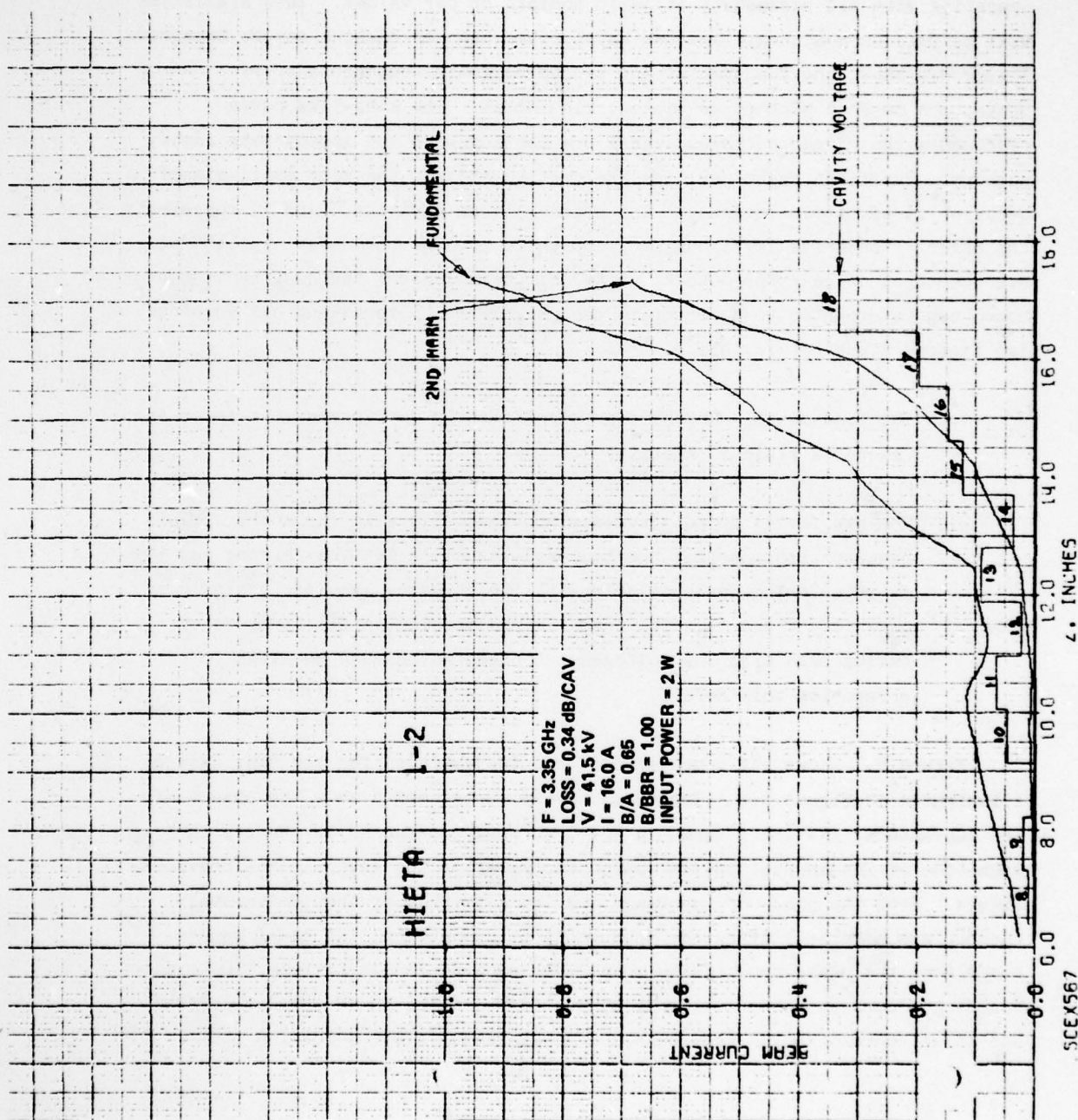


FIGURE 4.6 COMPUTED RF BEAM CURRENTS AND GAP VOLTAGES VS DISTANCE IN SIMULATED COUPLED-CAVITY TWT WITH NINE CAVITIES IN EACH SECTION

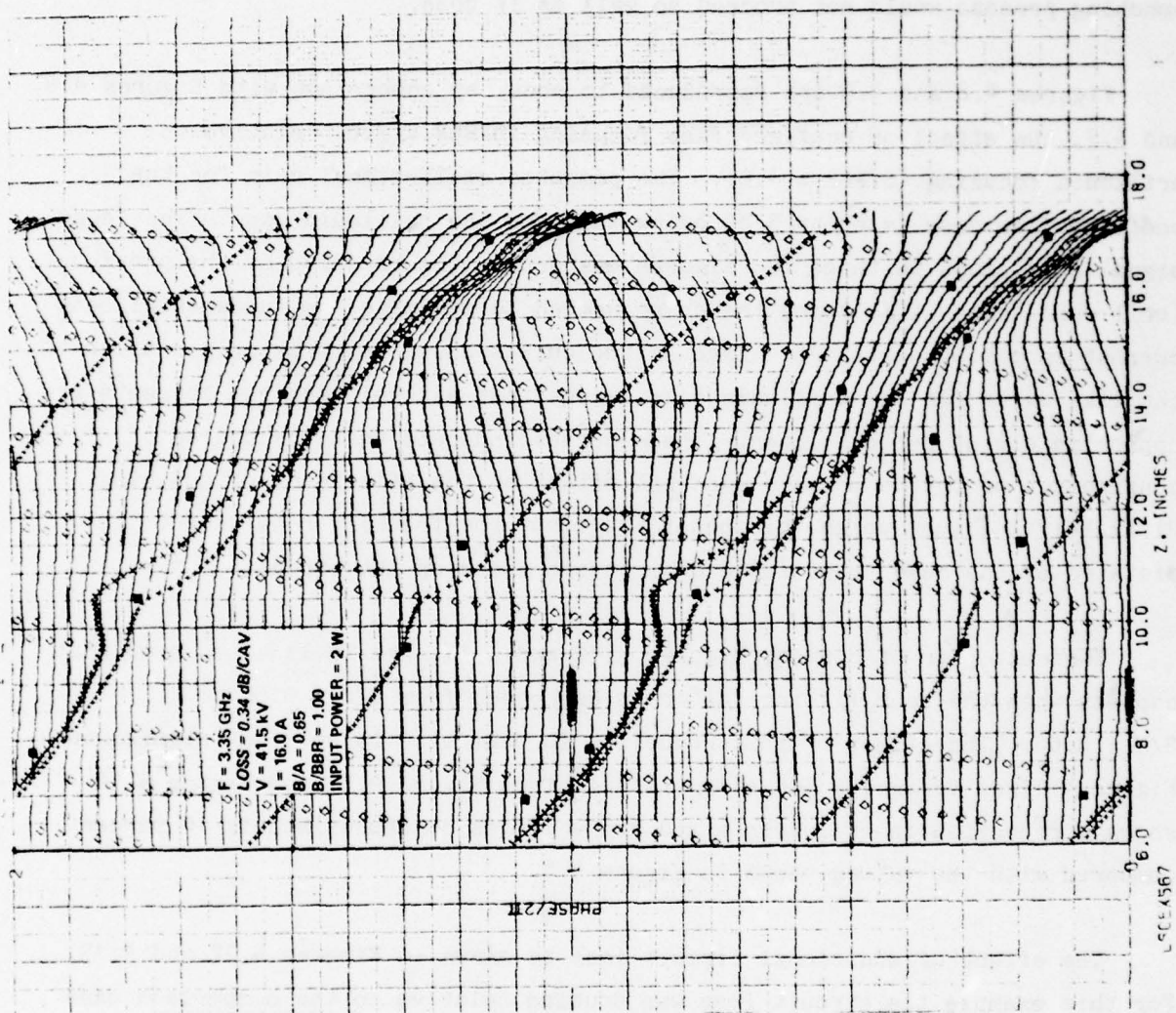


FIGURE 4.7 COMPUTED RELATIVE PHASES OF ELECTRON DISKS VS DISTANCE IN SIMULATED COUPLED-CAVITY TWT WITH NINE CAVITIES IN EACH SECTION

optimized when the marker is $2 \frac{1}{2}$ divisions (or 90°) above the bunch ("X" curve). For maximum energy extraction the small square boxes should coincide with the "X's." In Figure 4.7 the maximum retarding field in cavities 10, 12 and 14 is behind the bunch, hence debunching can be expected. Perhaps it is fortunate that these fields are weak, as shown in Figure 4.6, otherwise the bunching process would not proceed so well as it does.

Figures 4.8 and 4.9 are reproduced to show, by comparison with Figures 4.6 and 4.7, the effect of confined flow focusing ($B/BBR = 3.0$) relative to brillouin focusing ($B/BBR = 1.0$). The computed small-signal gain for the confined flow case is about 5 dB below that for the brillouin case. The large-signal case shown in these two figures has double the rf drive of the previous (brillouin) case, this being the drive needed to maximize the fundamental beam current in cavity number 18. Each of the curves shown is strikingly similar to the like curve for the brillouin case except that all voltages and currents are approximately 30 percent lower. These curves indicate that the degree of confinement of the beam has a material effect on the efficiency of bunching. Ultimately one must weigh this benefit against the focusing requirements dictated by the need to minimize beam interception on the circuit.

The next pair of curves, Figures 4.10 and 4.11, are included to show what happens when the beam filling factor is decreased from $B/A = 0.65$ to $B/A = 0.60$. The effect of this reduction in beam size is not very significant. Figure 4.11 is virtually indistinguishable from Figure 4.7, and Figure 4.10 shows a reduction in rf currents and gap voltages of approximately 10 percent compared with the values shown in Figure 4.6.

The effect of additional circuit loss is shown in Figures 4.12 and 4.13. For this example the circuit loss was doubled relative to the comparison case shown in Figures 4.6 and 4.7. Even though the loss has been increased by more

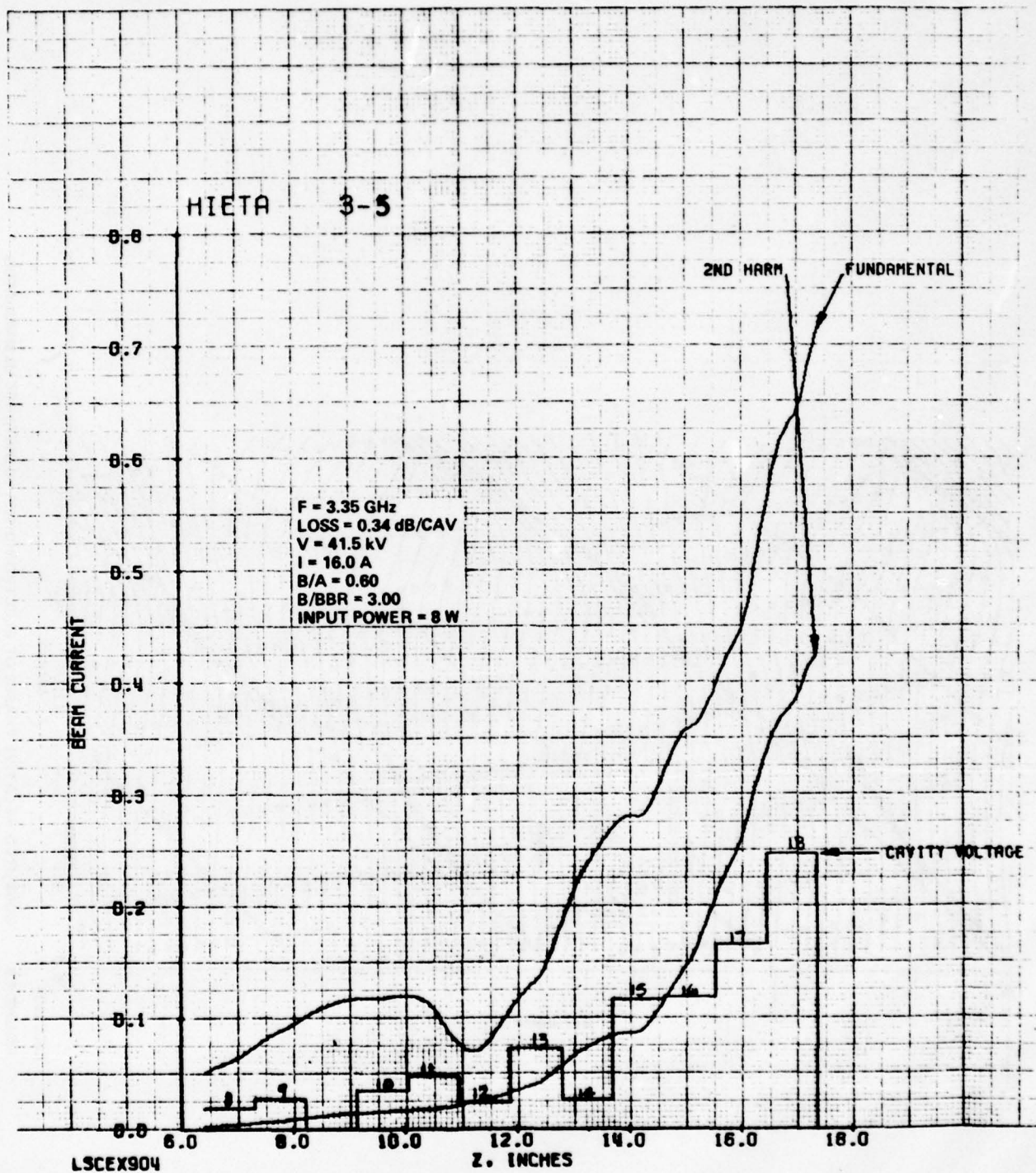


FIGURE 4.8 COMPUTED RF BEAM CURRENTS AND GAP VOLTAGES VS DISTANCE IN SIMULATED COUPLED-CAVITY TWT WITH NINE CAVITIES IN EACH SECTION

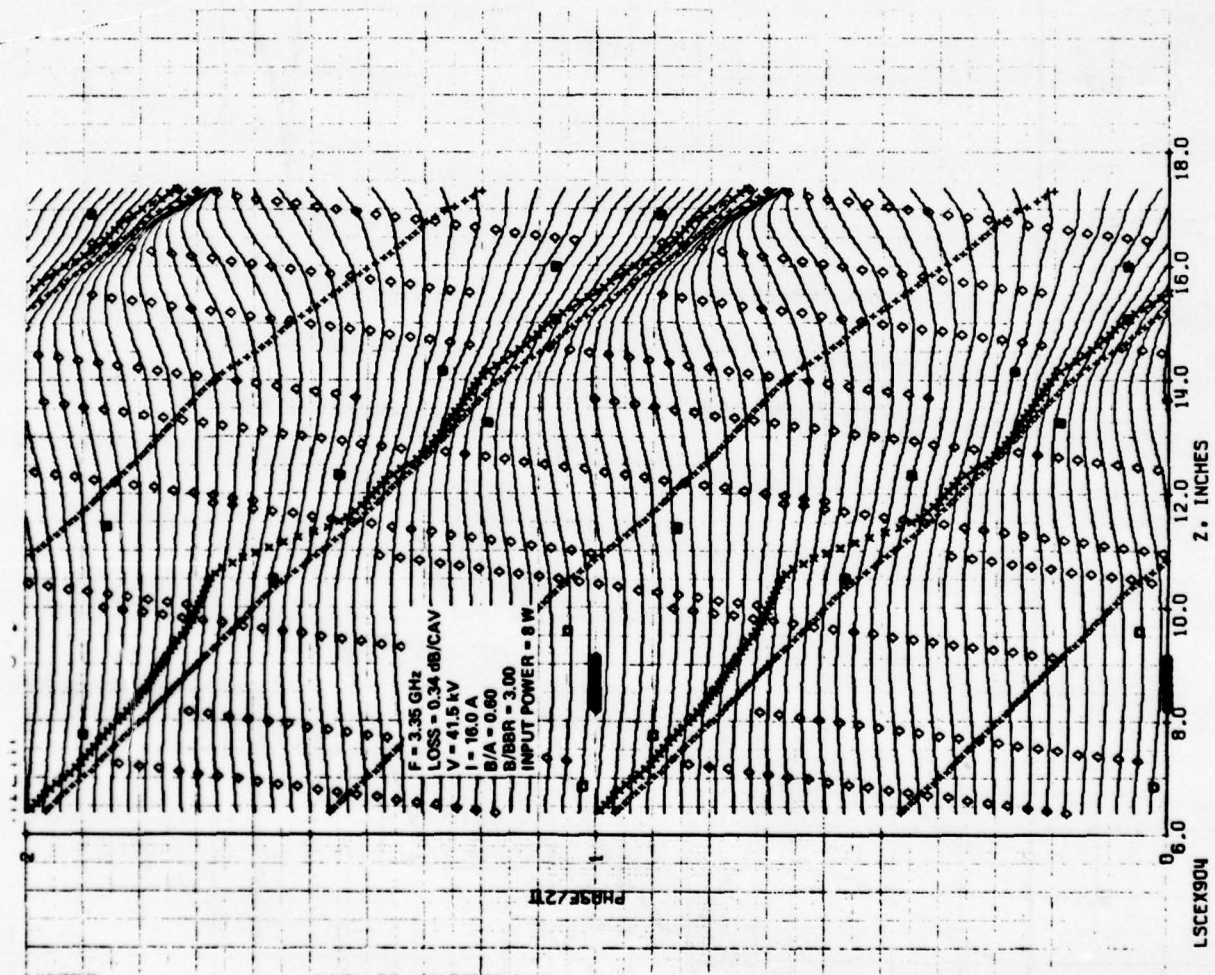


FIGURE 4.9 COMPUTED RELATIVE PHASES OF ELECTRON DISKS VS DISTANCE IN SIMULATED COUPLED-CAVITY TWT WITH NINE CAVITIES IN EACH SECTION

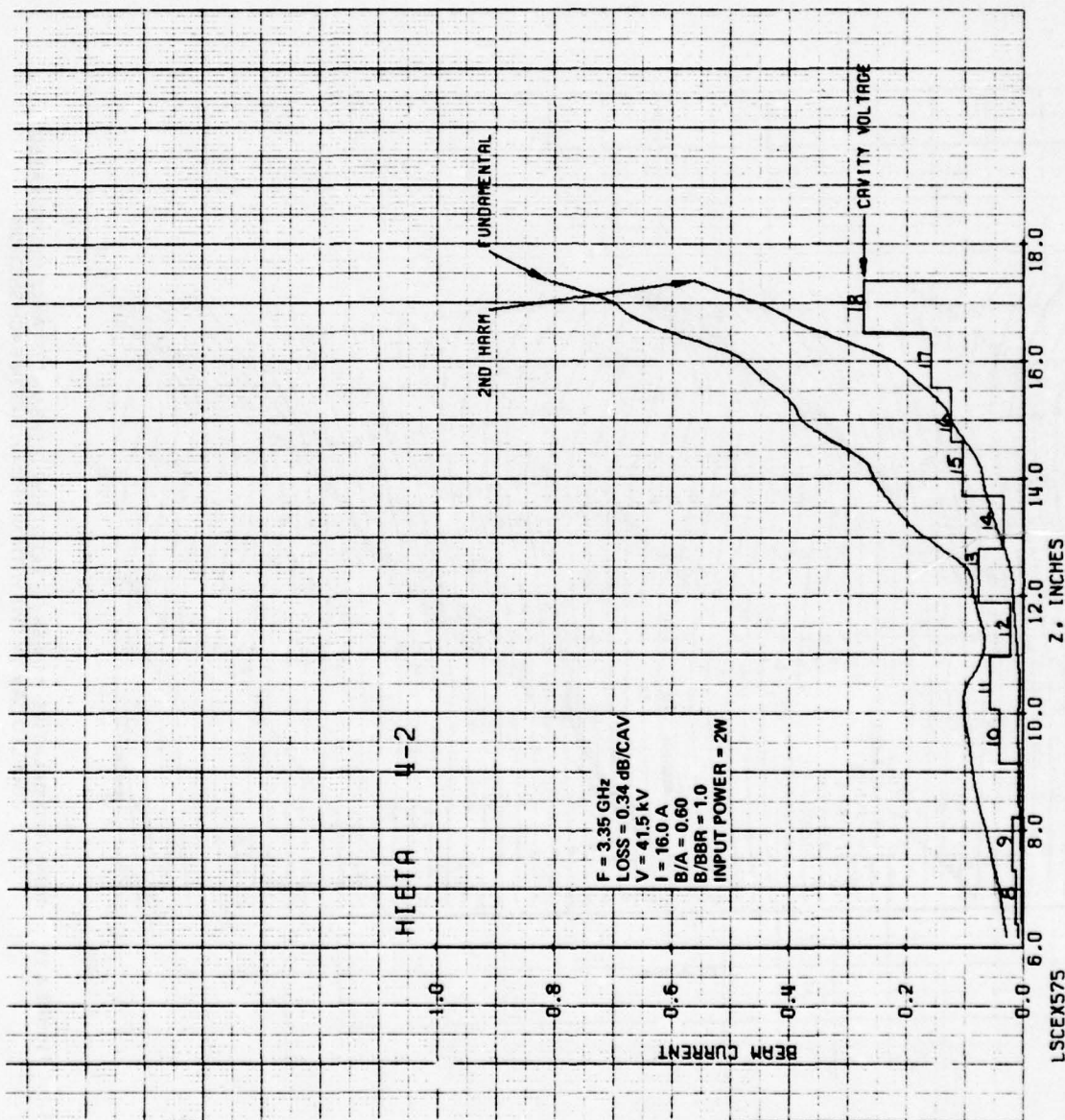


FIGURE 4.10 COMPUTED RF BEAM CURRENTS AND GAP VOLTAGES VS DISTANCE IN SIMULATED COUPLED-CAVITY TWT WITH NINE CAVITIES IN EACH SECTION

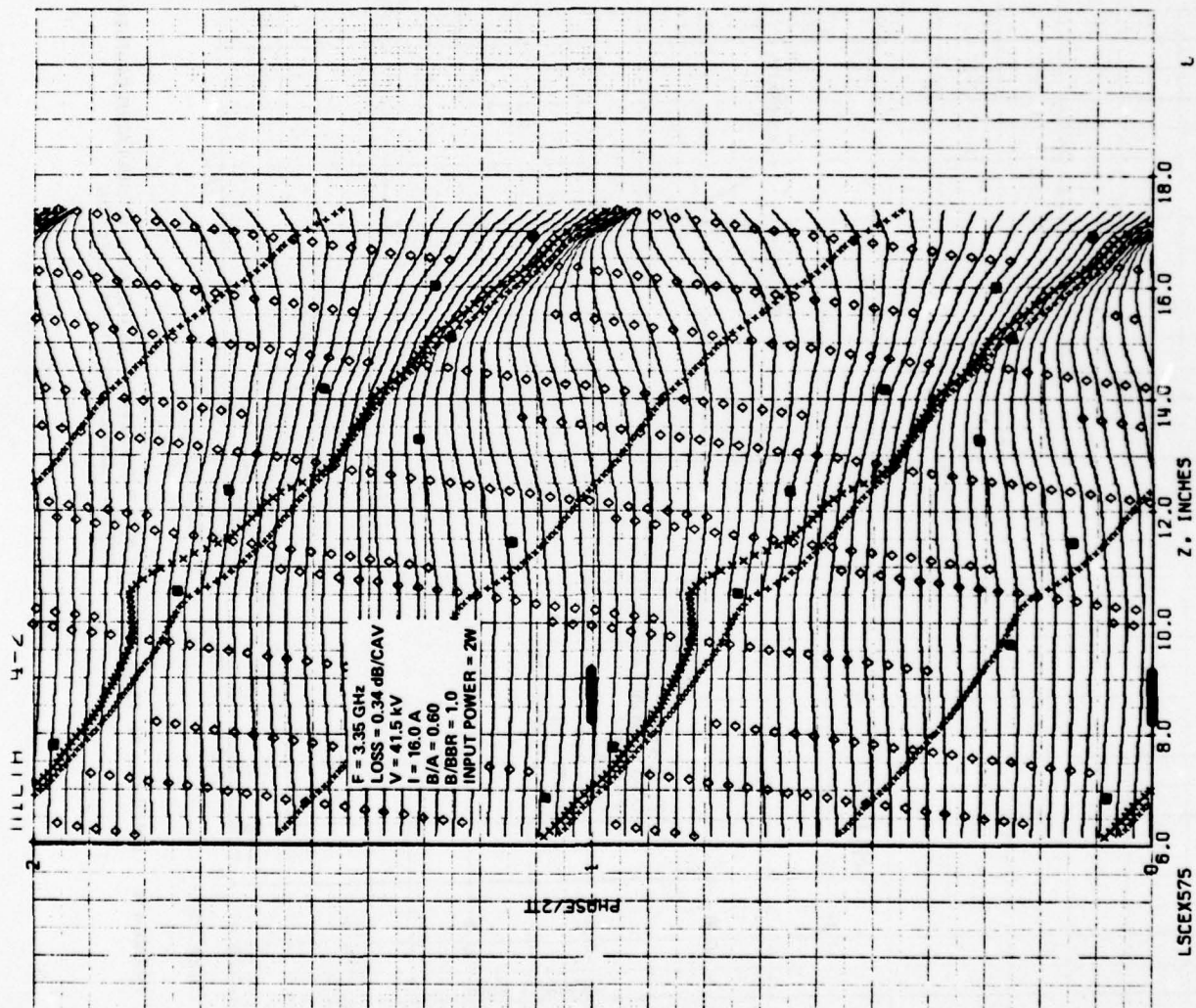


FIGURE 4.11 COMPUTED RELATIVE PHASES OF ELECTRON DISKS VS DISTANCE IN SIMULATED COUPLED-CAVITY TWT WITH NINE CAVITIES IN EACH SECTION

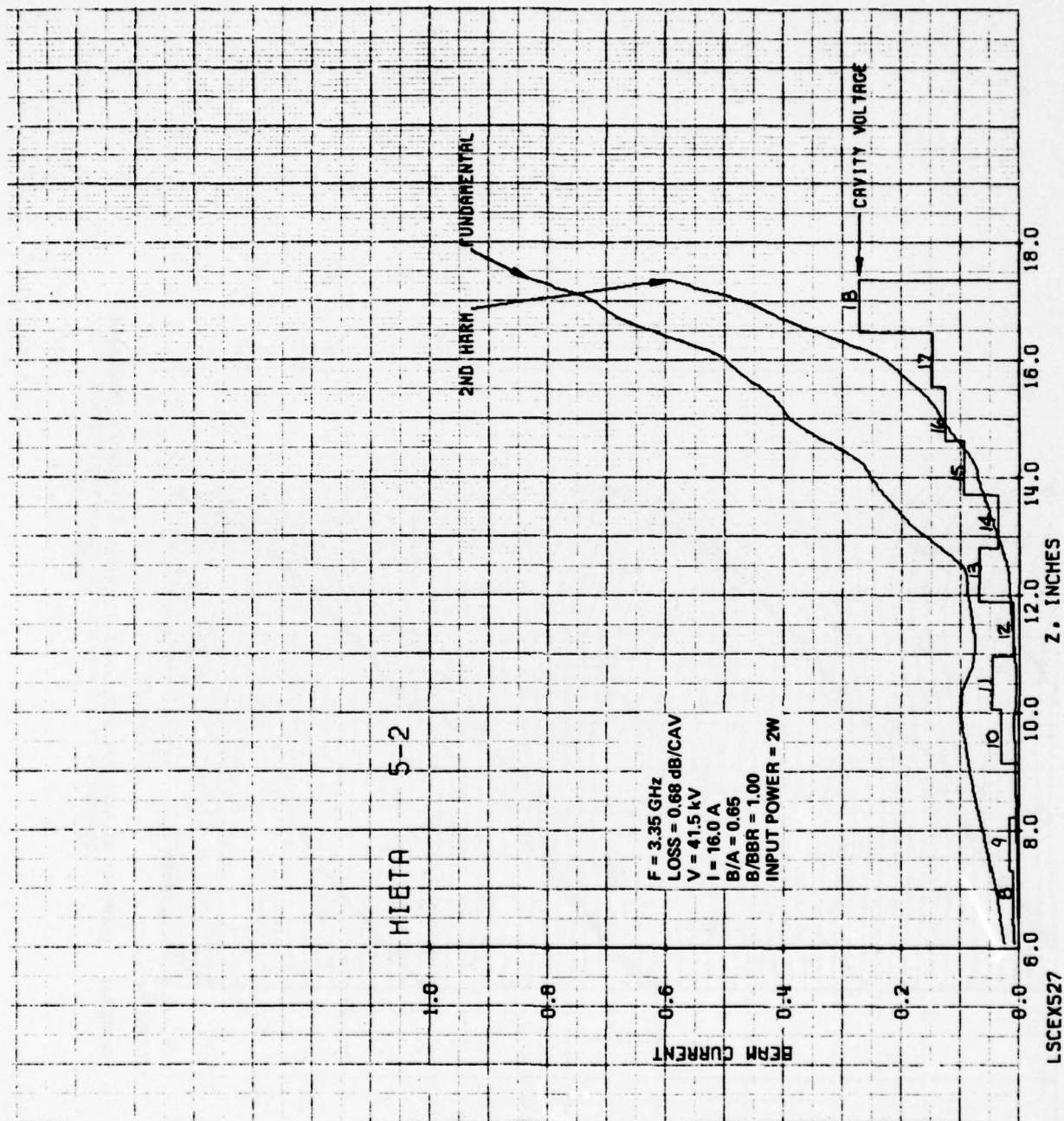


FIGURE 4.12 COMPUTED RF BEAM CURRENTS AND GAP VOLTAGES VS DISTANCE IN SIMULATED COUPLED-CAVITY TWT WITH NINE CAVITIES IN EACH SECTION

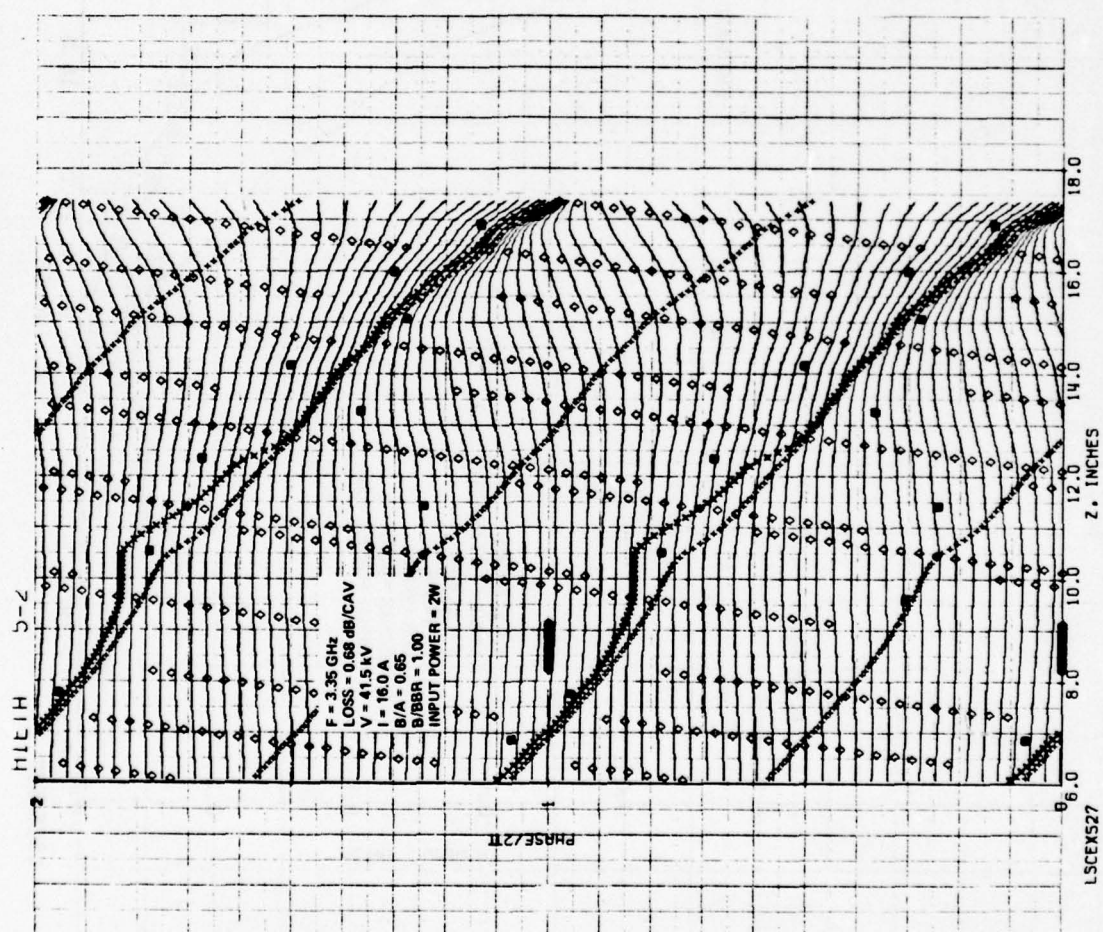


FIGURE 4.13 COMPUTED RELATIVE PHASES OF ELECTRON DISKS VS DISTANCE IN SIMULATED COUPLED-CAVITY TWT WITH NINE CAVITIES IN EACH SECTION

than 3 dB per circuit section, there is no appreciable effect on bunching. Since circuit loss is essential for stability, it is useful to know that reasonable levels of loss can be employed without ruinous effect on beam bunching.

Figures 4.14 and 4.15 illustrate the effect of synchronism between beam and circuit wave. In these two figures the Pierce velocity parameter b has been reduced to 0.50 relative to a value of 0.93 for the comparison case illustrated in Figures 4.6 and 4.7. The reduction in b was achieved by reducing the beam voltage to 38 kV from a nominal value of 41.5 kV. The overall effect of reducing b appears to be almost insignificant, with an increase in fundamental component of rf convection current of about 2 percent. However, the phases of the gap voltages, with the exception of that in cavity number 11, lie more nearly where they should be for optimum bunching and, in fact, the bunching proceeds more quickly than in the former case right up to the beginning of the 18th cavity. At this point overtaking begins to occur and the rf beam currents begin to saturate. The circuit velocity in the last few cavities appears to be too low to achieve optimum bunching, i.e., the bunch sees retarding fields rather than bunching fields.

In Varian Technical Proposal PAMTD 77-11462 in response to RFQ F30602-77-R-0333, several design concepts for improvement of conversion efficiency are discussed. One of these concepts is the notion that the electron velocity spread in a beam with predominant excitation of the slow space-charge wave is large by the very nature of this beam wave. For the slow space-charge wave, the electrons at the highest density modulation have the lowest velocity. A high rf beam current cannot, therefore, be achieved without severe electron overtaking. This velocity spread can be reduced by simultaneous excitation of the fast space-charge wave.

One method of increasing the fast space-charge wave excitation is to increase the positive beam loading in the interaction gaps by using long interaction gaps. Another method of increasing the fast space-charge wave

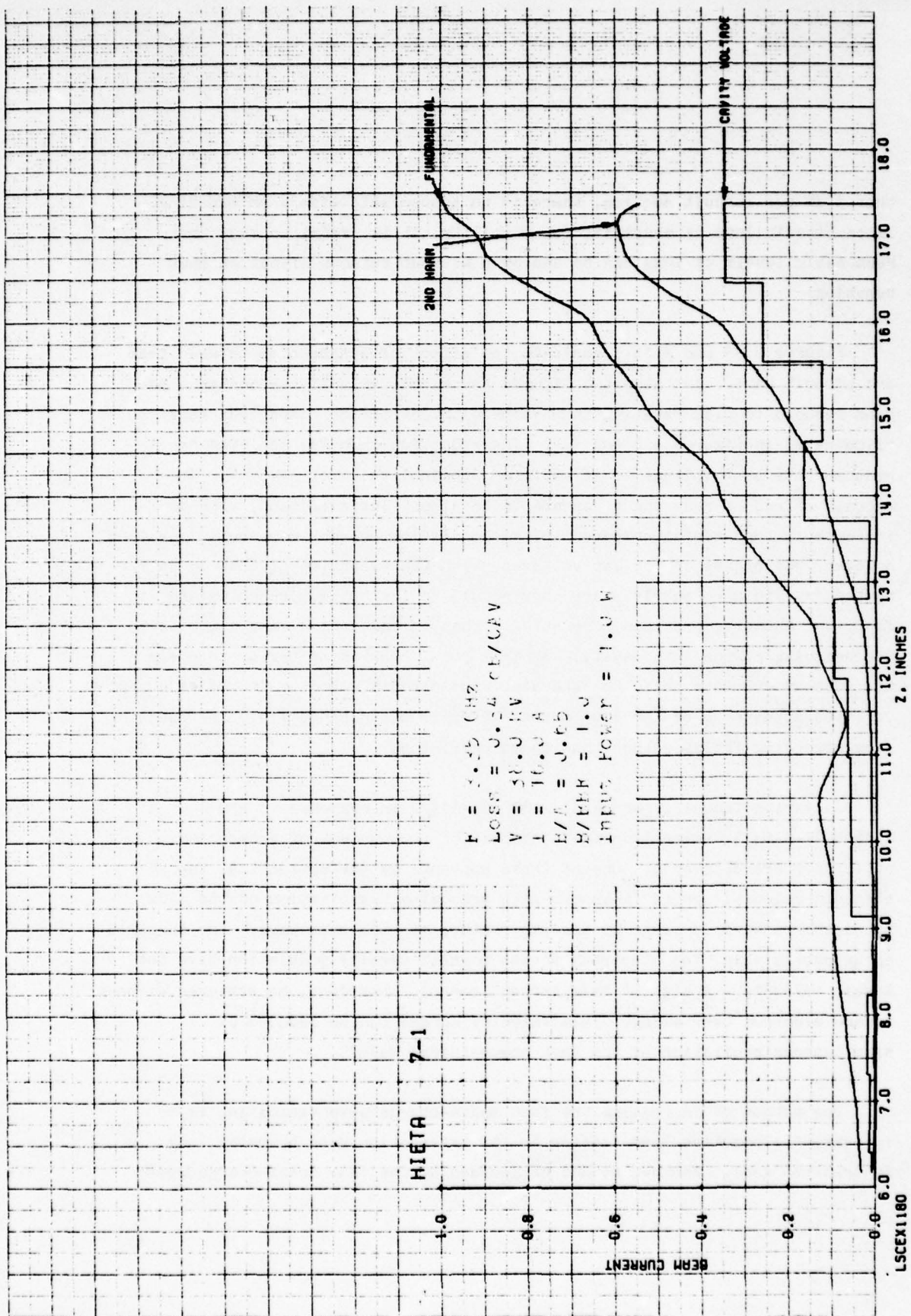


FIGURE 4.14 COMPUTED RF BEAM CURRENTS AND GAP VOLTAGES VS DISTANCE IN SIMULATED COUPLED-CAVITY TWT WITH NINE CAVITIES IN EACH SECTION

HIETA 7-1

$f = 3.35 \text{ GHz}$
 $\text{Loss} = 0.34 \text{ dB/CAV}$
 $V = 38.0 \text{ kV}$
 $I = 16.0 \text{ A}$
 $B/A = 0.65$
 $B/\text{EBK} = 1.0$
 $\text{Input Power} = 1.0 \text{ W}$

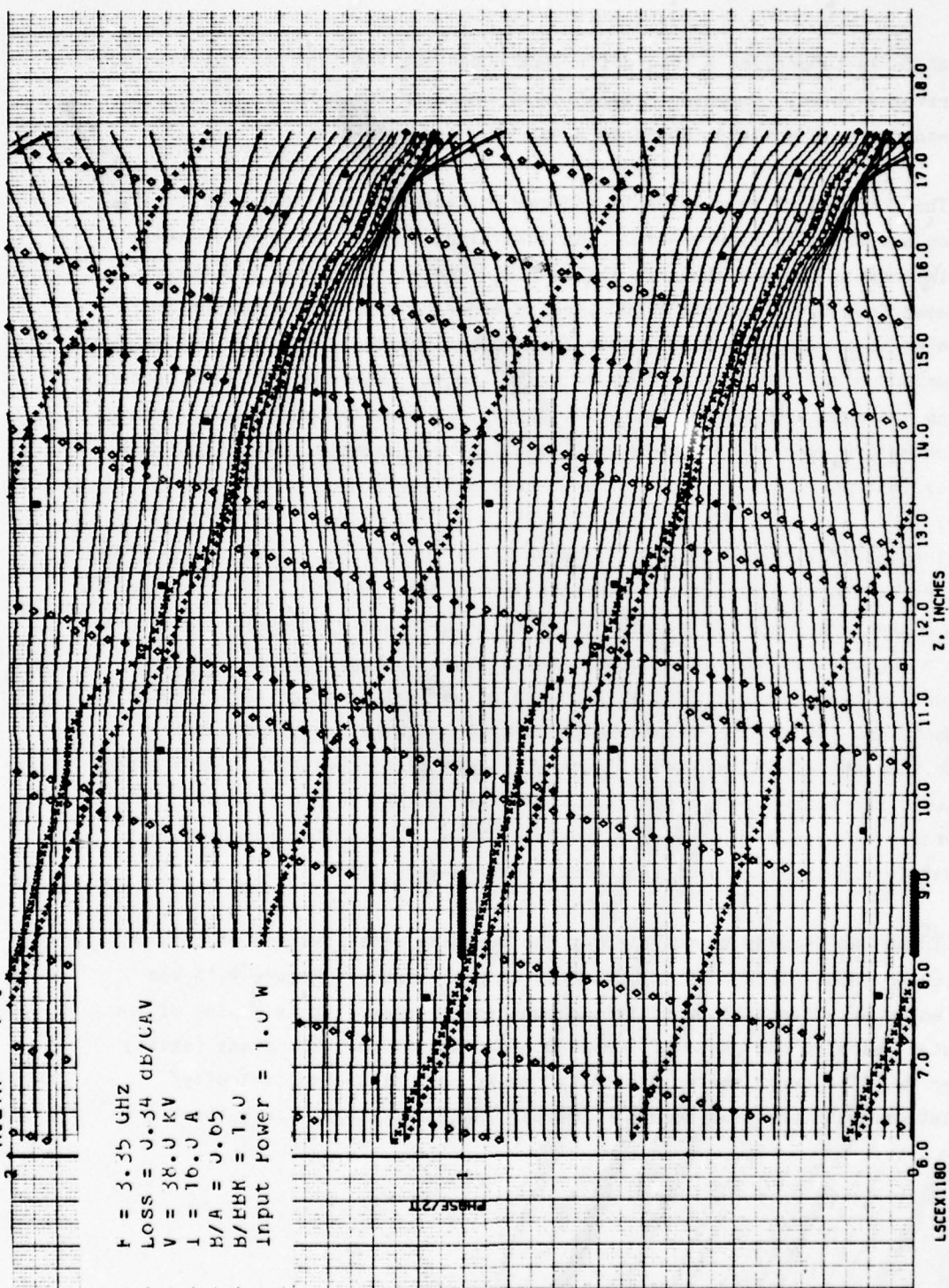


FIGURE 4.15 COMPUTED RELATIVE PHASES OF ELECTRON DISKS VS DISTANCE IN SIMULATED COUPLED-CAVITY TWT WITH NINE CAVITIES IN EACH SECTION

excitation is to provide a long drift length between the last two cavities of the driver section. Computer simulation of bunching for both the above fast space-charge wave enhancement schemes has been accomplished.

The computed rf beam currents and gap voltages for a nine-cavity input section are shown in Figure 4.16. The equivalent circuit employed in these calculations is the one shown in Figure 4.2. The cavity period has been increased from 0.914 inch to 1.000 inch in order to lower the synchronism parameter to a value $B = 0.095$, near synchronism, which is a better choice for optimum bunching. The gap spacing is 0.300 inches. The computed beam currents and gap voltages are much as one would expect. The gap voltages do not grow monotonically, even in this relatively small-signal example, due to backward-wave excitation.

The phase diagram Figure 4.17, shows an anomalous jump in the phase of the fundamental and second harmonic currents in the first cavity. This artifact is of no consequence since it simply reflects the difficulty of making an accurate calculation of the phase of a current which is vanishingly small. The gap voltages in the second and fourth gaps exhibit anomalous phase as indicated by the fact that the maximum retarding field (small square) points are below rather than above the fundamental current (curve marked by "Xs"). This effect is due to the backward-wave and illustrates once more the significant difference between coupled-cavity and helix TWTs. The latter can usually be adequately simulated without including backward-wave effects.

These two figures do not display the bunching effectiveness of this particular input circuit in any dramatic or obvious way. Figure 4.18 was plotted in an attempt to quantify the bunching process. It is a plot of the computed velocity and phase of the electron disks at the exit plane (cavity number 9). The curve marked "velocity" shows near sinusoidal velocity modulation, with the peak somewhat sharper than the trough, i.e., there are

$F = 3.35 \text{ GHz}$
 $L_{\text{loss}} = 0.34 \text{ dB/CAV}$
 $V = 41.5 \text{ kV}$
 $I = 16.0 \text{ A}$
 $E/A = 0.65$
 $B/EER = 1.0$
 $\text{Gap Length} = 0.20''$
 $\text{Input Power} = 4.0 \text{ W}$

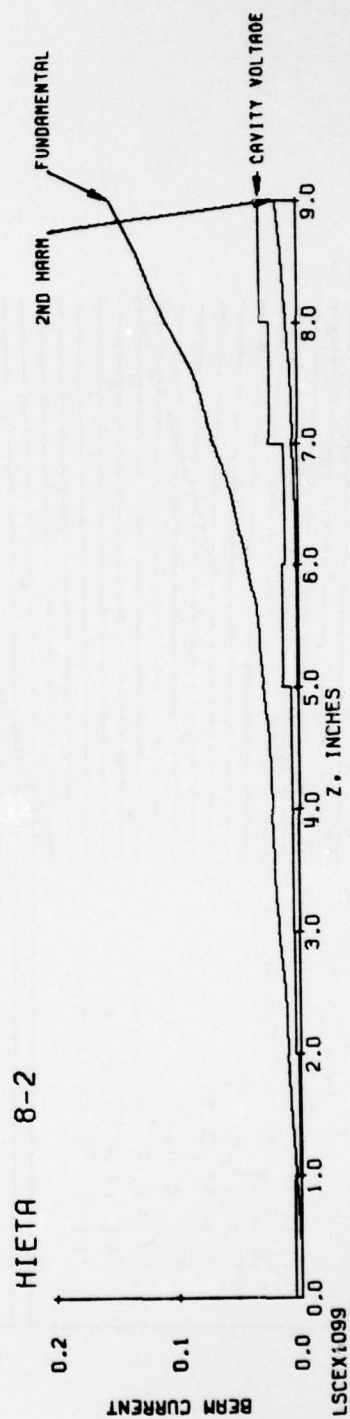


FIGURE 4.16 COMPUTED RF BEAM CURRENTS AND GAP VOLTAGES VS DISTANCE IN SIMULATED NINE CAVITY DRIVER SECTION

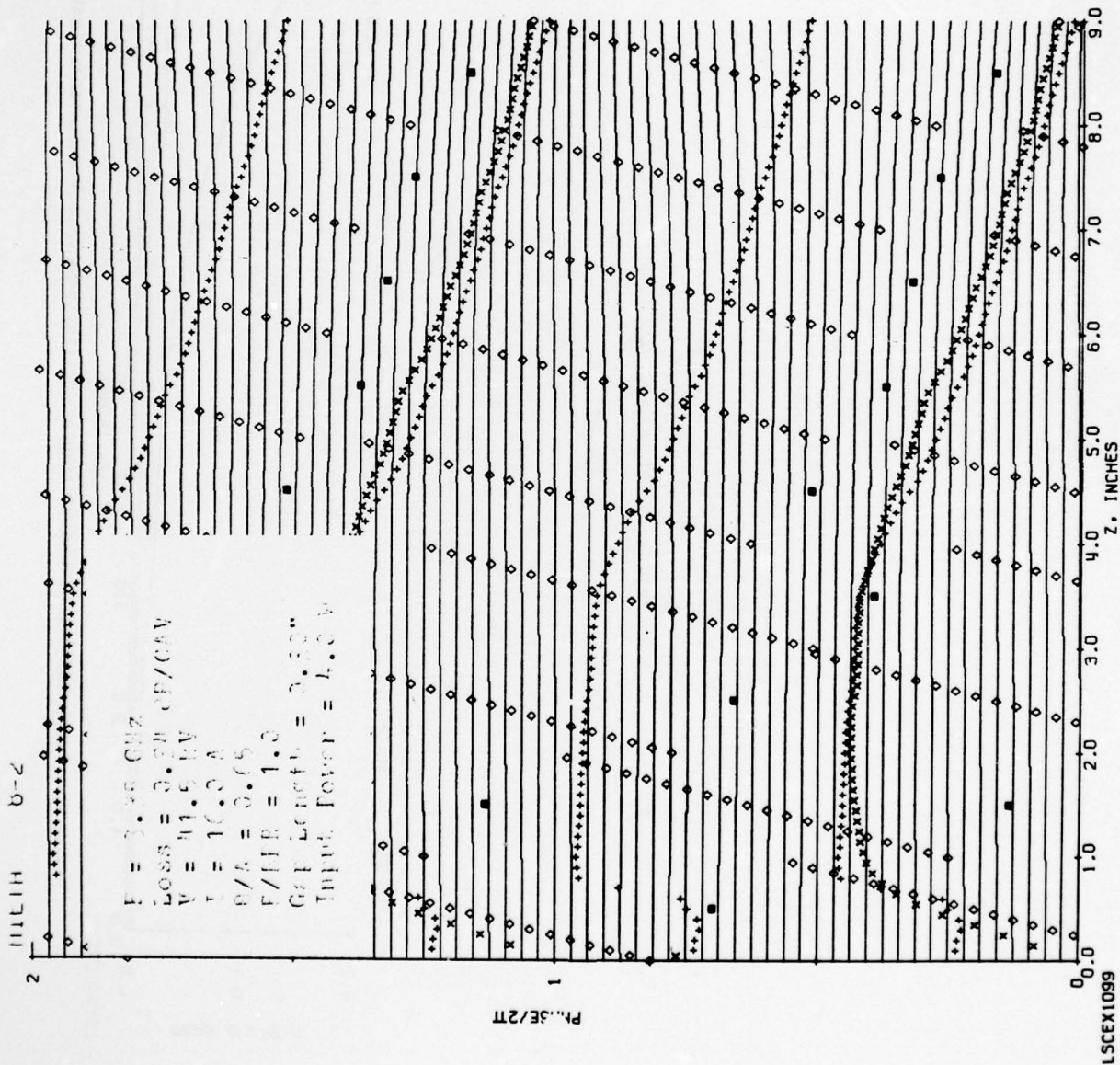


FIGURE 4.17 COMPUTED RELATIVE PHASES OF ELECTRON DISKS VS DISTANCE IN SIMULATED NINE CAVITY DRIVER SECTION

THIS PAGE IS BEST QUALITY PAGE
 FROM COPY 941000 TO DDC

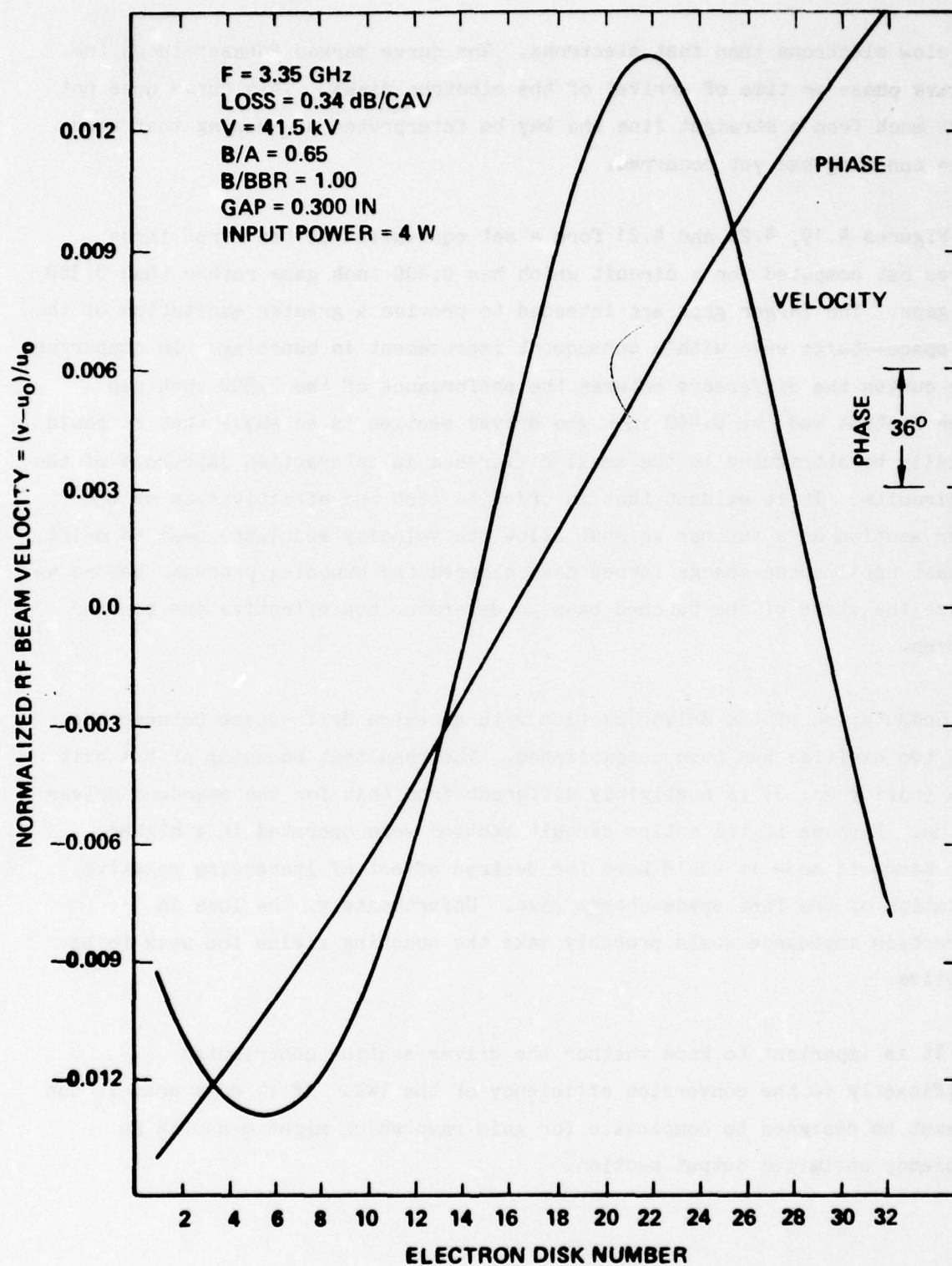


FIGURE 4.18 COMPUTED VELOCITY SPECTRUM AND PHASES OF ELECTRON DISKS IN SIMULATED NINE-CAVITY DRIVER SECTION

more slow electrons than fast electrons. The curve marked "phase" shows the relative phase or time of arrival of the electron disks. This curve does not depart much from a straight line and may be interpreted as showing that very little bunching has yet occurred.

Figures 4.19, 4.20 and 4.21 form a set equivalent to the first three figures but computed for a circuit which has 0.400 inch gaps rather than 0.300 inch gaps. The larger gaps are intended to provide a greater excitation of the fast space-charge wave with a consequent improvement in bunching. In comparing these curves the difference between the performance of the 0.300 inch gap driver section and the 0.400 inch gap driver section is so small that it could logically be attributed to the small difference in interaction impedance of the two circuits. It is evident that in order to test the effectiveness of the driver section as a buncher we must allow the velocity modulated beam to drift, at least until space-charge forces have stopped the bunching process, before we analyze the state of the bunched beam to determine how effective the buncher has been.

Computation of the driver section with an extra drift-space between the final two cavities has been accomplished. The resultant bunching at the exit plane (cavity No. 9) is negligibly different from that for the standard driver section. Perhaps if the entire circuit section were operated in a higher space-harmonic mode it would have the desired effect of increasing relative excitation of the fast space-charge wave. Unfortunately, the loss in interaction impedance would probably make the bunching fields too weak to be effective.

It is important to know whether the driver section contributes significantly to the conversion efficiency of the TWT. If it does not, it can at least be designed to compensate for gain ramp which might occur in an efficiency optimized output section.

$F = 3.35 \text{ GHz}$
 $\text{Loss} = 0.34 \text{ dB/CAV}$
 $V = 41.5 \text{ kV}$
 $I = 16.0 \text{ A}$
 $E/A = 0.65$
 $B/FBR = 1.0$
 $\text{Gap Length} = 0.40''$
 $\text{Input Power} = 4.0 \text{ W}$

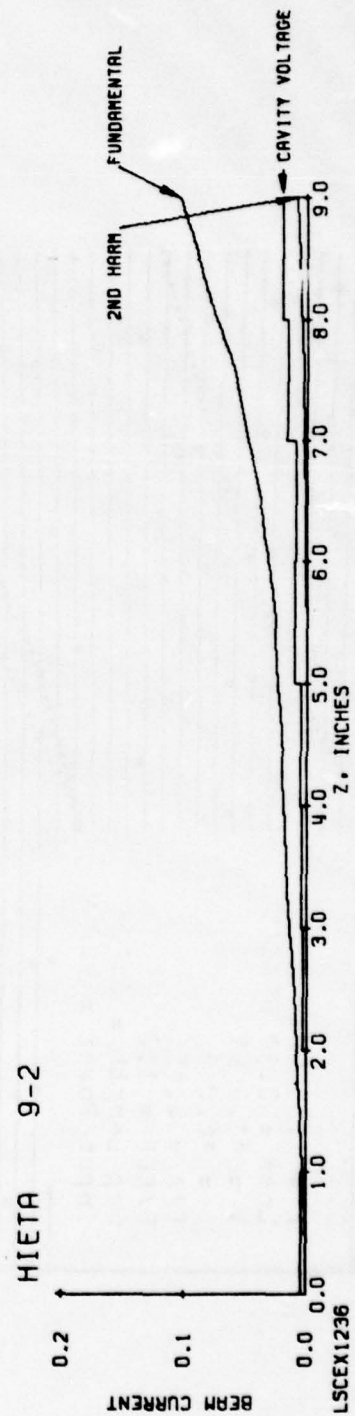


FIGURE 4.19 COMPUTED RF BEAM CURRENTS AND GAP VOLTAGES VS DISTANCE IN SIMULATED NINE CAVITY DRIVER SECTION

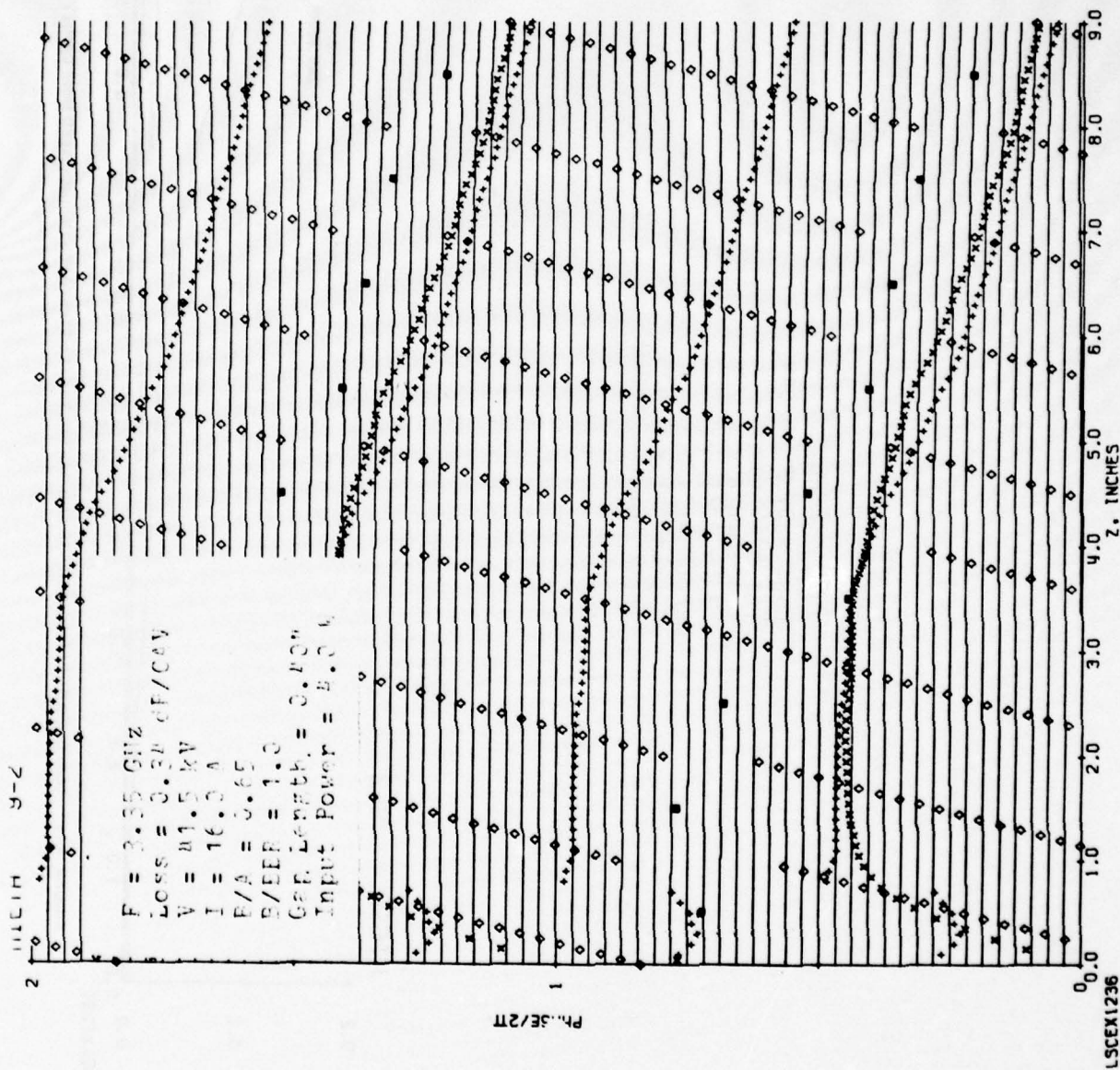


FIGURE 4.20 COMPUTED RELATIVE PHASES OF ELECTRON DISKS VS DISTANCE IN SIMULATED NINE CAVITY DRIVER SECTION

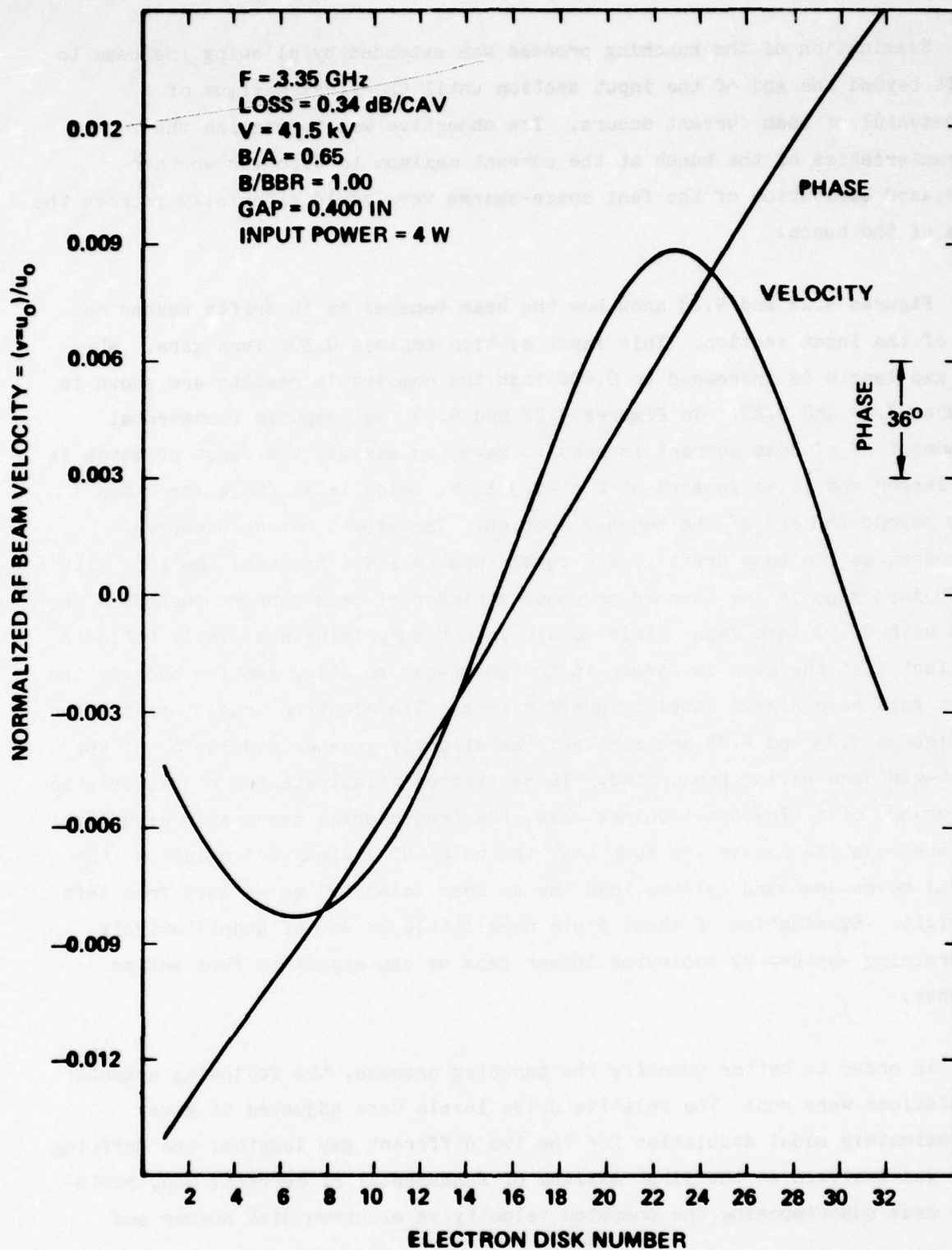


FIGURE 4.21 COMPUTED VELOCITY SPECTRUM AND PHASES OF ELECTRON DISKS IN SIMULATED NINE-CAVITY DRIVER SECTION

Examination of the bunching process was extended by allowing the beam to drift beyond the end of the input section until the first maximum of fundamental rf beam current occurs. The objective was to examine the characteristics of the bunch at the current maximum to discover whether increased excitation of the fast space-charge wave could materially improve the form of the bunch.

Figures 4.22 and 4.23 show how the beam behaves as it drifts beyond the end of the input section. This input section employs 0.300 inch gaps. When the gap length is increased to 0.400 inch the comparable results are shown in Figures 4.24 and 4.25. In Figures 4.22 and 4.24 the computed fundamental component of rf beam current is seen to have two maxima, the first of which is the larger and it is located at $Z = 10.3$ inch, which is a little more than 1 inch beyond the end of the buncher section. The second harmonic current increases as the beam drifts. For equal input drive (16 watts) the tube with 0.300 inch gaps in the buncher produces a higher rf beam current than does the tube with 0.400 inch gaps. This result is not surprising and simply reflects the fact that the gain is larger in the short-gap bunching section because the short gaps have higher coupling coefficients. The electron trajectories shown in Figures 4.23 and 4.25 are similar; the slightly greater modulation of the short-gap case having been noted. These figures illustrate the characteristic appearance of a slow space-charge wave; the trajectories are nearly sinusoidal but the relative phases are such that the point of maximum accumulation (the bunch) moves downward (slower than the dc beam velocity) as we move from left to right. Examination of these plots does little by way of quantitatively determining whether by employing longer gaps we can expect to form better bunches.

In order to better quantify the bunching process, the following computer simulations were run: The relative drive levels were adjusted to give approximately equal modulation for the two different gap lengths; the drifting beam was analyzed at the first maximum of fundamental rf current; and, plots were made superimposing the computed velocity vs electron disk number and

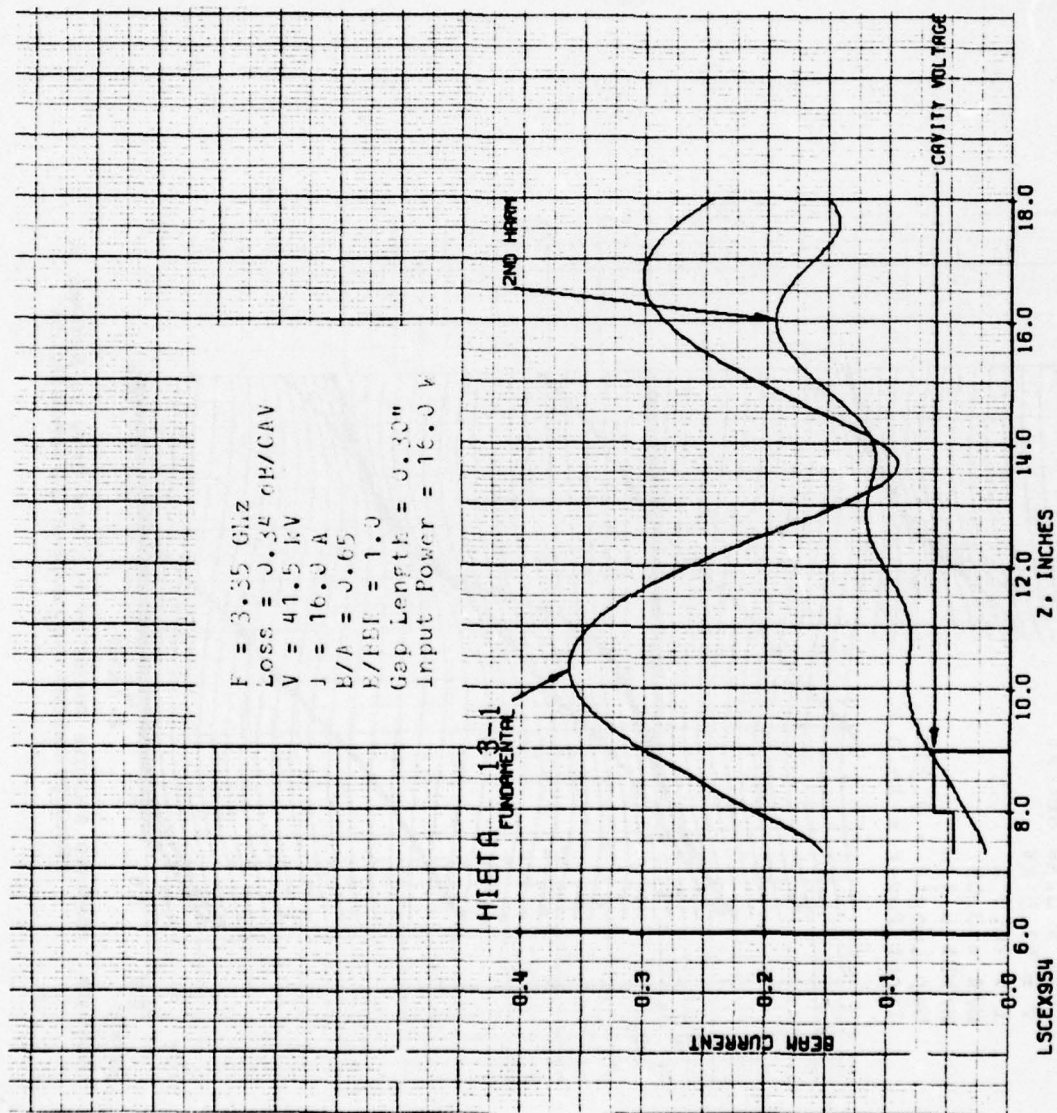


FIGURE 4.22 COMPUTED RF BEAM CURRENTS AND GAP VOLTAGES VS DISTANCE IN SIMULATED NINE INCH DRIFT SPACE BEYOND DRIVER SECTION

THIS PAGE IS BEST QUALITY PRINTING
FROM COPY FURNISHED TO DDC

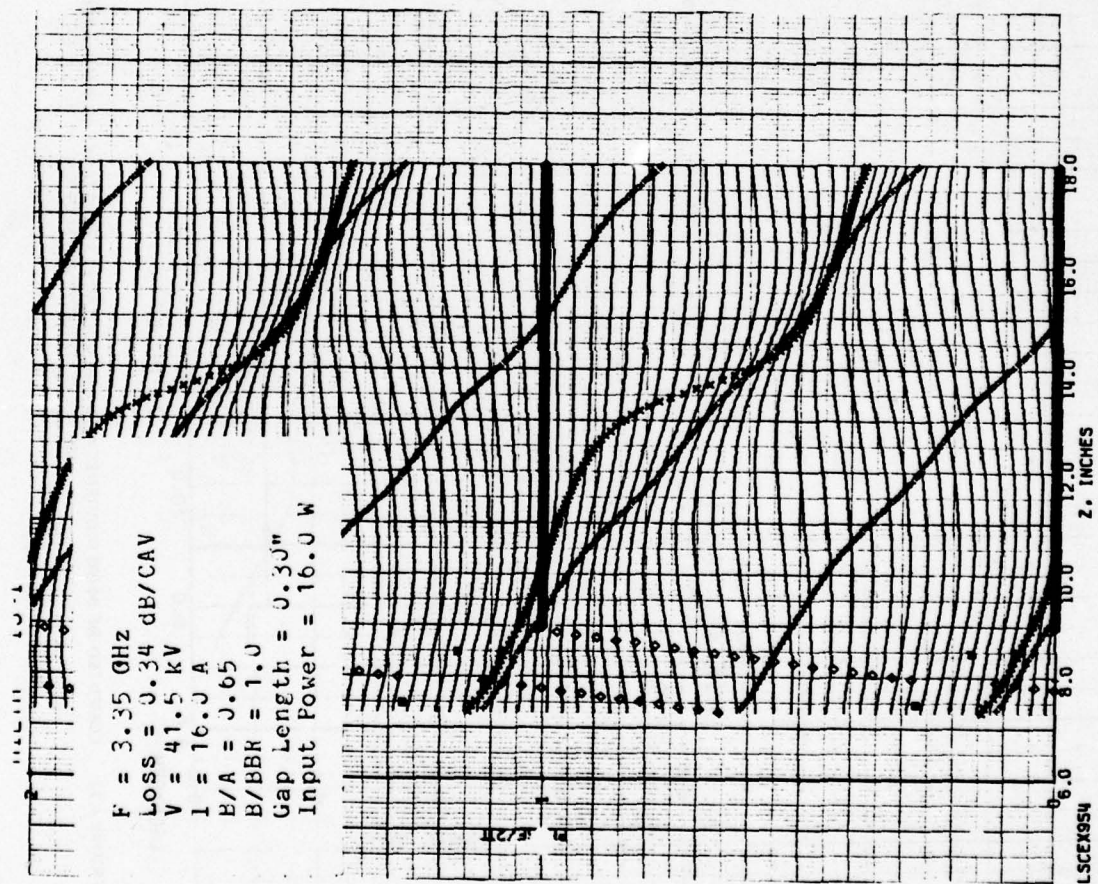


FIGURE 4.23 COMPUTED RELATIVE PHASES OF ELECTRON DISKS VS DISTANCE IN SIMULATED NINE INCH DRIFT SPACE BEYOND DRIVER SECTION

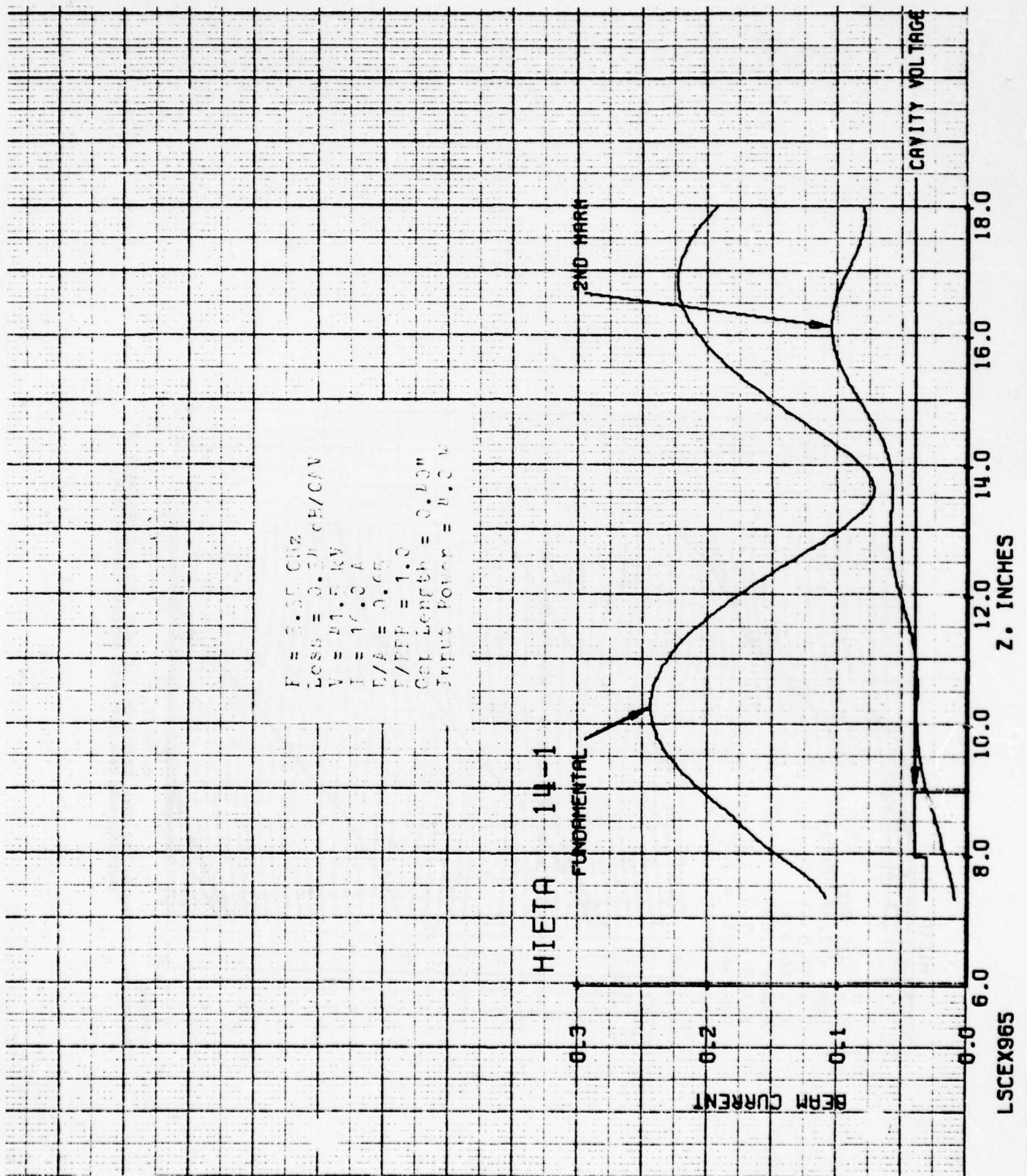


FIGURE 4.24 COMPUTED RF BEAM CURRENTS AND GAP VOLTAGES VS DISTANCE IN SIMULATED NINE INCH DRIFT SPACE BEYOND DRIVER SECTION

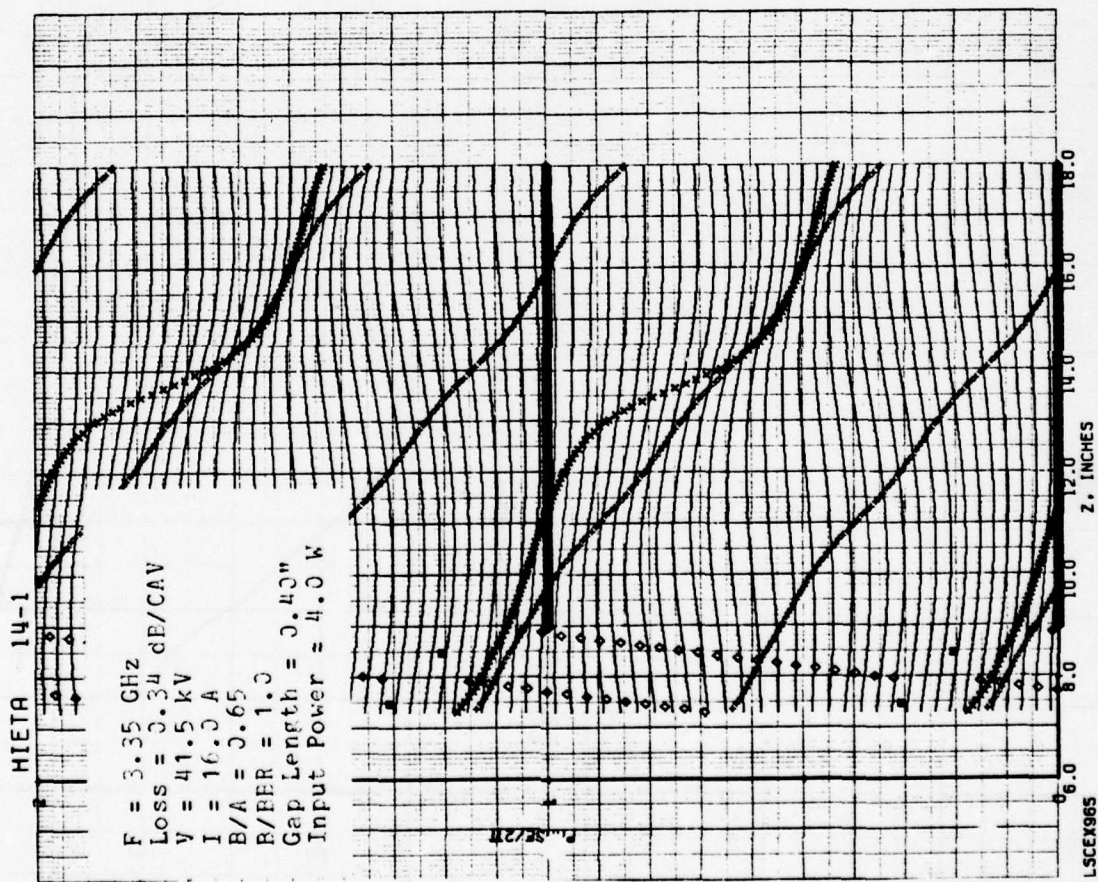


FIGURE 4.25 COMPUTED RELATIVE PHASES OF ELECTRON DISKS VS DISTANCE IN
SIMULATED NINE INCH DRIFT SPACE BEYOND DRIVER SECTION

$-d\theta/dN$, the negative derivative of the arrival phase of the electron disks. The minus sign is chosen so that the resultant curves may be superimposed with minimum confusion. $d\theta/dN$ is a measure of bunch density; the smaller the $d\theta/dN$, the closer packed the electron disks. The negative sign switches the phase so that the maximum bunch density occurs where $-d\theta/dN$ is maximum.

Figures 4.26 and 4.27 show the velocities and bunching densities vs disk number for the two comparable cases: in Figure 4.26, the short-gap buncher is employed with 4 W drive power; in Figure 4.27, the long gap buncher is employed with 9.5 W drive power, the increased drive being necessary to make up for the reduced gain. In both case, the bunches are being analyzed at the first maximum of fundamental rf current, approximately 1 inch beyond the end of the buncher. These two figures are virtually identical; in each case the maximum bunch density coincides with the minimum electron velocity. Increased excitation of the fast space-charge would be expected to move these two curves into quadrature; the rf velocity should be smallest where the bunch is most dense. These results show that increasing the gaplength has an insignificant effect on the character of the bunch. It would appear that the best bunches possible in a TWT might be those which have a reasonable fraction of the electrons arriving within a small phase interval with nearly equal velocities, even though the bunch velocity would need be a little lower than the beam velocity.

Figures 4.28 and 4.29 illustrate the buildup of convection current in the beam after the sever. In Figure 4.28 the sever length is 0.914 inch whereas in Figure 4.29 the sever length is zero. The fundamental and second harmonic currents are seen to be virtually unaffected by changes in sever length of the order of one period. Even the gap voltages are nearly identical. In both cases the gap voltages exhibit rather erratic, non-monotonic behavior, a consequence of the destructive interference of the backward-wave. In future calculations a zero sever length will be assumed in order to minimize the number of computed cases.

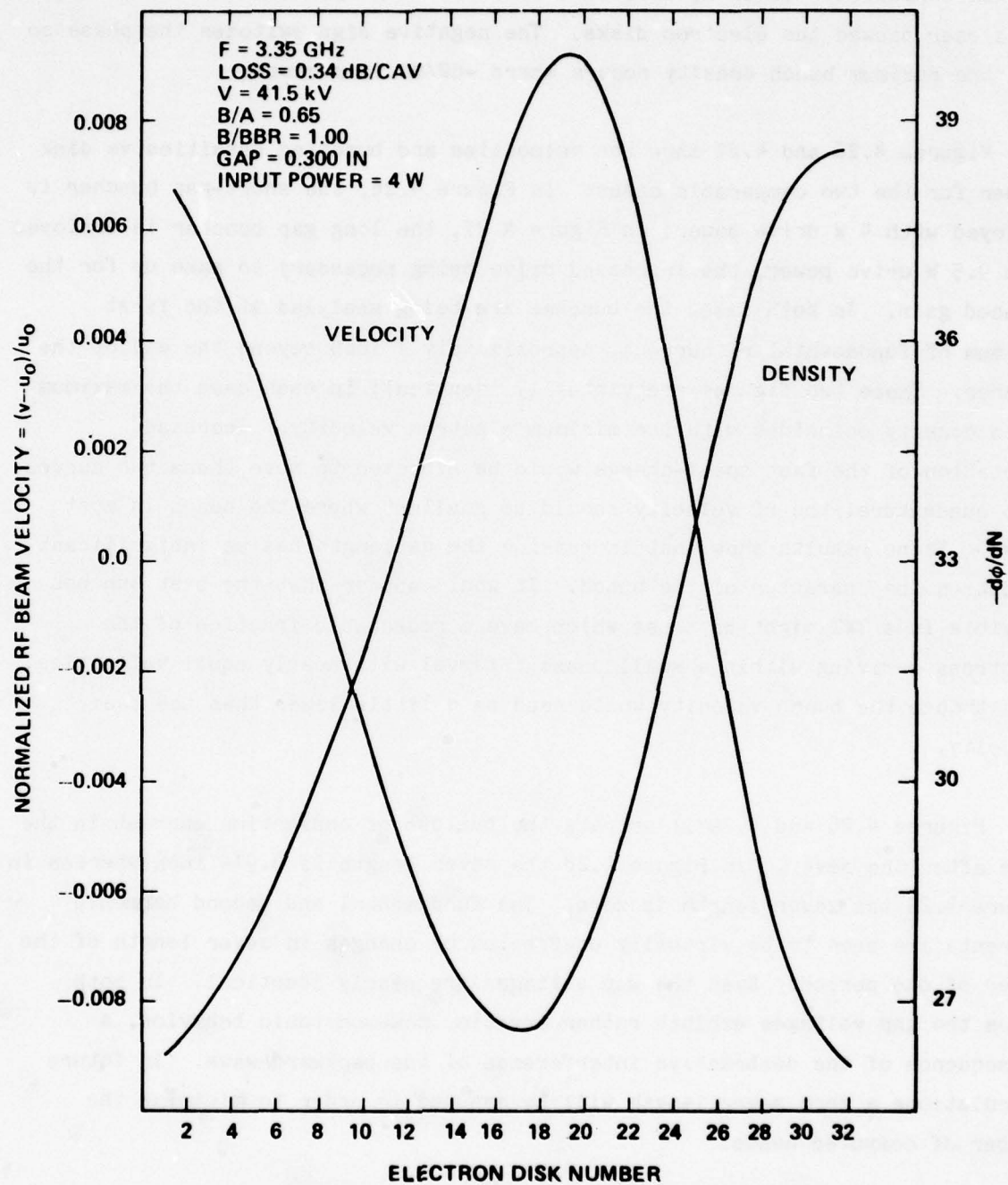


FIGURE 4.26 COMPUTED VELOCITY SPECTRUM AND BUNCHED DENSITY
 OF ELECTRON DISKS ONE INCH INTO SEVER

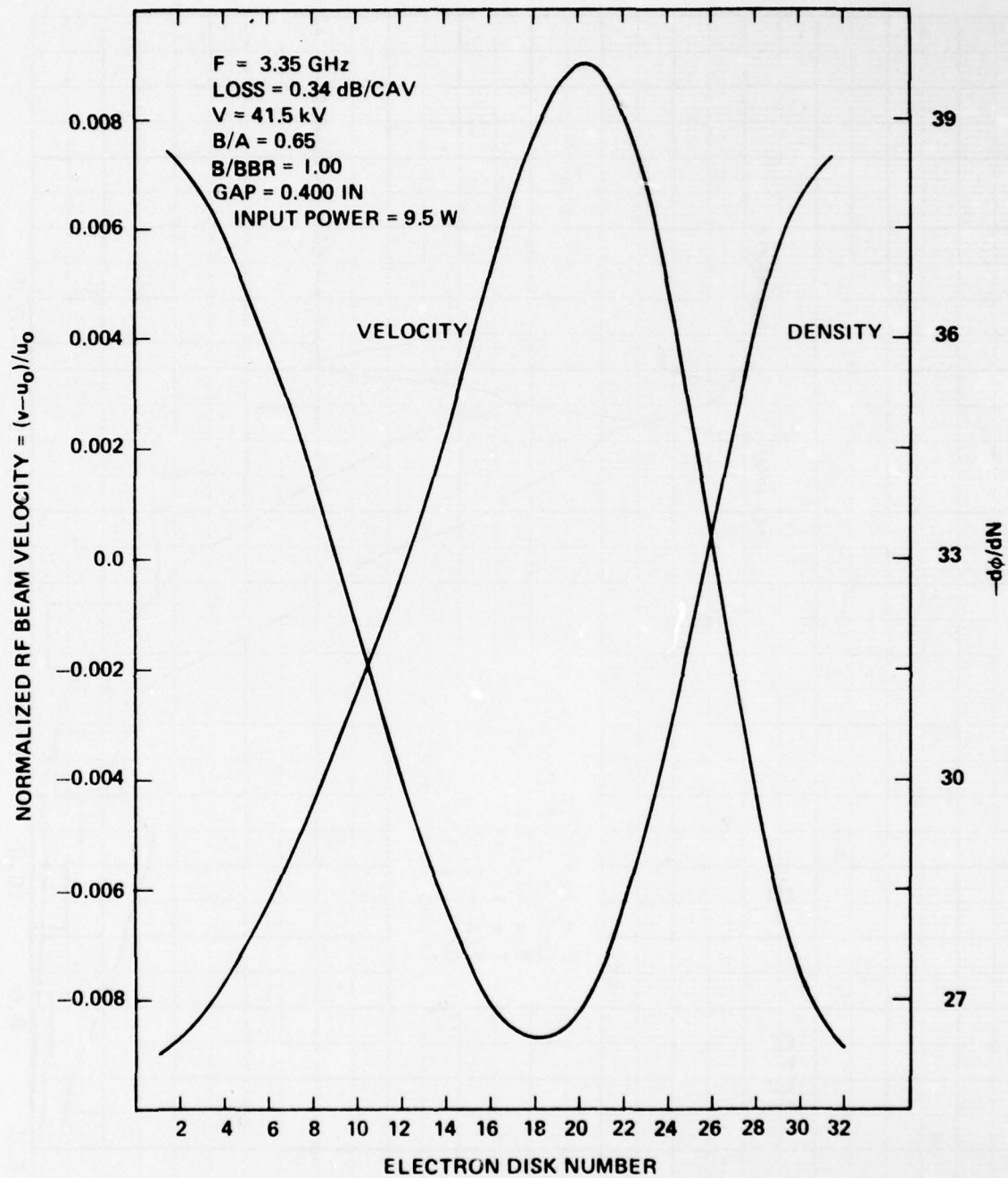


FIGURE 4.2.7 COMPUTED VELOCITY SPECTRUM AND BUNCHED DENSITY OF ELECTRON DISKS ONE INCH INTO SEVER

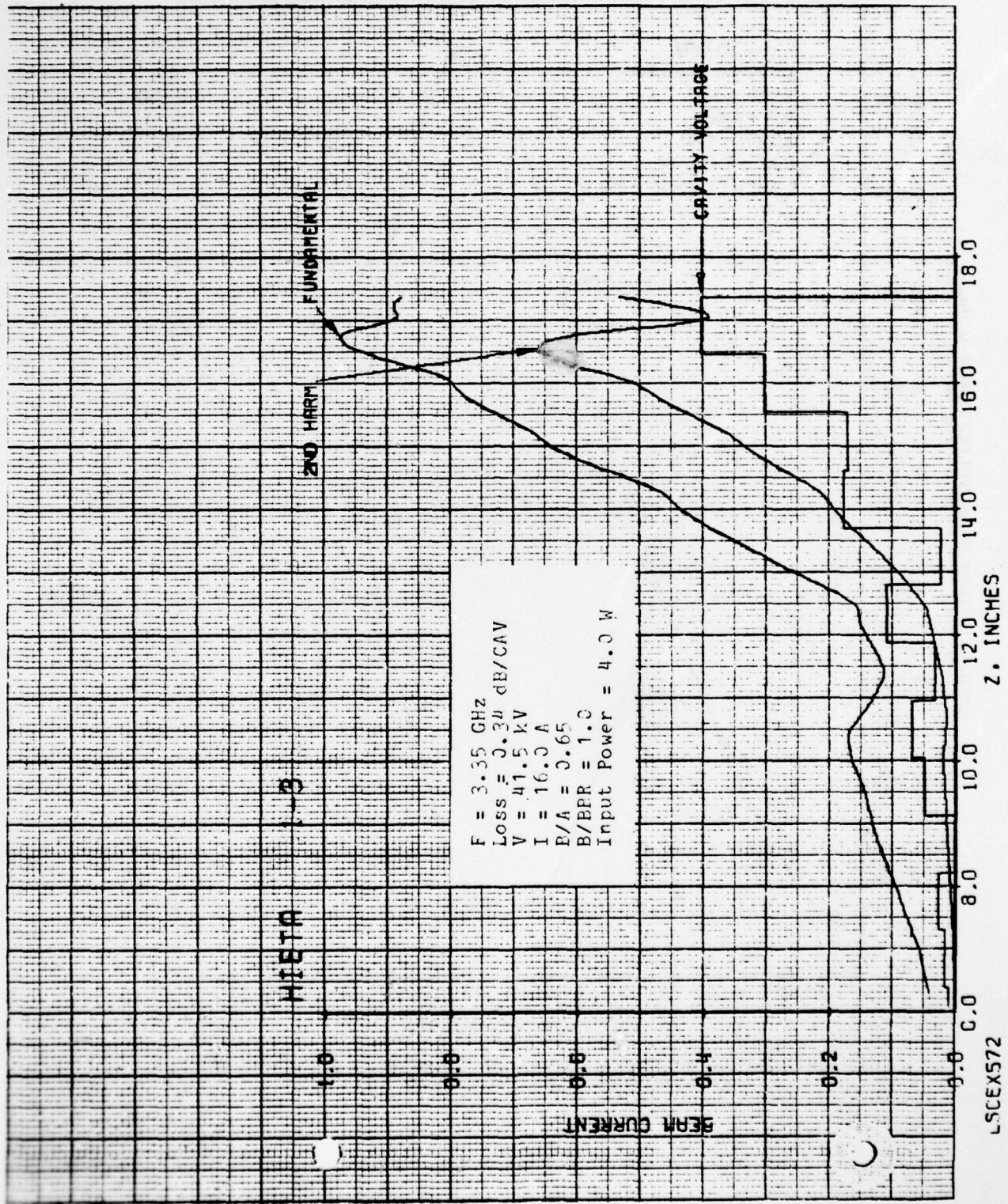


FIGURE 4.28 COMPUTED RF BEAM CURRENTS AND GAP VOLTAGES VS DISTANCE IN SIMULATED COUPLED-CAVITY TWT WITH SEVERE

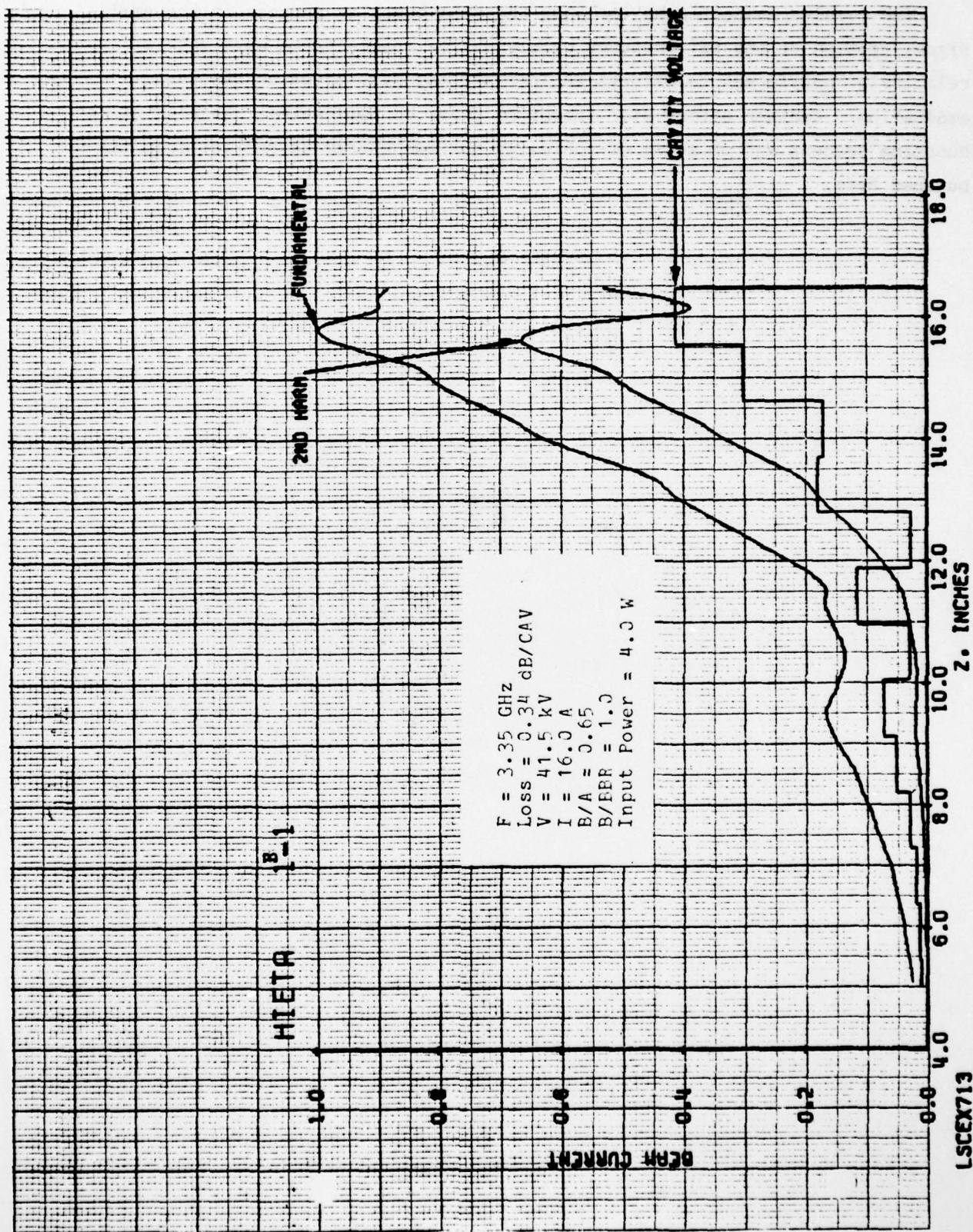


FIGURE 4.29 COMPUTED RF BEAM CURRENTS AND GAP VOLTAGES VS DISTANCE IN SIMULATED COUPLED-CAVITY TWT WITHOUT SEVER

The results presented so far show that the bunching process in the small-signal section of the TWT produces mainly a slow space-charge wave and is relatively indifferent to efforts to increase the fast space-charge wave excitation. Further effort will therefore focus on large-signal aspects of the bunching process and on means of achieving maximum energy extraction from the bunched beam.

5.0 OPTIMIZING THE OUTPUT CIRCUIT SECTION

5.1 Introduction

This section of the report starts with an investigation of bunching and energy extraction in the output section using a simplified circuit model which supports no backward-wave. The study of tube performance with no backward-wave is made as a basis for comparison, to better understand the effects of the backward-wave when a tube with a real circuit is examined. The output circuit including backward-wave effects is examined and compared with the idealized calculations. An effort is made to reduce the anomalous effects of the backward-wave by incorporating a pretaper into the output circuit section. After optimizing the output circuit in a TWT design employing a 2 μ perv beam, a thorough investigation is made of the effect of a major reduction in beam current leading to an optimized design for a TWT meeting the required power objective but employing only a 1 μ perv beam. This low current design is then optimized for best performance over the required 3.1 to 3.6 GHz frequency band.

5.2 Circuits Which Do Not Support a Backward-Wave

Figures 5.1 and 5.2 illustrate some of the features of the bunching process computed for a simplified output circuit. The circuit model employed does not support propagation in the backward direction, permitting a somewhat idealized capability for adjusting the circuit velocity without encountering anomalous gap fields due to backward-wave generation. For the case illustrated in Figure 5.1, the output circuit has nine cavities, all of the same period. The figure shows the electron trajectories in the last four cavities. The small squares represent maximum retarding field at the center of each gap. If the squares were 2 1/2 divisions above the "Xs" this would imply a circuit wave in quadrature with the fundamental component of beam current, i.e., electrons on the front of the bunch (above the "Xs") would encounter retarding fields while those electrons behind the bunch (below the "Xs") would encounter

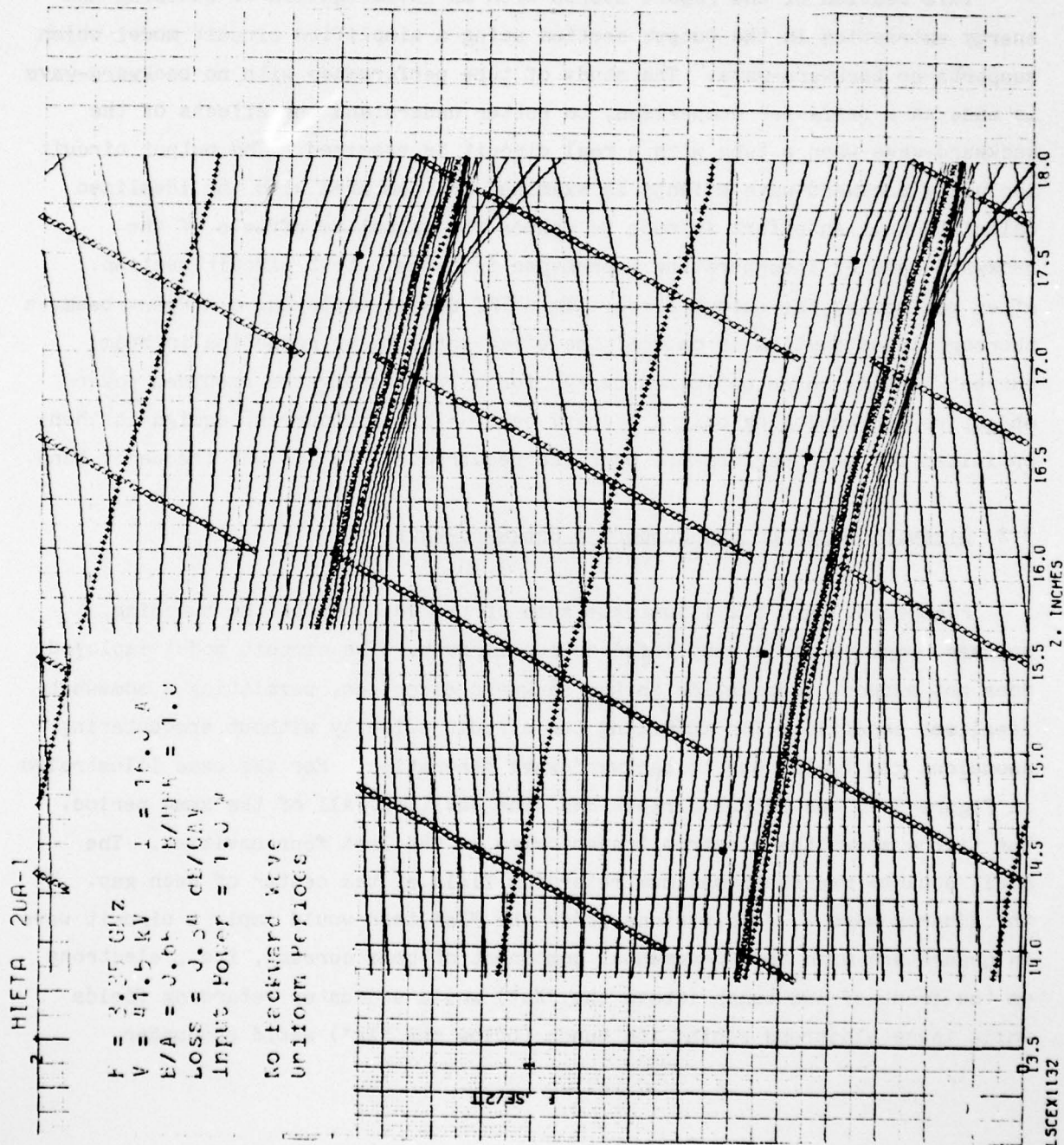


FIGURE 5.1 COMPUTED RELATIVE PHASES OF ELECTRON DISKS VS DISTANCE IN SIMULATED COUPLED-CAVITY TWT WITH UNIFORM PERIODS

HIETA 22-1

$F = 3.35 \text{ GHz}$
 $V = 41.5 \text{ kV}$
 $B/A = 0.65$
 $I = 16.0 \text{ A}$
 $B/PER = 1.0$
 $Loss = 0.34 \text{ dB/CAV}$
 $Input Power = 1.0 \text{ W}$

No Backward Wave
 Tapered Periods

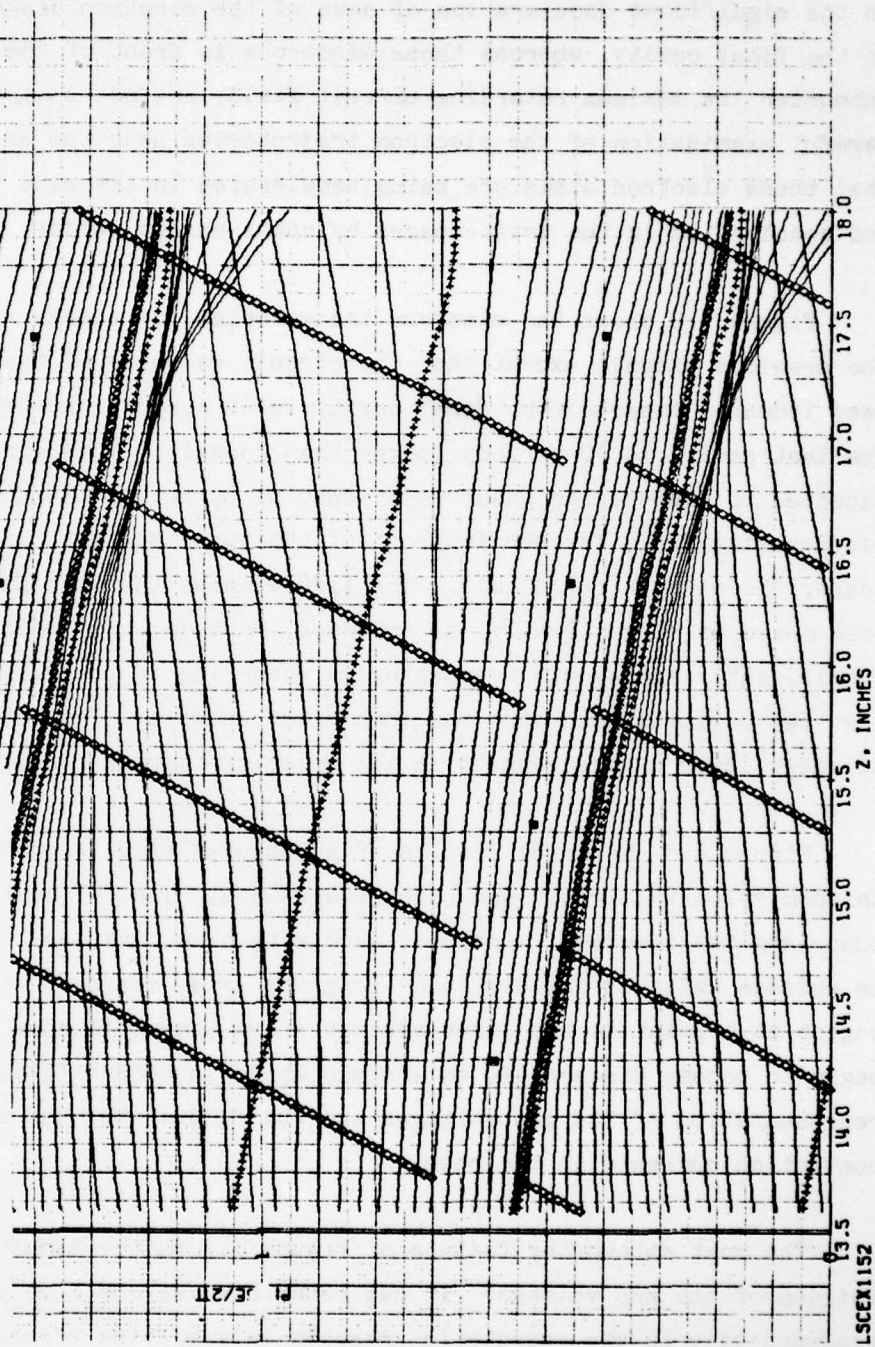


FIGURE 5.2 COMPUTED RELATIVE PHASES OF ELECTRON DISKS VS DISTANCE IN SIMULATED COUPLED-CAVITY TWT WITH TAPERED PERIODS

accelerating fields. In the present example, the bunch is forming in the retarding field rather than at the field null. Space-charge forces are evident in the significant deceleration of some of the electron disks behind the bunch in the final cavity, whereas those electrons in front of the bunch, which encounter the maximum retarding circuit field, are not so greatly decelerated. Careful examination of the electron trajectories near the small squares reveals that these electron disks are being decelerated in the gaps by circuit fields and accelerated in the drift-spaces by space-charge forces.

Figure 5.2 shows the electron trajectories for a case which is the same as the previous example except that the circuit velocity of the output circuit has been linearly tapered (the first cavity is 10 percent shorter than normal -- the last cavity is 10 percent longer than normal). This arrangement was expected to improve the phase relationships by moving the point of the maximum decelerating field farther in front of the bunch so that the bunch would be nearer the circuit field null. The figure shows that the small squares have been moved up very slightly, as intended; however, the bunching has not been significantly improved. Overtaking is occurring in the drift-space between the last two cavities much like the comparison example. The interbunch space has a slightly lower charge density in the velocity-tapered circuit.

Figure 5.3 shows the results of a computer simulation of a TWT with a uniform velocity circuit and no backward-wave. The TWT being simulated comprises two identical sections, each with nine cavities. The figure employs an abscissa which is the distance along the axis, measured in inches. Plotting begins at a point in the input section where the amplitudes of the gap voltages begin to become discernible on a scale which is chosen to provide a convenient representation of the gap voltages and the fundamental and second harmonic rf convection currents in the beam.

The most noteworthy feature of Figure 5.3 is the almost uniform monotonic buildup of the gap voltage. It has been noted before that inclusion of the backward-wave in the computation results in a beating effect between the

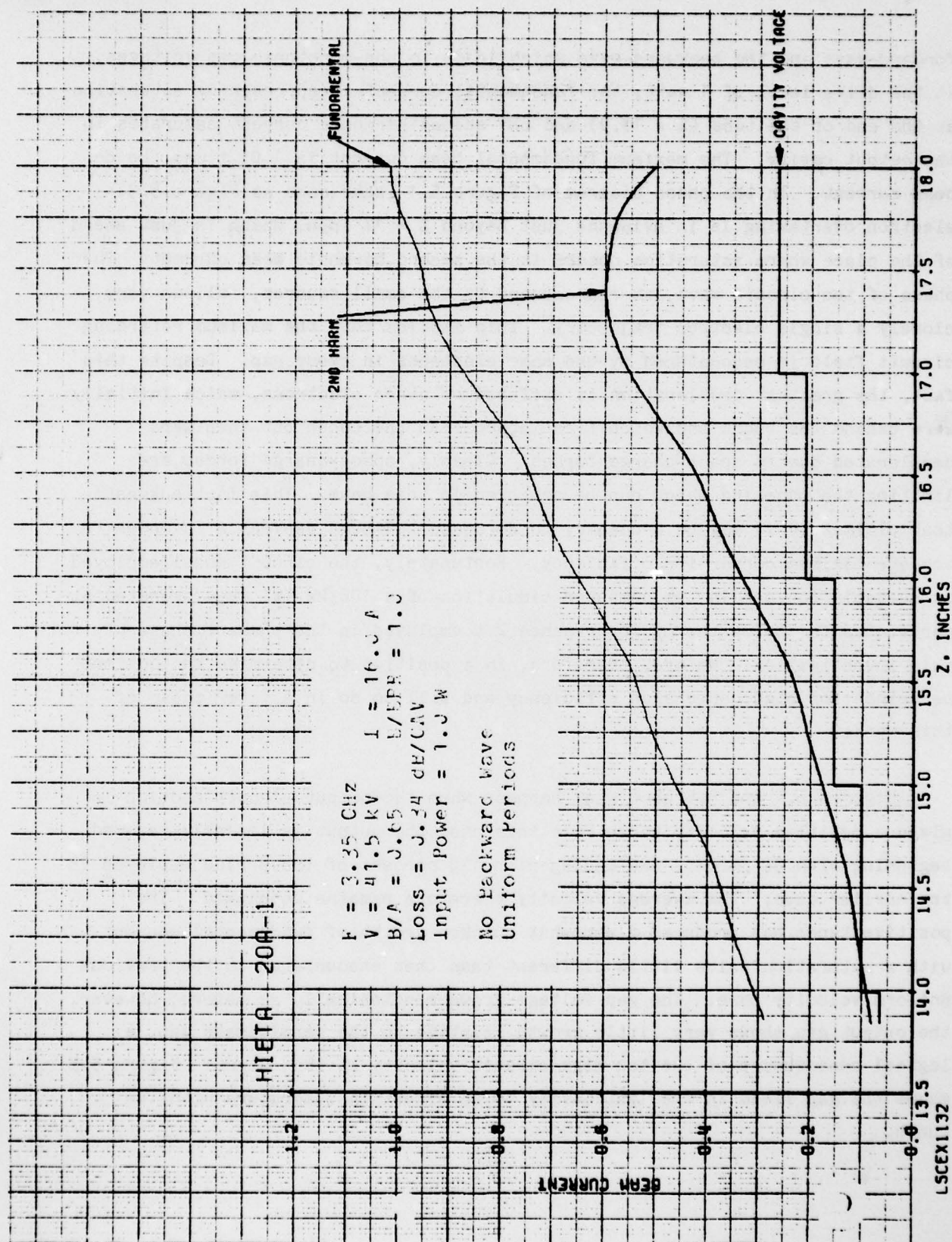


FIGURE 5.3 COMPUTED RF BEAM CURRENTS AND GAP VOLTAGES VS DISTANCE IN SIMULATED COUPLED-CAVITY TWT WITH UNIFORM PERIODS

forward-wave and the backward-wave which leads to non-monotonic gap voltages. At the drive level of 1 watt, the fundamental current is approaching saturation at the end of the tube ($Z = 18.0$) and the second harmonic current saturates in the output cavity. The maximum fundamental beam current is 1.05 times the dc beam current. In the phase diagram of Figure 5.1 (same case as Figure 5.3) electron overtaking is in evidence just beyond $Z = 17$ inch, which is just ahead of the place where saturation occurs in the second harmonic beam current. The phase of the circuit wave, as represented by the small squares, follows very closely a single electron trajectory. This implies that the maximum retarding circuit field is encountered by the same electrons in every gap. Despite this fact, the greatest deceleration is suffered by other electrons, which initially were behind the bunch and which first approached the bunch but then were decelerated due to space-charge forces. Clearly, space-charge forces are limiting the bunching which can be achieved in this beam. This fact suggests that ultimately it may be necessary to decrease the beam perveance in order to achieve maximum conversion efficiency. Fortunately, the circuit model employed is suitable for use in the computer simulation of a 100 kW TWT when operated at perveances far below the microperveance 2.0 employed in the present phase of this investigation. We are, therefore, in a position to determine the optimum perveance for high conversion efficiency and will do so in a later phase of this work.

Figures 5.4 and 5.5 show what happens when the output circuit section is given a positive velocity taper. In this case the output is linearly tapered beginning with 90 percent and ending with 110 percent of the period employed in the earlier case. The average velocity therefore remains unchanged. The positive taper has produced a somewhat quicker growth of fundamental current with a saturation value little different than that encountered in the previous uniform velocity case. The gap voltage grows monotonically as before; however, the output gap shows very little growth relative to the penultimate gap, a logical consequence of the too high circuit velocity at the output. Figure 5.5 shows the gap field in the last cavity to be almost in quadrature with the bunch.

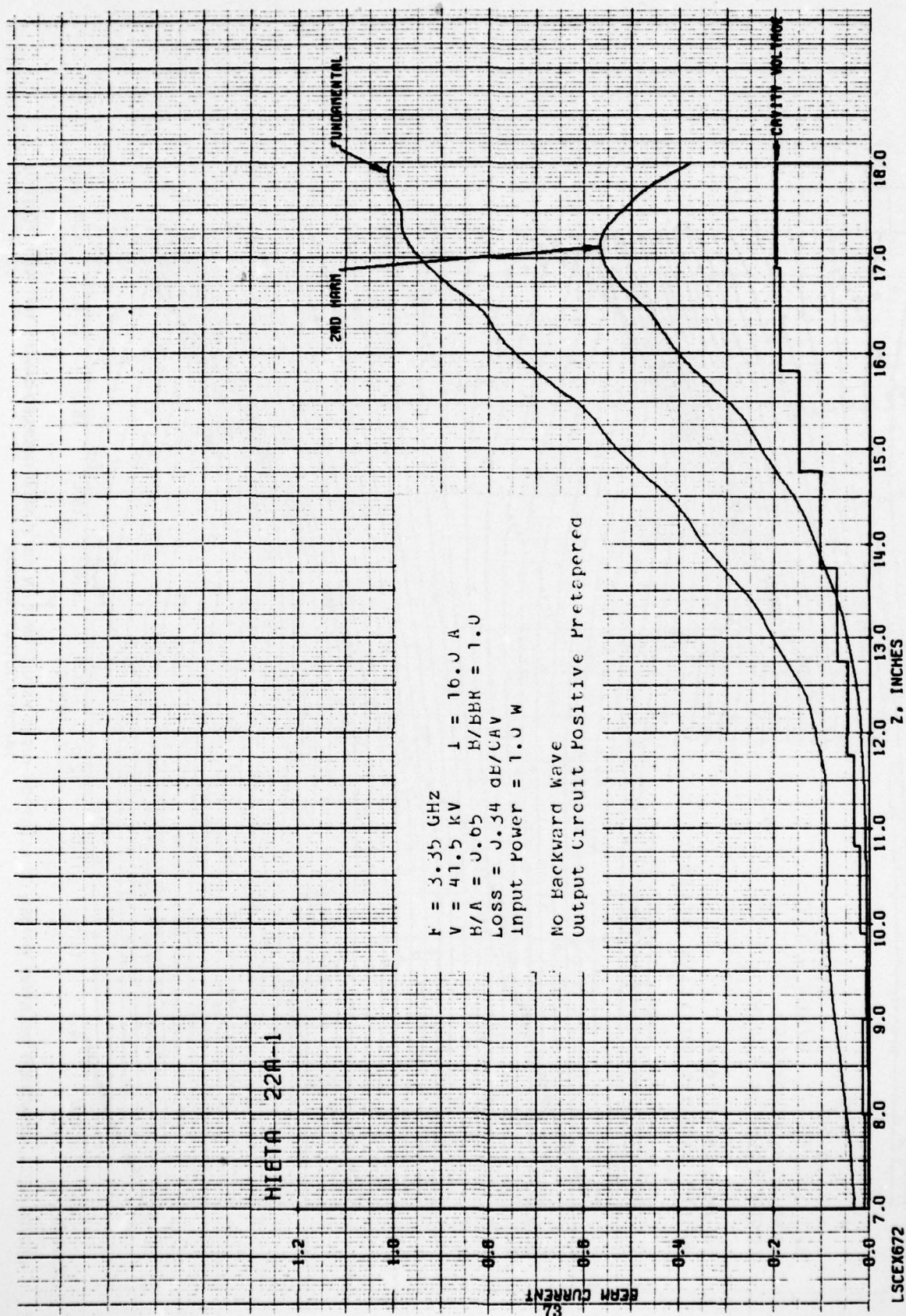


FIGURE 54 COMPUTED RF BEAM CURRENTS AND GAP VOLTAGES VS DISTANCE IN SIMULATED COUPLED-CAVITY TWT WITH POSITIVE TAPERED OUTPUT PERIODS

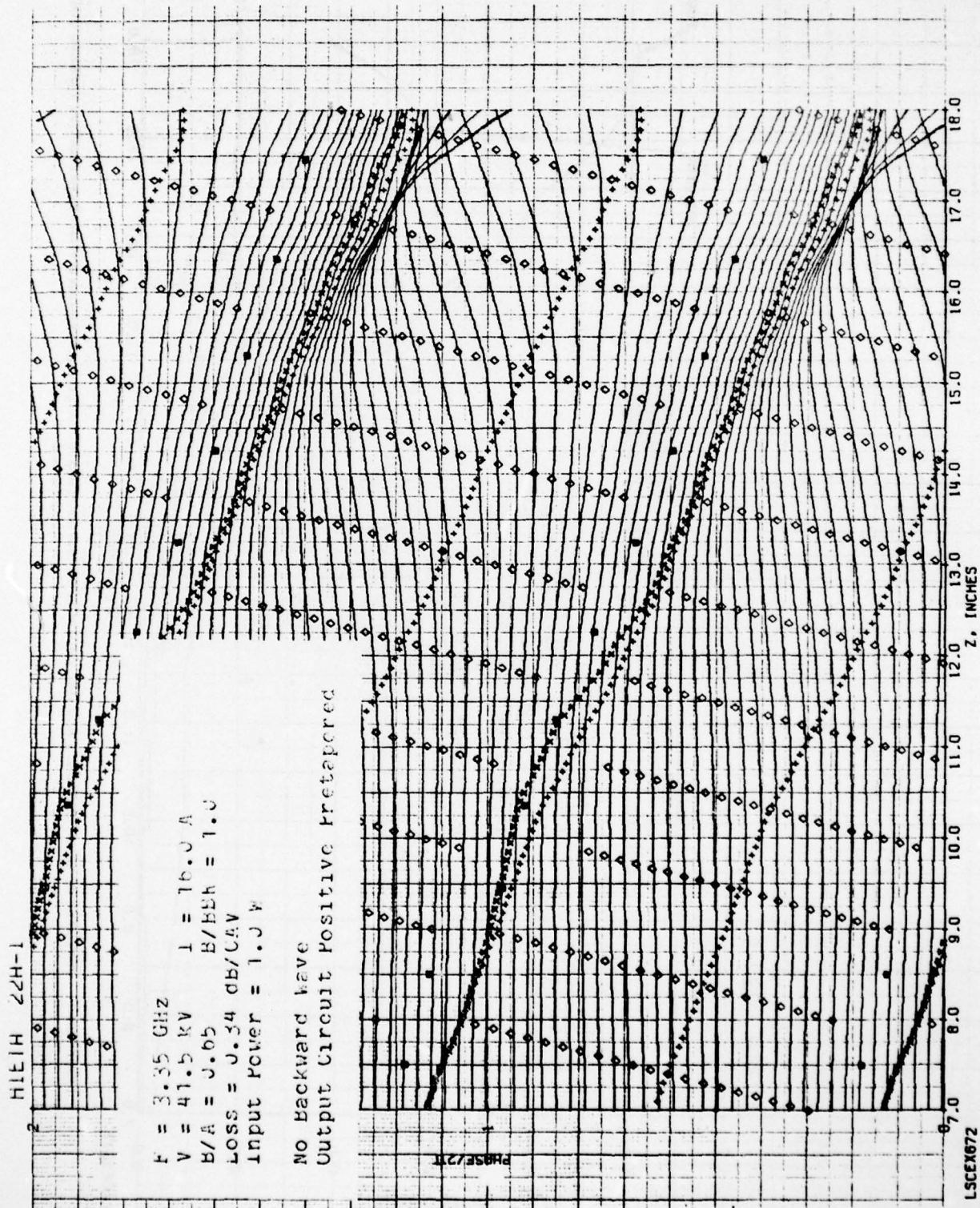


FIGURE 5.5 COMPUTED RELATIVE PHASES OF ELECTRON DISKS VS DISTANCE IN SIMULATED COUPLED-CAVITY TWT WITH POSITIVE TAPERED OUTPUT PERIODS

Figures 5.6 and 5.7 illustrate the bunching process in a TWT with a negative velocity taper. The fundamental current builds up more slowly than it did in the two previous cases. However, the maximum second harmonic is greater than before and the maximum fundamental current has not yet been reached at the drive level employed. It appears likely that the maximum fundamental current will be at least as large and possibly larger than in the two previous cases. The gap voltage grows more slowly near the input but increases dramatically toward the output reaching a larger value than in either of the previous cases. On examination of Figure 5.7 it is apparent that the "hot" circuit wave is traveling more slowly than the bunch. Near the output the bunches pass through the gaps shortly after the gap fields reach their maximum retarding value. While this condition favors energy extraction, it is not clear whether the bunches produced by the negatively tapered circuit will ultimately yield more energy to the circuit.

Figures 5.8 and 5.9 show the results of a computer simulation of a TWT with a uniform velocity circuit. There are nine cavities in each of the two circuit sections; the output section having four lossless cavities at its output end. This circuit supports only a forward-wave and is driven at the input by 1 watt. Figure 5.8 shows cavity voltage, and fundamental and second harmonic beam current vs axial position. Each step in cavity voltage has a width equal to the cavity period. Gap-to-gap spacing is equal to the distance between the centers of adjacent steps. This figure shows a monotonic buildup in cavity voltage and fundamental current in the output section. The second harmonic current is seen to saturate in the output cavity.

Figure 5.9 shows the electron phase trajectories vs axial distance. Some electron overtaking is occurring in the output cavity. The small squares, which mark the maximum retarding field, remain above (in front of) the line of "Xs" which mark the center of the bunch. This phase relationship between the fields and the bunch is approximately midway between a "bunching" field and a "stopping" field -- a necessary condition to obtain a growing wave.

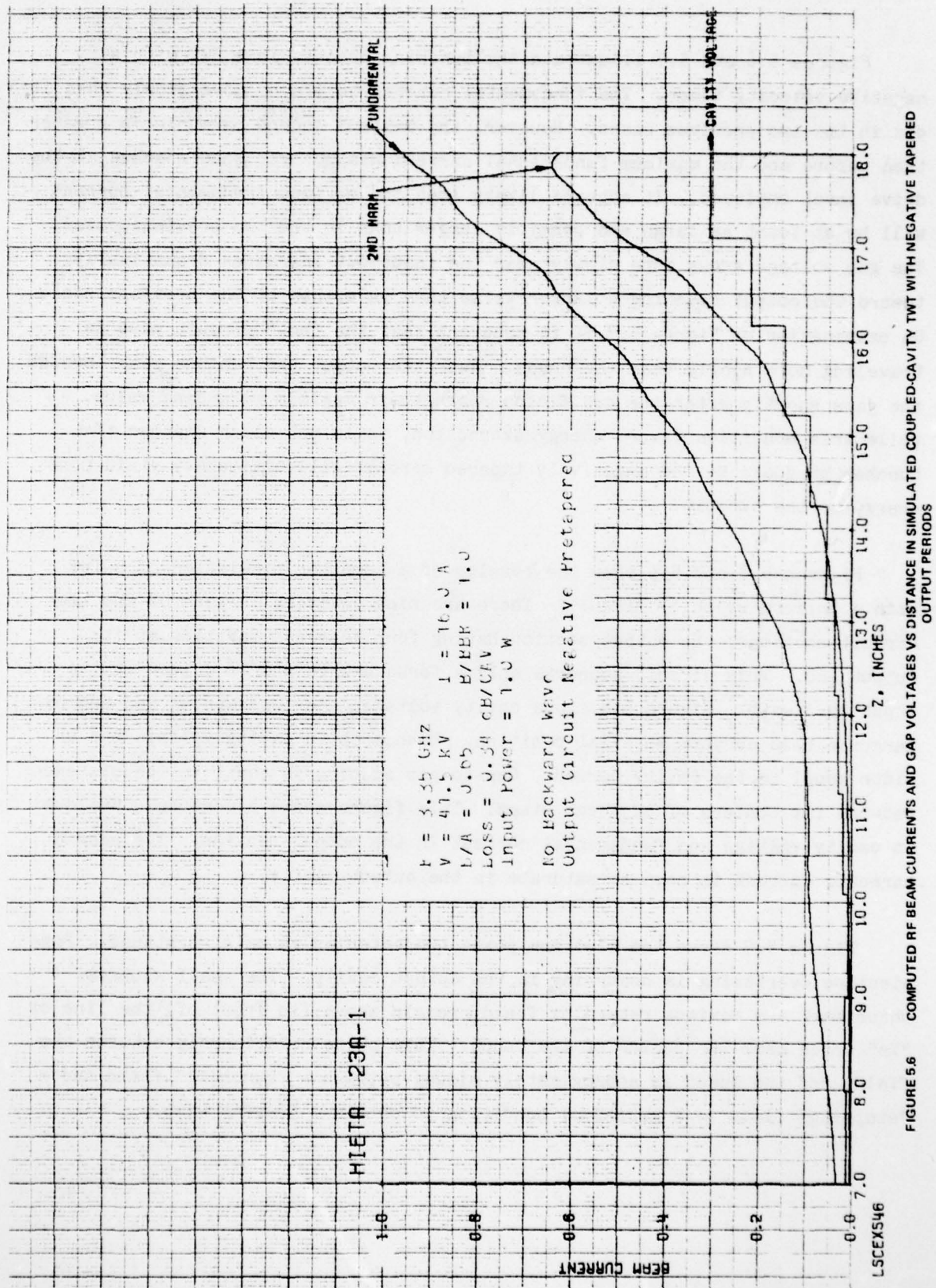


FIGURE 5.6 COMPUTED RF BEAM CURRENTS AND GAP VOLTAGES VS DISTANCE IN SIMULATED COUPLED-CAVITY TWT WITH NEGATIVE TAPERED OUTPUT PERIODS

HIETA 23A-1

$f = 3.35 \text{ GHz}$
 $V = 41.5 \text{ kV}$
 $B/A = 0.05$
 $\text{Loss} = 0.34 \text{ CH/CAV}$
 $\text{Input Power} = 1.0 \text{ W}$

No Backward Wave
 Output Circuit Negative Pretapered

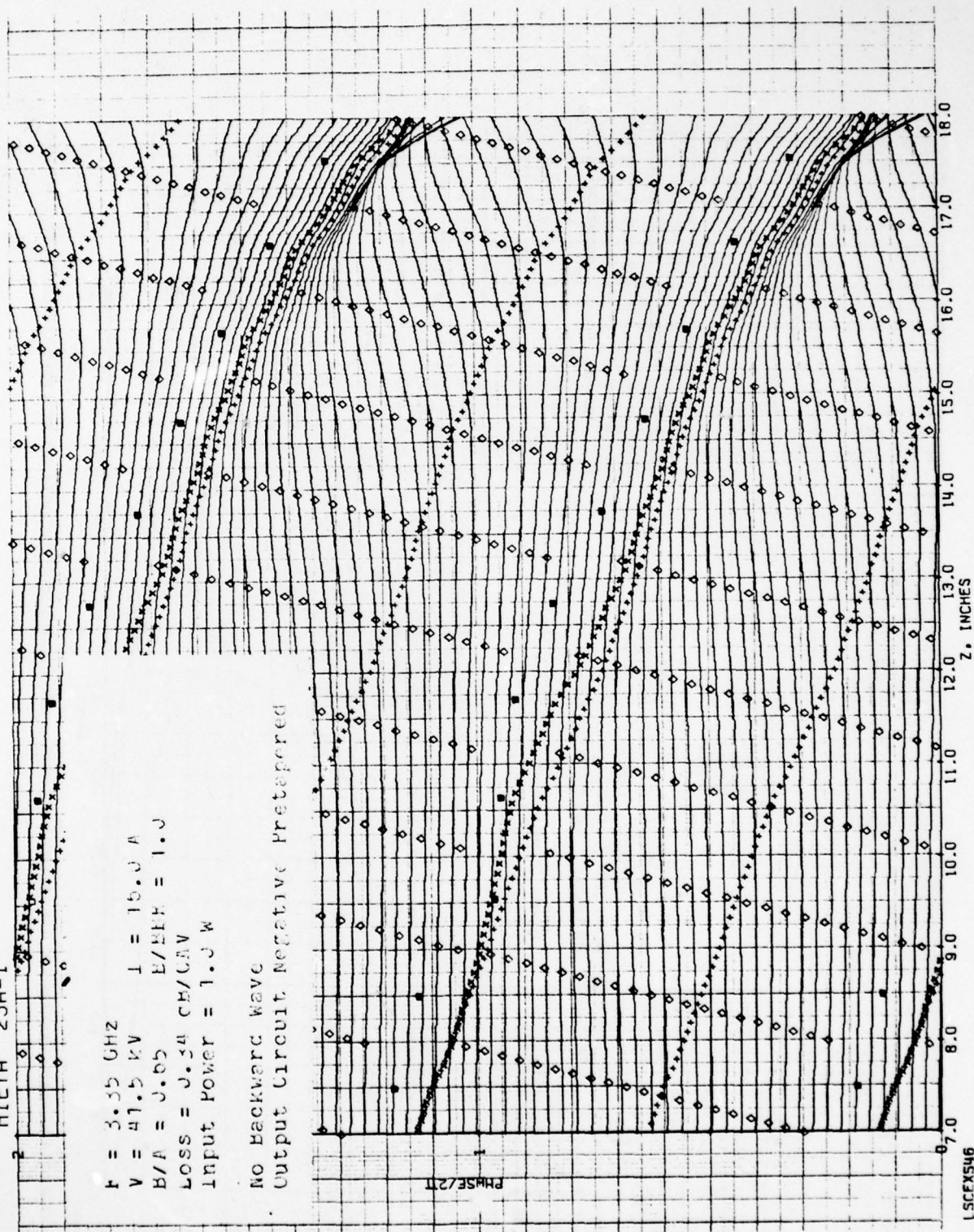


FIGURE 5.7 COMPUTED RELATIVE PHASES OF ELECTRON DISKS VS DISTANCE IN SIMULATED COUPLED-CAVITY TWT WITH NEGATIVE TAPERED OUTPUT PERIODS

AD-A080 961

VARIAN ASSOCIATES INC PALO ALTO CA PALO ALTO MICROWAVE--ETC F/G 9/1
EFFICIENCY IMPROVEMENTS IN COUPLED CAVITY TRAVELING WAVE TUBES.(U)
OCT 79 W R AYERS, F R WALKER

F30602-78-C-0117

UNCLASSIFIED

RADC-TR-79-264

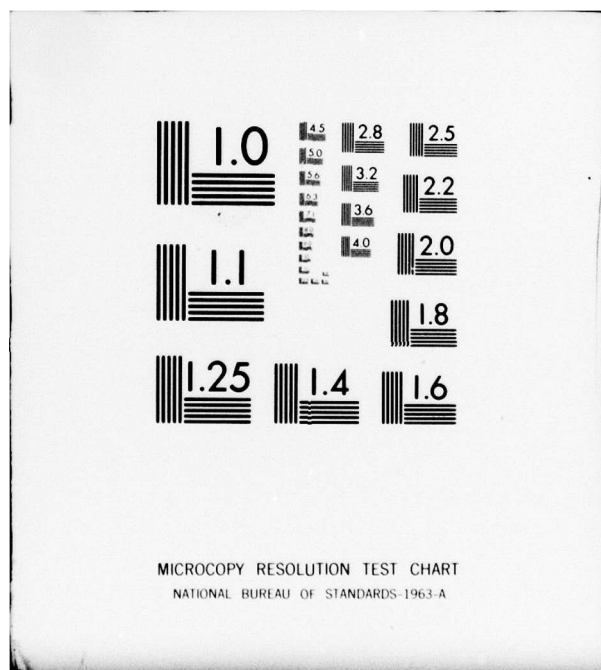
NL

2 OF 3

AD-

AOB0961





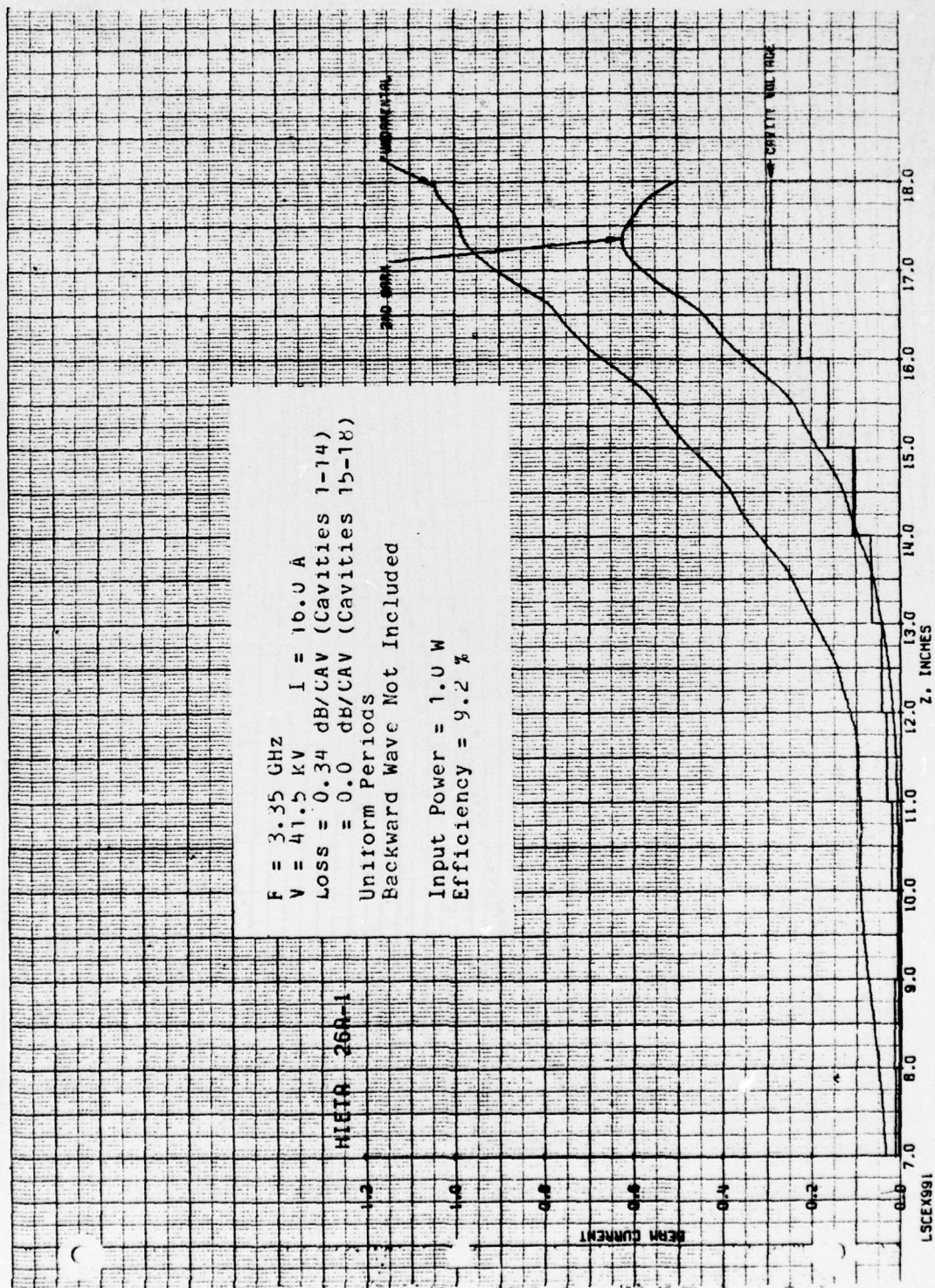


FIGURE 5.8 COMPUTED RF BEAM CURRENTS AND GAP VOLTAGES VS DISTANCE IN SIMULATED COUPLED-CAVITY TWT WITH FOUR LOSSLESS OUTPUT CAVITIES

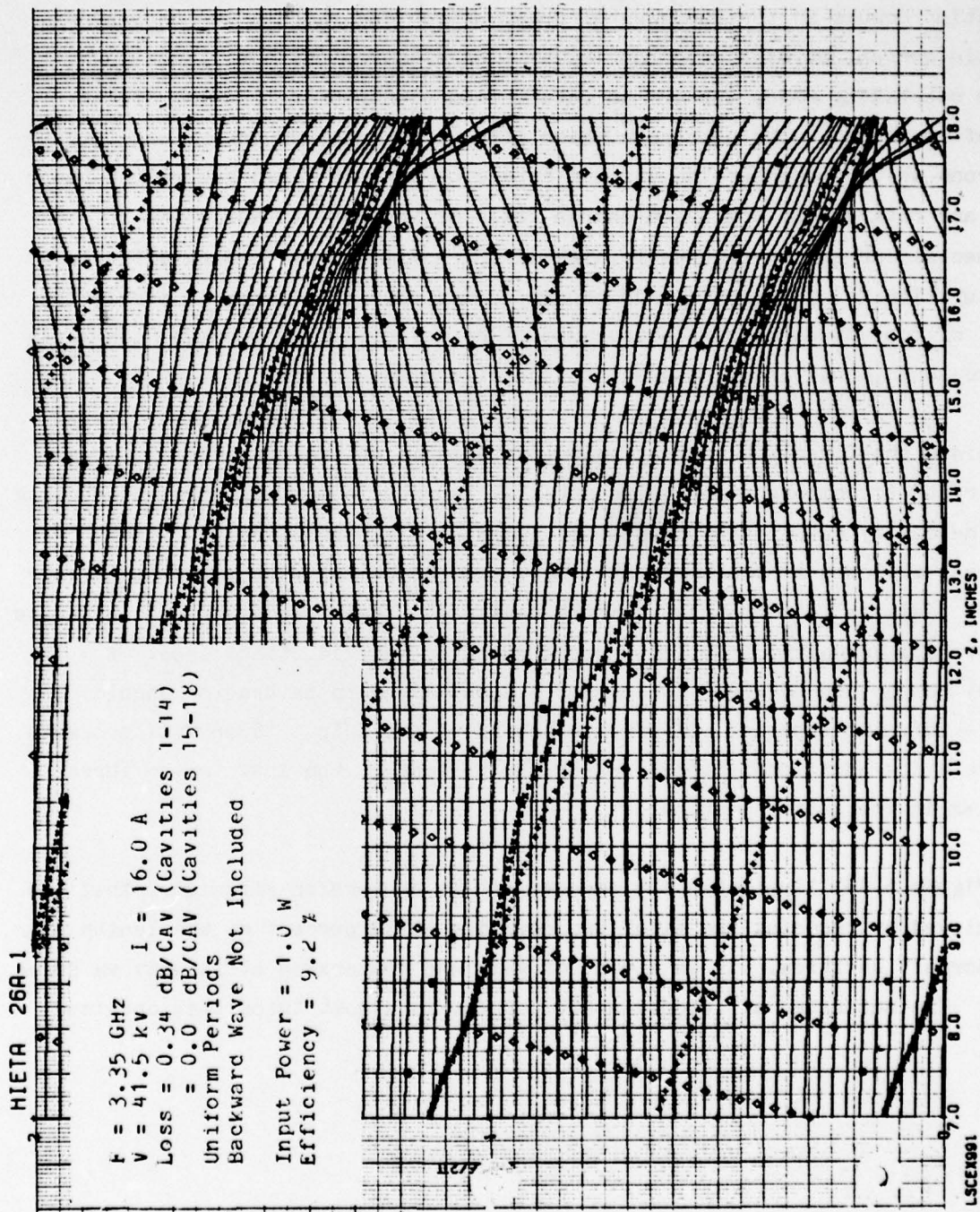


FIGURE 5.9 COMPUTED RELATIVE PHASES OF ELECTRON DISKS VS DISTANCE IN SIMULATED COUPLED-CAVITY TWT WITH FOUR LOSSLESS OUTPUT CAVITIES

Figures 5.10 and 5.11 are similar to the two previous figures except that the drive power has been increased by 3 dB to 2 watts. Figures 5.12 and 5.13 similarly are for a drive power of 4 watts. As the drive level is increased, saturation occurs in the fundamental beam current and the dip in the second harmonic current moves toward the input. The electron phase diagram shows severe overtaking which appears to result from electrons reflecting off the back of the bunch. The electrons which give up the maximum energy are not the electrons which encounter the maximum retarding circuit field but rather those which are retarded by the space-charge field of the bunch. While the fundamental current is reasonably high ($I_{\max} \approx 1$), the conversion efficiency at saturation is approximately 15 percent. The poor efficiency is partly the result of poor synchronization (because of no velocity taper) between the wave and the bunch, and partly because of excessive space-charge.

Since the foregoing test of velocity taper is not conclusive, it seems appropriate to compare positive vs negative taper by computing efficiency using two nine-cavity output circuit models; one with seven positively tapered cavities, followed by two short cavities, and the other, with seven negatively tapered cavities followed by two short cavities. These circuits would have the same overall velocity, identical output cavities, and identical loss. A careful comparison of these two circuits when driven to saturation should resolve which is superior. The optimization of the output taper will probably require a few additional iterations of the periods of the last two or three cavities in the output section.

Figure 5.14 illustrates the improvement in conversion efficiency that can be achieved by reducing the final two cavities to 70 percent of the length of the "normal" cavities. It is a plot of gain and conversion efficiency vs drive level. The saturated efficiency at 28 percent is almost twice that obtained

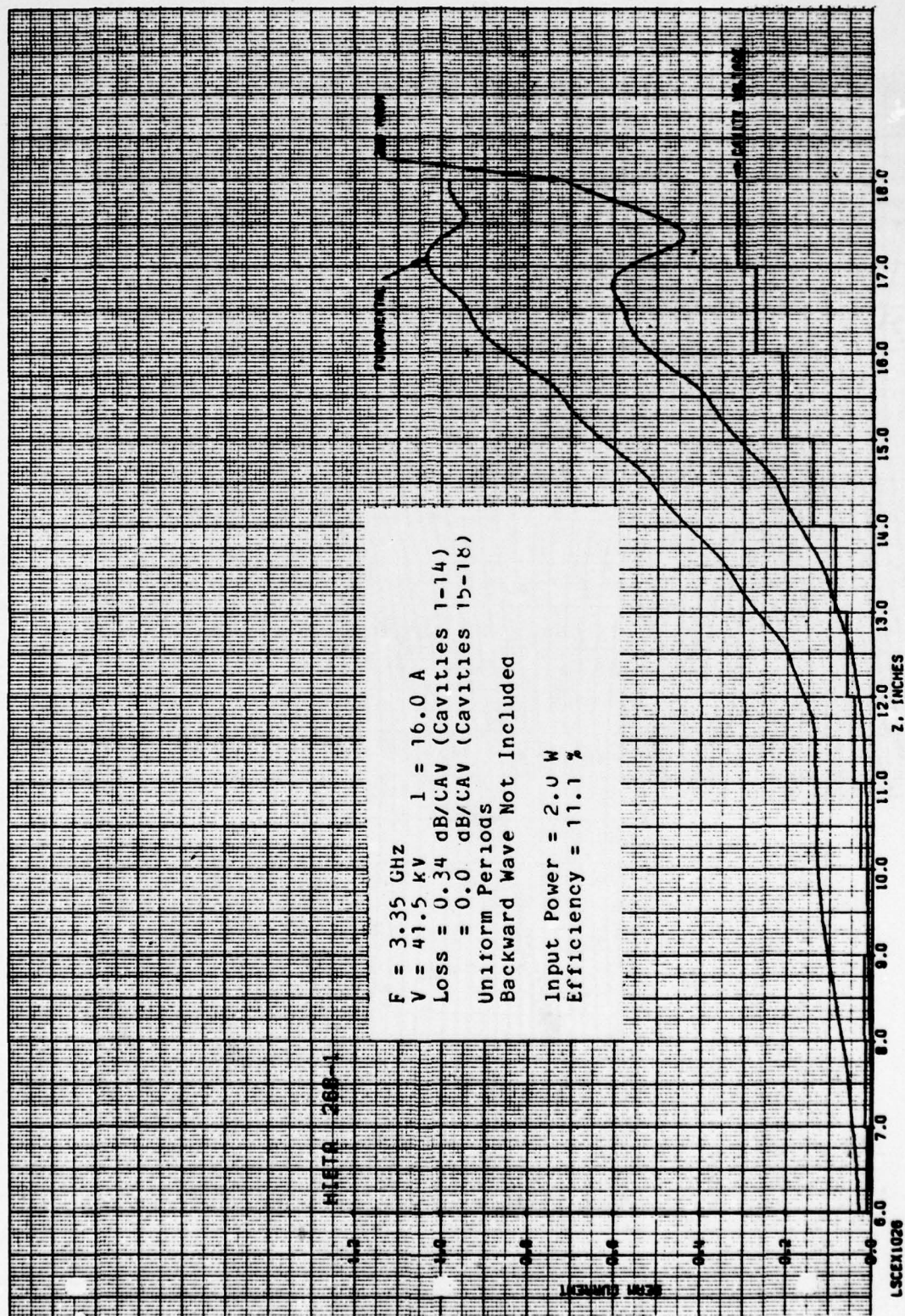


FIGURE 5.10 COMPUTED RF BEAM CURRENTS AND GAP VOLTAGES VS DISTANCE IN SIMULATED COUPLED-CAVITY TWT WITH FOUR LOSSLESS OUTPUT CAVITIES

HIETA 268-1

$F = 3.35 \text{ GHz}$
 $V = 41.5 \text{ kV}$
 $I = 16.0 \text{ A}$
 $\text{Loss} = 0.34 \text{ dB/CAV (Cavities 1-14)}$
 $= 0.0 \text{ dB/CAV (Cavities 15-18)}$
 Uniform Periods
 Backward Wave Not Included

Input Power = 2.0 W
 Efficiency = 11.1 %

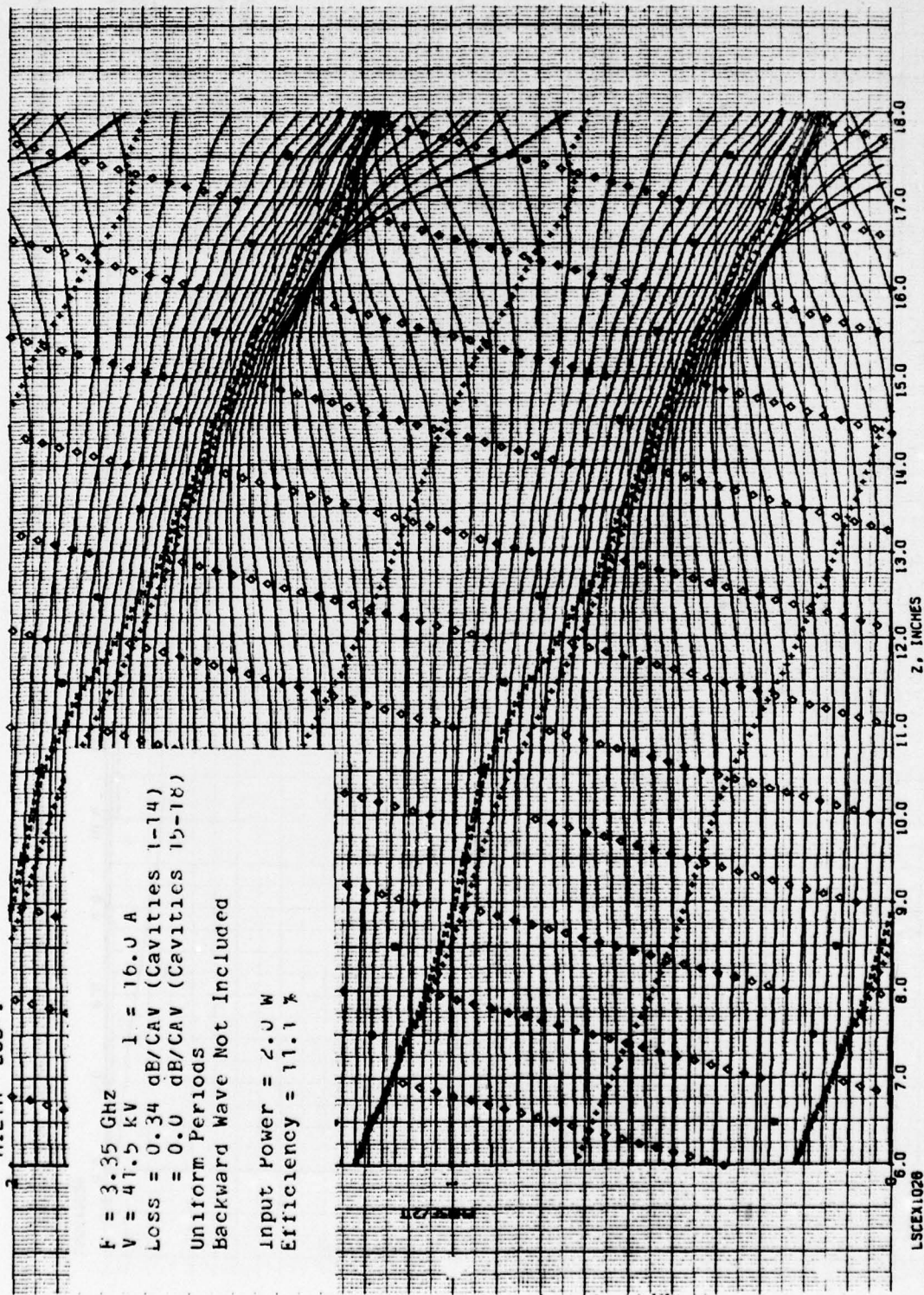


FIGURE 5.11 COMPUTED RELATIVE PHASES OF ELECTRON DISKS VS DISTANCE IN SIMULATED COUPLED-CAVITY TWT WITH FOUR LOSSLESS OUTPUT CAVITIES

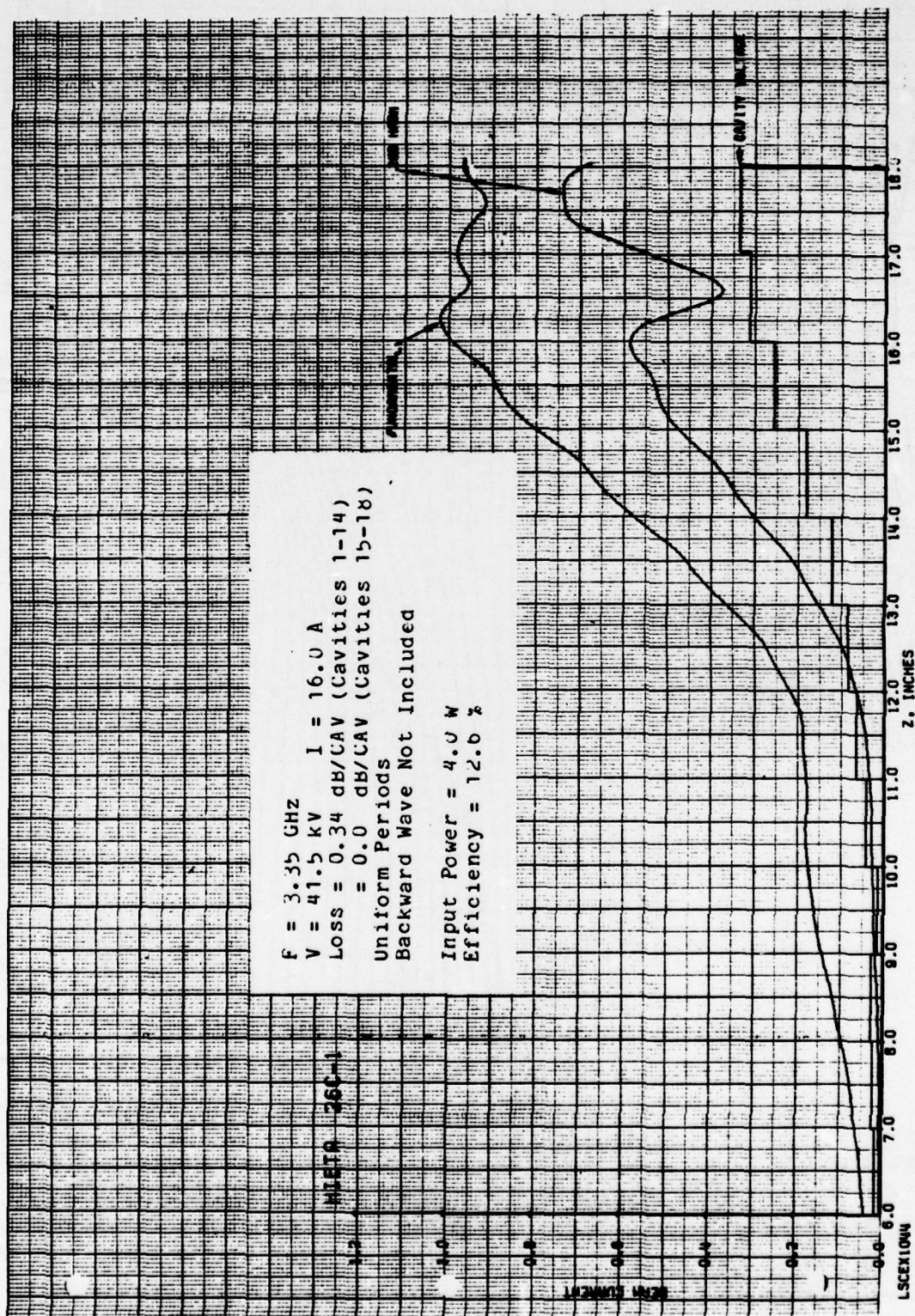


FIGURE 5.12 COMPUTED RF BEAM CURRENTS AND GAP VOLTAGES VS DISTANCE IN SIMULATED COUPLED-CAVITY TWT WITH FOUR LOSSLESS OUTPUT CAVITIES

HIEIA 26C-1

$F = 3.35 \text{ GHz}$
 $V = 41.5 \text{ kV}$
 $I = 16.0 \text{ A}$
 $\text{Loss} = 0.34 \text{ dB/CAV (Cavities 1-14)}$
 $= 0.0 \text{ dB/CAV (Cavities 15-18)}$
 Uniform Periods
 Backward Wave Not Included
 Input Power = 4.0 W
 Efficiency = 12.6 %

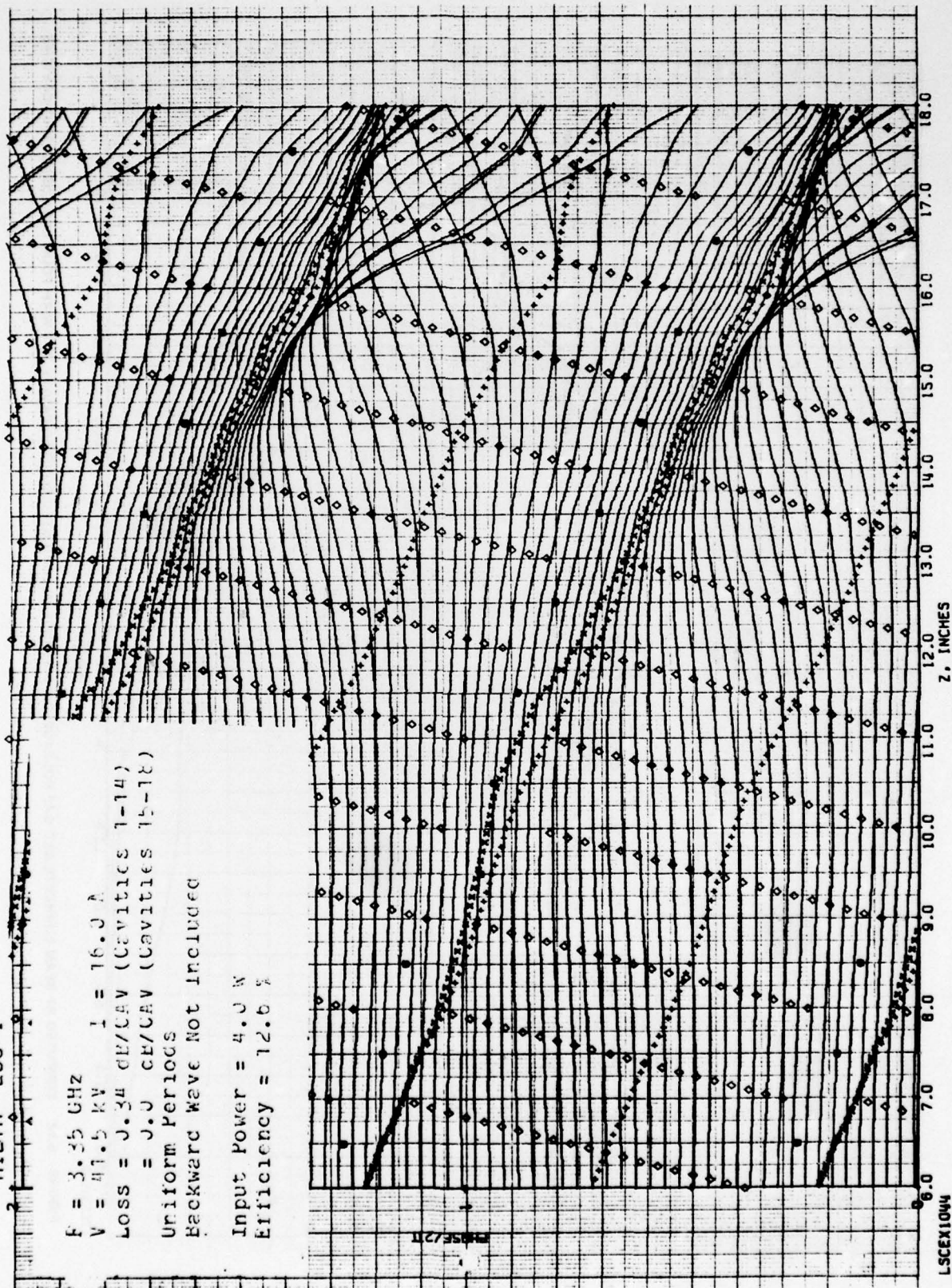


FIGURE 5.13 COMPUTED RELATIVE PHASES OF ELECTRON DISKS VS DISTANCE IN SIMULATED COUPLED-CAVITY TWT WITH FOUR LOSSLESS OUTPUT CAVITIES

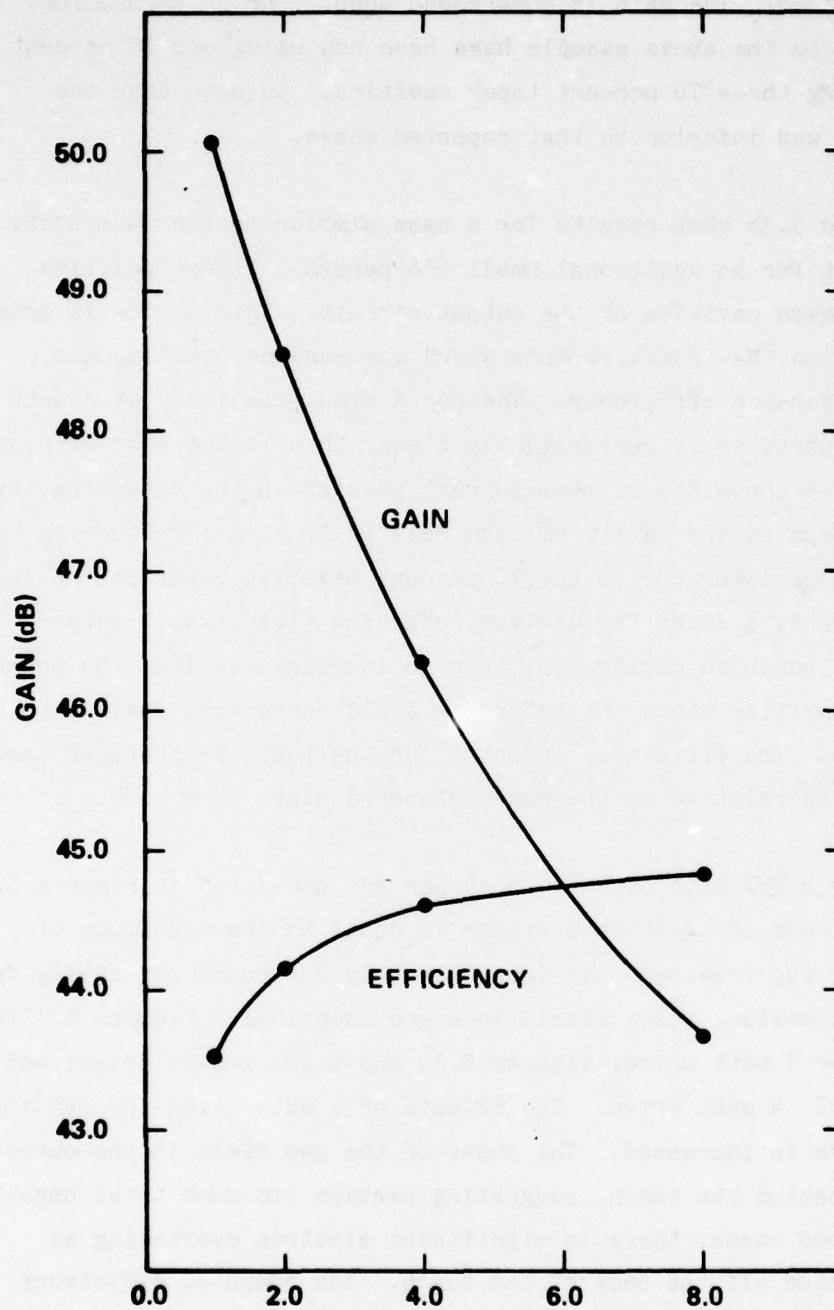


FIGURE 5.14 POWER GAIN AND CONVERSION EFFICIENCY VERSUS INPUT POWER IN SIMULATED COUPLED CAVITY TWT, WITH 4 LOSSLESS OUTPUT CAVITIES, AND FINAL 2 CAVITIES WITH DECREASED PERIOD.

without a velocity taper. The gain is compressed about 7 dB at saturation. Calculations similar to the above example have been run using one 70 percent taper cavity and using three 70 percent taper cavities. In each case the resultant efficiency was inferior to that reported above.

Figures 5.15 and 5.16 show results for a case similar to the two-cavity velocity taper except for an additional small (16 percent) linear positive taper in the first seven cavities of the output circuit. This choice is made to test the proposition that positive "pretaper" can enhance bunching and thereby increase conversion efficiency. The conversion efficiency at 1 watt drive with positive pretaper is very slightly higher than in the case with no pretaper. Figure 5.15 shows the rf beam current peaking in the output cavity, with the last two steps in the cavity voltage relatively large; reflecting the effective extraction of power due to the 70 percent negative taper in the least two cavities. Figure 5.16 shows the maximum retarding field (small square) to be in phase with the bunch in cavity ten, then to increasingly lead the bunch until the last two cavities where the retarding field comes once again into phase with the bunch. The efficiency computed for the positive pretaper case is negligibly improved relative to the non-pretapered case.

The results for a TWT with negative pretaper are presented in Figures 5.17 and 5.22. The magnitude of negative pretaper is equal to the magnitude of positive pretaper in the previous case (approximately 2 percent per cavity for seven cavities). Otherwise, these simulations are identical. Figures 5.17 and 5.18 show results for 1 watt drive; Figures 5.19 and 5.20, 2 watt drive; and Figures 5.21 and 5.22, 4 watt drive. The effects of a saturation are readily apparent as the drive is increased. The phase of the gap field in the output cavity is retarded behind the bunch, suggesting perhaps too much total negative taper. As in previous cases, there is significant electron overtaking as electrons are reflected off the back of the bunch. The computed efficiency with 4 watt drive is 23.9 percent compared to 25 percent for the non-pretapered case (Figure 7-7). This difference is not thought to be significant.

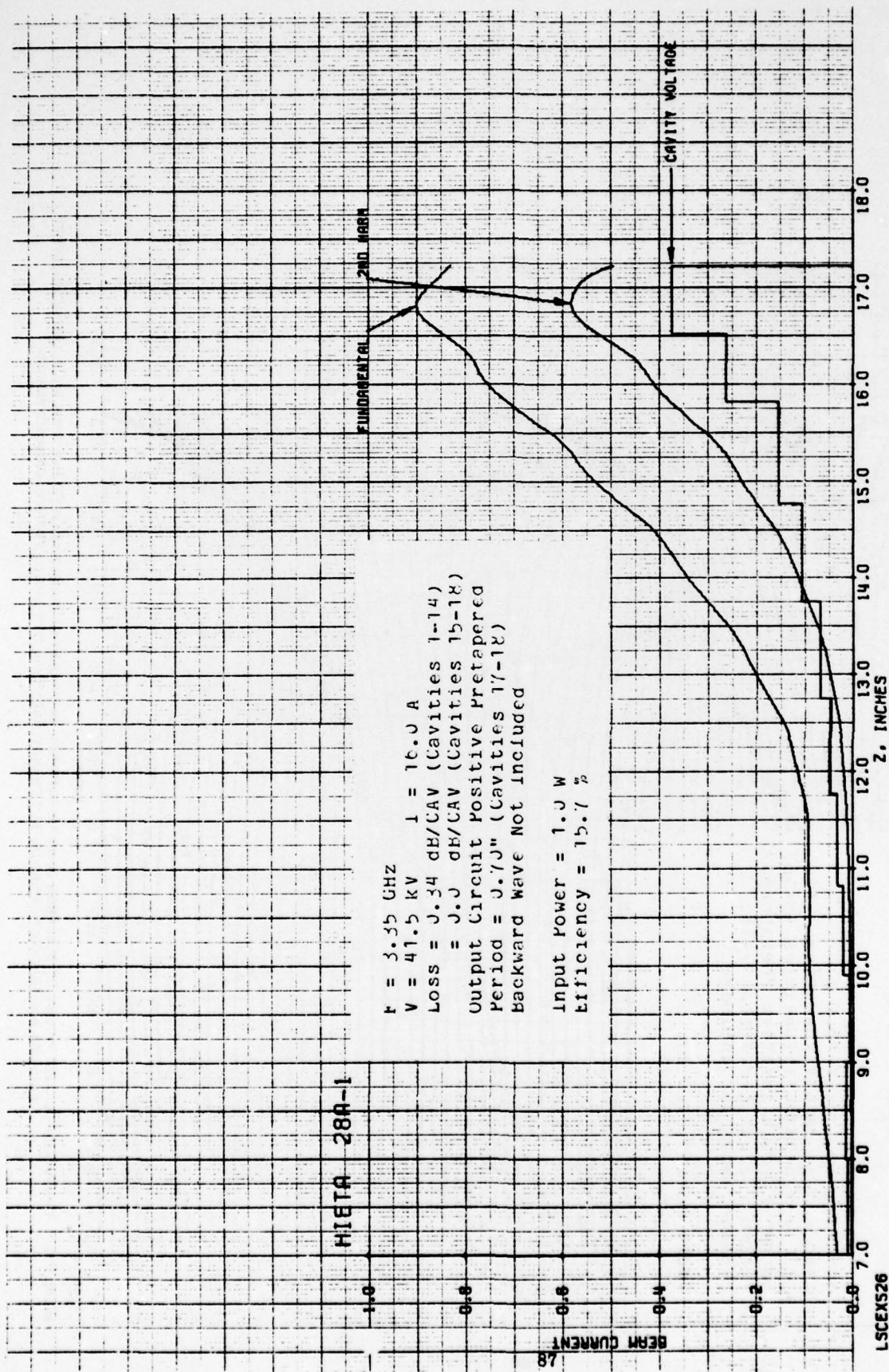


FIGURE 5.15 COMPUTED RF BEAM CURRENTS AND GAP VOLTAGES VS DISTANCE IN SIMULATED COUPLED-CAVITY TWT WITH FOUR LOSSLESS OUTPUT CAVITIES, POSITIVE PRETAPERED OUTPUT CIRCUIT, AND FINAL TWO CAVITIES WITH DECREASED PERIODS

THIS PAGE IS BEST QUALITY PRINTING
 FROM COPY FURNISHED TO DDO

MIETA 28A-1

$f = 3.35$ GHz
 $V = 41.5$ kV
 $I = 16.0$ A
 $\text{Loss} = 0.34$ dB/CAV (Cavities 1-14)
 $\text{Loss} = 0.0$ dB/CAV (Cavities 15-18)
 Output Circuit Positive Pretapered
 Period = 0.70 " (Cavities 17-18)
 Backward Wave Not Included

Input Power = 1.0 W
 Efficiency = 15.7%

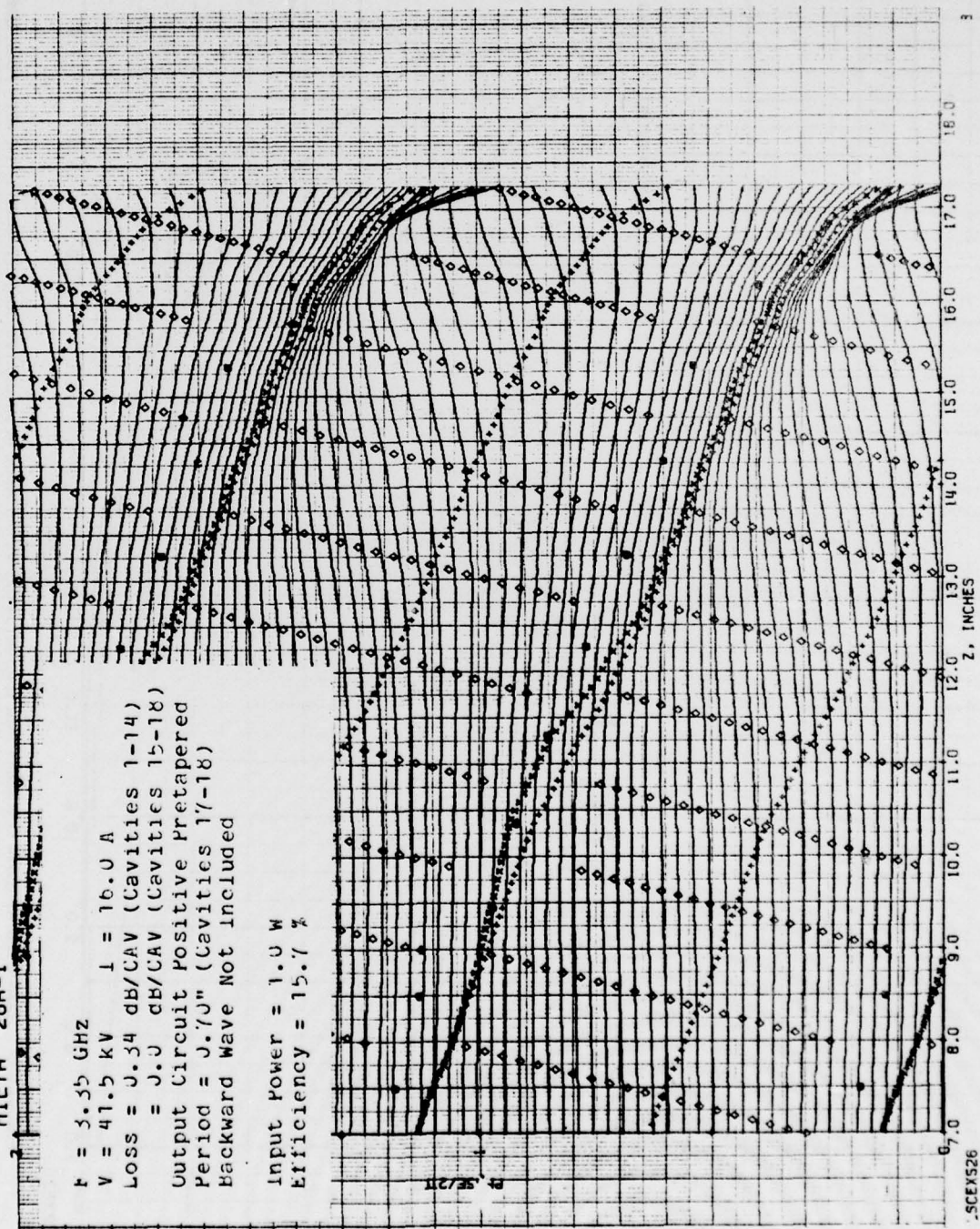


FIGURE 5.16 COMPUTED RELATIVE PHASES OF ELECTRON DISKS VS DISTANCE IN SIMULATED COUPLED-CAVITY TWT WITH FOUR LOSSLESS OUTPUT CAVITIES, POSITIVE PRETAPERED OUTPUT CIRCUIT, AND FINAL TWO CAVITIES WITH DECREASED PERIODS

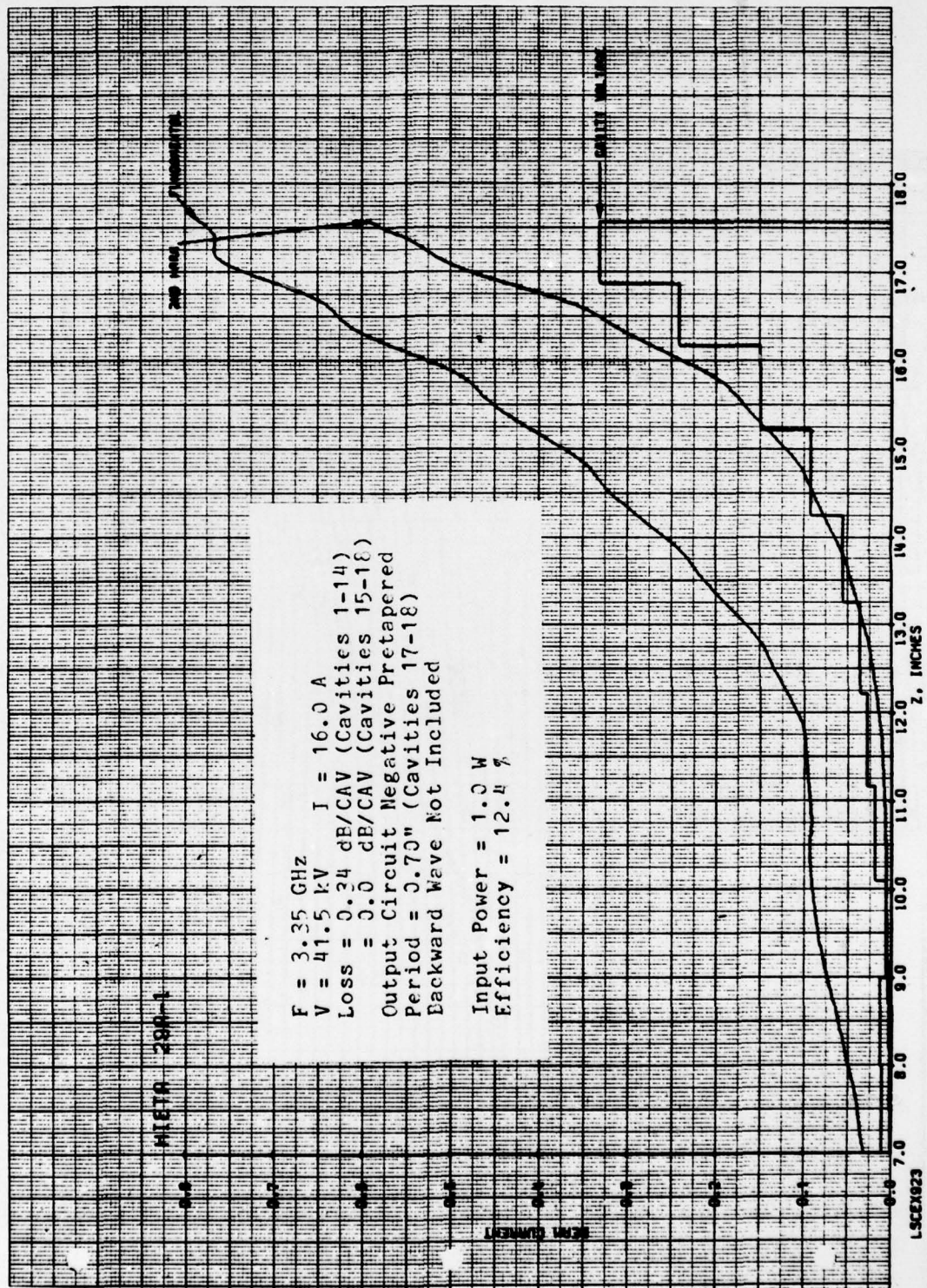


FIGURE 5.17 COMPUTED RF BEAM CURRENTS AND GAP VOLTAGES VS DISTANCE IN SIMULATED COUPLED-DAVITY TWT WITH FOUR LOSSLESS OUTPUT CAVITIES, NEGATIVE PRETAPERED OUTPUT CIRCUIT, AND FINAL TWO CAVITIES WITH DECREASED PERIODS

MIETA 29A-1

$F = 3.35 \text{ GHz}$
 $V = 41.5 \text{ kV}$ $I = 16.0 \text{ A}$
 $\text{Loss} = 0.34 \text{ dB/CAV (Cavities 1-14)}$
 $\quad = 0.0 \text{ dB/CAV (Cavities 15-18)}$
 $\text{Output Circuit Negative Pretapered}$
 $\text{Period} = 0.70'' \text{ (Cavities 17-18)}$
 $\text{Backward Wave Not Included}$

$\text{Input Power} = 1.0 \text{ W}$
 $\text{Efficiency} = 12.4 \%$

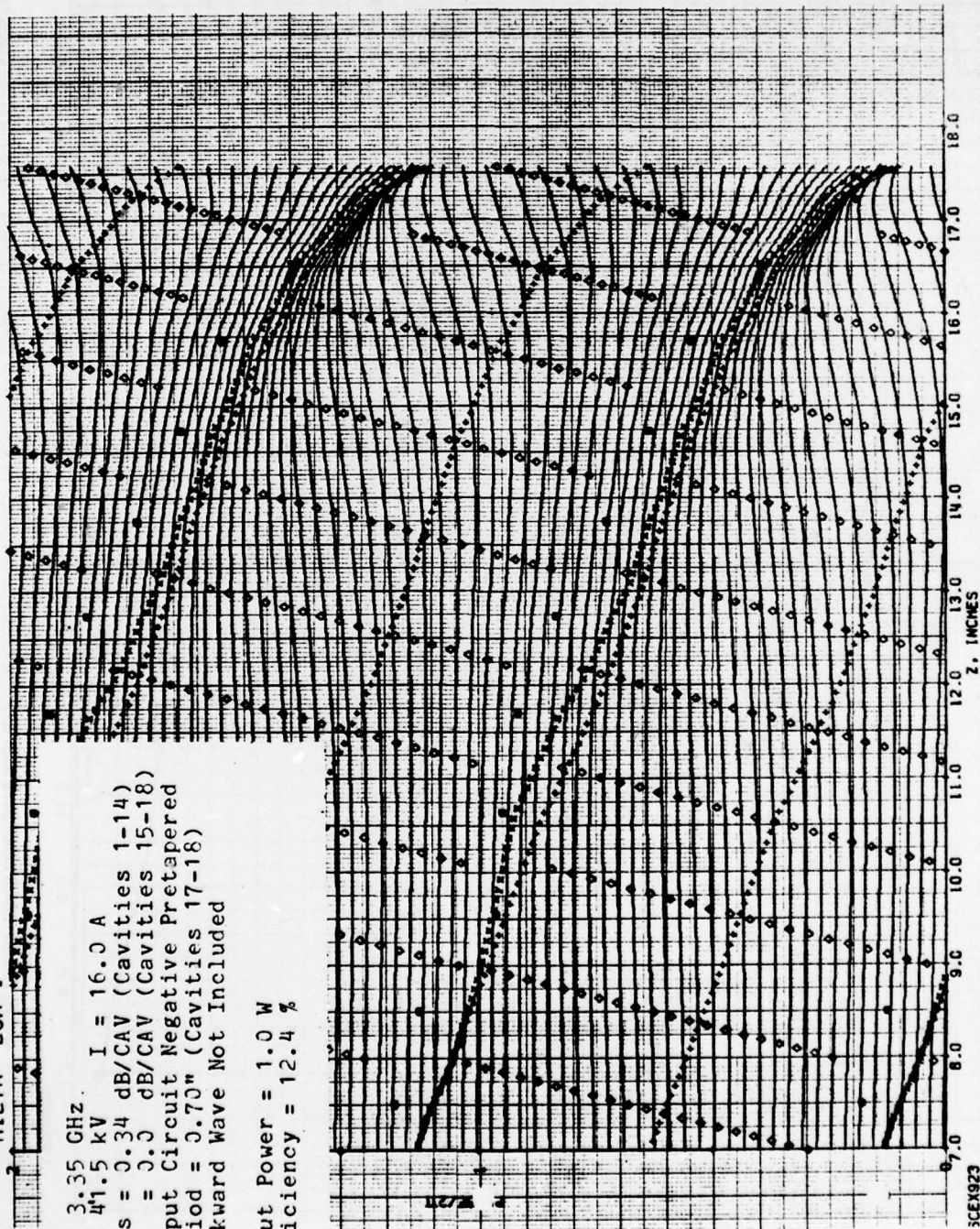


FIGURE 5.18 COMPUTED RELATIVE PHASES OF ELECTRON DISKS VS DISTANCE IN SIMULATED COUPLED-DAVITY TWT WITH FOUR LOSSLESS OUTPUT CAVITIES, NEGATIVE PRETAPERED OUTPUT CIRCUIT, AND FINAL TWO CAVITIES WITH DECREASED PERIODS

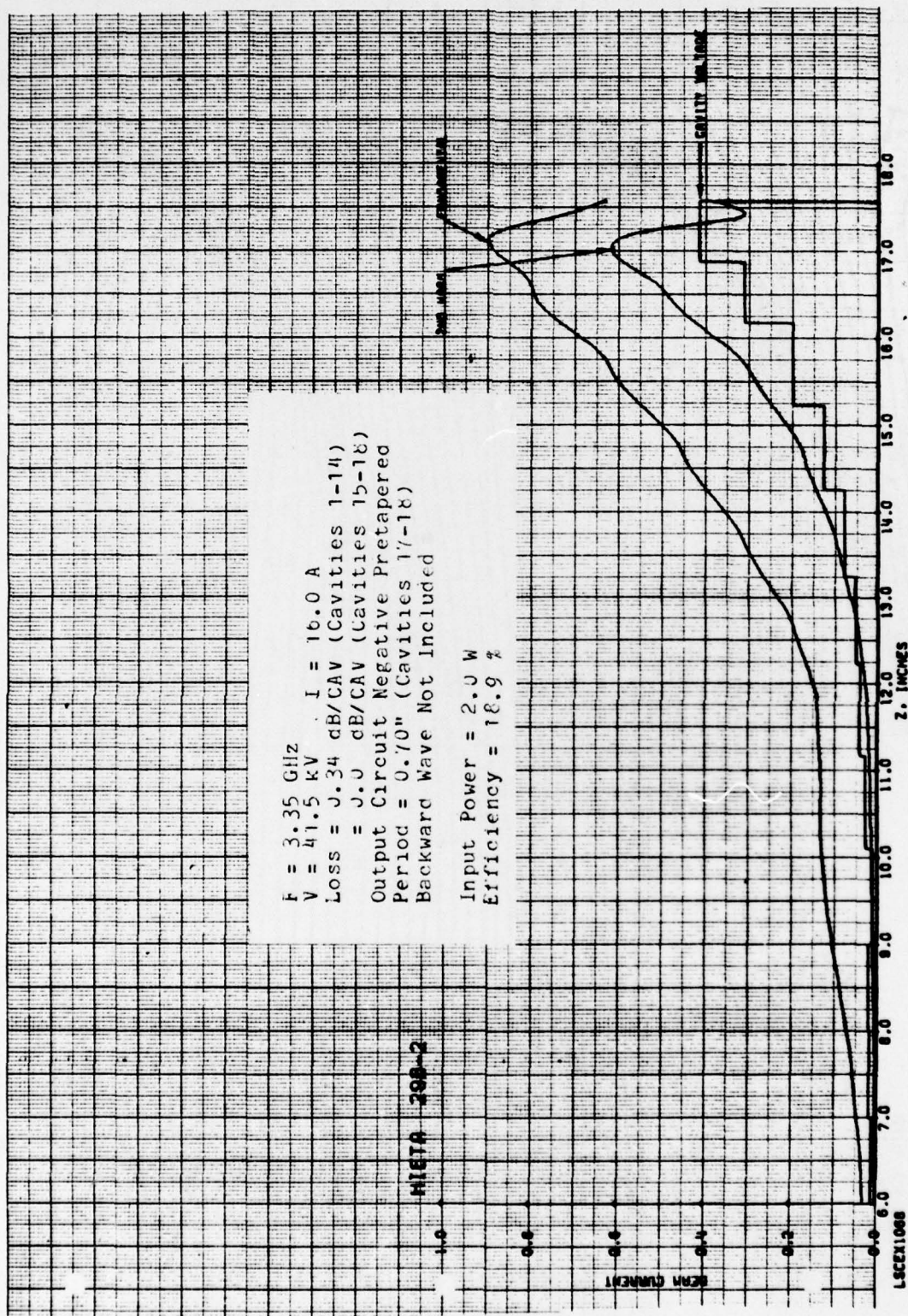


FIGURE 5.19 COMPUTED RF BEAM CURRENTS AND GAP VOLTAGES VS DISTANCE IN SIMULATED COUPLED-CAVITY TWT WITH FOUR LOSSLESS OUTPUT CAVITIES, NEGATIVE PRETAPERED OUTPUT CIRCUIT, AND FINAL TWO CAVITIES WITH DECREASED PERIODS

HIETA 29B-2

$F = 3.35 \text{ GHz}$
 $V = 41.5 \text{ kV}$
 $I = 16.0 \text{ A}$
 $\text{Loss} = 0.34 \text{ dB/CAV. (Cavities 1-14)}$
 $= 0.0 \text{ dB/CAV. (Cavities 15-18)}$
 $\text{Output Circuit Negative Pretapered}$
 $\text{Period} = 0.70'' \text{ (Cavities 17-18)}$
 $\text{Backward Wave Not Included}$

$\text{Input Power} = 2.0 \text{ W}$
 $\text{Efficiency} = 18.9\%$

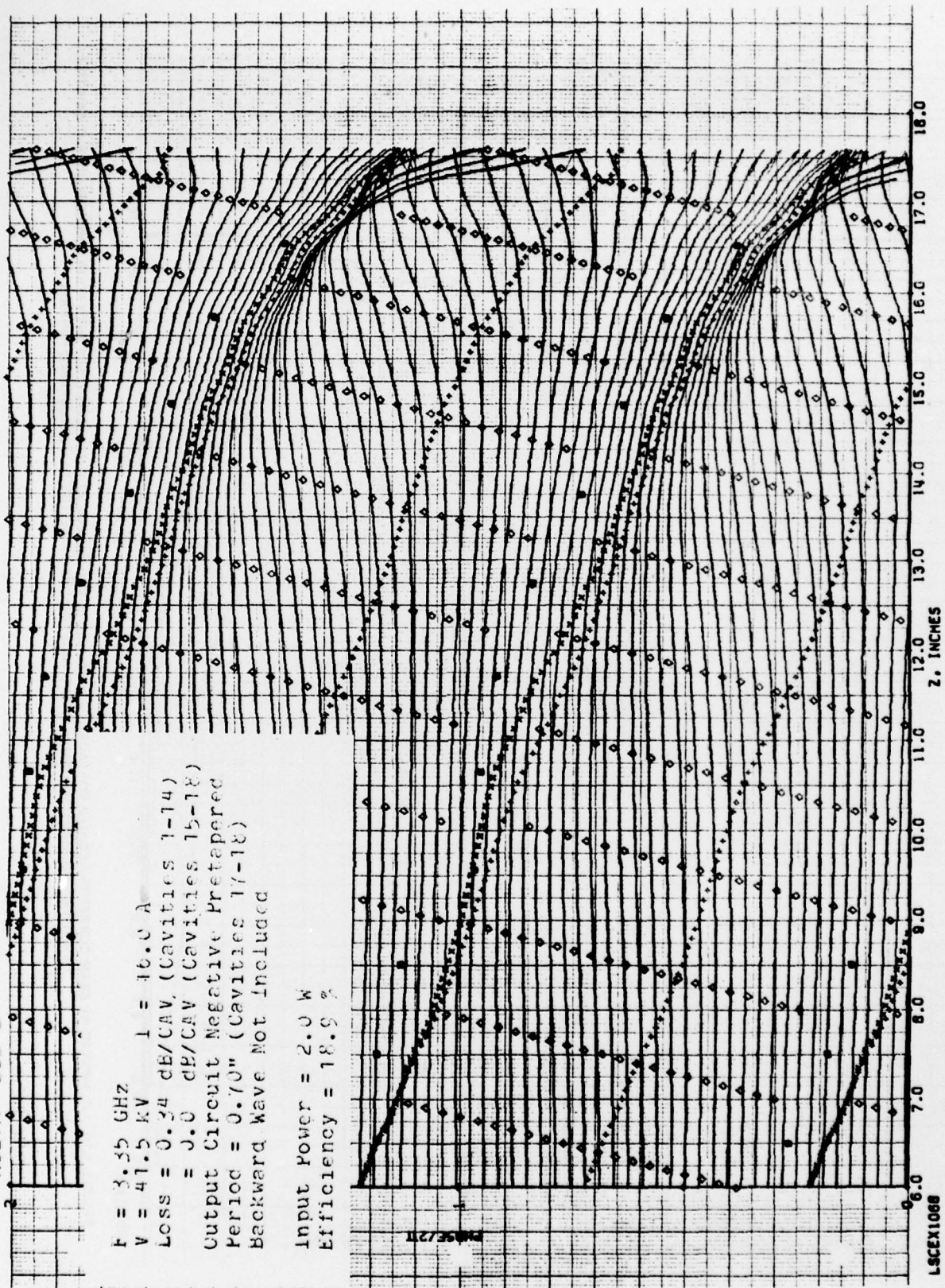


FIGURE 5.20 COMPUTED RELATIVE PHASES OF ELECTRON DISKS VS DISTANCE IN SIMULATED COUPLED-CAVITY TWT WITH FOUR LOSSLESS OUTPUT CAVITIES, NEGATIVE PRETAPERED OUTPUT CIRCUIT, AND FINAL TWO CAVITIES WITH DECREASED PERIODS

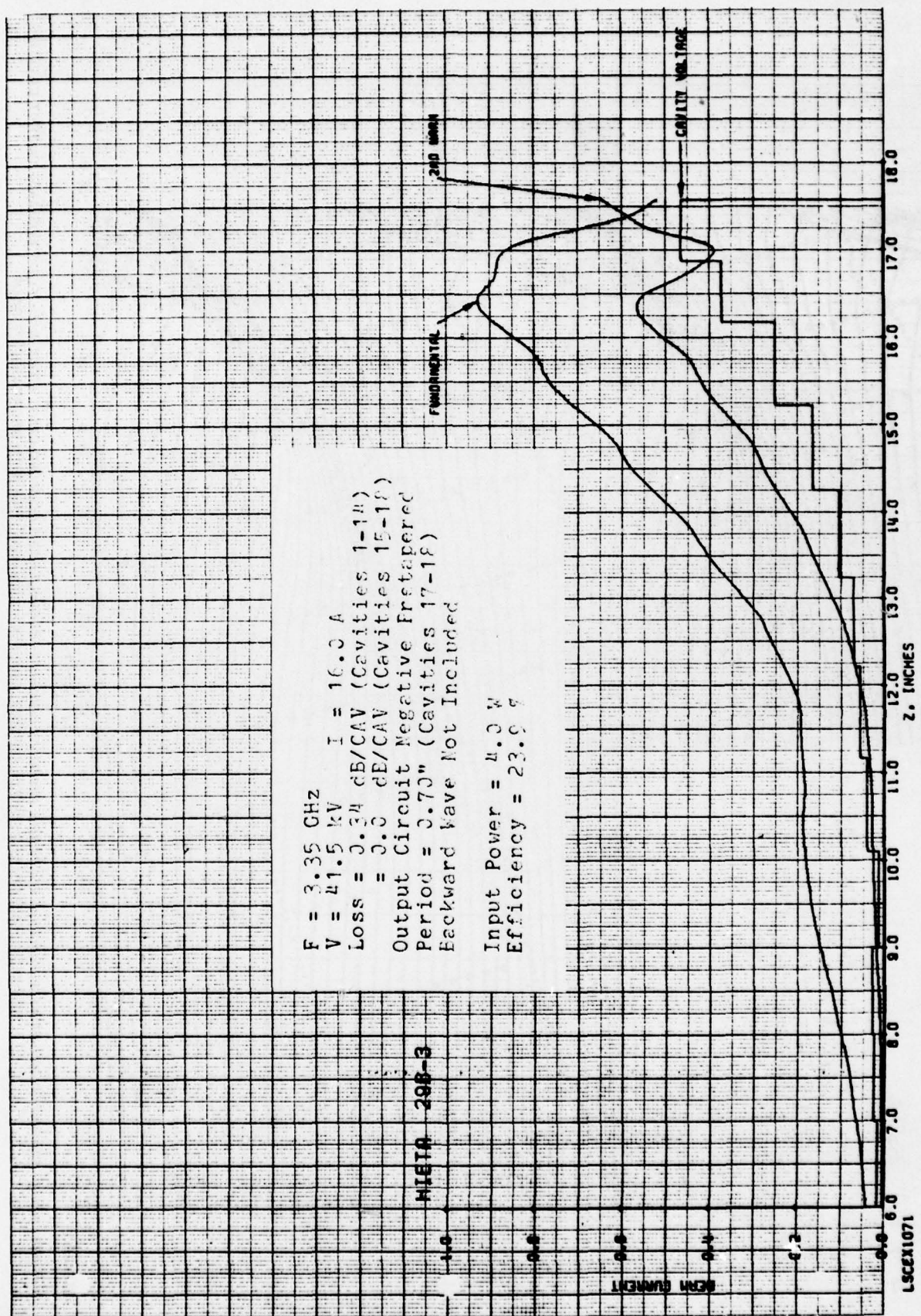


FIGURE 5.21 COMPUTED RF BEAM CURRENTS AND GAP VOLTAGES VS DISTANCE IN SIMULATED COUPLED-CAVITY TWT WITH FOUR LOSSLESS OUTPUT CAVITIES, NEGATIVE PRE-TAPERED OUTPUT CIRCUIT, AND FINAL TWO CAVITIES WITH DECREASED PERIODS

HIETA 29B-3

$F = 3.35 \text{ CHz}$
 $V = 41.5 \text{ KV}$
 $I = 16.0 \text{ A}$
 $\text{Loss} = 0.34 \text{ dB/CAV (Cavities 1-14)}$
 $\text{Loss} = 0.3 \text{ dB/CAV (Cavities 15-16)}$
 $\text{Output Circuit Negative Preapered}$
 $\text{Period} = 0.70'' \text{ (Cavities 17-18)}$
 $\text{Backward Wave Not Included}$

$\text{Input Power} = 4.0 \text{ W}$
 $\text{Efficiency} = 23.6\%$

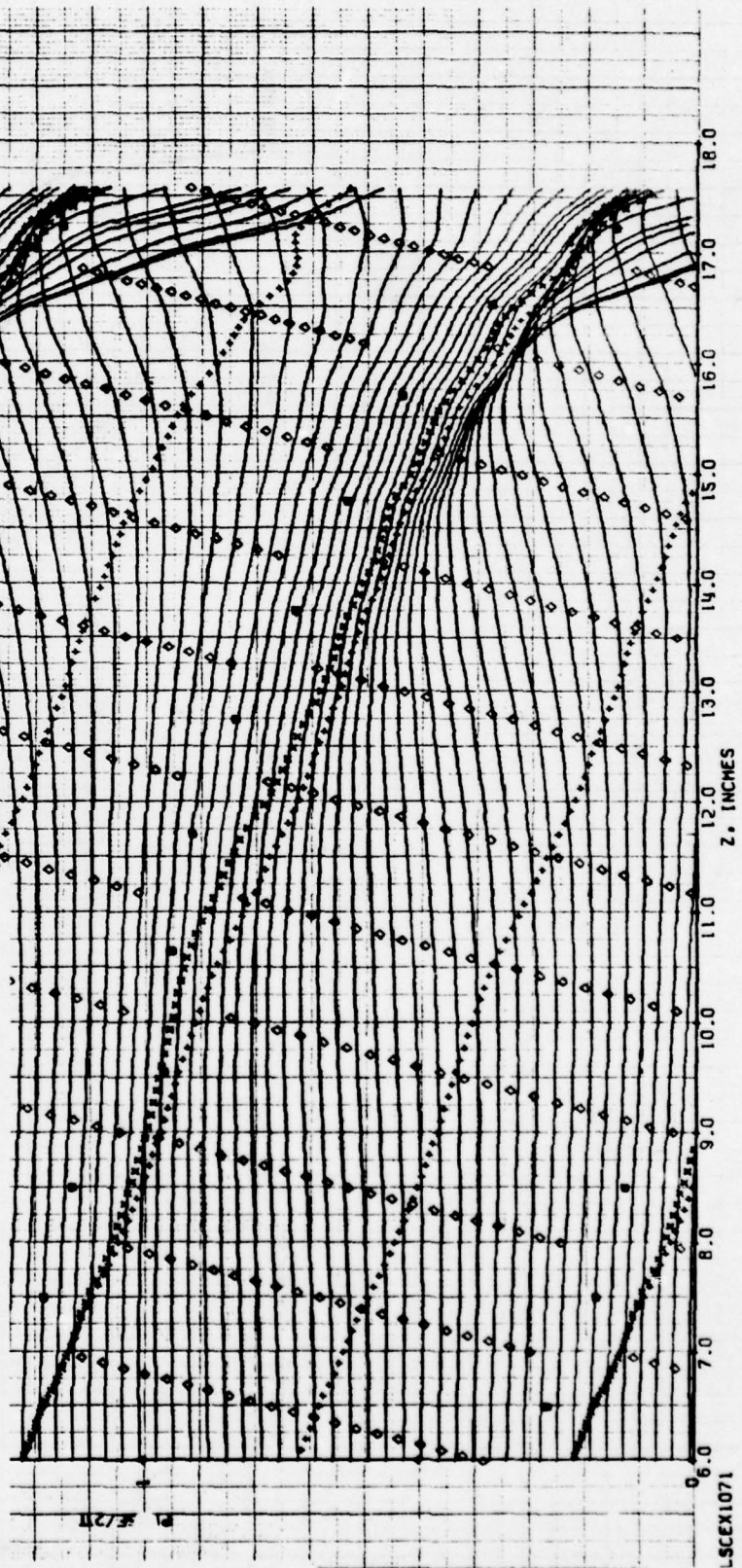


FIGURE 5.22 COMPUTED RELATIVE PHASES OF ELECTRON DISKS VS DISTANCE IN SIMULATED COUPLED-CAVITY TWT WITH FOUR LOSSLESS OUTPUT CAVITIES, NEGATIVE PREAPERED OUTPUT CIRCUIT, AND FINAL TWO CAVITIES WITH DECREASED PERIODS

The case illustrated in Figures 5.23 and 5.24 was run to demonstrate the effect of reduction of dc beam current. This case is identical to that illustrated by Figures 5.8 and 5.9 except that the beam current has been reduced by 10 percent. This reduction in beam current produced a negligible change in conversion efficiency at the 1 watt drive level. One expects a reduction in efficiency with reduced beam current at fixed drive power because of the reduction in gain. The fact that the efficiency did not decline is encouraging.

5.3 Backward-Wave Effects in the Output Circuit Section

Figures 5.25 and 5.26 show the computed performance of a TWT which is identical to the TWT simulation of Figures 5.3 and 5.1 except that the backward-wave is included and is seen to yield non-monotonic gap voltages and the phases of the gap fields are seen to fluctuate more or less randomly. In spite of these apparent defects, the maximum fundamental current is larger than that calculated for the non backward-wave circuit.

Figure 5.26 shows the gap voltage in cavity 13 ($Z = 12.5$) to be advanced in phase and that in cavity 14 ($Z = 13.5$) to be retarded relative to the ideal phase for small-signal bunching. To test whether a local perturbation can materially affect bunching, the thirteenth cavity was lengthened by 30 percent and the fourteenth cavity was shortened by 30 percent in the hope that the gap fields in these cavities would be brought closer in phase to their ideal values. The results of this computation are shown in Figures 5.27 and 5.28. The gap voltages are still non-monotonic. The phase in gap 13 is nearer the ideal value but the phase in gap 14 is even farther advanced than in the previous example. However, this perturbation has yielded a small increase in rf beam current.

Figures 5.29 and 5.30 show what happens if cavities 13 and 14 are reversed relative to the previous case. As anticipated, the bunching suffers from this change; the normalized fundamental current falls from 1.04 to 0.94.

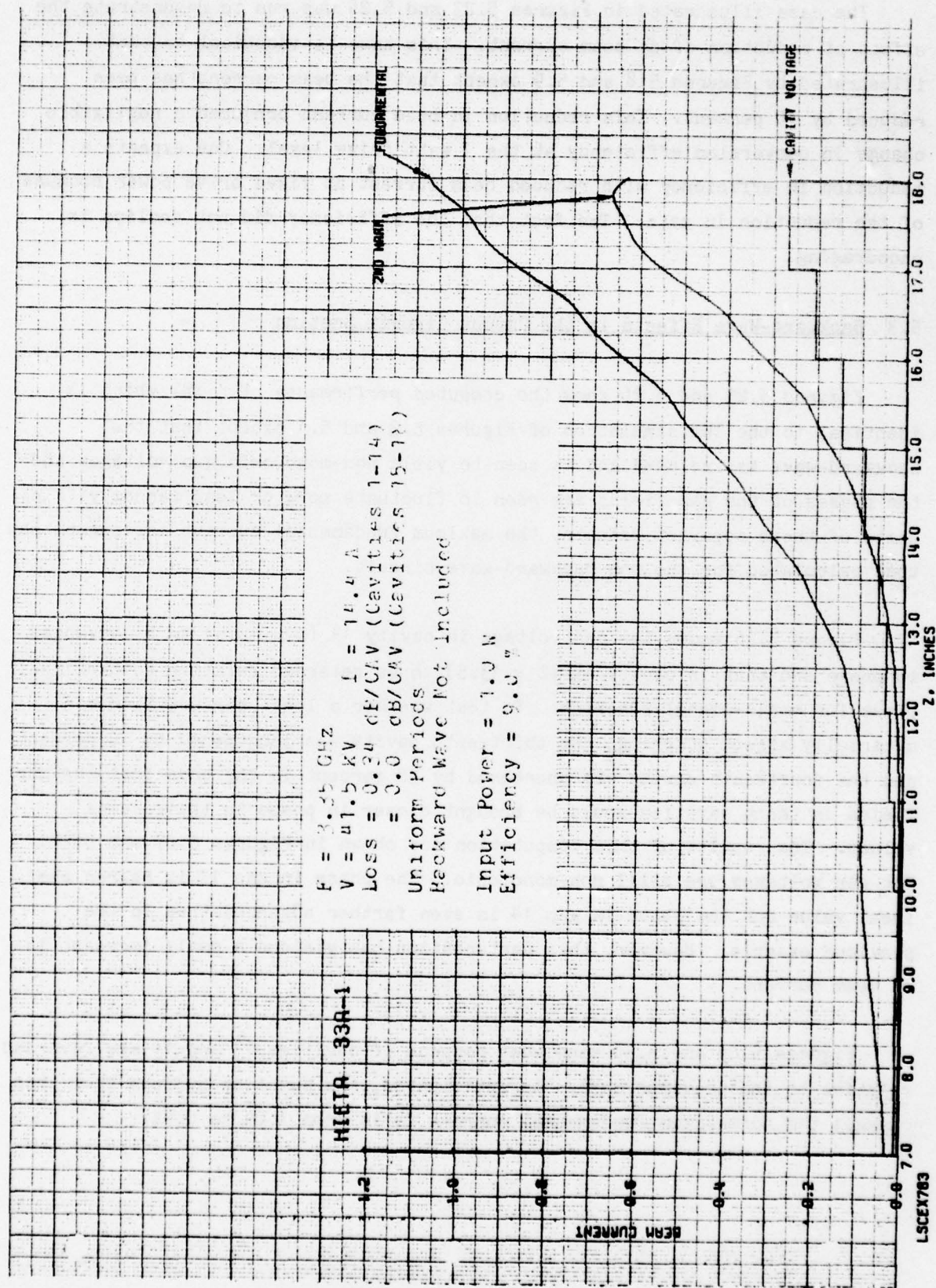


FIGURE 5.23 COMPUTED RF BEAM CURRENTS AND GAP VOLTAGES VS DISTANCE IN SIMULATED COUPLED-CAVITY TWT WITH FOUR LOSSLESS OUTPUT CAVITIES

HIETA 33A-1

$F = 3.35 \text{ GHz}$
 $V = 41.5 \text{ kV}$
 $I = 14.4 \text{ A}$
 $\text{Loss} = 0.34 \text{ dB/CAV (Cavities 1-14)}$
 $= 0.0 \text{ dB/CAV (Cavities 15-18)}$
 Uniform Periods
 Backward Wave Not Included

Input Power = 1.0 W
 Efficiency = 9.0 %

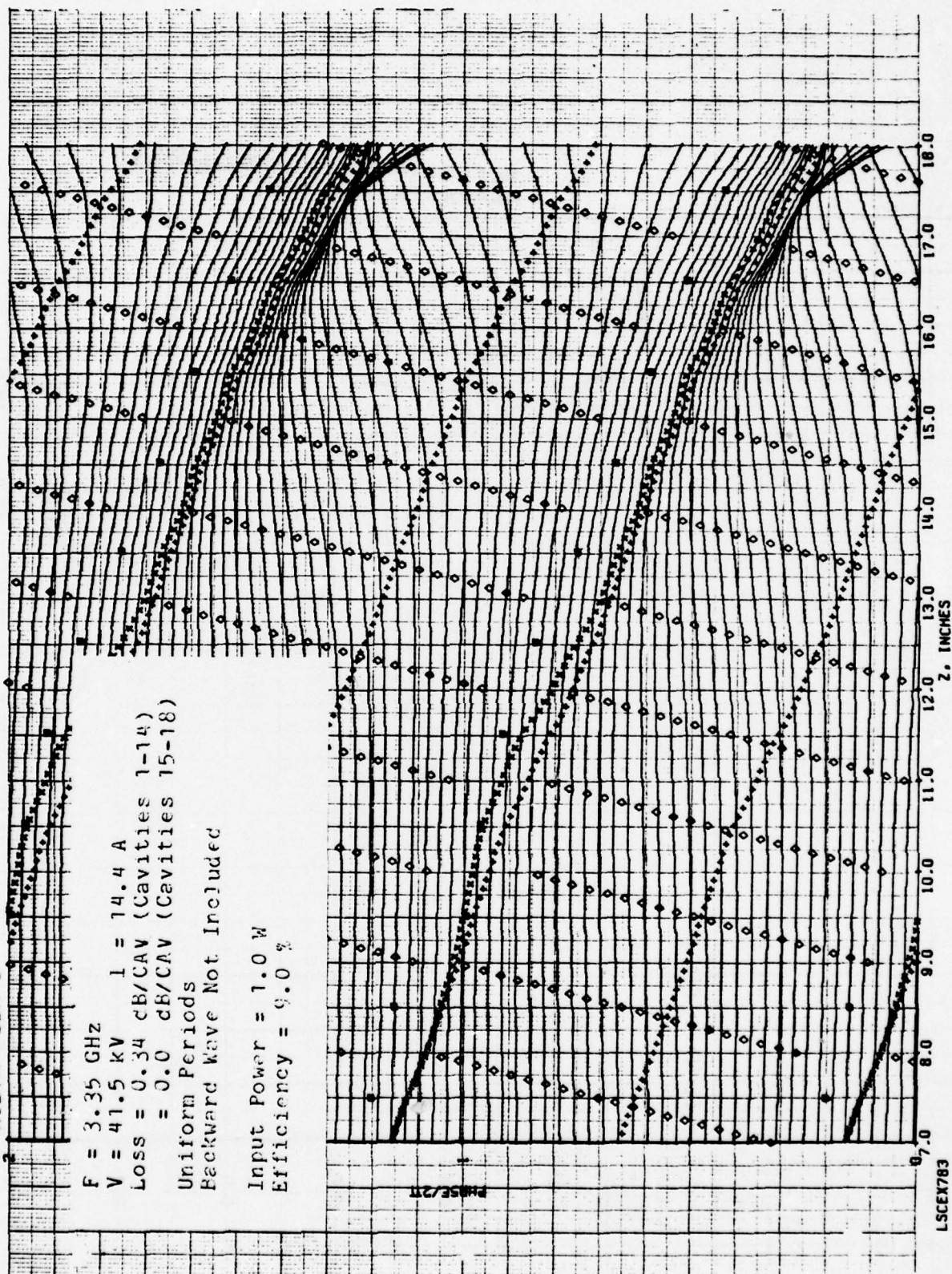


FIGURE 5.24 COMPUTED RELATIVE PHASES OF ELECTRON DISKS VS DISTANCE IN SIMULATED COUPLED-CAVITY TWT WITH FOUR LOSSLESS OUTPUT CAVITIES

THIS PAGE IS BEST QUALITY REPRODUCTION
FROM COPY FURNISHED TO DDC

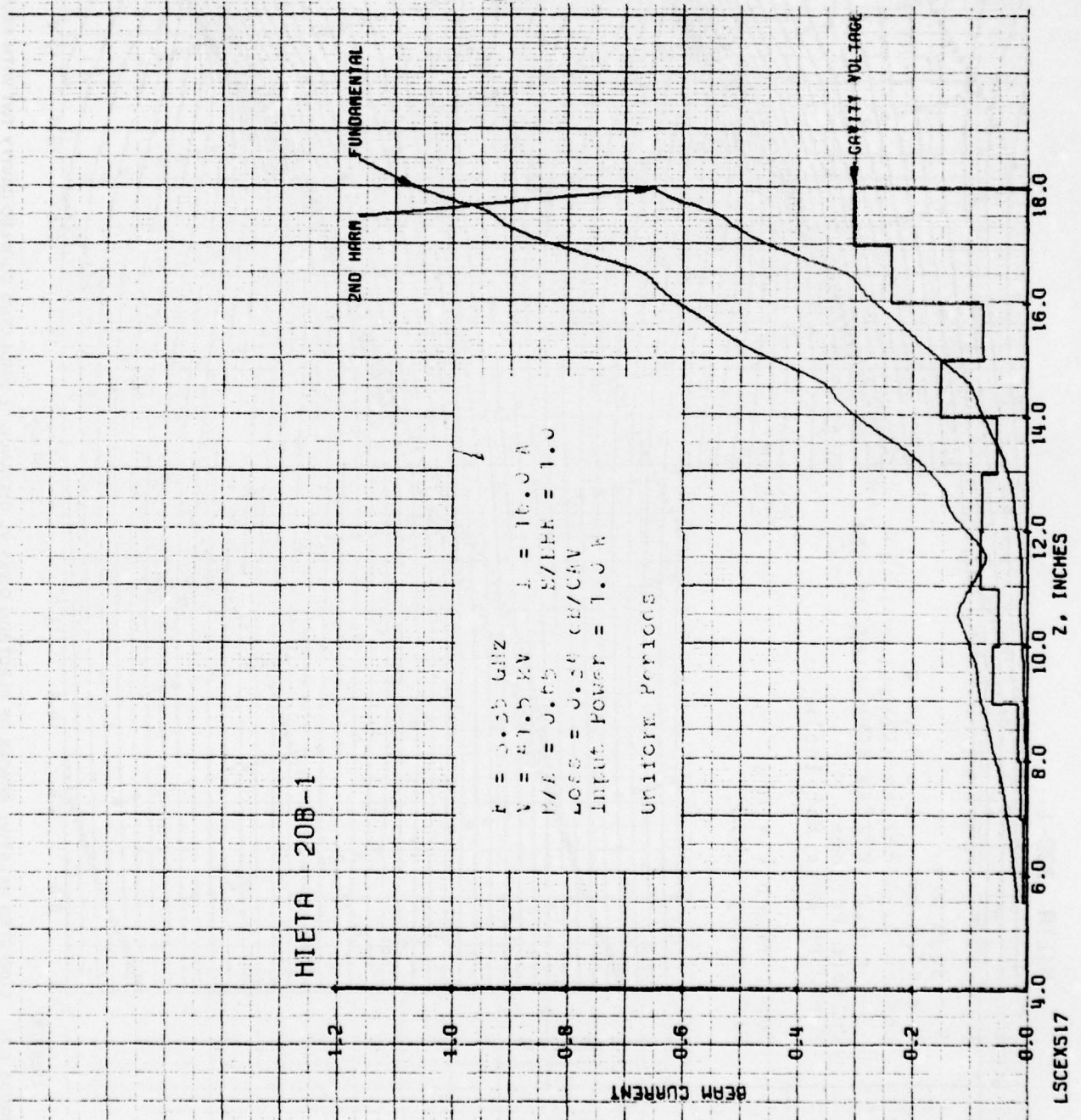


FIGURE 5.25 COMPUTED RF BEAM CURRENTS AND GAP VOLTAGES VS DISTANCE IN SIMULATED COUPLED-CAVITY TWT WITH UNIFORM PERIODS

HIETA 20B-1

$f = 3.35 \text{ GHz}$
 $V = 41.5 \text{ kV}$
 $I = 16.0 \text{ A}$
 $B/A = 0.05$
 $H/PER = 1.0$
 $LOSS = 0.34 \text{ CE/CAV}$
 $Input \text{ Power} = 1.0 \text{ W}$

Uniform Periods

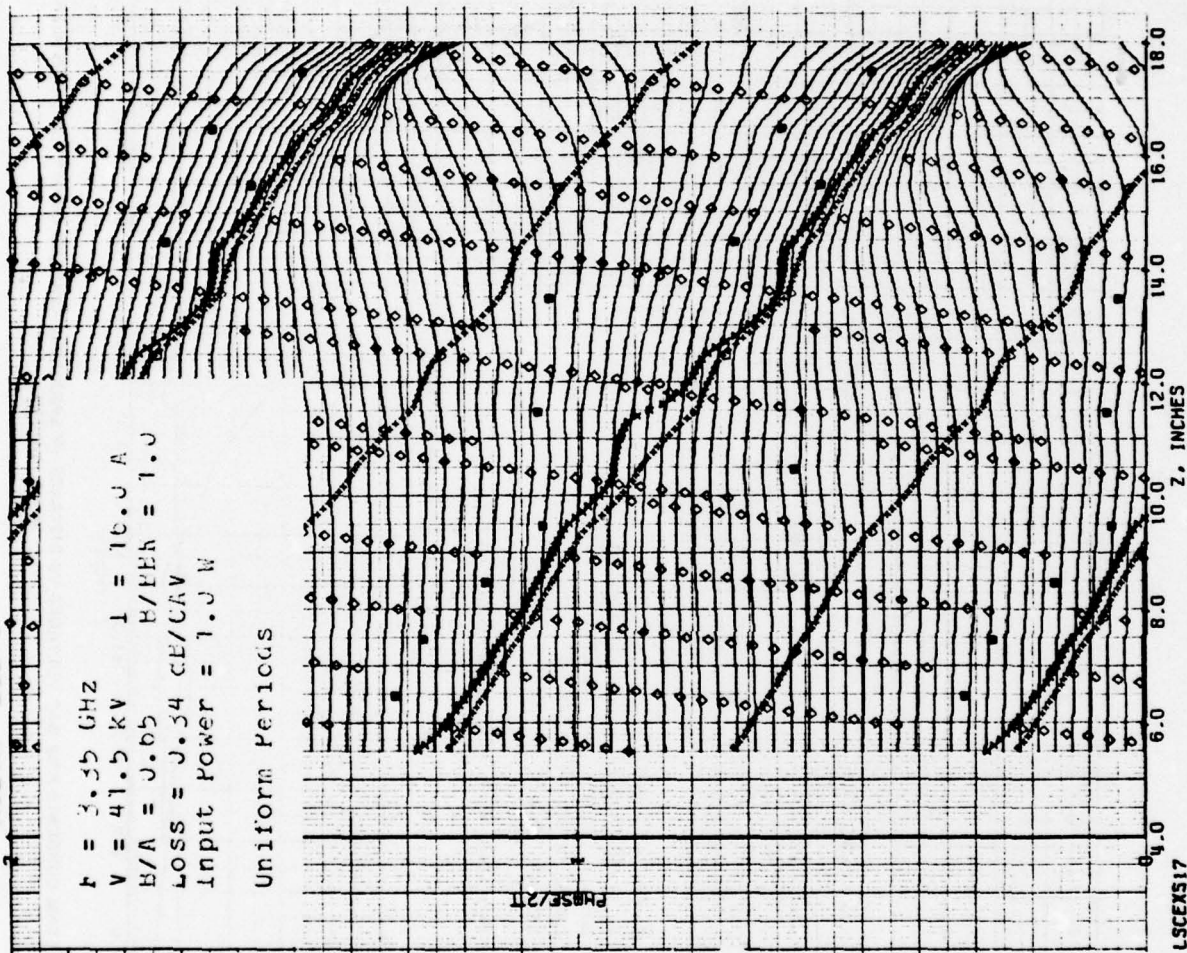


FIGURE 5.26 COMPUTED RELATIVE PHASES OF ELECTRON DISKS VS DISTANCE z SIMULATED COUPLED-CAVITY TWT WITH UNIFORM PERIODS

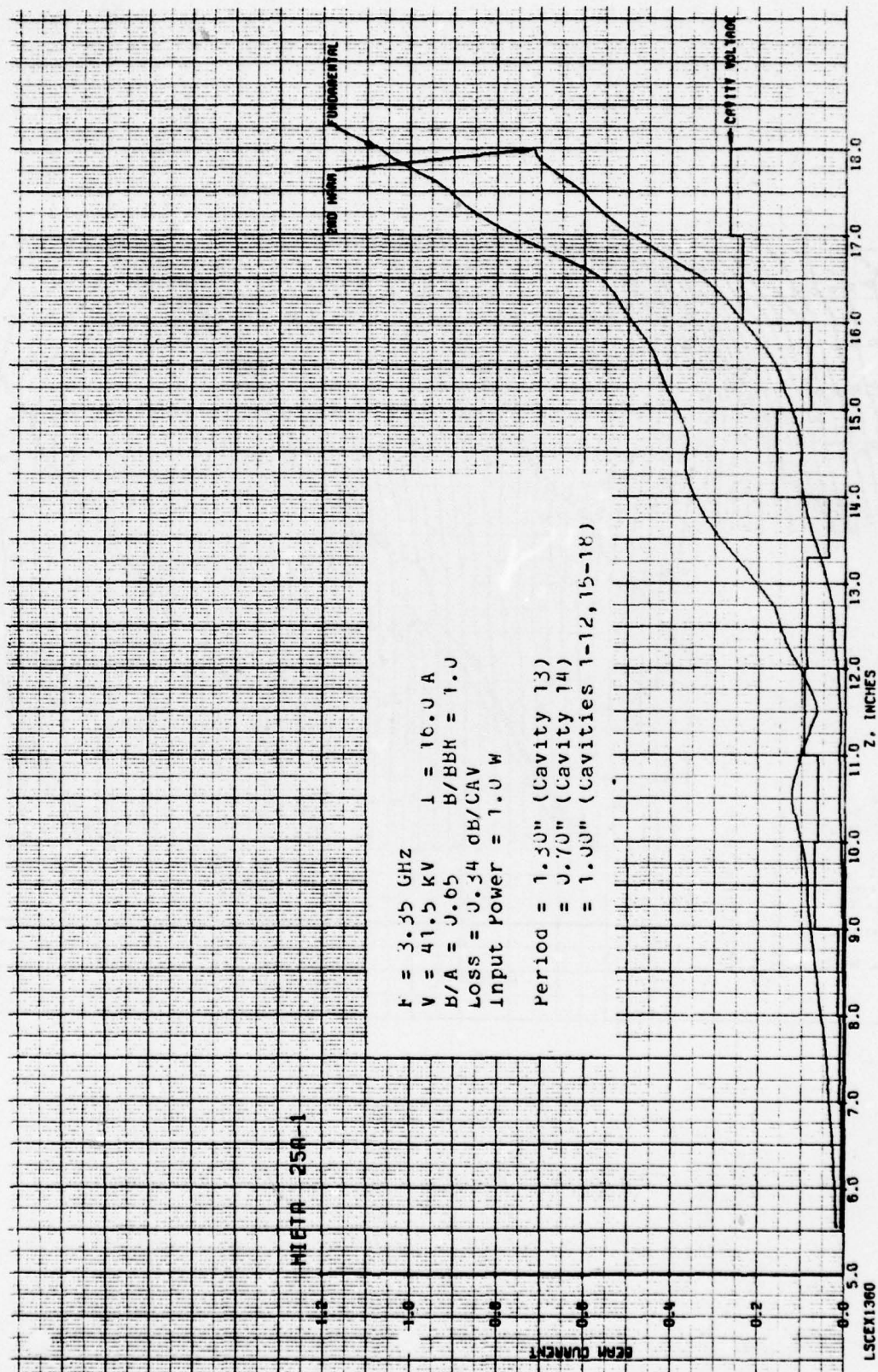


FIGURE 5.27 COMPUTED RF BEAM CURRENTS AND GAP VOLTAGES VS DISTANCE IN SIMULATED COUPLED-CAVITY TWT WITH A TWO CAVITY PERIOD MODIFICATION

HIETA 25A-1

$f = 3.55$ GHz
 $V = 41.5$ KV $I = 16.0$ A
 $B/A = 0.65$ $B/ERR = 1.0$
 $LOSS = 0.34$ dB/CAV
 $Input\ Power = 1.0$ W

Period = $1.30''$ (Cavity 13)
 $= 0.70''$ (Cavity 14)
 $= 1.00''$ (Cavities 1-12, 15-18)

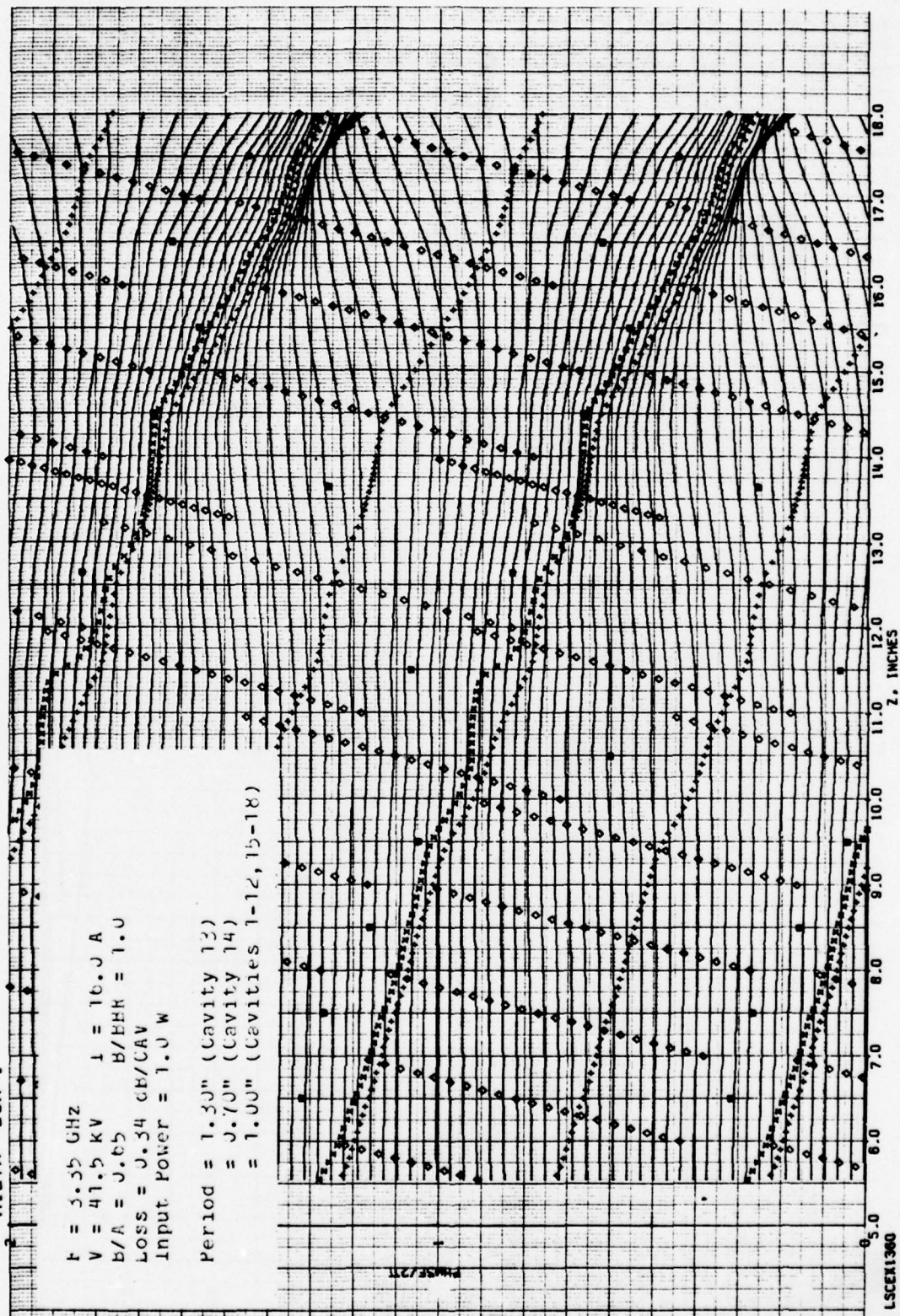


FIGURE 5.28 COMPUTED RELATIVE PHASES OF ELECTRON DISKS VS DISTANCE IN SIMULATED COUPLED-CAVITY TWT WITH A TWO-CAVITY PERIOD MODIFICATION

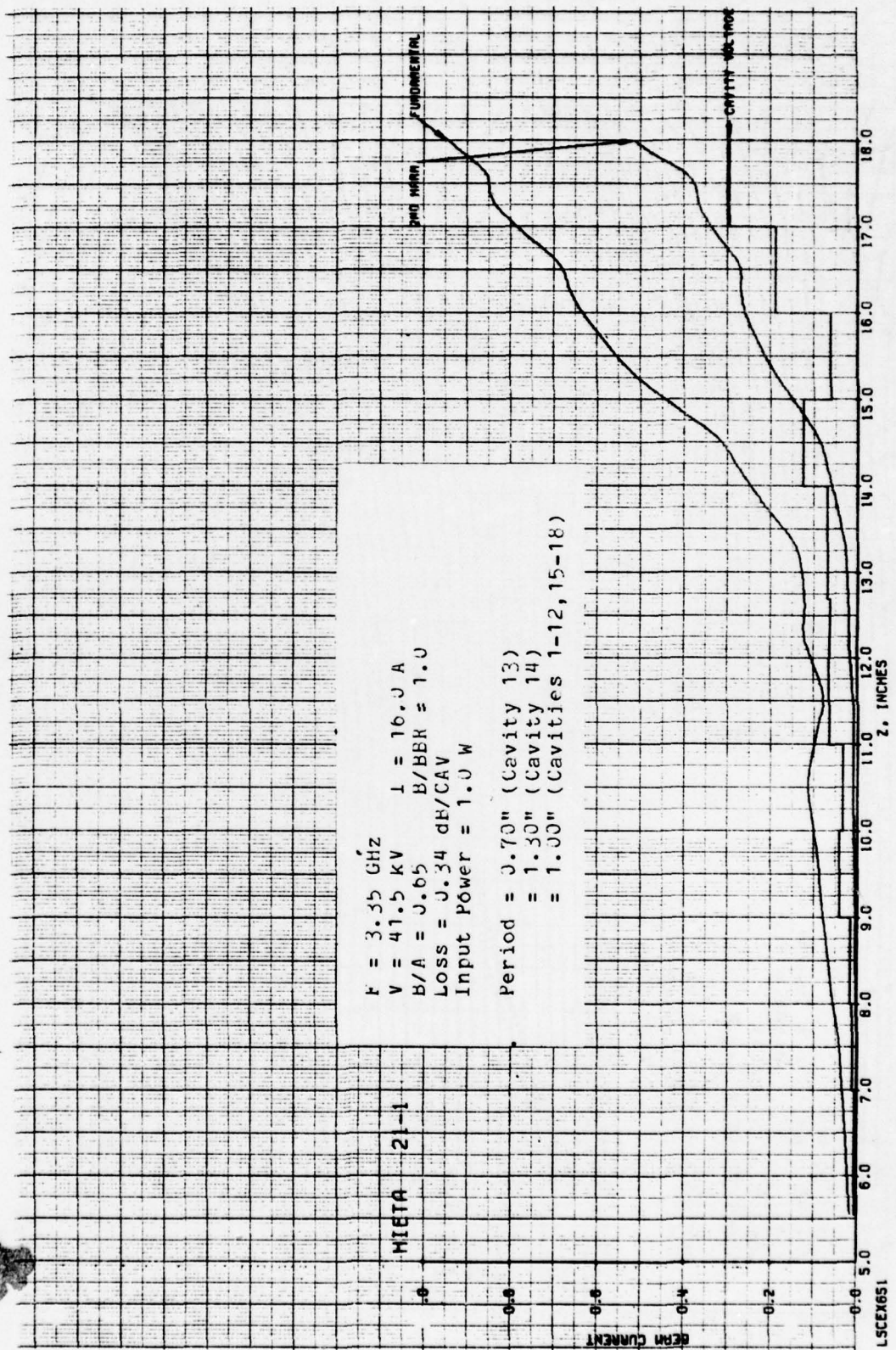


FIGURE 5.29 COMPUTED RF BEAM CURRENTS AND GAP VOLTAGES VS DISTANCE IN SIMULATED COUPLED-CAVITY TWT WITH A TWO CAVITY PERIOD MODIFICATION

HIETA 21-1

$F = 3.35$ GHz
 $V = 41.5$ KV
 $B/A = 0.65$
 $I = 16.0$ A
 $B/EPR = 1.0$
 $Loss = 0.34$ dB/CAV
 $Input Power = 1.0$ W

Period = $0.70''$ (Cavity 13)
 $= 1.30''$ (Cavity 14)
 $= 1.00''$ (Cavities 1-12, 15-18)

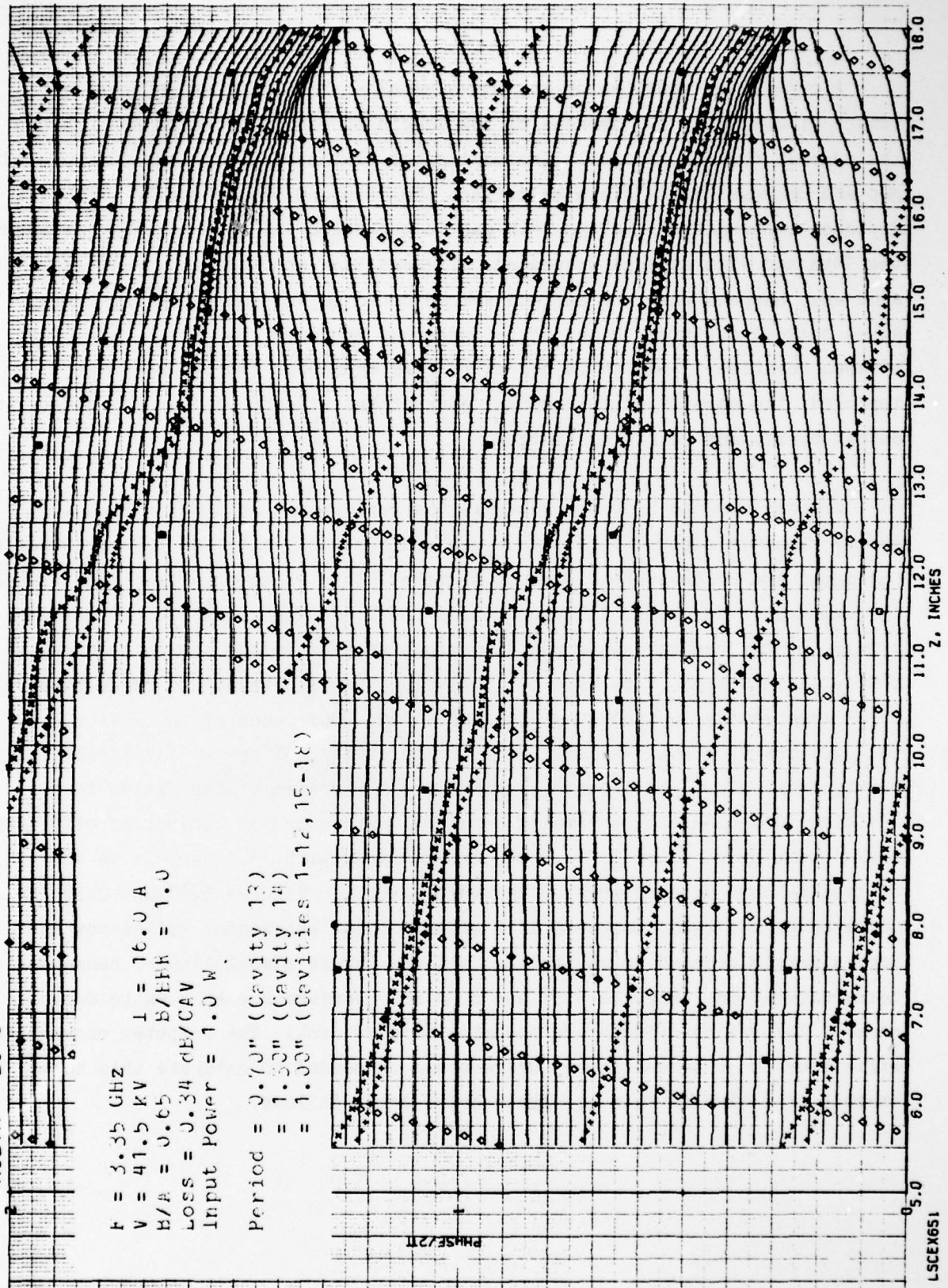


FIGURE 5.30 COMPUTED RELATIVE PHASES OF ELECTRON DISKS VS DISTANCE IN SIMULATED COUPLED-CAVITY TWT WITH A TWO-CAVITY PERIOD MODIFICATION

A careful examination of the above results shows that by increasing the length of cavity 13 and decreasing the length of cavity 14 we do not achieve the desired results of simply increasing the distance between the 12th and 13th gap and decreasing the distance between the 13th and 14th gap. In fact, the distance between the 13th and 14th gap is unchanged while the distance between the 14th and 15th gaps is decreased. Figures 5.31 and 5.32 are included to show what happens when the periods are adjusted so that only the gap-to-gap space between cavities 12 and 13 is increased and only the gap-to-gap space between cavities 13 and 14 is decreased. As expected, the bunching has improved; the normalized fundamental current has risen to 1.1 at the end of the output cavity and is rising rapidly.

Figures 5.33 to 5.38 characterize the performance of a TWT with a two-cavity negative taper at the output end and a seven-cavity positive pretaper at the input end of the output circuit section. This is exactly the circuit whose performance is described in Figures 5.15 and 5.16 except that in the former simulation the backward-wave was suppressed whereas in the present example a complete simulation is carried out including the effects of the backward-wave. It is immediately apparent that the phases and amplitudes of the cavity voltages are erratic. The amplitude of the cavity voltage in cavity 15 (fourth cavity from output) is abnormally low while the phases of the fields in cavities 10 and 12 are abnormally retarded. The computed conversion efficiency with 1 watt drive power is 11.6 percent compared with 15.7 percent in the equivalent case with suppressed backward-wave. In Figures 5.35 and 5.36 the drive power has been increased to 2 watts and the conversion efficiency has approximately doubled which implies that the TWT is almost linear, hence well below saturation. Figures 5.37 and 5.38 show performance at 4 watts drive power. Saturation effects are becoming more evident. The computed conversion efficiency is 30 percent. More drive would be needed to saturate this tube. An example of a similar tube at higher drive level follows.

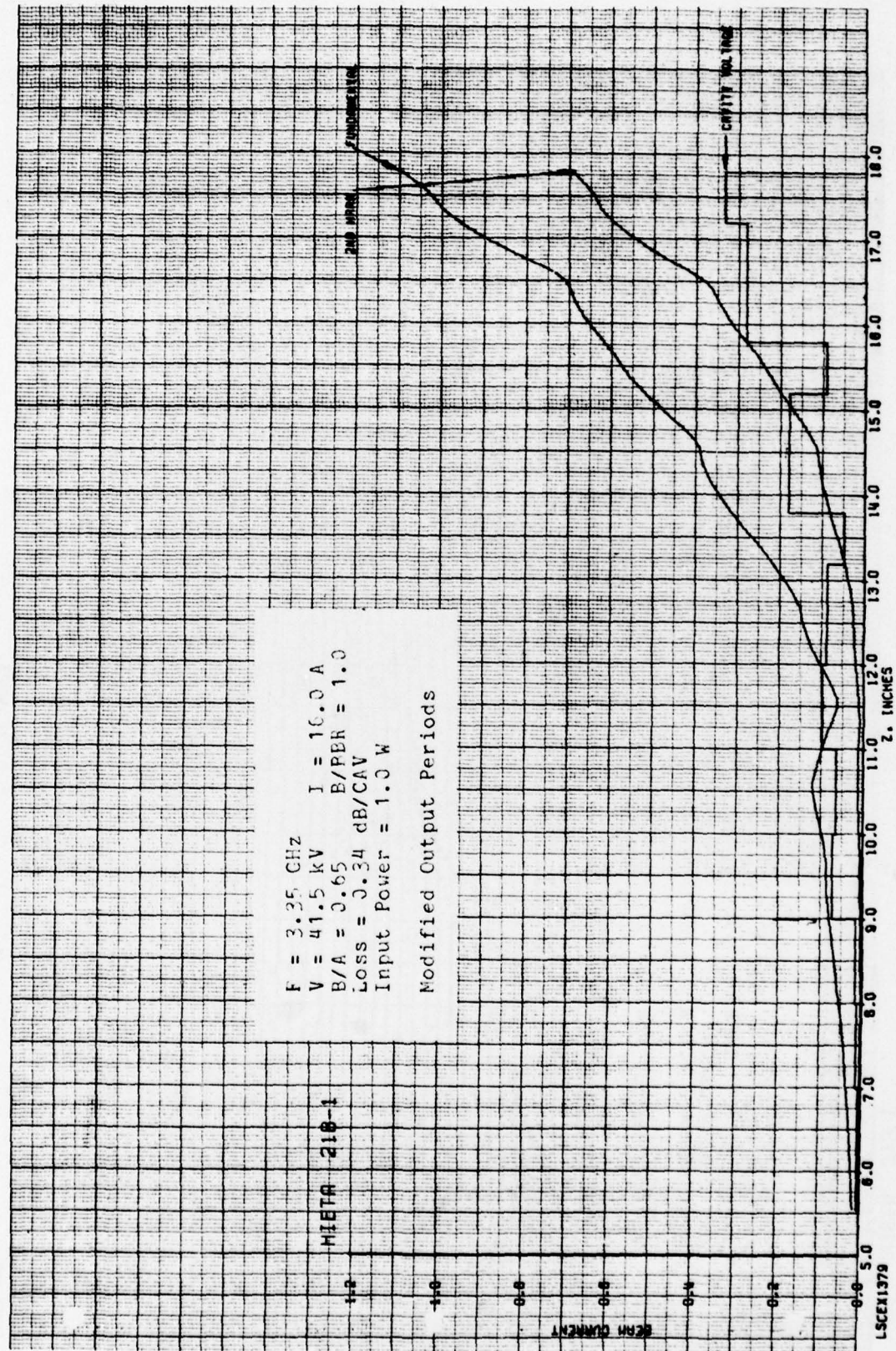


FIGURE 5.31 COMPUTED RF BEAM CURRENTS AND GAP VOLTAGES VS DISTANCE IN SIMULATED COUPLED-CAVITY TWT WITH MODIFIED OUTPUT PERIODS

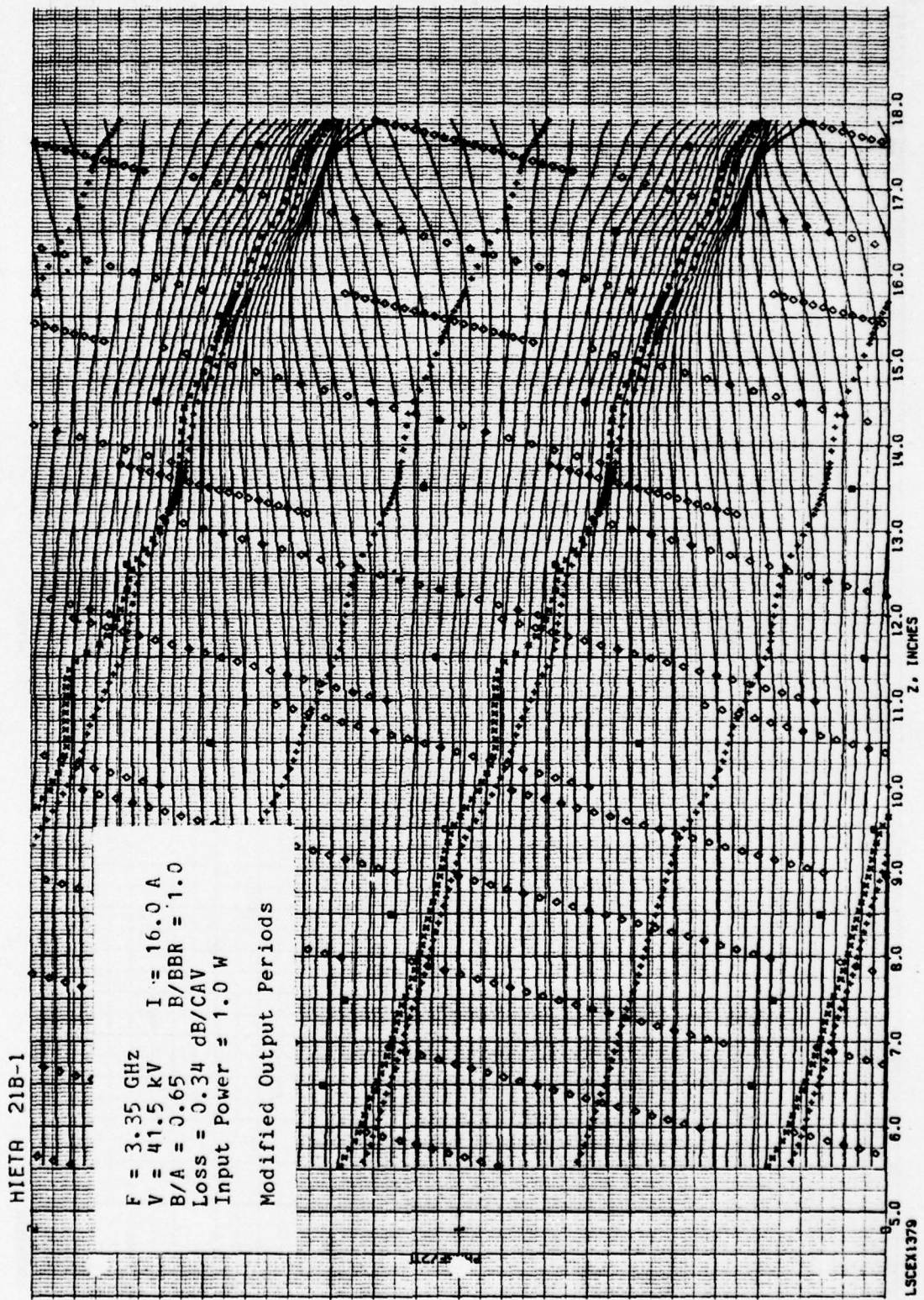
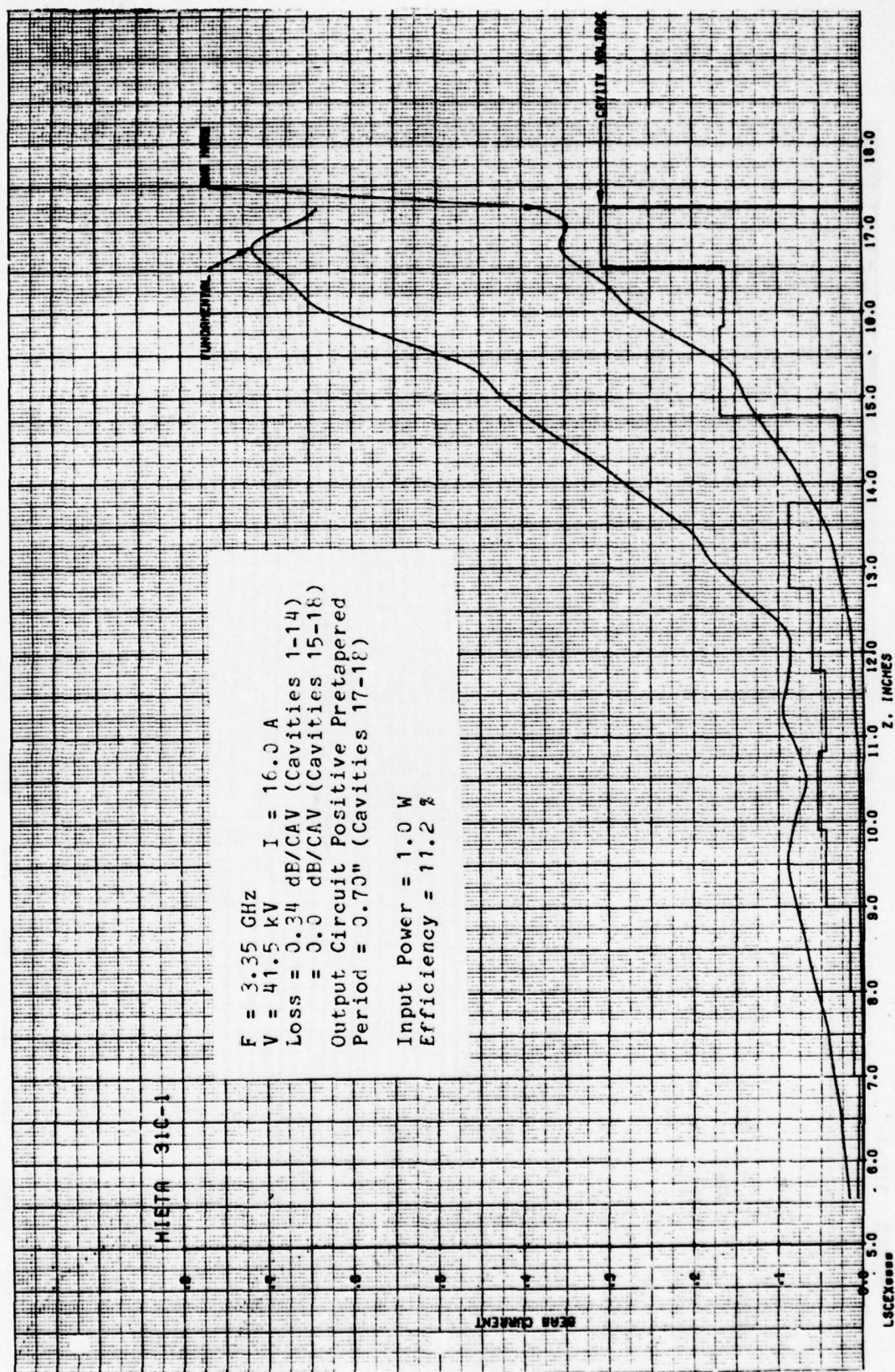


FIGURE 5.32 COMPUTED RELATIVE PHASES OF ELECTRON DISKS VS DISTANCE IN SIMULATED COUPLED-CAVITY TWT WITH MODIFIED OUTPUT PERIODS



MIETA 31C-1

$F = 3.35 \text{ GHz}$
 $V = 41.5 \text{ kV}$
 $I = 16.0 \text{ A}$
 $\text{Loss} = 0.34 \text{ dB/CAV (Cavities 1-14)}$
 $\text{Output} = 0.0 \text{ dB/CAV (Cavities 15-18)}$
 $\text{Period} = 0.70'' \text{ (Cavities 17-18)}$

$\text{Input Power} = 1.0 \text{ W}$
 $\text{Efficiency} = 11.2 \%$

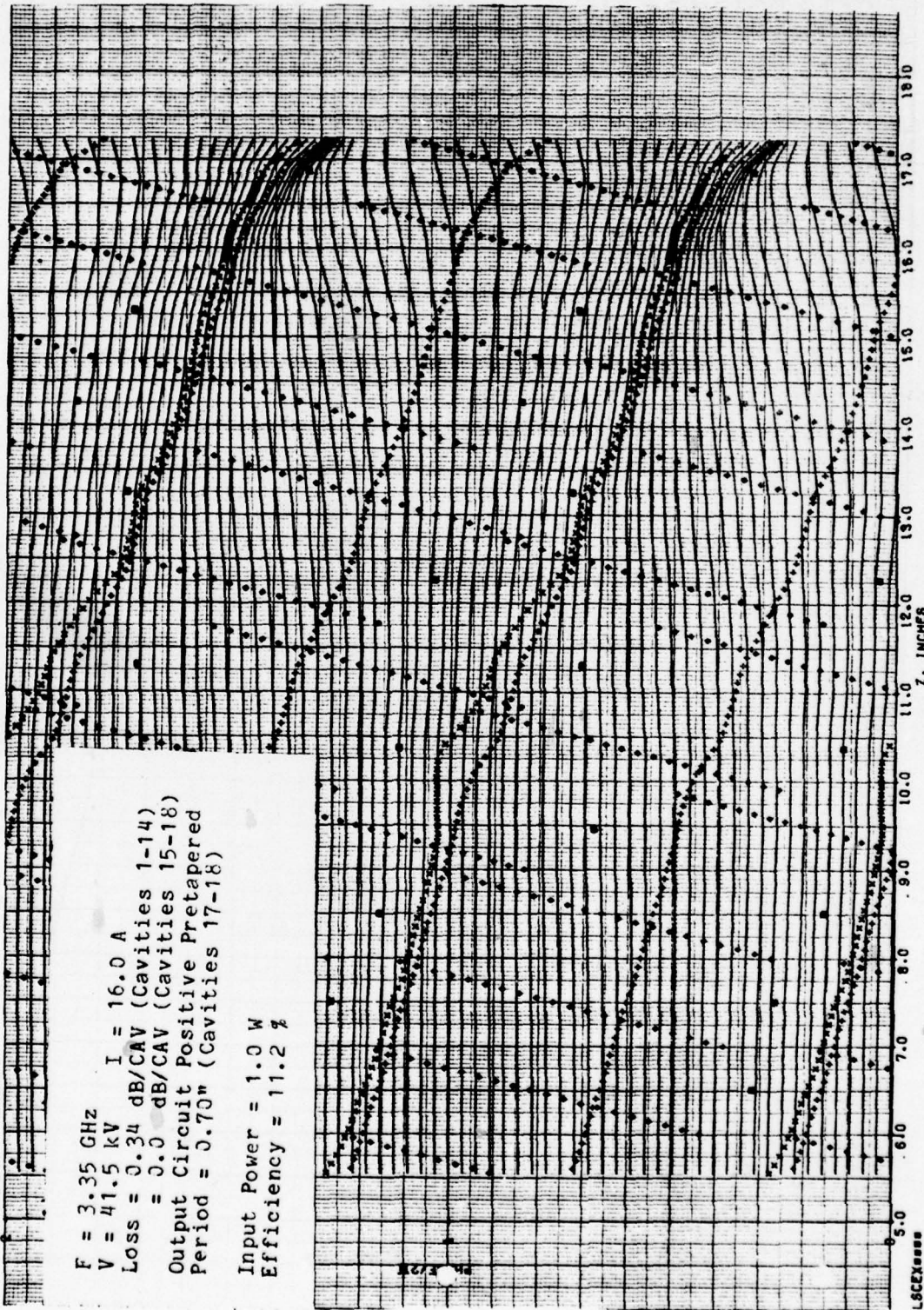


FIGURE 5.34 COMPUTED RELATIVE PHASES OF ELECTRON DISKS VS DISTANCE IN SIMULATED COUPLED-CAVITY TWT WITH FOUR LOSSLESS OUTPUT CAVITIES, POSITIVE PRETAPERED OUTPUT CIRCUIT, AND FINAL TWO CAVITIES WITH DECREASED PERIODS

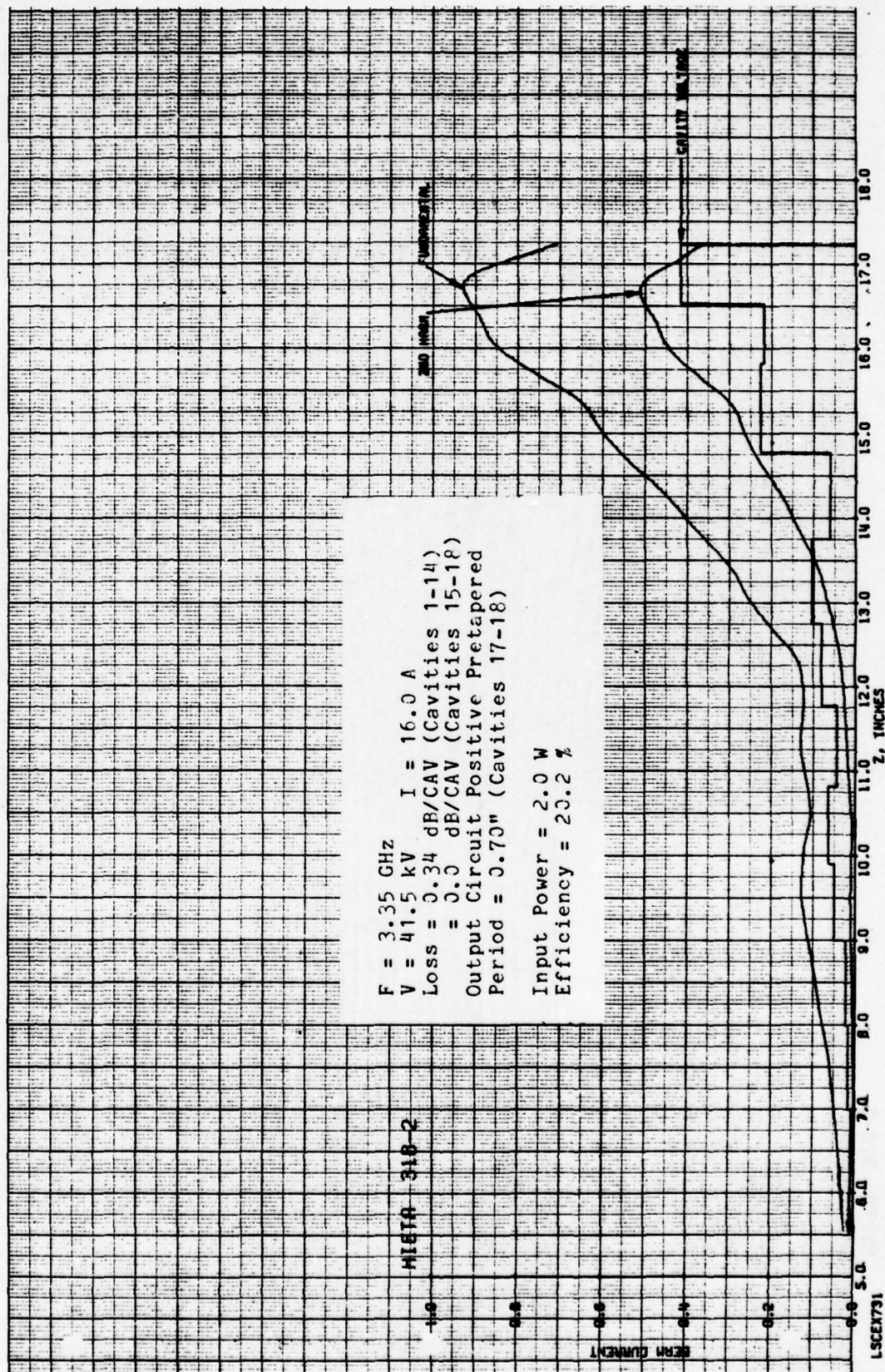


FIGURE 5.36 COMPUTED RF BEAM CURRENTS AND GAP VOLTAGES VS DISTANCE IN SIMULATED COUPLED-CAVITY TWT WITH FOUR LOSSLESS OUTPUT CAVITIES, POSITIVE PRETAPERED OUTPUT CIRCUIT, AND FINAL TWO CAVITIES WITH DECREASED PERIODS

HIETA 318-2

$F = 3.35 \text{ GHz}$
 $V = 41.5 \text{ kV}$ $I = 16.0 \text{ A}$
 $\text{Loss} = 0.34 \text{ dB/CAV (Cavities 1-14)}$
 $\quad = 0.0 \text{ dB/CAV (Cavities 15-18)}$
 $\text{Output Circuit Positive Pretapered}$
 $\text{Period} = 0.70'' \text{ (Cavities 17-18)}$
 $\text{Input Power} = 2.0 \text{ W}$
 $\text{Efficiency} = 20.2 \%$

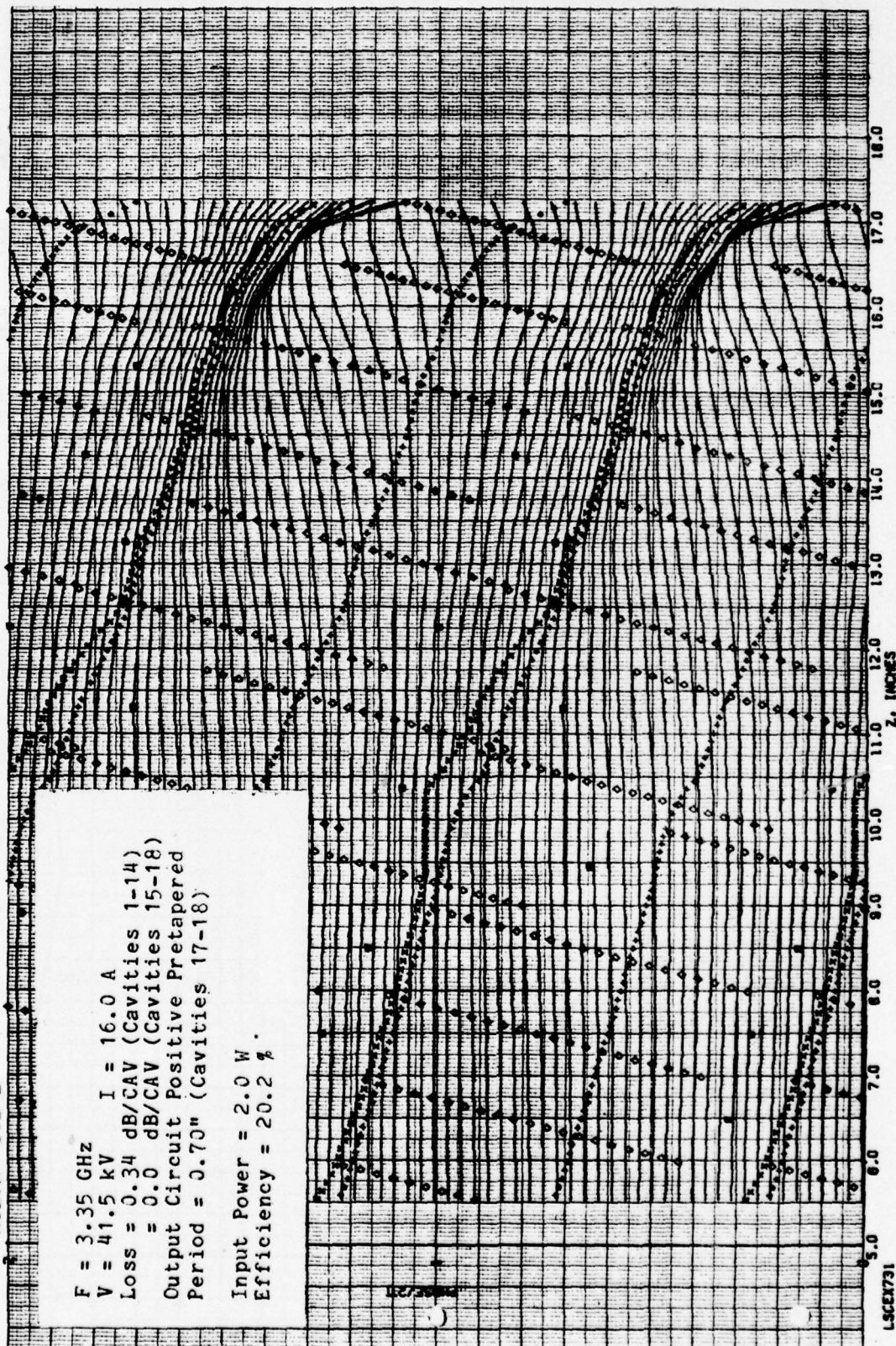


FIGURE 5.36 COMPUTED RELATIVE PHASES OF ELECTRON DISKS VS DISTANCE IN SIMULATED COUPLED-CAVITY TWT WITH FOUR LOSSLESS OUTPUT CAVITIES, POSITIVE PRETAPERED OUTPUT CIRCUIT, AND FINAL TWO CAVITIES WITH DECREASED PERIODS

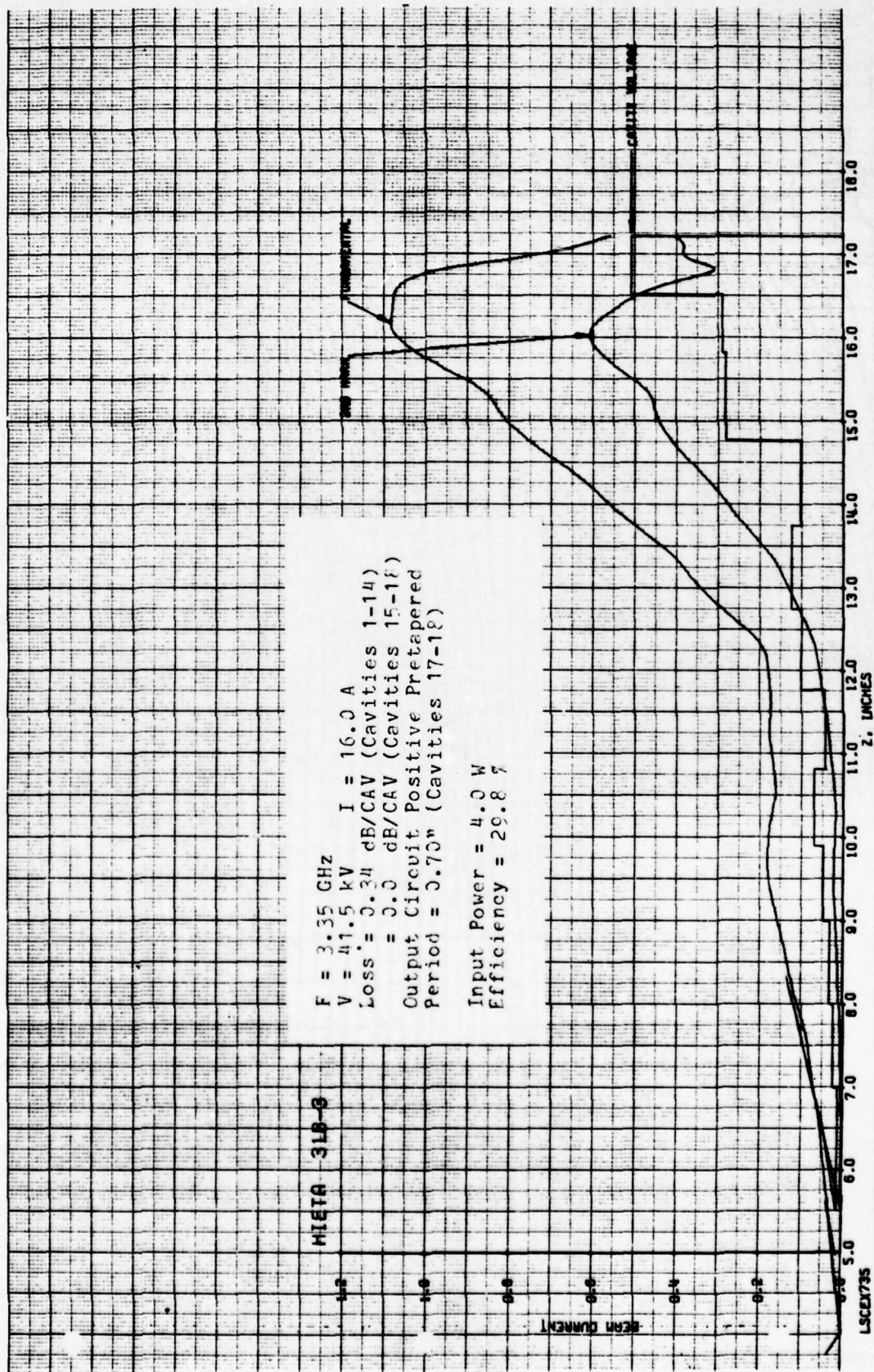


FIGURE 5.37 COMPUTED RF BEAM CURRENTS AND GAP VOLTAGES VS DISTANCE IN SIMULATED COUPLED-CAVITY TWT WITH FOUR LOSSLESS OUTPUT CAVITIES, POSITIVE PRETAPERED OUTPUT CIRCUIT, AND FINAL TWO CAVITIES WITH DECREASED PERIODS

HIETA 31B-3

$F = 3.35 \text{ GHz}$
 $V = 41.5 \text{ kV}$
 $I = 16.0 \text{ A}$
 $\text{Loss} = 0.34 \text{ dB/CAV (Cavities 1-14)}$
 $= 0.0 \text{ dB/CAV (Cavities 15-18)}$
 $\text{Output Circuit Positive Pretapered}$
 $\text{Period} = 0.70'' \text{ (Cavities 17-18)}$

$\text{Input Power} = 4.0 \text{ W}$
 $\text{Efficiency} = 29.8 \%$

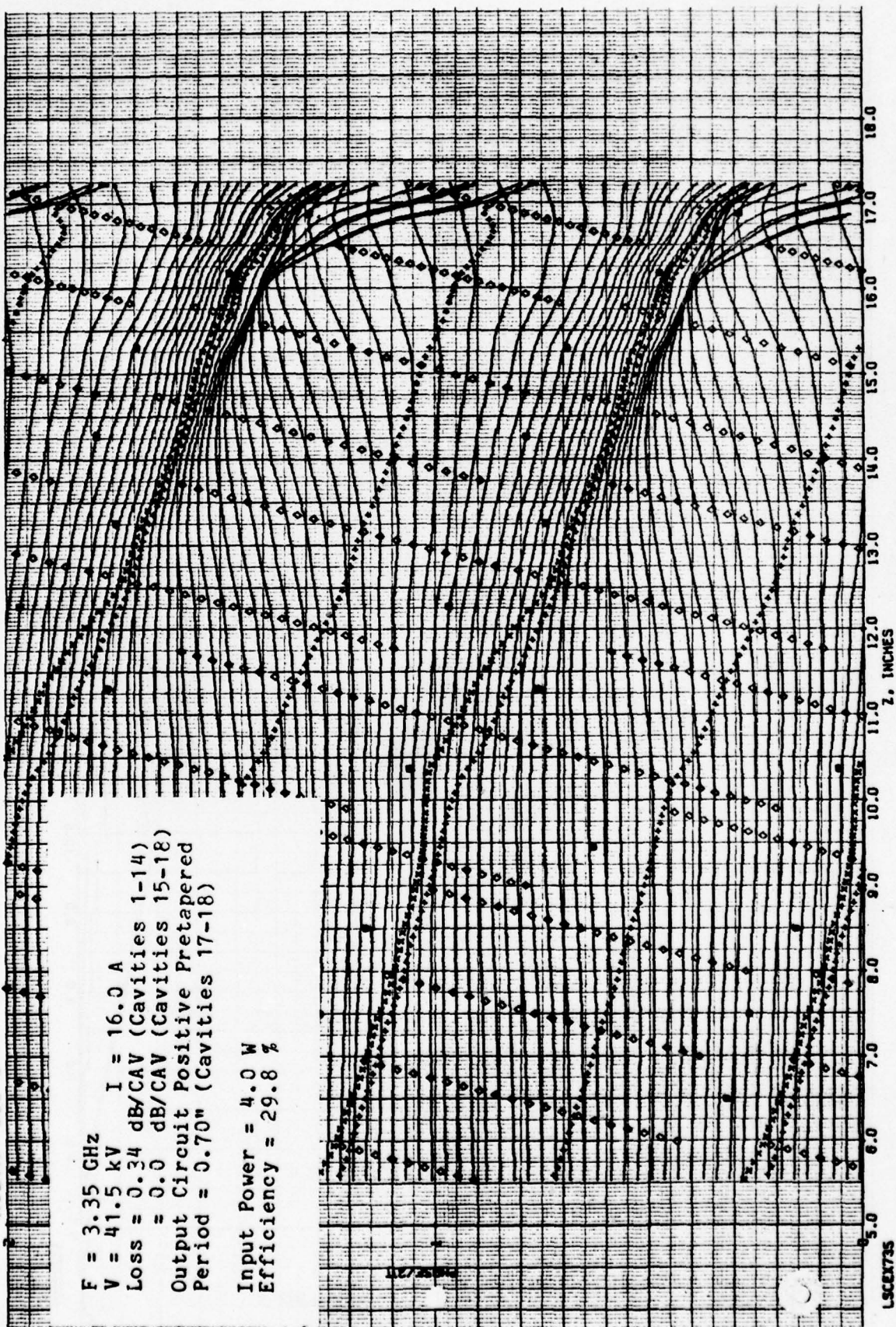


FIGURE 5.38 COMPUTED RELATIVE PHASES OF ELECTRON DISKS VS DISTANCE IN SIMULATED COUPLED-CAVITY TWT WITH FOUR LOSSLESS OUTPUT CAVITIES, POSITIVE PRETAPERED OUTPUT CIRCUIT, AND FINAL TWO CAVITIES WITH DECREASED PERIODS

Figures 5.39 through 5.46 illustrate the computed performance -- including backward-wave interaction -- of a TWT with negative pretaper. This TWT employs exactly the same circuit used in the simulation illustrated in Figures 5.17 through 5.22. Once again the backward-wave manifests itself in the erratic behavior of the cavity voltages. However, a most interesting characteristic is revealed as the drive power is increased. In Figures 5.39 and 5.40 the drive power is one watt. In each successive pair of figures, the drive power is doubled. As the drive power level is increased, both the amplitudes and the phases of the gap fields become normalized and, at 8 watts drive power, approach the relatively smooth monotonic behavior characteristic of the simulation with suppressed backward-wave. The computed conversion efficiency at 8 watts drive power is 38 percent and the saturated efficiency at approximately 20 watts drive power is 43 percent as shown in Figure 5.47 which is a plot of efficiency and gain vs drive power.

5.4 Analysis of Pretaper

In a coupled-cavity TWT of the type under investigation, in which the gain per cavity is relatively large, the voltage in any particular gap is the vector sum of a number of components arising from the interaction in all the gaps. The downstream gaps tend to produce backward-wave components which are comparable in magnitude (even with some circuit loss) to the component induced in a particular gap by the bunched beam. In consequence we find, under small-signal conditions, that the gap voltages do not grow exponentially with distance, as one would anticipate from a simple three wave model, but rather show an erratic variation both in amplitude and phase. Since good bunching depends on maintaining approximate phase quadrature between the bunch and the gap fields, it seems almost certain that the noted erratic phase behavior will be deleterious to bunching and to efficiency. Figures 5.48 and 5.49 show the computed behavior of a typical TWT at a drive level approximately 10 dB below saturation. The gap voltages (Figure 5.48) are seen to fluctuate erratically. In cavity No. 10 ($Z = 9.5''$), the first cavity of the output section, the gap voltage is more than twice that in cavity No. 9 even though the forward-wave

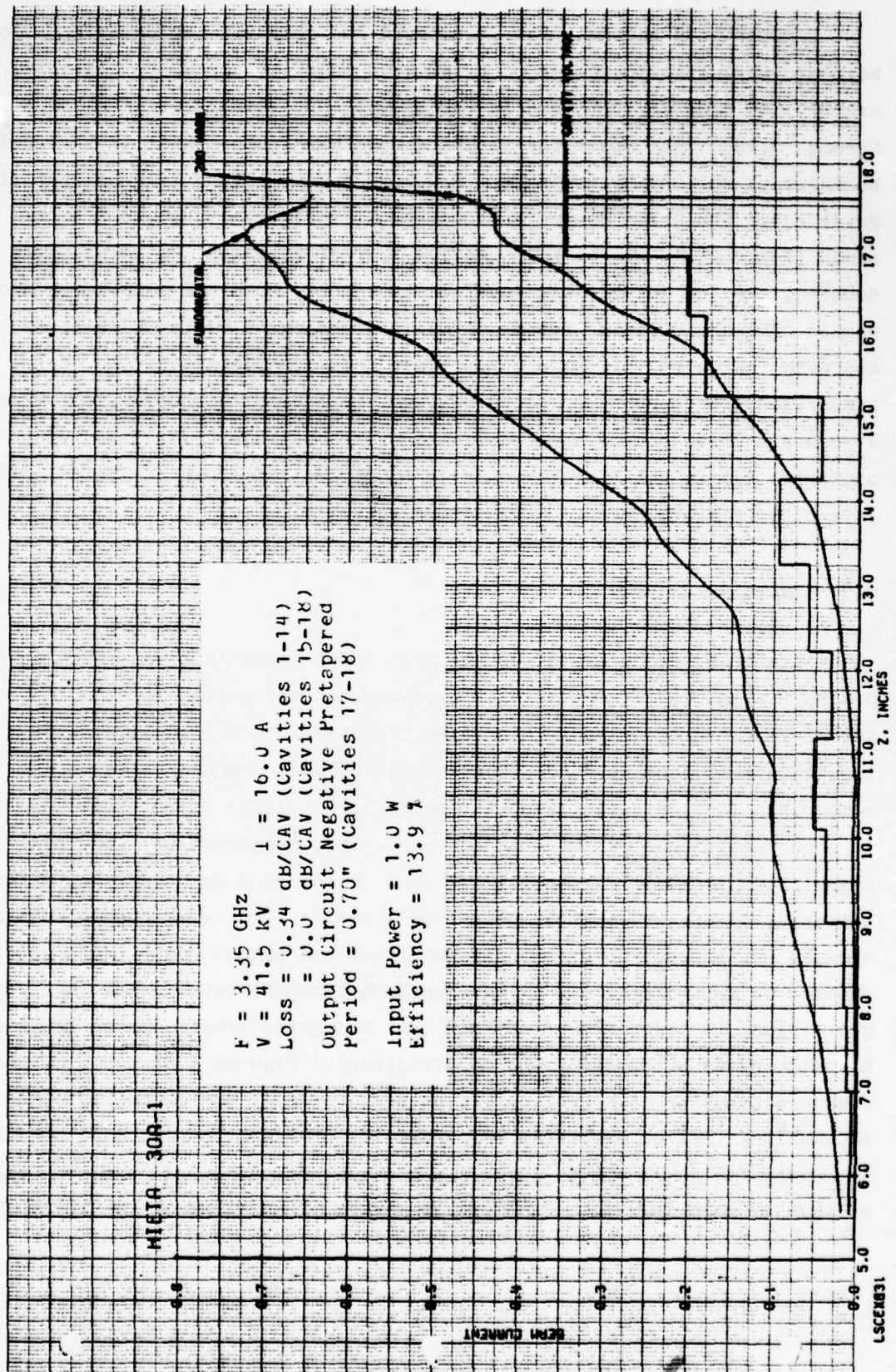
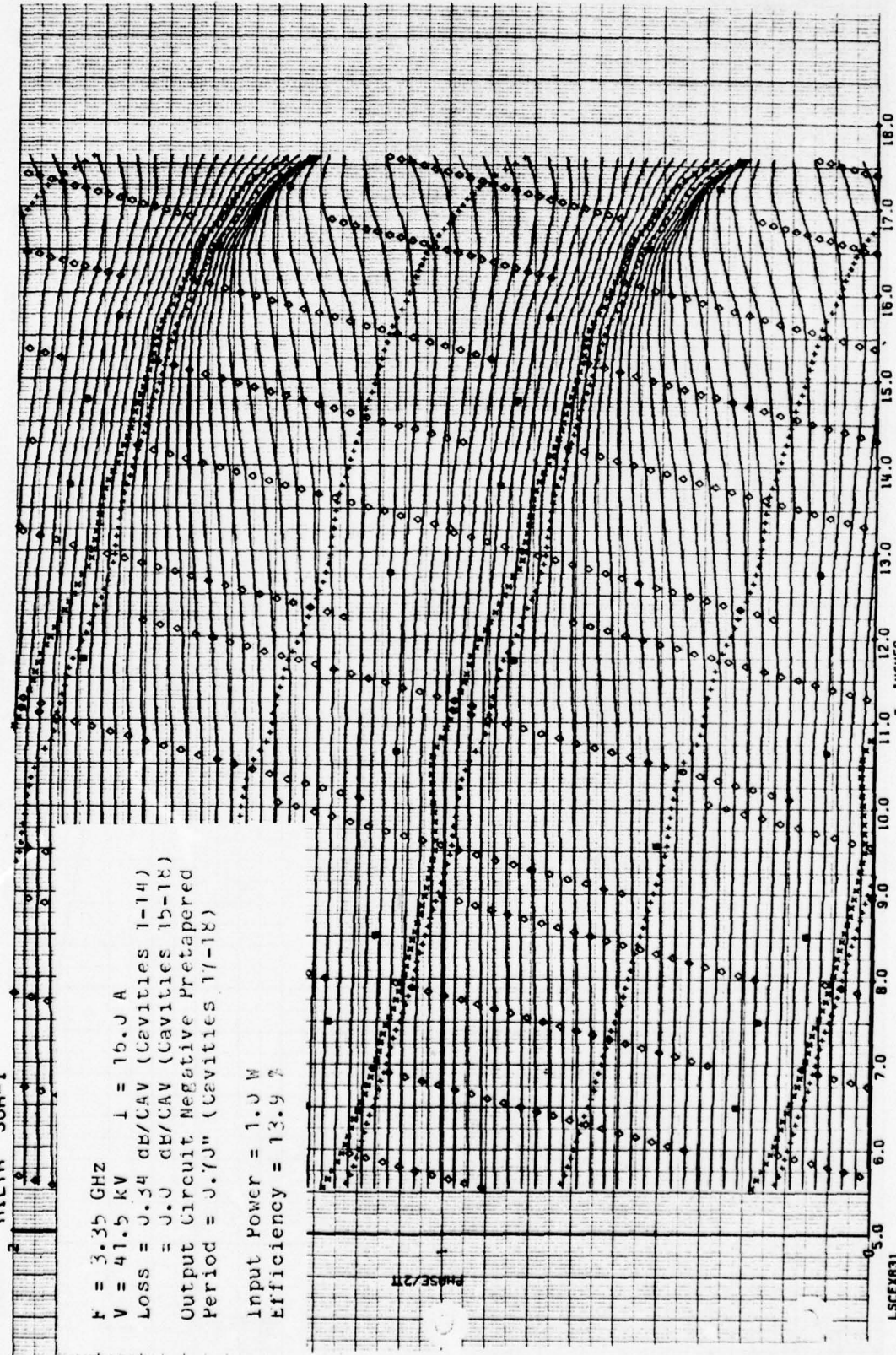


FIGURE 5.38 COMPUTED RF BEAM CURRENTS AND GAP VOLTAGES VS DISTANCE IN SIMULATED COUPLED-CAVITY TWT WITH FOUR LOSSLESS OUTPUT CAVITIES, NEGATIVE PRETAPERED OUTPUT CIRCUIT, AND FINAL TWO CAVITIES WITH DECREASED PERIODS

HIETA 30A-1



$F = 3.35 \text{ GHz}$
 $V = 41.5 \text{ kV}$
 $I = 15.0 \text{ A}$
 $\text{Loss} = 0.34 \text{ dB/CAV (Cavities 1-14)}$
 $= 0.70 \text{ dB/CAV (Cavities 15-18)}$
 $\text{Output Circuit Negative Pretapered}$
 $\text{Period} = 0.70'' \text{ (Cavities 17-18)}$

$\text{Input Power} = 1.0 \text{ W}$
 $\text{Efficiency} = 13.9 \%$

FIGURE 5.40 COMPUTED RELATIVE PHASES OF ELECTRON DISKS VS DISTANCE IN SIMULATED COUPLED-CAVITY TWT WITH FOUR LOSSLESS OUTPUT CAVITIES, NEGATIVE PRETAPERED OUTPUT CIRCUIT, AND FINAL TWO CAVITIES WITH DECREASED PERIODS

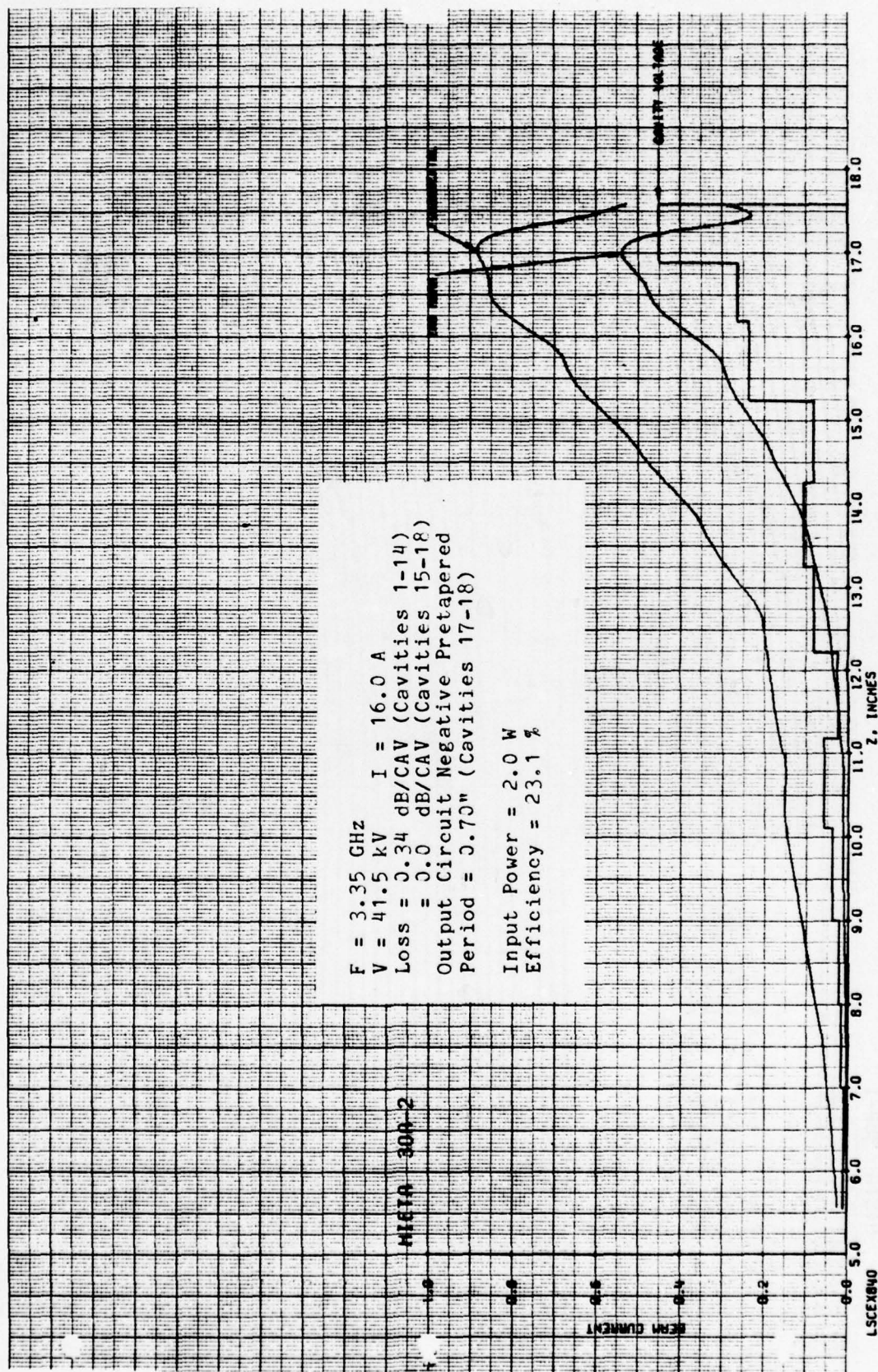


FIGURE 5.41 COMPUTED RF BEAM CURRENTS AND GAP VOLTAGES VS DISTANCE IN SIMULATED COUPLED-CAVITY TWT WITH FOUR LOSSLESS OUTPUT CAVITIES, NEGATIVE PRETAPERED OUTPUT CIRCUIT, AND FINAL TWO CAVITIES WITH DECREASED PERIODS

HIETA 30A-2

$F = 3.35 \text{ GHz}$
 $V = 41.5 \text{ kV}$
 $I = 16.0 \text{ A}$
 $\text{Loss} = 0.34 \text{ dB/CAV (Cavities 1-14)}$
 $\text{Loss} = 0.0 \text{ dB/CAV (Cavities 15-18)}$
 $\text{Output Circuit Negative Pretapered}$
 $\text{Period} = 0.70'' \text{ (Cavities 17-18)}$

$\text{Input Power} = 2.0 \text{ W}$
 $\text{Efficiency} = 23.1 \%$

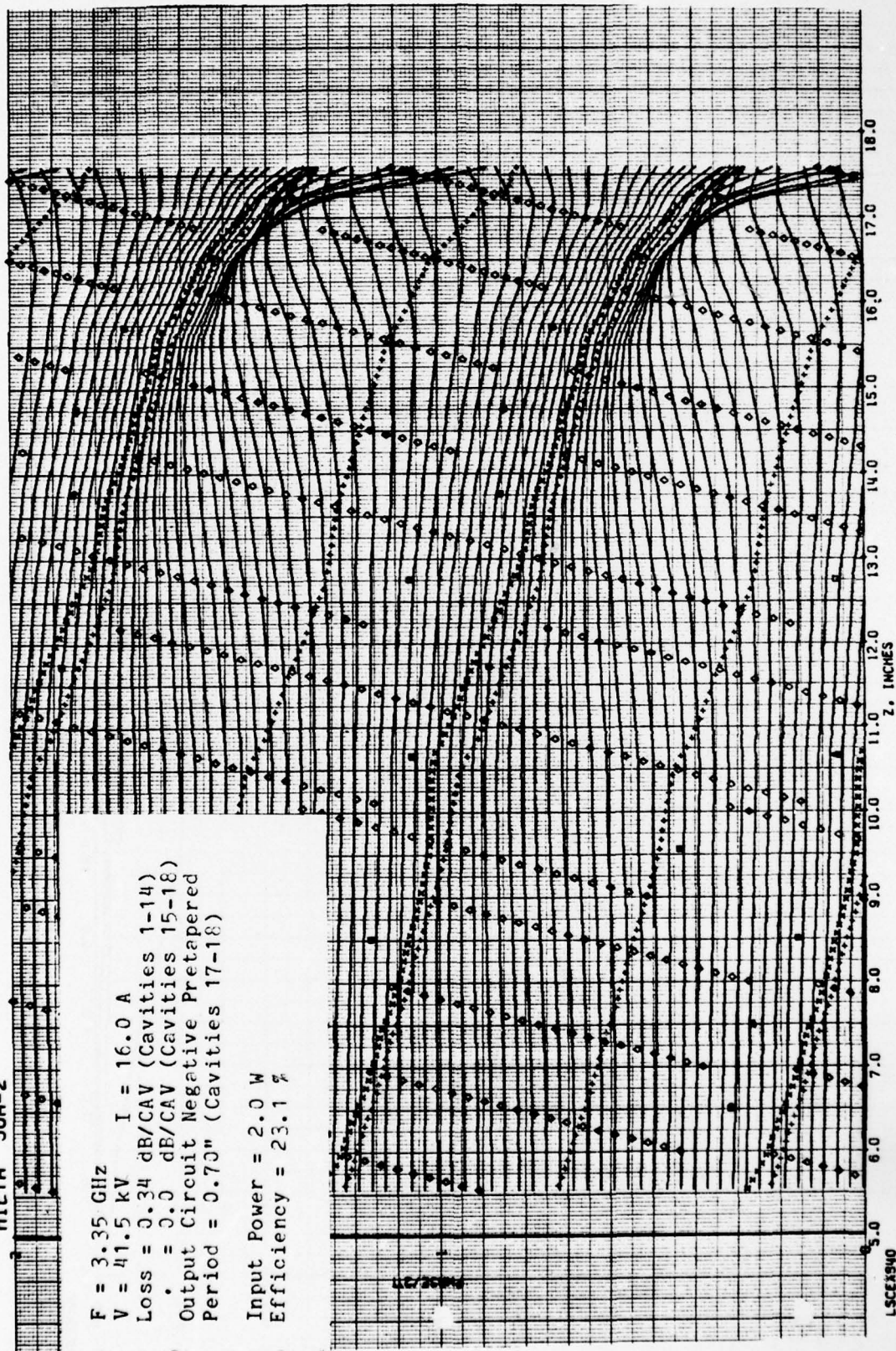


FIGURE 5.42 COMPUTED RELATIVE PHASES OF ELECTRON DISKS VS DISTANCE IN SIMULATED COUPLED-CAVITY TWT WITH FOUR LOSSLESS OUTPUT CAVITIES, NEGATIVE PRETAPERED OUTPUT CIRCUIT, AND FINAL TWO CAVITIES WITH DECREASED PERIODS

$F = 3.35 \text{ GHz}$
 $V = 41.5 \text{ kV}$
 $I = 16.0 \text{ A}$
 $\text{Loss} = 0.34 \text{ dB/CAV (Cavities 1-14)}$
 $\text{Output} = 0.3 \text{ dB/CAV (Cavities 15-18)}$
 $\text{Output Circuit Negative Pretapered}$
 $\text{Period} = 0.70'' \text{ (Cavities 17-18)}$
 $\text{Input Power} = 4.0 \text{ W}$
 $\text{Efficiency} = 30.6 \%$

HIETA 30A-3

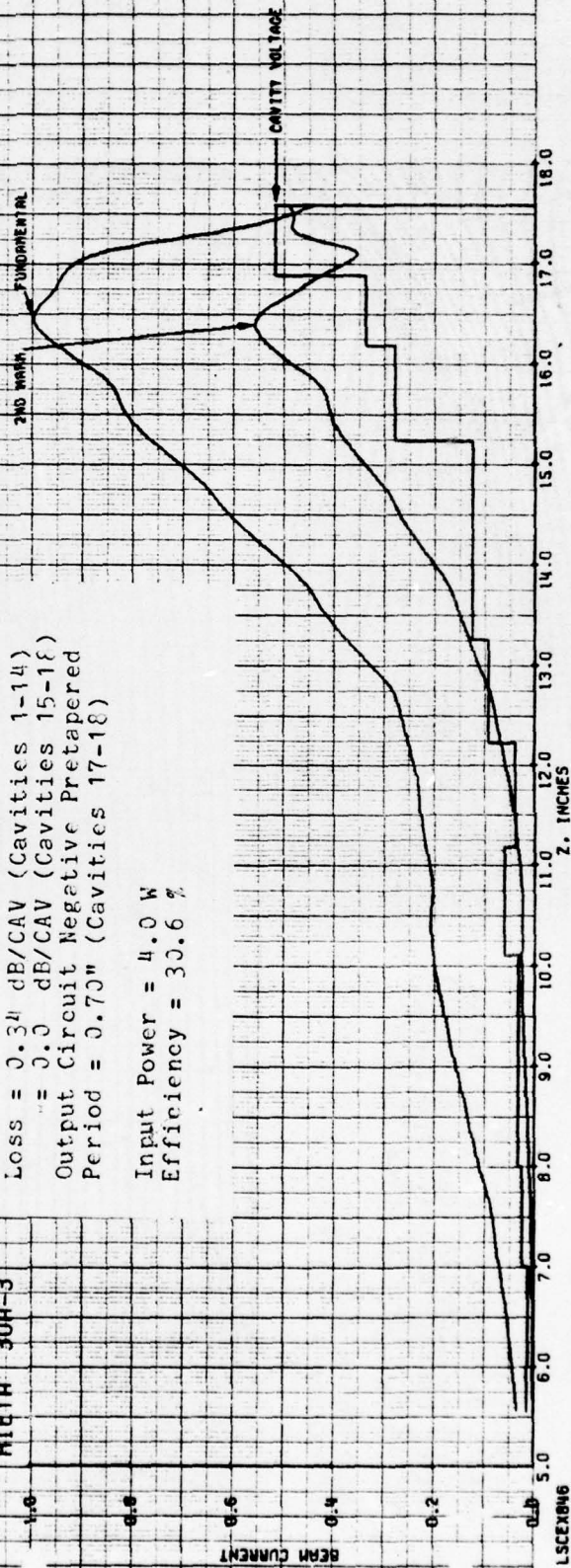


FIGURE 5.43 COMPUTED RF BEAM CURRENTS AND GAP VOLTAGES VS DISTANCE IN SIMULATED COUPLED-CAVITY TWT WITH FOUR LOSSLESS OUTPUT CAVITIES, NEGATIVE PRETAPERED OUTPUT CIRCUIT, AND FINAL TWO CAVITIES WITH DECREASED PERIODS

HIETA 30A-3

$F = 3.35 \text{ GHz}$
 $V = 41.5 \text{ kV}$
 $I = 16.0 \text{ A}$
 $\text{Loss} = 0.34 \text{ dB/CAV (Cavities 1-14)}$
 $= 0.0 \text{ dB/CAV (Cavities 15-18)}$
 $\text{Output Circuit Negative Pretapered}$
 $\text{Period} = 0.70'' \text{ (Cavities 17-18)}$

$\text{Input Power} = 4.0 \text{ W}$
 $\text{Efficiency} = 30.6 \%$

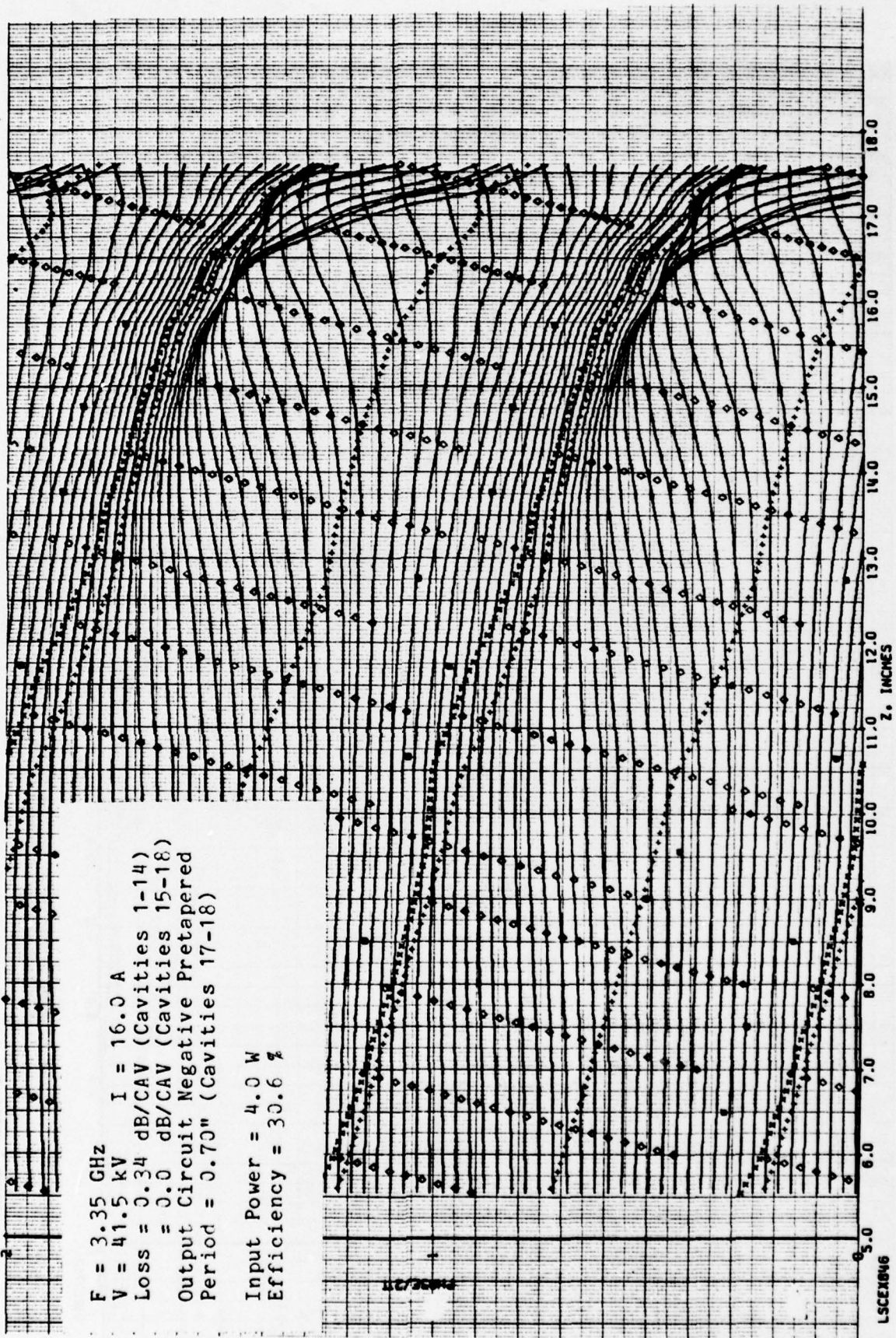


FIGURE 5.44 COMPUTED RELATIVE PHASES OF ELECTRON DISKS VS DISTANCE IN SIMULATED COUPLED-CAVITY TWT WITH FOUR LOSSLESS OUTPUT CAVITIES, NEGATIVE PRETAPERED OUTPUT CIRCUIT, AND FINAL TWO CAVITIES WITH DECREASED PERIODS

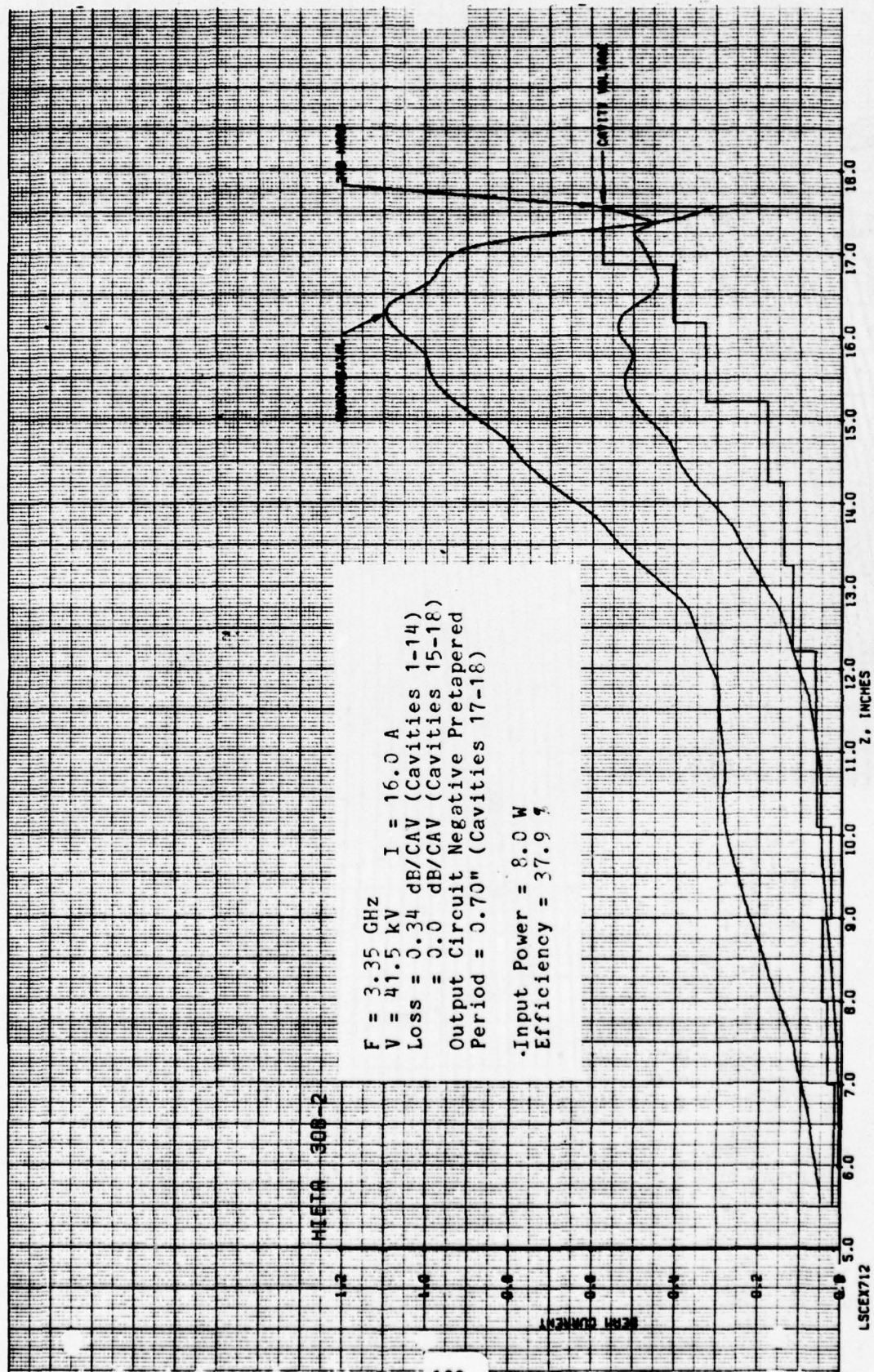


FIGURE 5.45 COMPUTED RF BEAM CURRENTS AND GAP VOLTAGES VS DISTANCE IN SIMULATED COUPLED-CAVITY TWT WITH FOUR LOSSLESS OUTPUT CAVITIES, NEGATIVE PRETAPERED OUTPUT CIRCUIT, AND FINAL TWO CAVITIES WITH DECREASED PERIODS

HIEIA 30B-2

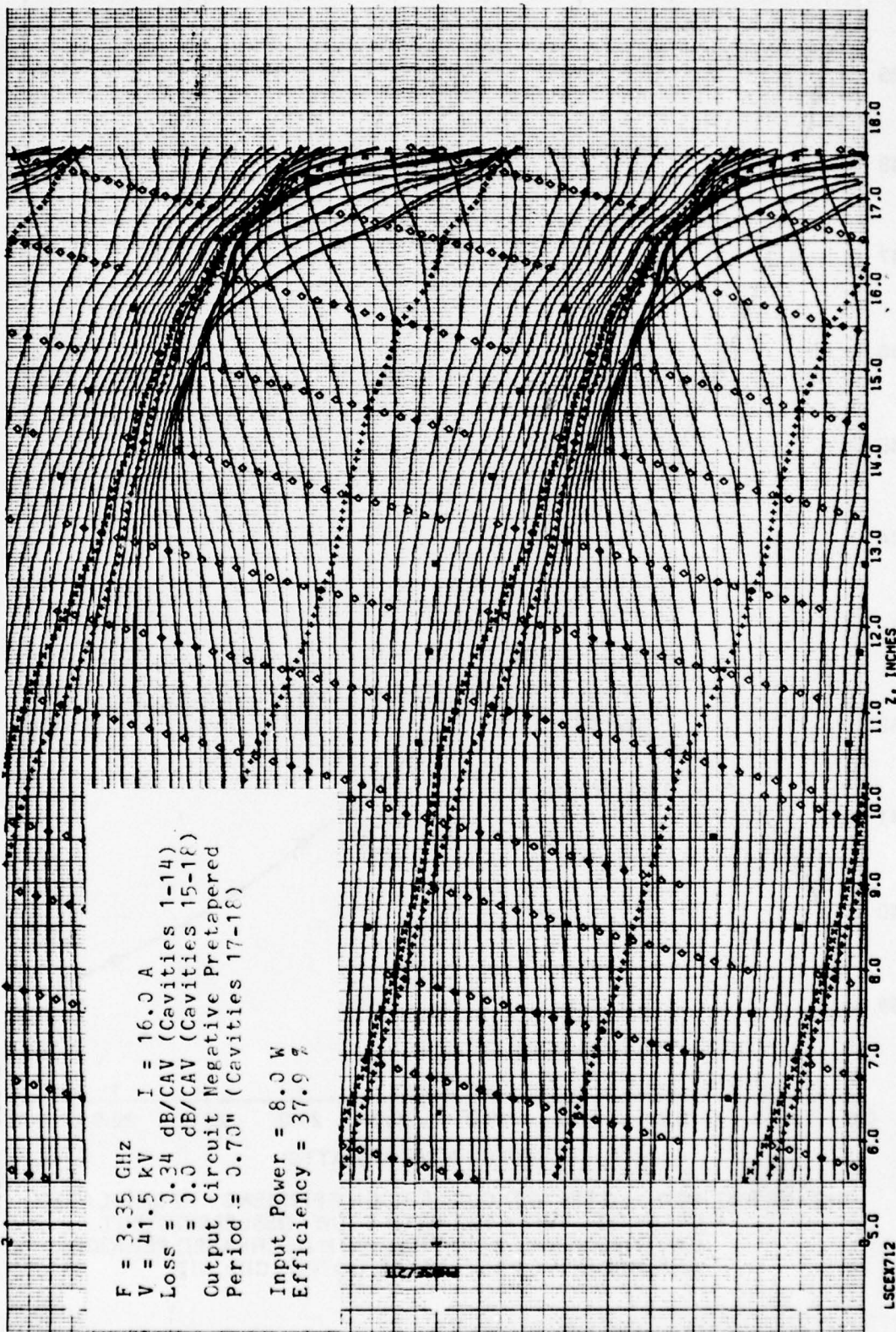


FIGURE 5.46 COMPUTED RELATIVE PHASES OF ELECTRON DISKS VS DISTANCE IN SIMULATED COUPLED-CAVITY TWT WITH FOUR LOSSLESS OUTPUT CAVITIES, NEGATIVE PRETAPERED OUTPUT CIRCUIT, AND FINAL TWO CAVITIES WITH DECREASED PERIODS

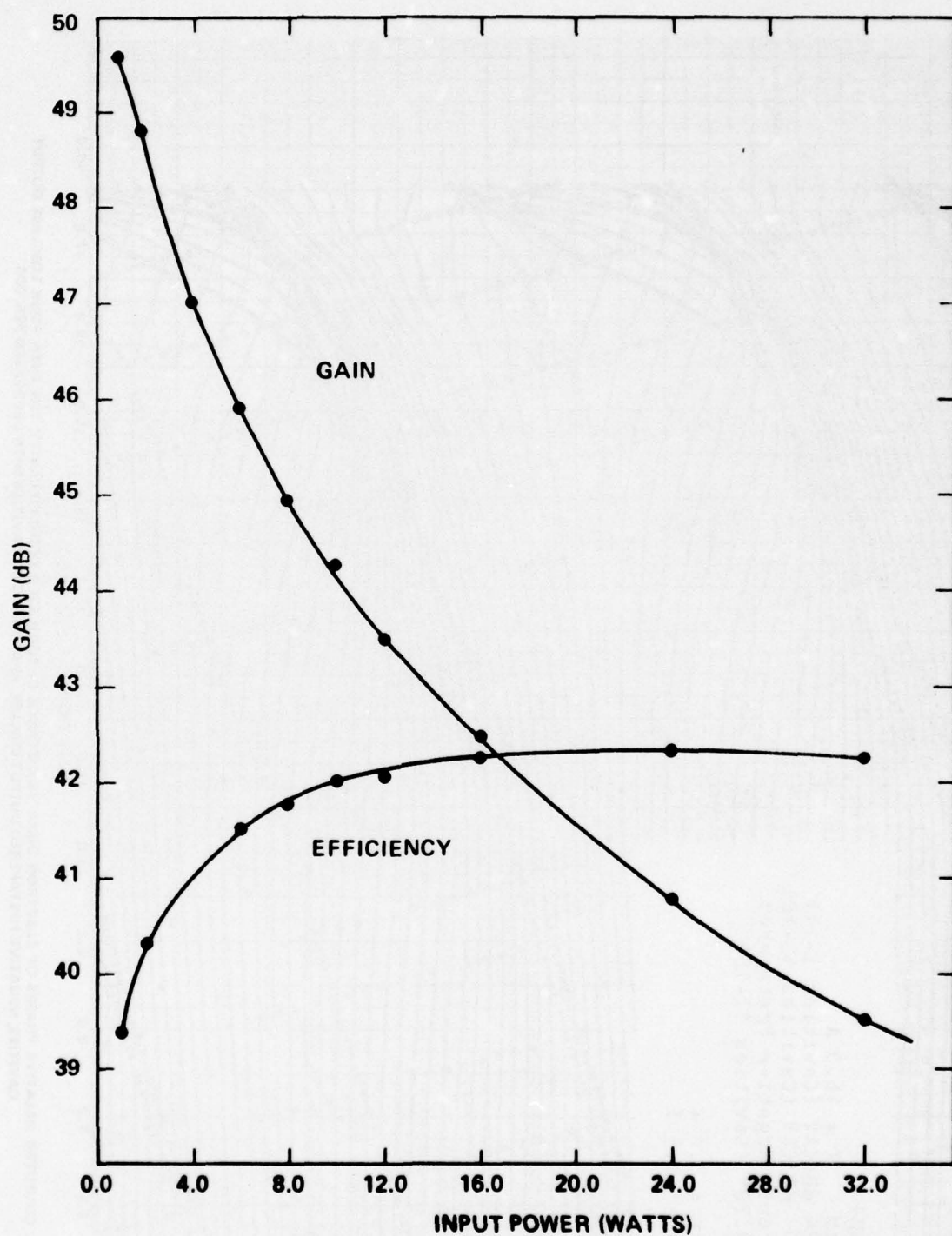


FIGURE 5.47 POWER GAIN AND CONVERSION EFFICIENCY IN SIMULATED COUPLED CAVITY TWT WITH FOUR LOSSLESS OUTPUT CAVITIES, FINAL 2 CAVITIES WITH DECREASED PERIODS, AND NEGATIVE PRETAPERED OUTPUT CIRCUIT.

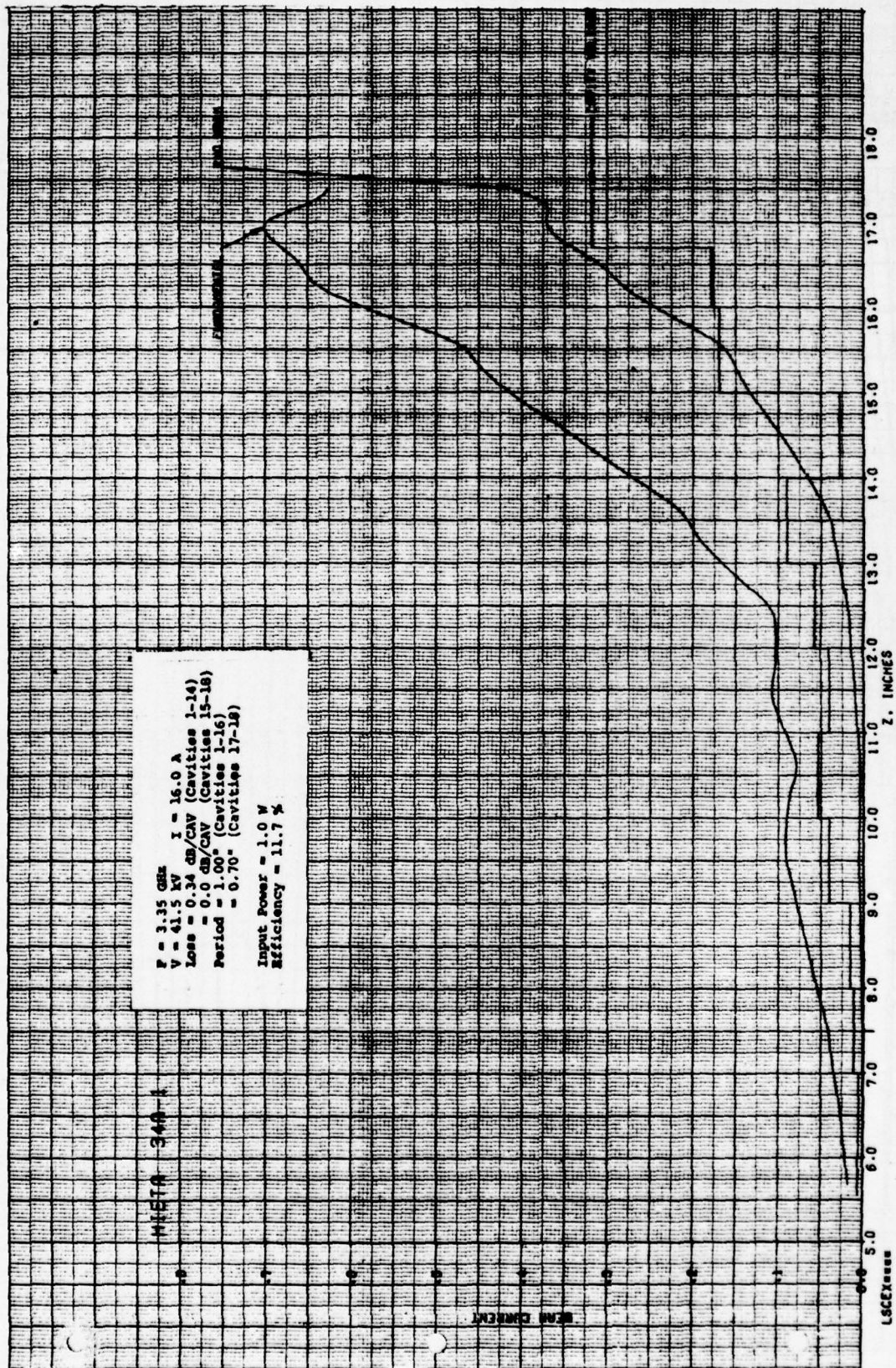


FIGURE 5.48 COMPUTED RF BEAM CURRENTS AND GAP VOLTAGES VS DISTANCE IN SIMULATED COUPLED-CAVITY TWT WITH FOUR LOSSLESS OUTPUT CAVITIES AND FINAL TWO WITH DECREASED PERIODS

H1ETA 34A-1

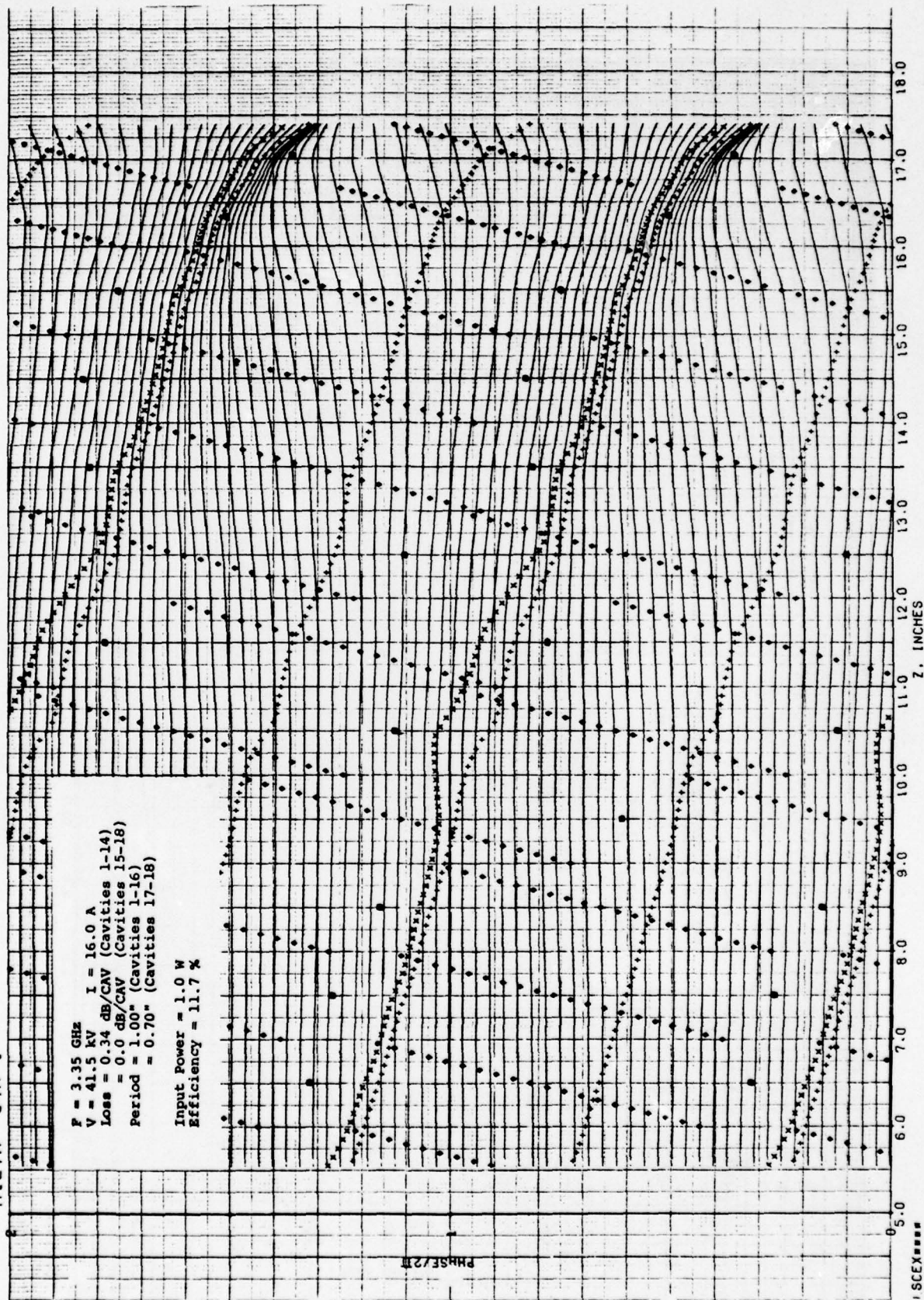


FIGURE 5.49 · COMPUTED RELATIVE PHASES OF ELECTRON DISKS VS DISTANCE IN SIMULATED COUPLED-CAVITY TWT WITH FOUR LOSSLESS OUTPUT CAVITIES AND FINAL TWO CAVITIES WITH DECREASED PERIODS

exiting cavity No. 10 is approximately 7 dB below that exiting cavity No. 9. (These latter data are contained in the computer printout rather than in the plots exhibited here.) It is apparent that the backward-wave plays a dominant role in determining the gap voltages at the front end of the output circuit section. Even in cavity No. 15 ($Z = 14.5''$) the effect of the backward-wave is evident in the anomalously low gap voltage in this cavity. Figure 5.49 shows the electron phase trajectories. The small squares represent the maximum decelerating phase of the gap fields. These squares should be approximately one quarter wavelength in front of the bunch. In this representation that would place them above the double line of "Xs" and "+s" about half way to the single line of "+s." As shown in the figure, the gap phases do not satisfy this criterion and, in fact, vary erratically.

Figures 5.39 through 5.46 illustrated how the gap voltages and phases tended to smooth out as the drive level was increased to saturation. Data presented in Figures 5.50 through 5.55 show a comparison between the computed results obtained employing different amounts of pretaper in the output circuit. Positive pretaper, as used in this example, refers to a uniform linear upward ramp in phase velocity in the first seven cavities of the nine-cavity output section. The average phase velocity in the pretapered section is identical to that in the non-pretapered case. A negative pretaper, in this example, refers to a uniform downward ramp in phase velocity over the first seven cavities. The pretapered sections have a total phase velocity ramp of approximately 16 percent. The final two output cavities are 70 percent of normal cavity period. This two-cavity section is normally referred to as a negative velocity taper or velocity step.

Figures 5.50 and 5.51 illustrate the computed performance of the non-pretapered TWT at a drive power level of 8 W. The amplitudes and phases of the gap voltages have been considerably smoothed relative to those illustrated in Figures 5.48 and 5.49, which represent the same TWT driven at 1 W.

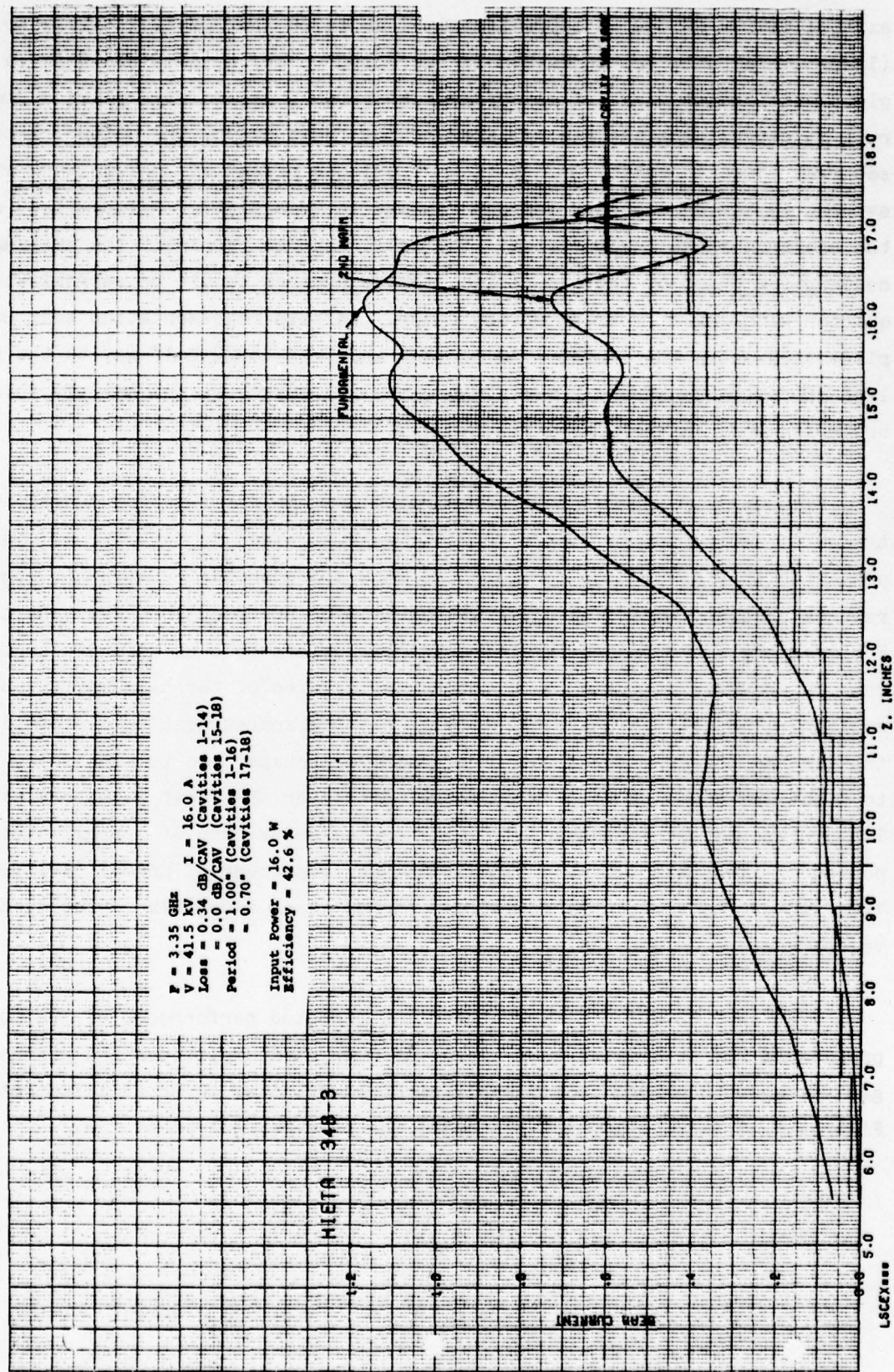


FIGURE 5.50 COMPUTED RF BEAM CURRENTS AND GAP VOLTAGES VS DISTANCE IN SIMULATED COUPLED-CAVITY TWT WITH FOUR LOSSLESS OUTPUT CAVITIES AND FINAL TWO WITH DECREASED PERIODS

HIETA 34B-3

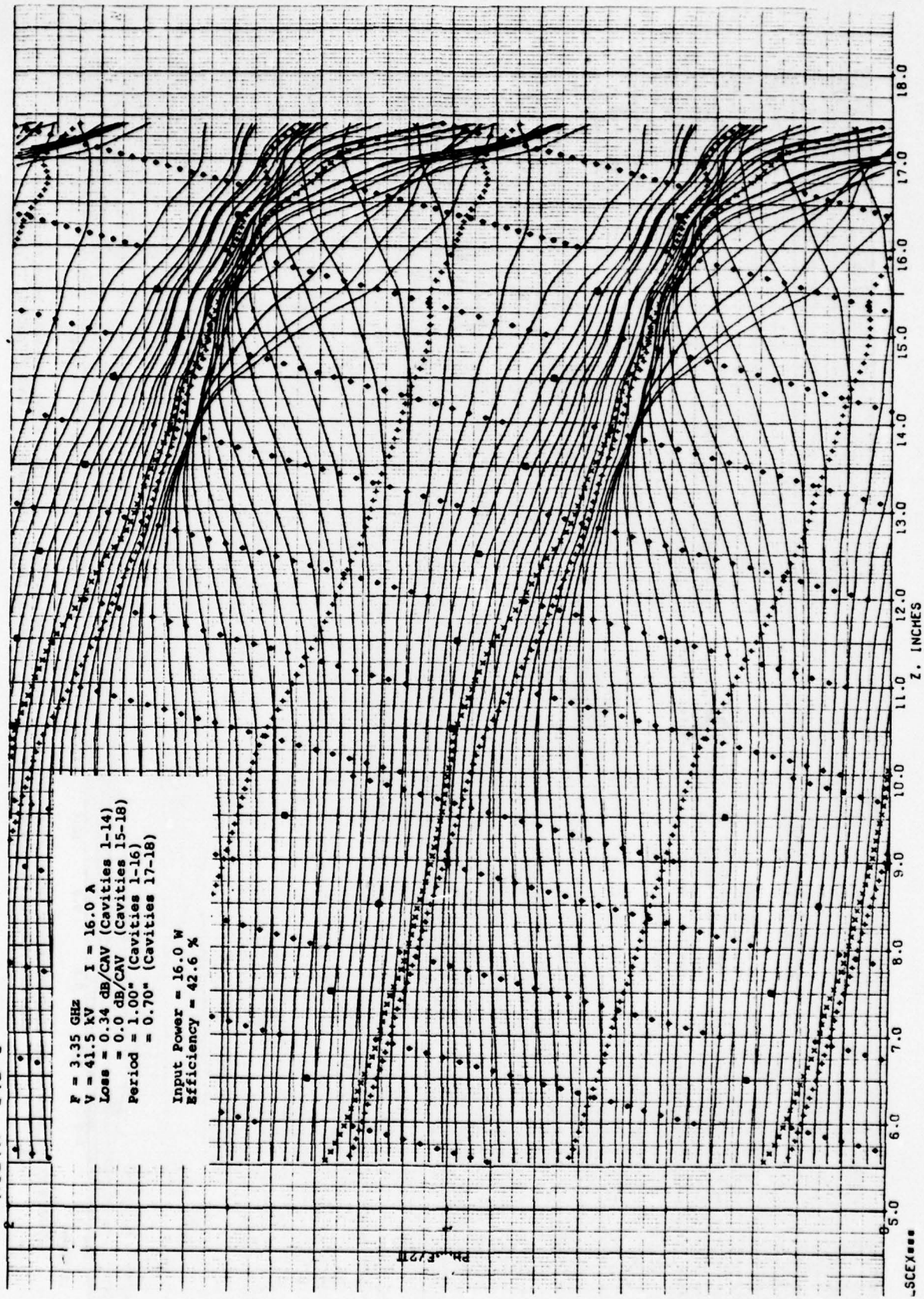


FIGURE 5.51 COMPUTED RELATIVE PHASES OF ELECTRON DISKS VS DISTANCE IN SIMULATED COUPLED-CAVITY TWT WITH FOUR LOSSLESS OUTPUT CAVITIES AND FINAL TWO CAVITIES WITH DECREASED PERIODS

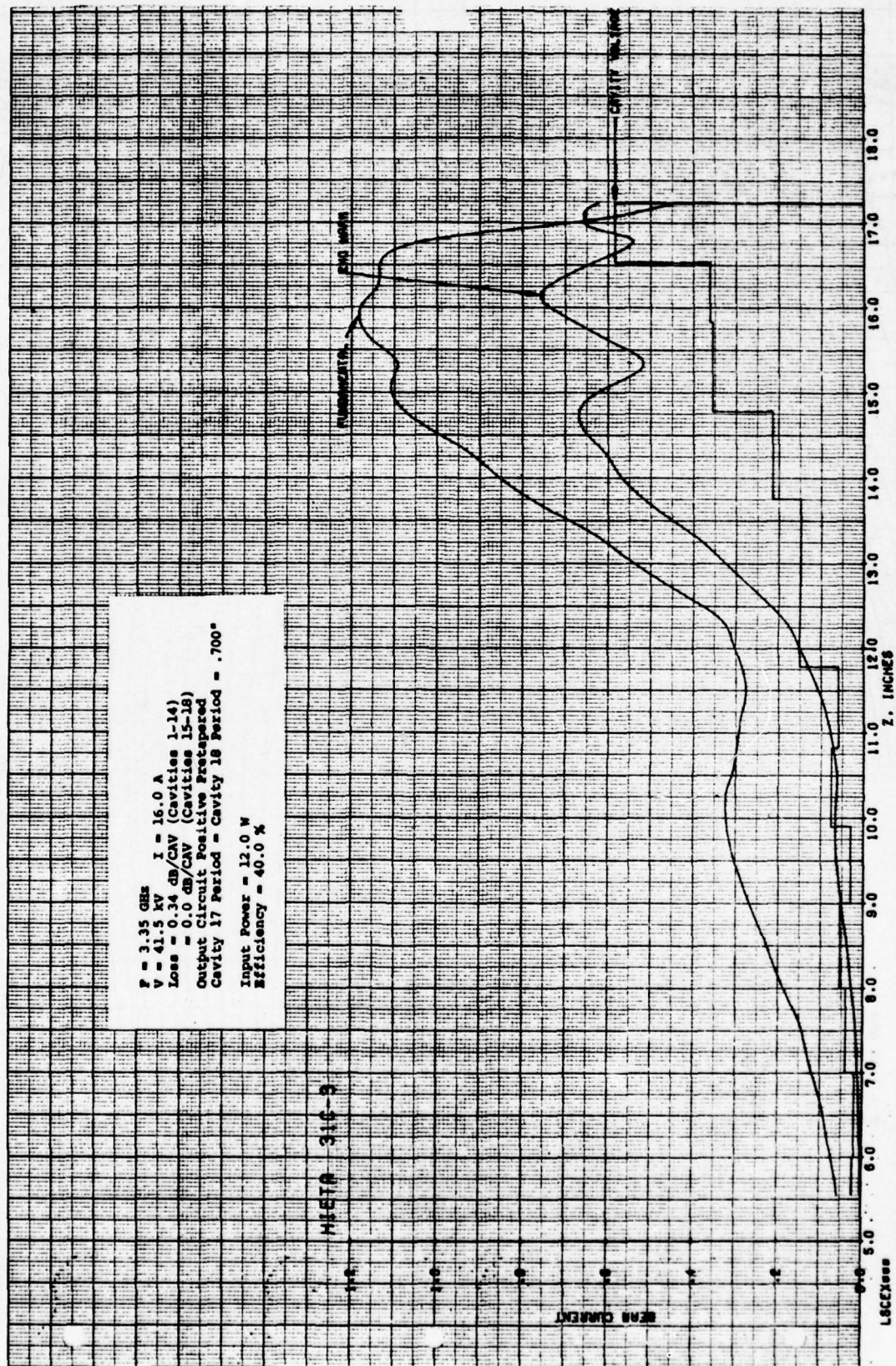


FIGURE 5.52 COMPUTED RF BEAM CURRENTS AND GAP VOLTAGES VS DISTANCE IN SIMULATED COUPLED-CAVITY TWT WITH FOUR LOSSLESS OUTPUT CAVITIES, POSITIVE PREAPERED OUTPUT CIRCUIT, AND FINAL TWO CAVITIES WITH DECREASED PERIODS

HIETA 31C-3

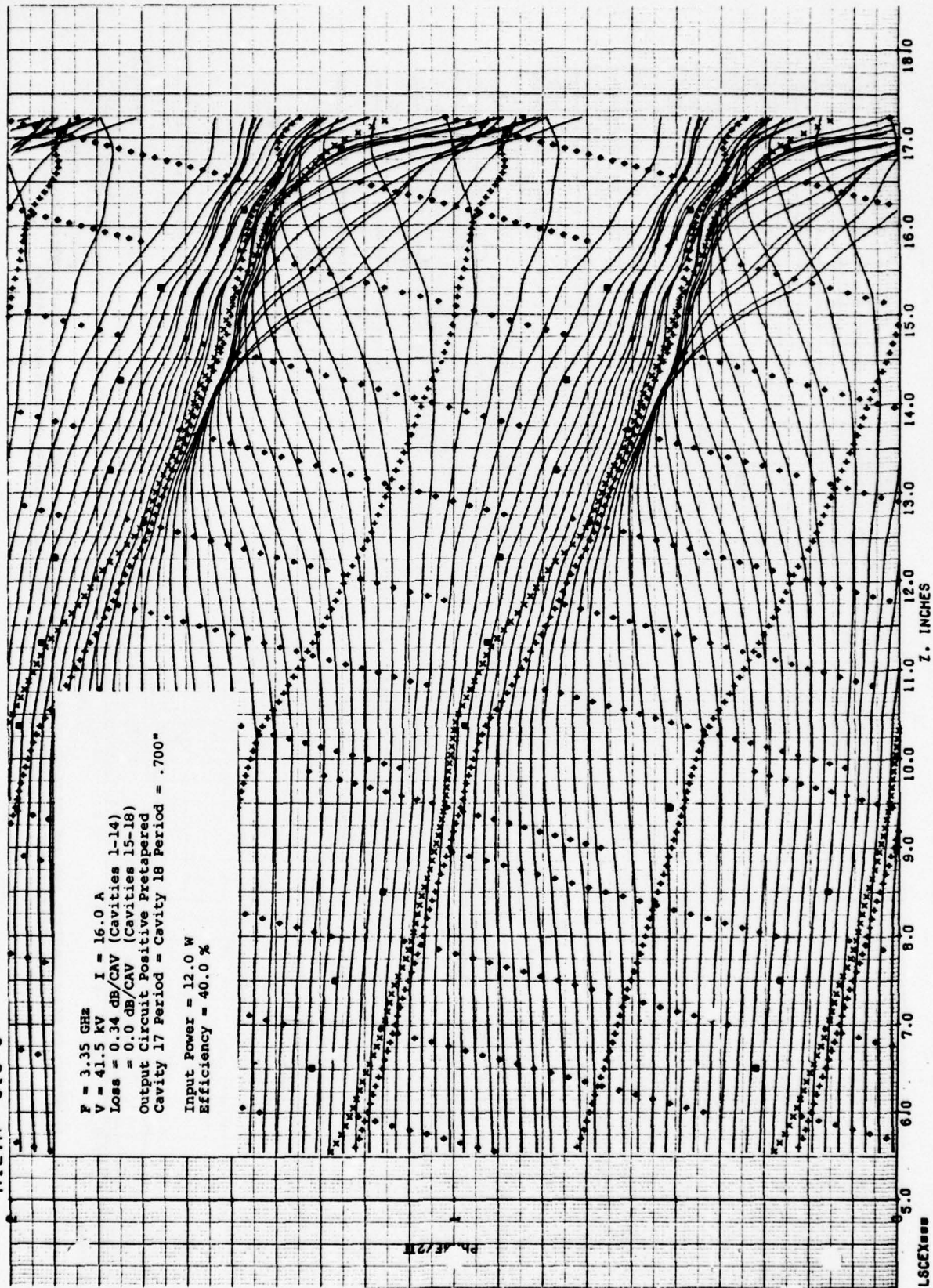
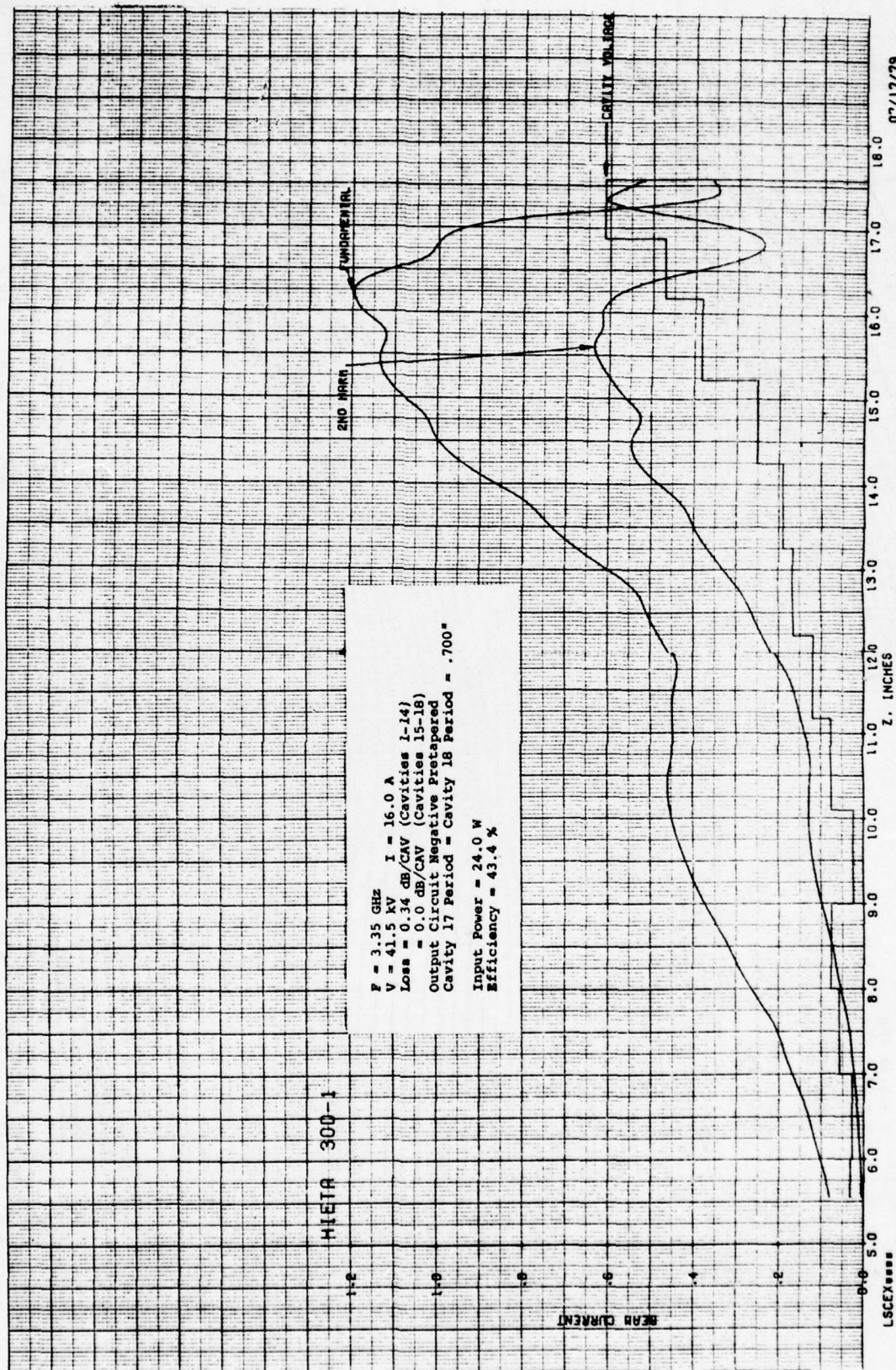


FIGURE 5.53 COMPUTED RELATIVE PHASES OF ELECTRON DISKS VS DISTANCE IN SIMULATED COUPLED-CAVITY TWT WITH FOUR LOSSLESS OUTPUT CAVITIES, POSITIVE PRETAPERED OUTPUT CIRCUIT, AND FINAL TWO CAVITIES WITH DECREASED PERIODS



07/17/79

FIGURE 5.54 COMPUTED RF BEAM CURRENTS AND GAP VOLTAGES VS DISTANCE IN SIMULATED COUPLED-CAVITY TWT WITH FOUR LOSSLESS OUTPUT CAVITIES, NEGATIVE PRETAPERED OUTPUT CIRCUIT, AND FINAL TWO CAVITIES WITH DECREASED PERIODS

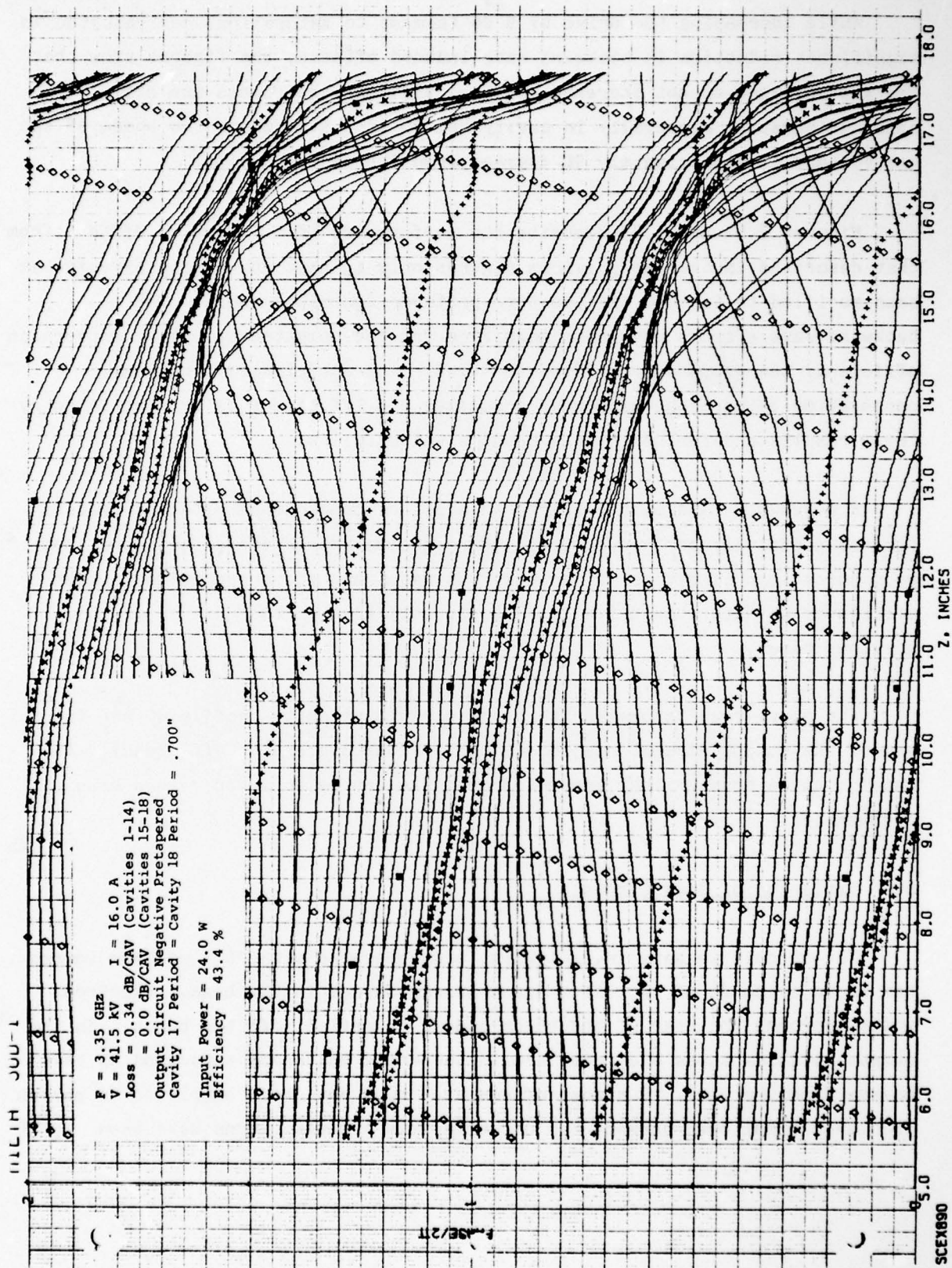


FIGURE 5.55 COMPUTED RELATIVE PHASES OF ELECTRON DISKS IN SIMULATED COUPLED-CAVITY TWT WITH FOUR LOSSLESS OUTPUT CAVITIES, NEGATIVE PRETAPERED OUTPUT CIRCUIT, AND FINAL TWO CAVITIES WITH DECREASED PERIODS

While increasing the drive by 9 dB (almost to saturation) has resulted in significant reduction in backward-wave induced effects, the figures show that the gap voltages do not increase monotonically and the phases are still somewhat erratic, especially in cavity No. 10 ($Z = 9.5$) where the phase of the gap voltage is approximately 90 degrees from its desired value.

Figures 5.52 and 5.53 describe the performance of a TWT which differs from that described in the two previous figures only in that the output circuit has been modified to include the positive pretaper described above. The backward-wave effects have been magnified and the computed saturated conversion efficiency has dropped from 42.6% to 40.0%. The anticipated negative correlation between backward-wave anomalies and efficiency is substantiated by these results and further by the results which follow.

Figures 5.54 and 5.55 complete this set of comparisons with the results for the negatively pretapered case. Here the backward-wave effects are less pronounced than in either of the previous cases and the computed conversion efficiency at saturated drive is 43.4 percent; greater than either of the previous cases.

The above results suggest that the circuit velocity profile at the front end of the output circuit has some impact on the conversion efficiency. It remains to be seen whether these improvements can be achieved over a band of frequencies.

5.5 Variation of Beam Current

The circuit we have investigated, when operated with 16 A of beam current, has shown evidence of excessive space-charge forces in the beam. Electrons which approach the rear of the bunch appear to reflect off the bunch. In the output cavities these electrons are in the wrong phase and thus tend to take energy from the wave. A number of computer runs have been completed to search for the optimum beam current for use with this circuit. Runs have been

completed at 12, 9 and 8 A. Additional standard cavities have been added to the circuit in order to bring the gain up to the approximate value it had in the 16 A version.

Table 5.1 is a summary of the results obtained over a two-to-one range in beam current. It is apparent, even though these results are not fully optimized, that beam current is not a strong determinant of conversion efficiency. Apparently the Pierce gain parameter C and space-charge parameter QC vary in such a way as to provide a broad plateau of nearly constant efficiency. When fully optimized we expect the computed efficiency will be in the range 45 to 50 percent at midband. Variation of efficiency with frequency will be computed after the midband efficiency has been optimized. The high current design would be expected to have the largest efficiency bandwidth product.

Figures 5.56 and 5.57 show some of the computed results for Run HIEFF 40, the final example of Table 5.1. This TWT runs with an 8 A beam current and has three additional cavities in each section. The output section has two additional standard cavities and one additional taper cavity. The three velocity taper cavities at the output are of 80 percent period.

In Figure 5.56 the 12-cavity output circuit begins at $Z = 12"$. The gap voltages appear to build up more regularly than was the case with the equivalent non-pretapered 16 A case shown in Figure 5.50. The maximum normalized rf beam current is 1.29 compared with 1.17 for the comparable 16 A case. Figure 5.57 shows an improved clearing out of the interbunch space and a relative decrease in the severity of reacceleration of the electrons at the back of the bunch. The computed saturated conversion efficiency for the 8 A TWT is 42.9 percent compared with 42.6 percent for the 16 A TWT.

TABLE 5.1

Computed characteristics of several TWT designs
with different beam currents and circuit tapers

RUN	BEAM CURRENT (A)	NO. OF CAVITIES	PRETAPER (%)	TAPER (%)	SATURATION DRIVE (W)	P OUT (kW)	EFFICIENCY (%)
HIEFF 34	16.0	9-9	NONE	70-70	16.0	282.6	42.6
31	16.0	9-9	+ 16	70-70	12.0	265.4	40.0
30	16.0	9-9	- 16	70-70	24.0	288.3	43.4
35	12.0	10-10	NONE	70-70	8.0	217.2	43.6
38	12.0	10-10	NONE	70-80	8.0	213.4	42.9
36	9.0	11-11	NONE	70-70	2.0	156.4	41.9
39	9.0	11-11	NONE	75-75	2.0	153.2	41.0
37	8.0	12-12	NONE	70-70-70	2.0	129.0	38.0
40	8.0	12-12	NONE	80-80-80	1.0	142.3	42.9

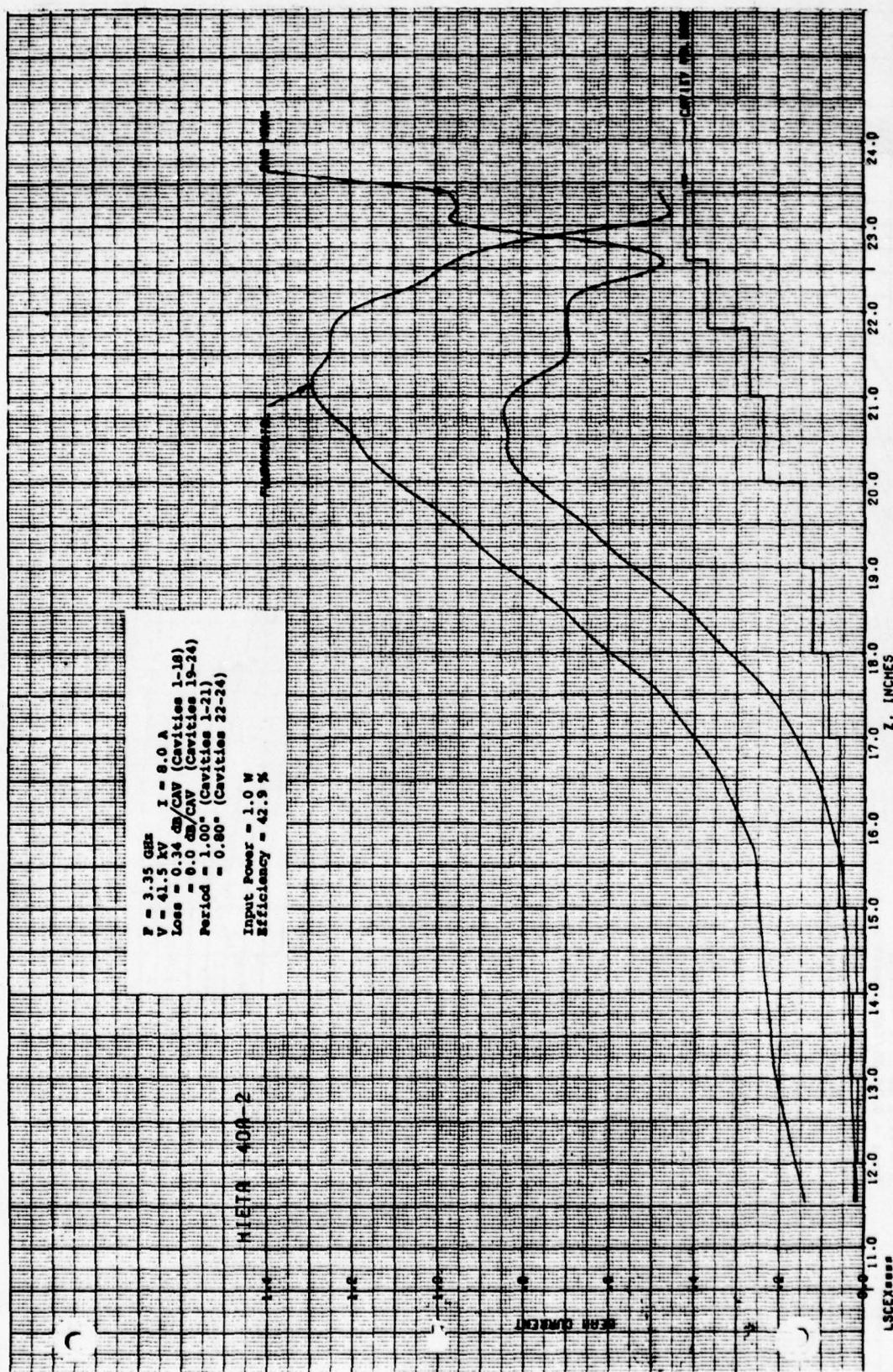


FIGURE 5.56 COMPUTED RF BEAM CURRENTS AND GAP VOLTAGES VS DISTANCE IN SIMULATED COUPLED-CAVITY TWT WITH SIX LOSSLESS OUTPUT CAVITIES AND FINAL THREE CAVITIES WITH DECREASED PERIODS

HIETA 40A-2

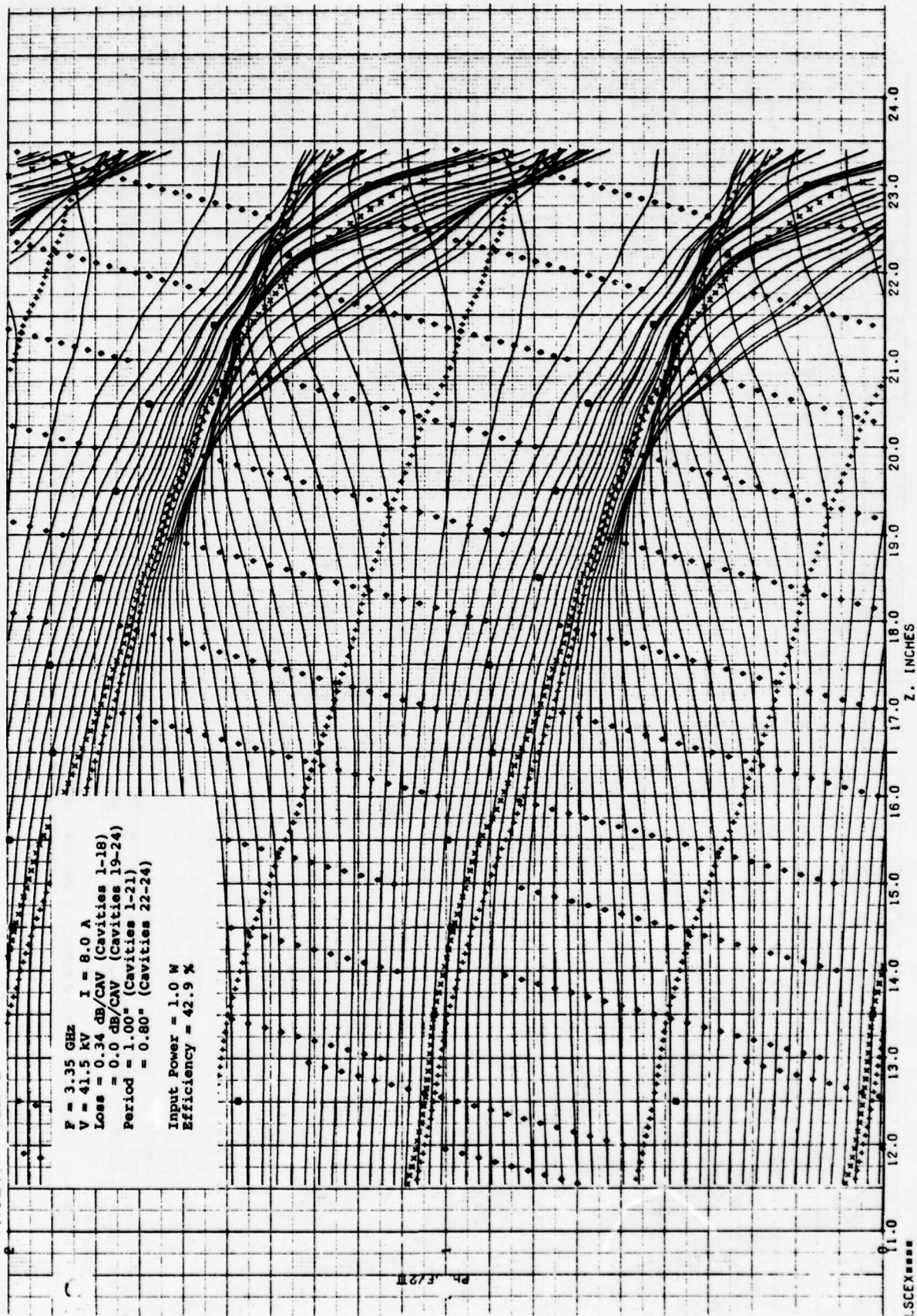


FIGURE 5.57 COMPUTED RELATIVE PHASES OF ELECTRON DISKS VS DISTANCE IN SIMULATED COUPLED-CAVITY TWT WITH SIX LOSSLESS OUTPUT CAVITIES AND FINAL THREE CAVITIES WITH DECREASED PERIODS

5.6 Optimization of Low Current TWT

Table 5.2 contains a tabulation of some of the salient parameters of the computer runs to be discussed in this section. The results will be discussed in the order in which they occur in this table. The figures are labeled with run numbers for cross indexing purposes.

Figures 5.56 through 5.61 (Run 40A) show the computed gap voltages, rf beam currents, and electron phase trajectories in the output section of a two-section TWT with 12 cavities in each section. There are two figures for each input drive level and three input drives. The output section comprises nine cavities each 1.00 inch long followed by three cavities each 0.80 inch long. This configuration is referred to as an 80-80-80 taper. The first six cavities are lossy and the last six cavities are lossless. The circuit sections are cold matched at both ends. This simple circuit will be used as a basis for comparison.

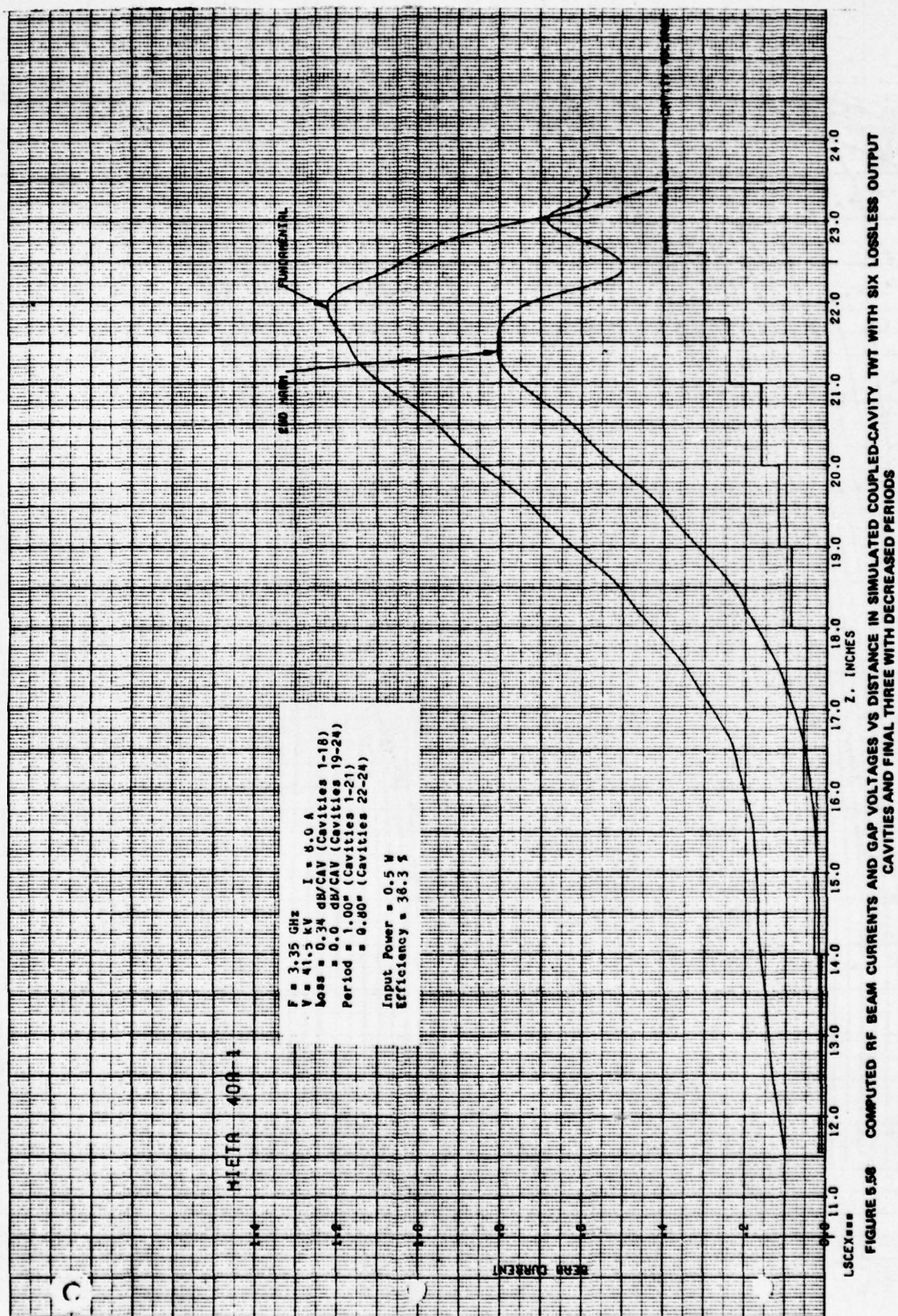
Run 40A saturates at 1 watt drive with 42.9 percent conversion efficiency. The maximum fundamental rf current is $1.29 I_0$ and occurs in cavity No. 22. The buildup in gap voltage is fairly regular at saturated drive (Figure 5.56) but less so when overdriven by 3 dB, as illustrated in Figure 5.60. The monotonicity of gap voltage is not felt to be important since we have found no consistent correlation between conversion efficiency and monotonic buildup in gap voltage. Figure 5.57 shows good electron bunching with a slight tendency for electron overtaking between the twentieth and twenty-first gaps. A sudden decrease in the velocity of the circuit in this region might be expected to improve the bunching and increase the efficiency.

Run 41C is illustrated in Figures 5.62 to 5.67. The circuit and the beam employed in this example are similar to the previous example (Run 40A) except that the first nine cavities of the output section have an 8 percent negative linear taper in cavity period. This arrangement is referred to as negative pretaper. The negative pretaper has resulted in a small loss in efficiency and

TABLE 5.2

Comparison of Computed TWT Characteristics

Run Number	Saturation Drive (Watts)	Saturation Conversion Efficiency (%)	Maximum Fundamental RF Current/ I_0	Comments
40A	1.0	42.9	1.29	Standard configuration, 1.00 inch gaps, 80-80-80 taper
41C	1.0	40.9	1.24	8% pretaper in cavities 13-21
42C	1.0	43.1	1.32	8% negative pretaper in cavities 13-21
42D	1.0	40.5	1.34	Same as 42C except 100-70-70 taper instead of 80-80-80
43A	4.0	39.2	1.14	Same as 40A except 0.500 inch gaps in cavities 13-21
43D	2.0	43.0	1.15	Same as 43A except two cavities added to make up for gain loss caused by large gaps
45A	1.0	42.9	1.32	Same as 42C except 90-80-70 taper instead of 80-80-80
45B	1.0	40.6	1.32	Same as 42C except 70-80-90 taper instead of 80-80-80
47A	2.0	42.7	1.42	Same as 40A except cavities 13-21 increased to 1.10 inch length
47B	4.0	29.8	1.37	Same as 40A except cavities 13-21 increased to 1.20 inch length
47E	2.0	40.2	1.44	Same as 47A except 90-70-75 taper instead of 80-80-80
48A	1.0	42.6	1.29	Same as 40A except sever load adjusted to give hot match at output



HIETA 40A-1

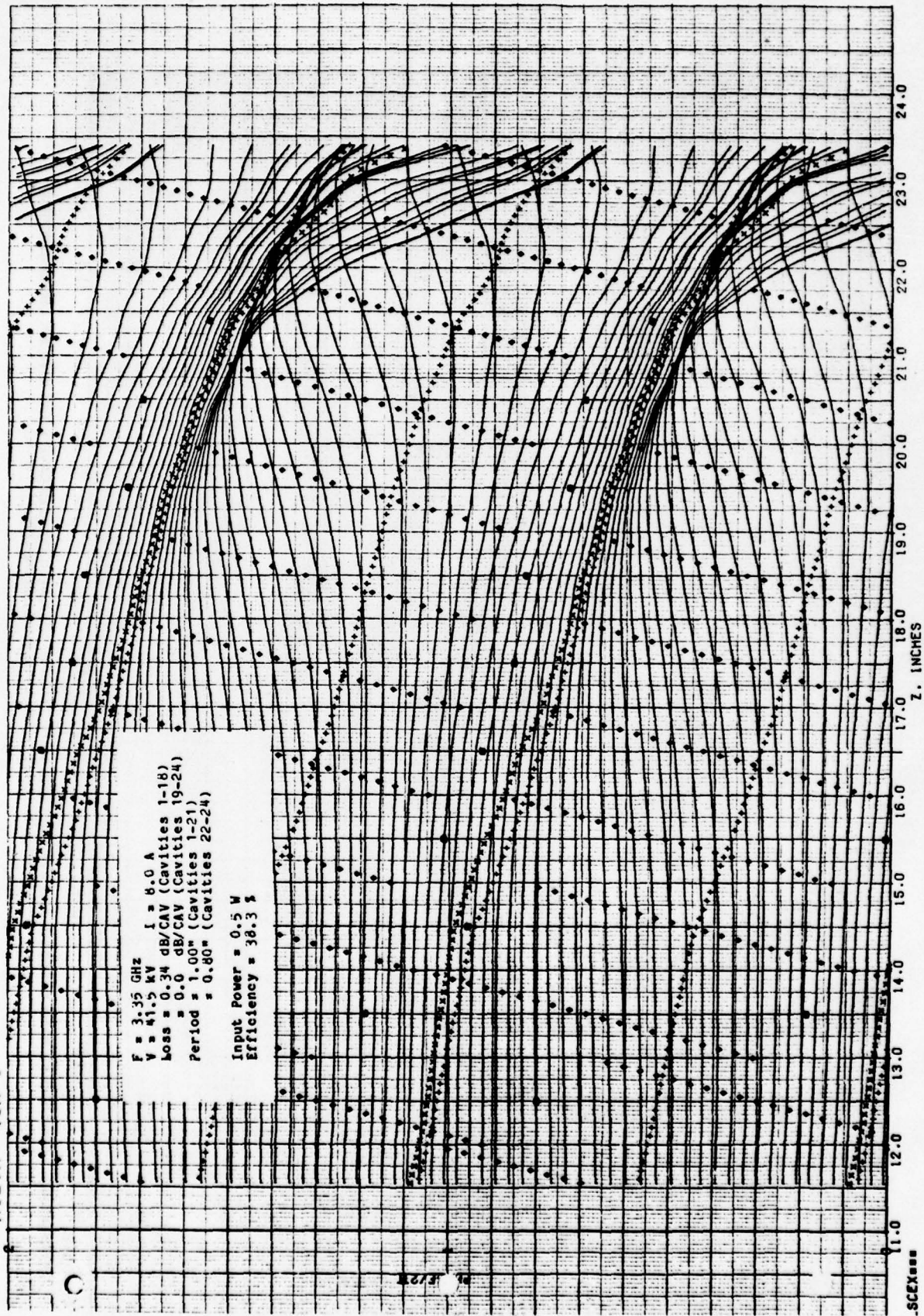


FIGURE 5.59 COMPUTED RELATIVE PHASES OF ELECTRON DISKS VS DISTANCE IN SIMULATED COUPLED-CAVITY TWT WITH SIX LOSSLESS OUTPUT CAVITIES AND FINAL THREE CAVITIES WITH DECREASED PERIODS

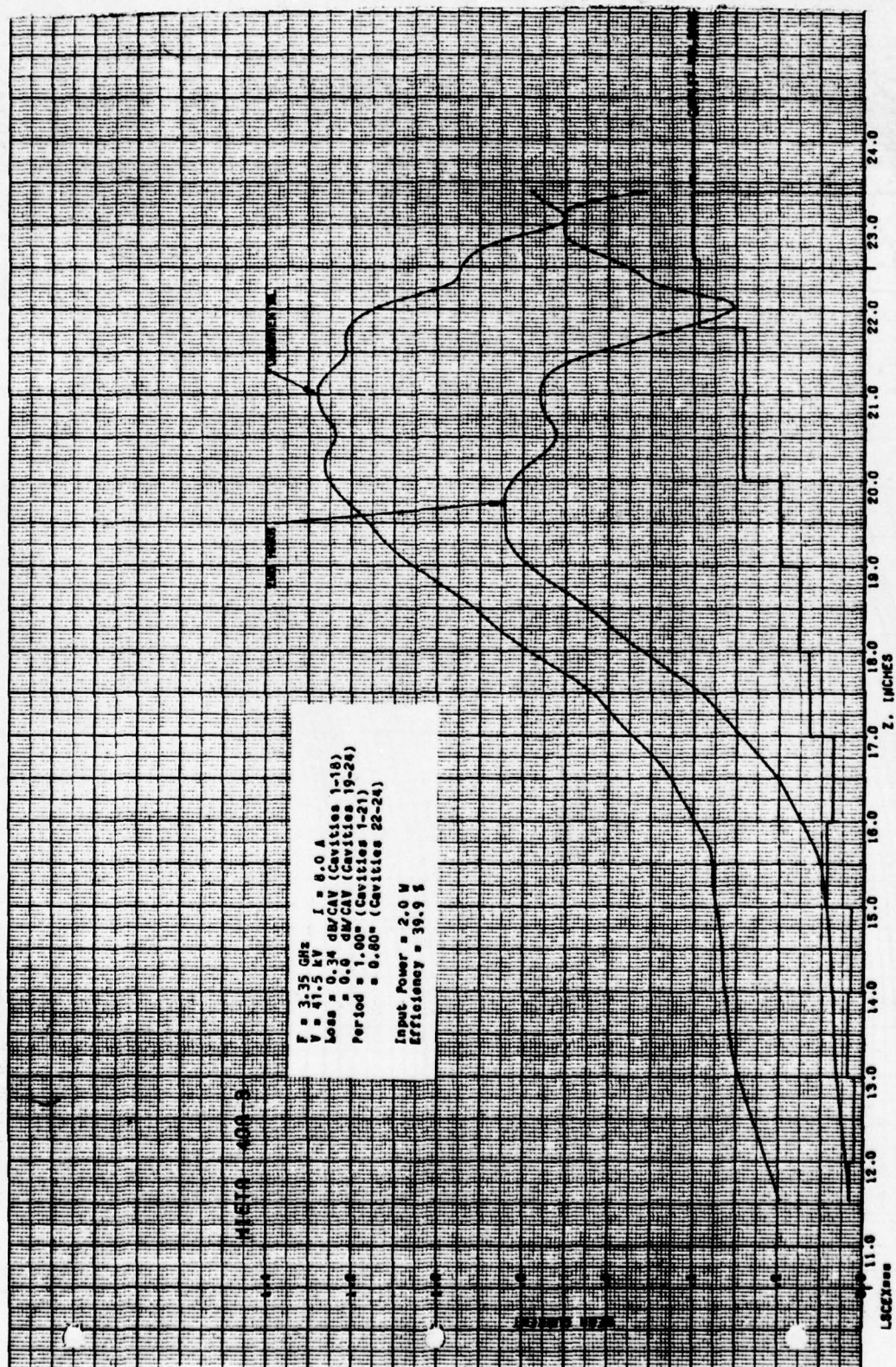


FIGURE 5.60 COMPUTED RF BEAM CURRENTS AND GAP VOLTAGES VS DISTANCE IN SIMULATED COUPLED-CAVITY TWT WITH SIX LOSSLESS OUTPUT CAVITIES AND FINAL THREE WITH DECREASED PERIODS

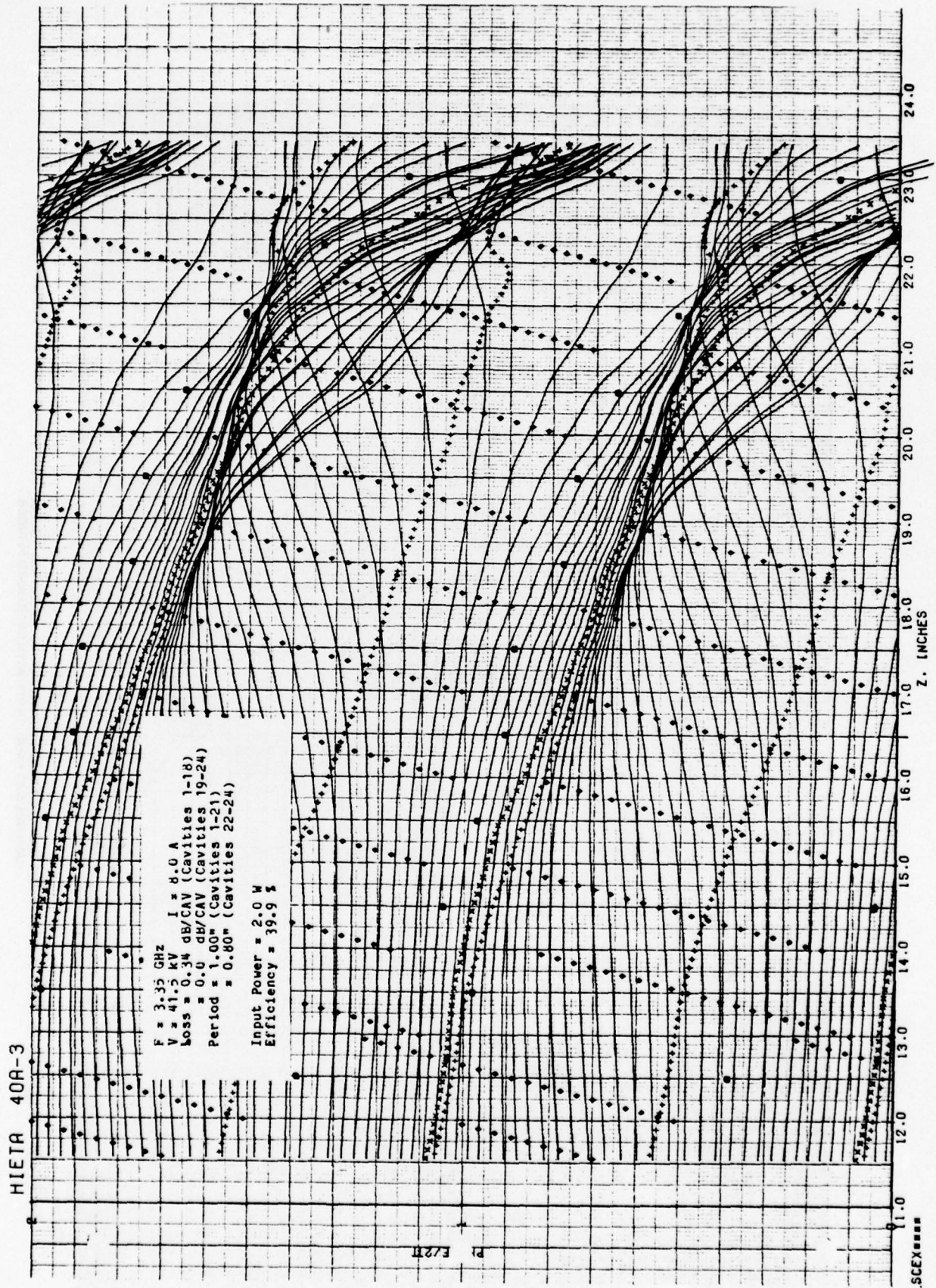


FIGURE 5.61 COMPUTED RELATIVE PHASES OF ELECTRON DISKS VS DISTANCE IN SIMULATED COUPLED-CAVITY TWT WITH SIX LOSSLESS OUTPUT CAVITIES AND FINAL THREE CAVITIES WITH DECREASED PERIODS

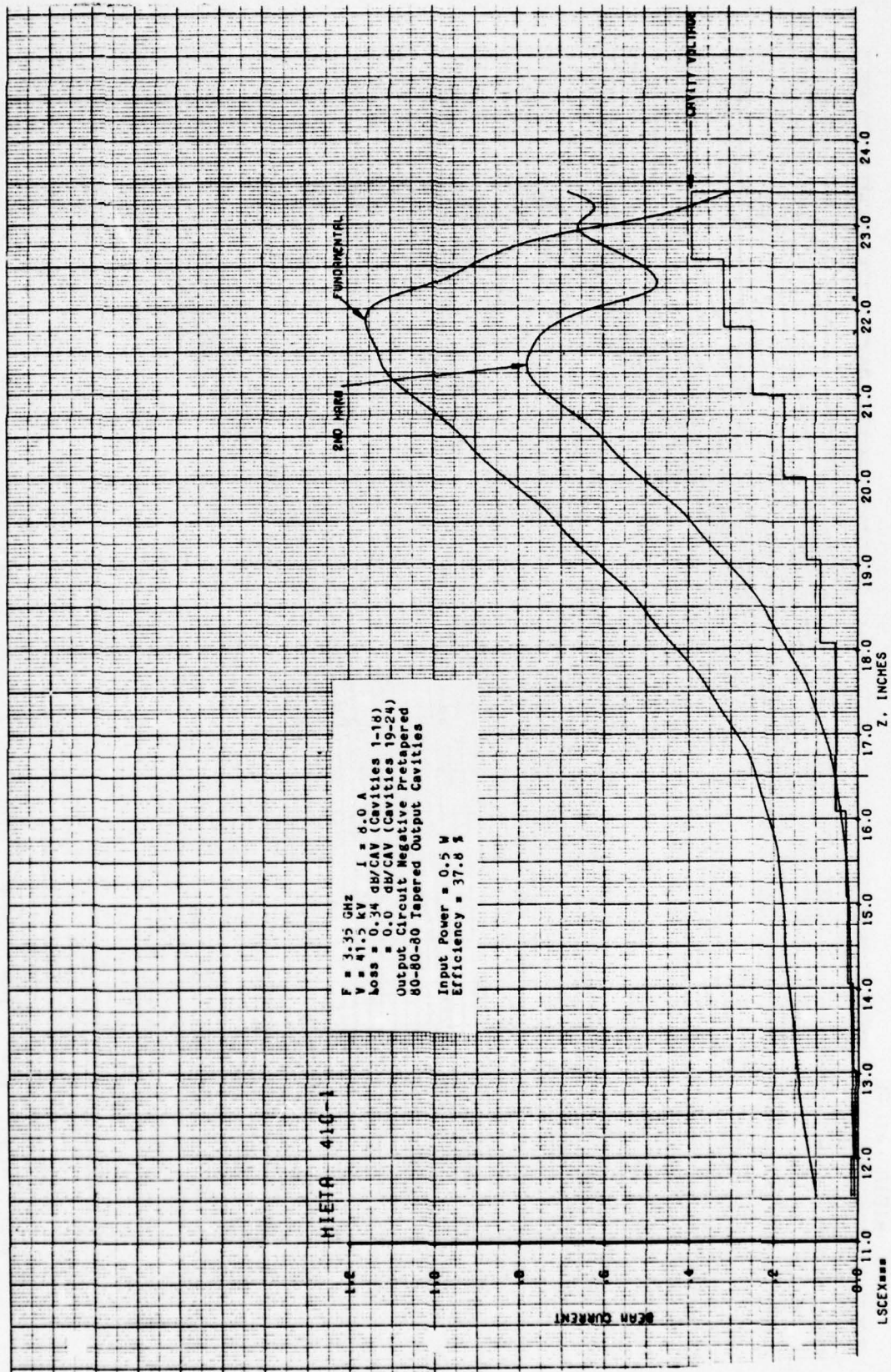


FIGURE 5.62 COMPUTED RF BEAM CURRENTS AND GAP VOLTAGES VS DISTANCE IN SIMULATED COUPLED-CAVITY TWT WITH SIX LOSSLESS OUTPUT CAVITIES, NEGATIVE PRETAPERED OUTPUT CIRCUIT, AND FINAL THREE CAVITIES WITH DECREASED PERIODS

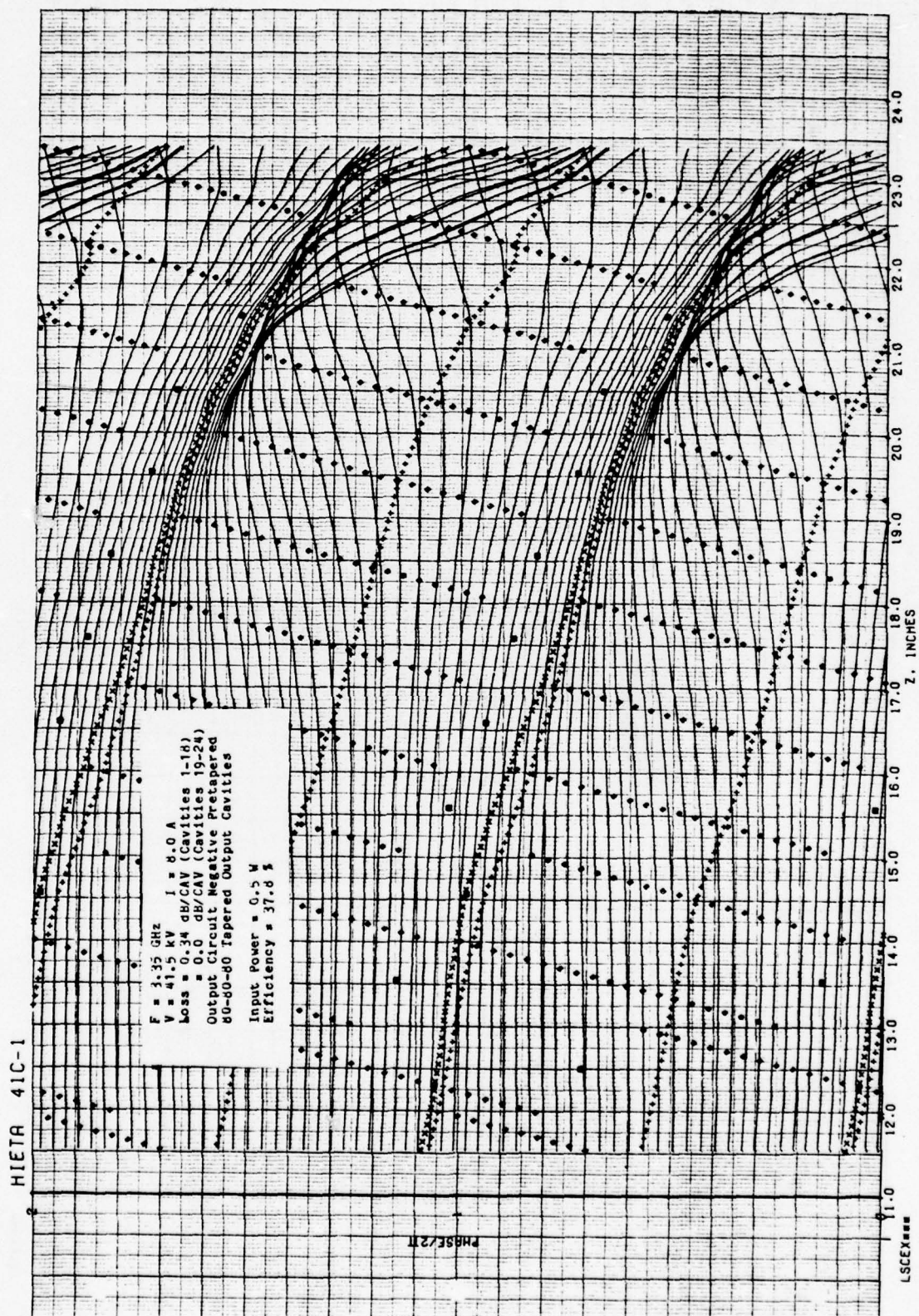


FIGURE 5.63 COMPUTED RELATIVE PHASES OF ELECTRON DISKS VS DISTANCE IN SIMULATED COUPLED-CAVITY TWT WITH SIX LOSSLESS OUTPUT CAVITIES, NEGATIVE PREAPERED OUTPUT CIRCUIT, AND FINAL THREE CAVITIES WITH DECREASED PERIODS

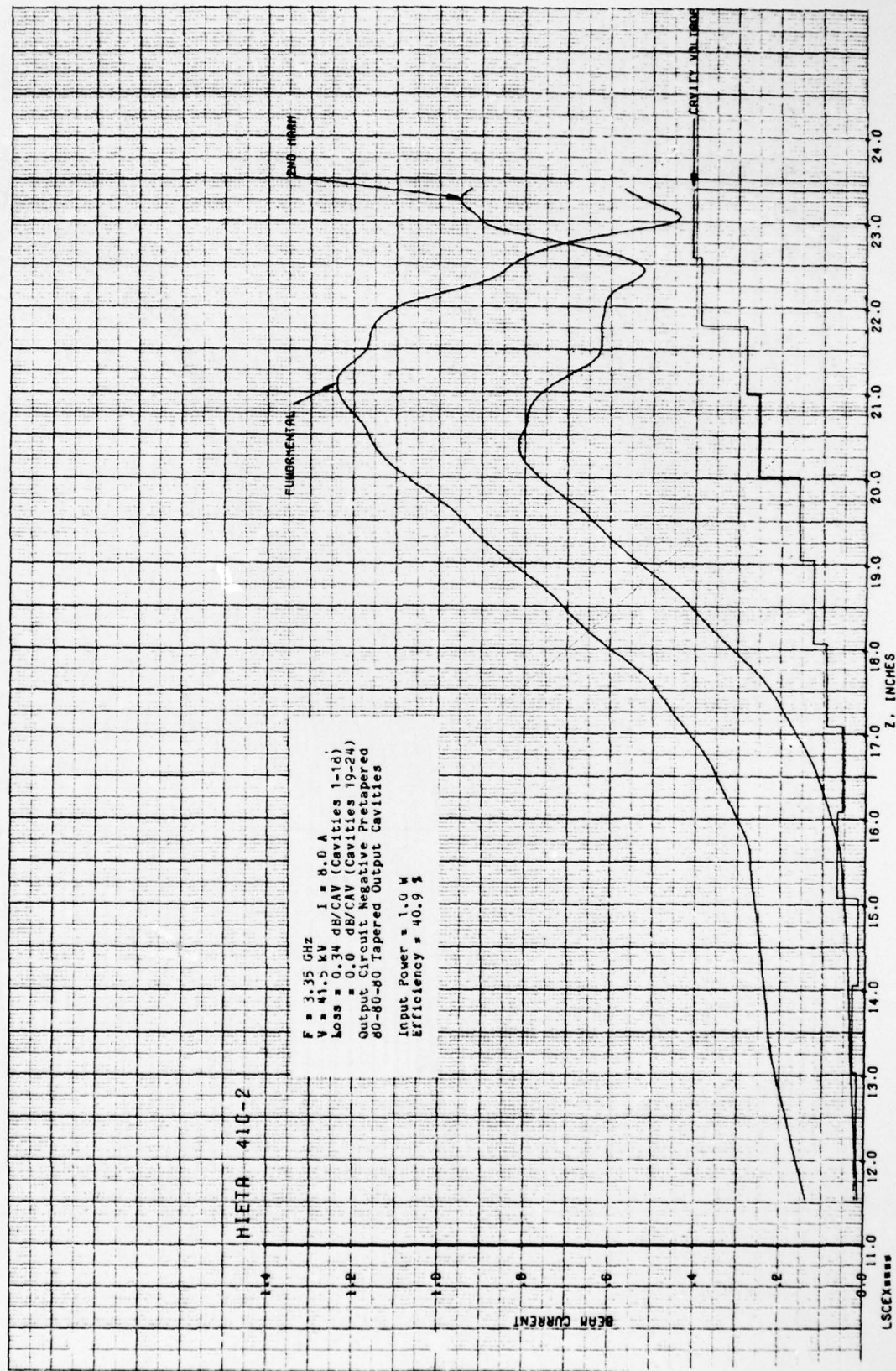


FIGURE 5.64 COMPUTED RF BEAM CURRENTS AND GAP VOLTAGES VS DISTANCE IN SIMULATED COUPLED-CAVITY TWT WITH SIX LOSSLESS OUTPUT CAVITIES, NEGATIVE PRETAPERED OUTPUT CIRCUIT, AND FINAL THREE CAVITIES WITH DECREASED PERIODS

HIEA 41C-2

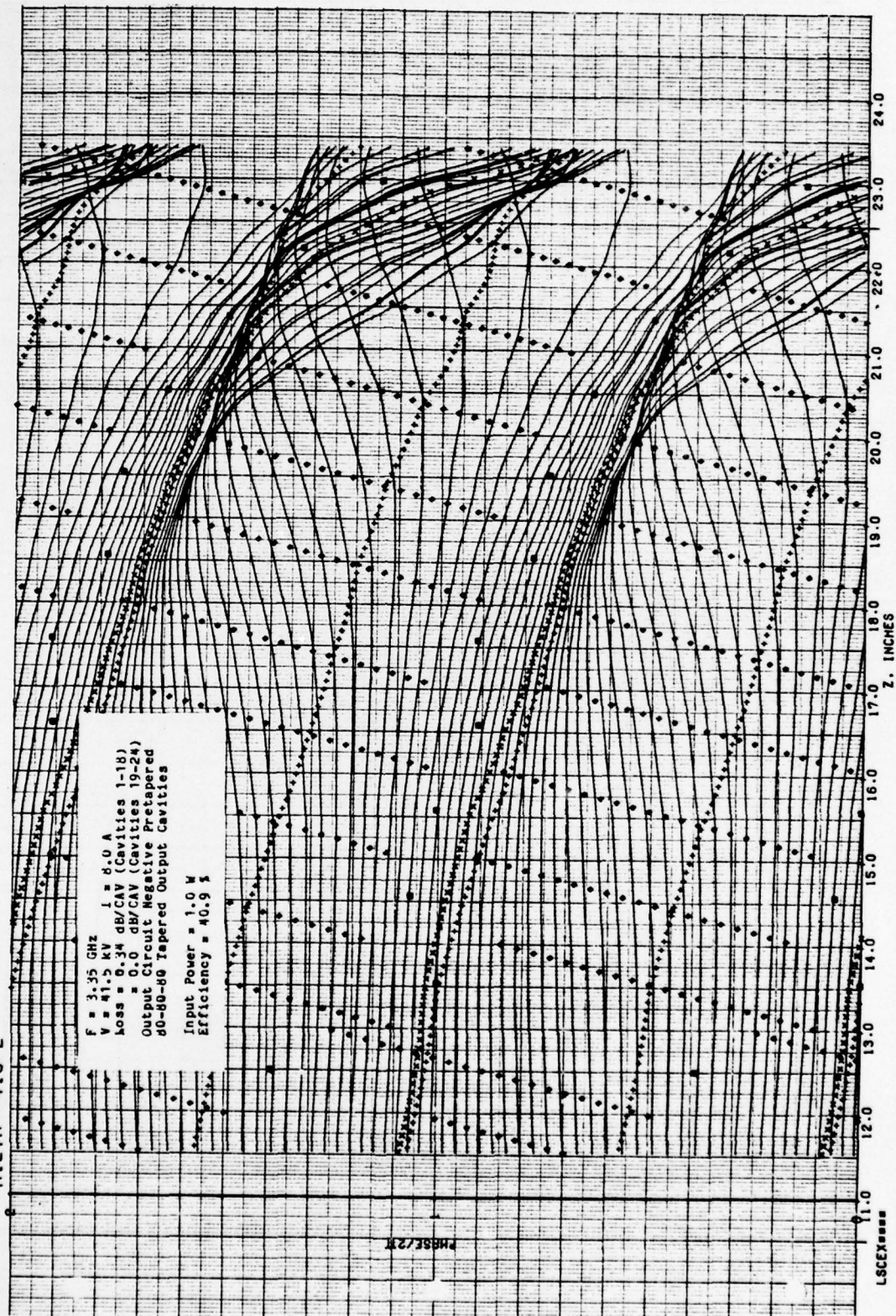


FIGURE 5.65 COMPUTED RELATIVE PHASES OF ELECTRON DISKS VS DISTANCE IN SIMULATED COUPLED-CAVITY TWT WITH SIX LOSSLESS OUTPUT CAVITIES, NEGATIVE PRETAPERED OUTPUT CIRCUIT, AND FINAL THREE CAVITIES WITH DECREASED PERIODS

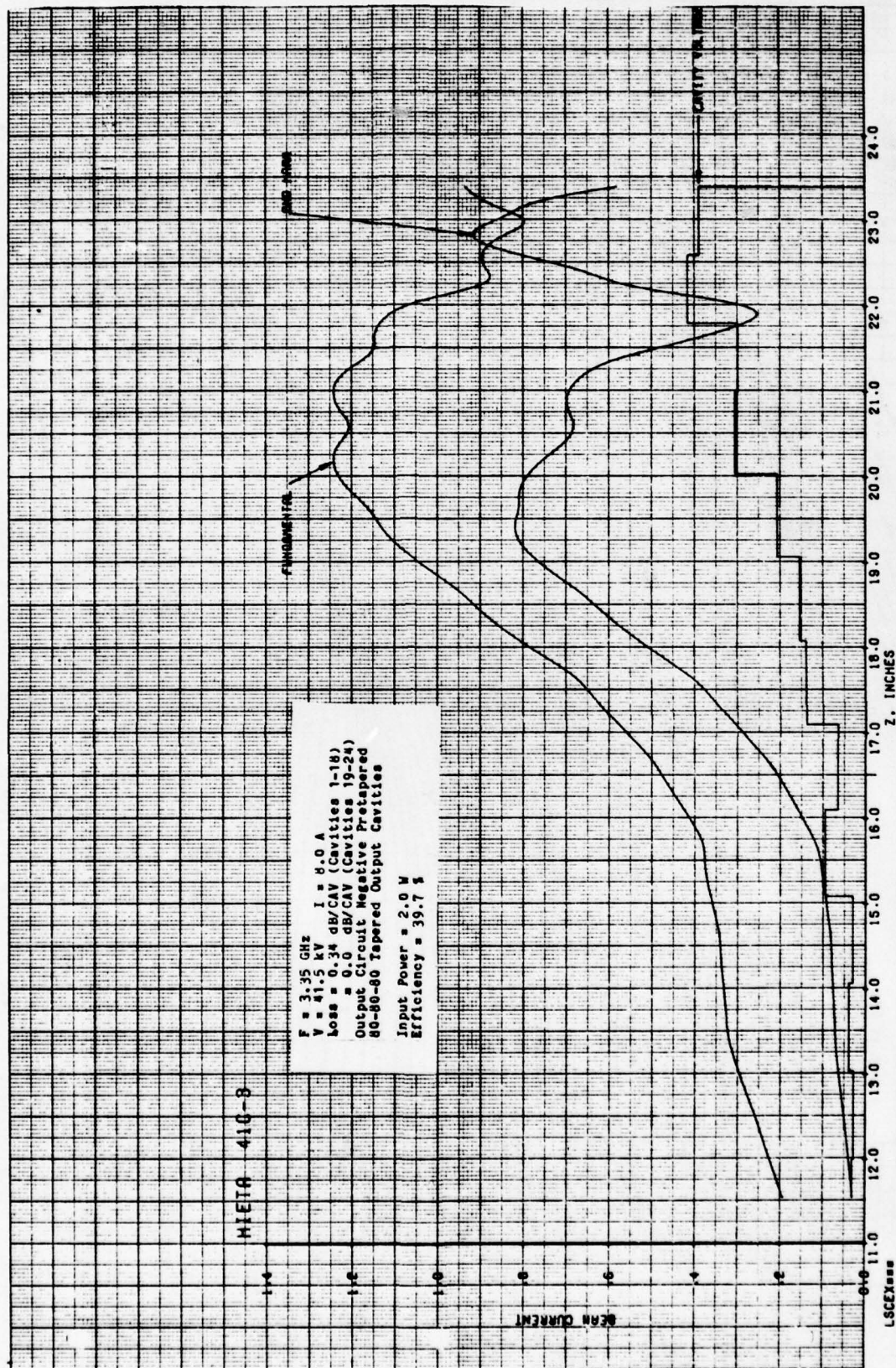


FIGURE 5-66 COMPUTED RF BEAM CURRENTS AND GAP VOLTAGES VS DISTANCE IN SIMULATED COUPLED-CAVITY TWT WITH SIX LOSSLESS OUTPUT CAVITIES, NEGATIVE PREAPERED OUTPUT CIRCUIT, AND FINAL THREE CAVITIES WITH DECREASED PERIODS

HIETA 41C-3

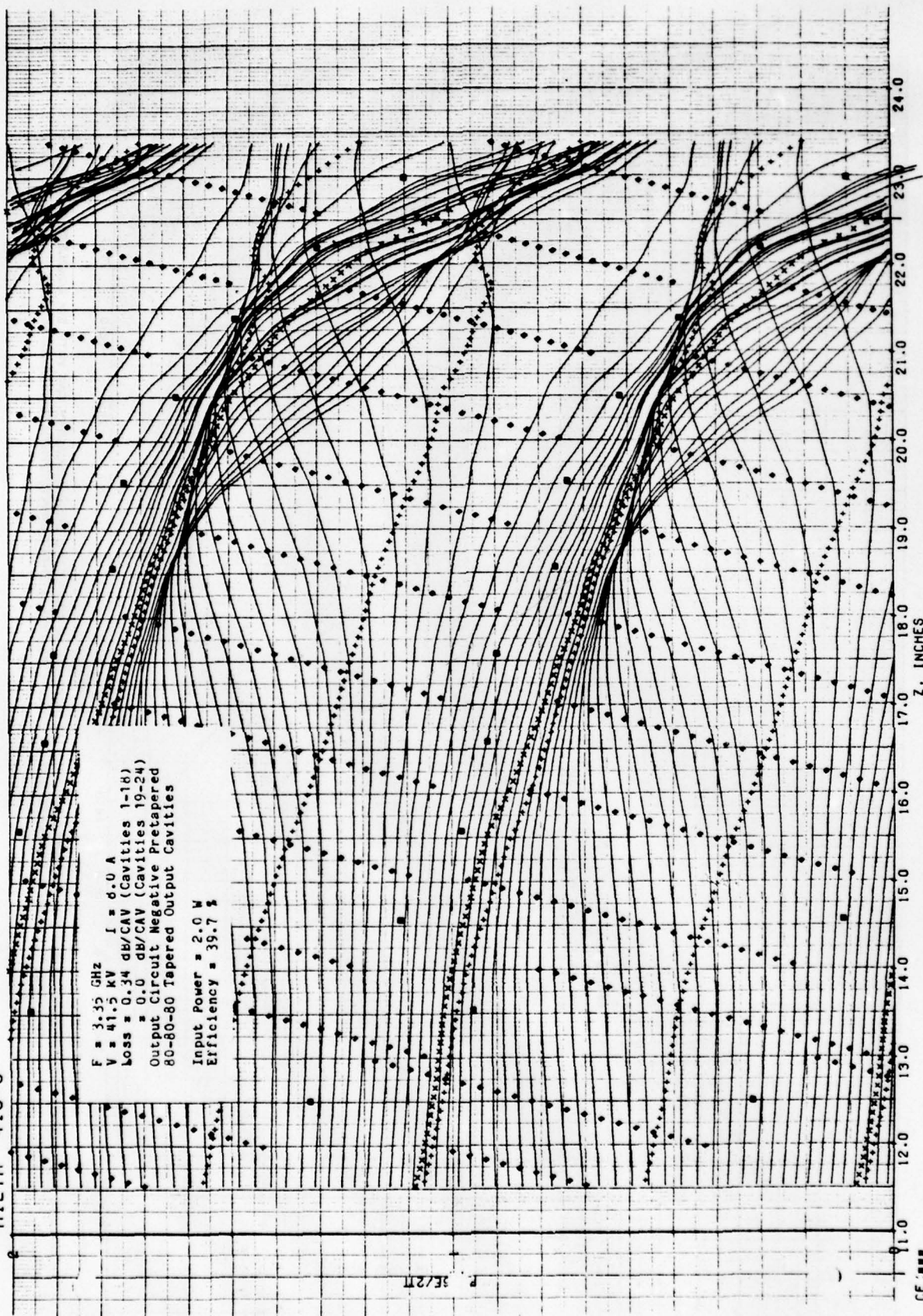


FIGURE 5.67 COMPUTED RELATIVE PHASES OF ELECTRON DISKS VS DISTANCE IN SIMULATED COUPLED-CAVITY TWT WITH SIX LOSSLESS OUTPUT CAVITIES, NEGATIVE PRETAPERED OUTPUT CIRCUIT, AND FINAL THREE CAVITIES WITH DECREASED PERIODS

in fundamental rf current. Figures 5.64 and 5.67 (employing saturated drive) are difficult to distinguish from Figures 5.56 and 5.57 (the non-pretapered case). The reduction in anomalous backward-wave effect noted in the 16A version of the TWT, in which negative pretaper resulted in a significant improvement in monotonicity of the gap voltages, has not been verified here. It must be concluded that factors other than pretaper are at least as important as pretaper in smoothing the gap voltage distribution. Other runs have been made employing more severe negative pretaper resulting in a continuing decline in performance.

Run 42C is illustrated in Figures 5.68 through 5.73. This example is dual to the previous example, with 8 percent positive pretaper. The positive pretaper has resulted in a small increase in efficiency and in fundamental rf current with $\eta = 43.1$ percent and $I_1 = 1.32 I_0$. Neither is this improvement in efficiency significant nor are the phase and amplitude plots sufficiently different from those derived for the non-pretapered case to recommend further search in this direction. A sixteen percent positive pretaper has been computed to produce a conversion efficiency of 41.4 percent. This is less than the non-pretapered case but not grossly different from it.

Run 42D represents an attempt to improve performance by modifying the shape of the velocity taper in the last three cavities of the output circuit. A more abrupt 70-70 velocity taper is used here relative to the 80-80-80 taper employed in the previous cases. The more abrupt taper was investigated in the expectation that better bunching might occur if the phase condition favoring bunching were preserved further along the circuit before the necessary final velocity taper. The results for this run are shown in Figures 5.74 to 5.79. The anticipated improvement in bunching has resulted, although the improvement is meager ($I_1 = 1.34 I_0$ vs. $I_1 = 1.32 I_0$) and has been gained at the expense of the efficiency which has been reduced from 43.1 percent to 40.5 percent. A three-cavity final velocity taper is clearly required in this TWT.

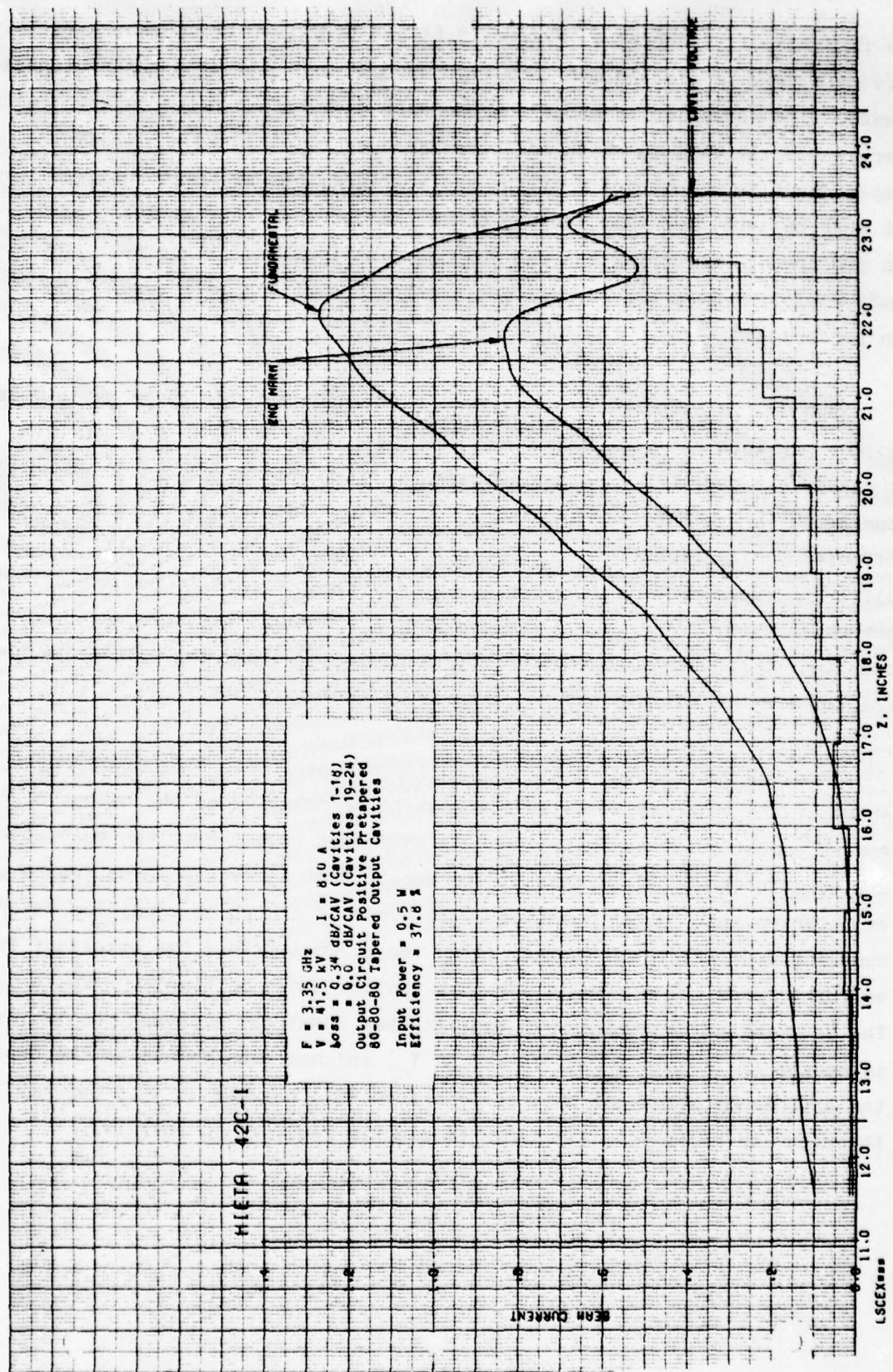


FIGURE 5.68 COMPUTED RF BEAM CURRENTS AND GAP VOLTAGES VS DISTANCE IN SIMULATED COUPLED-CAVITY TWT WITH SIX LOSSLESS OUTPUT CAVITIES, POSITIVE PRETAPERED OUTPUT CIRCUIT, AND FINAL THREE CAVITIES WITH DECREASED PERIODS

HIETA 42C-1

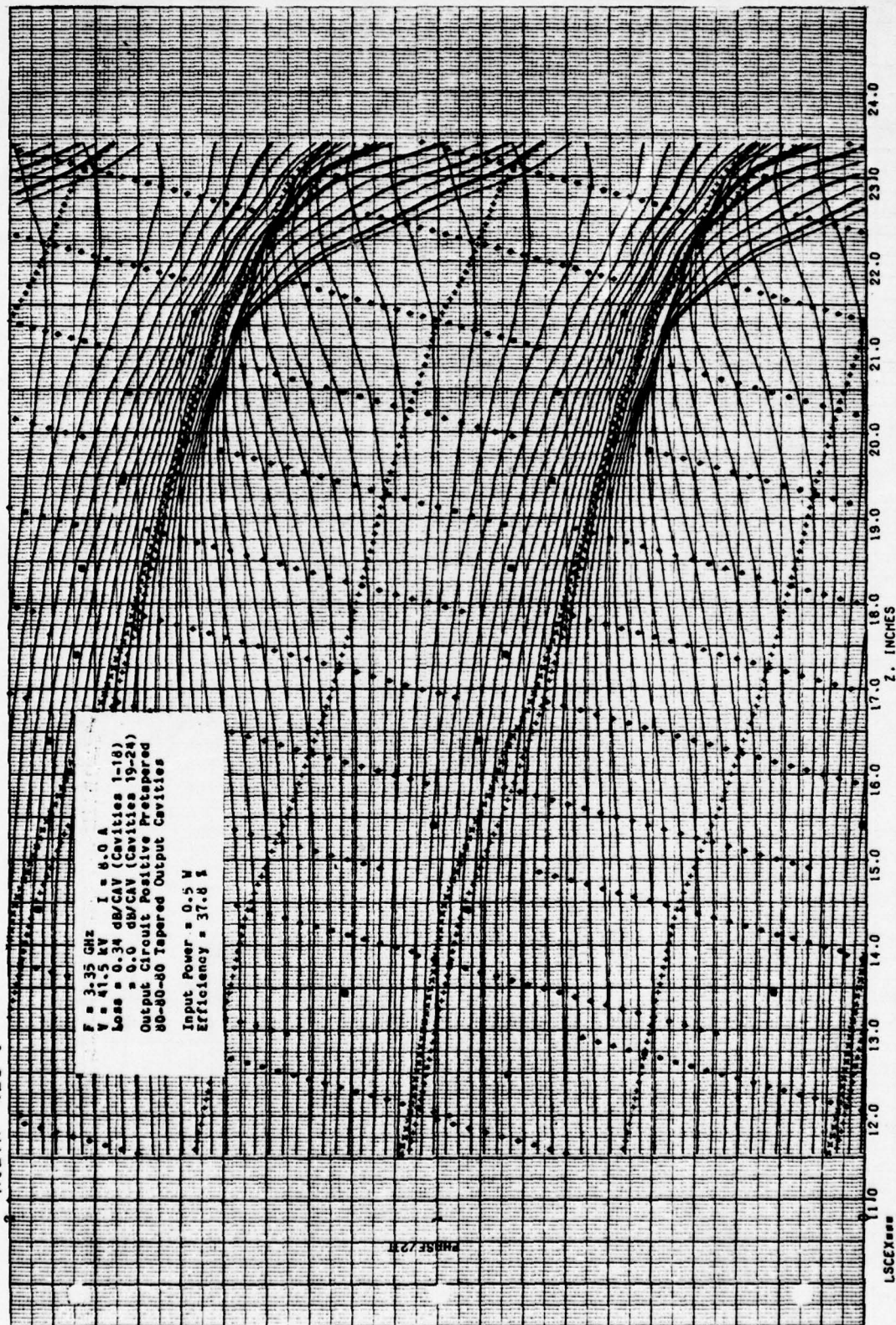


FIGURE 5.69 COMPUTED RELATIVE PHASES OF ELECTRON DISKS VS DISTANCE IN SIMULATED COUPLED-CAVITY TWT WITH SIX LOSSLESS OUTPUT CAVITIES, POSITIVE PRETAPERED OUTPUT CIRCUIT, AND FINAL THREE CAVITIES WITH DECREASED PERIODS

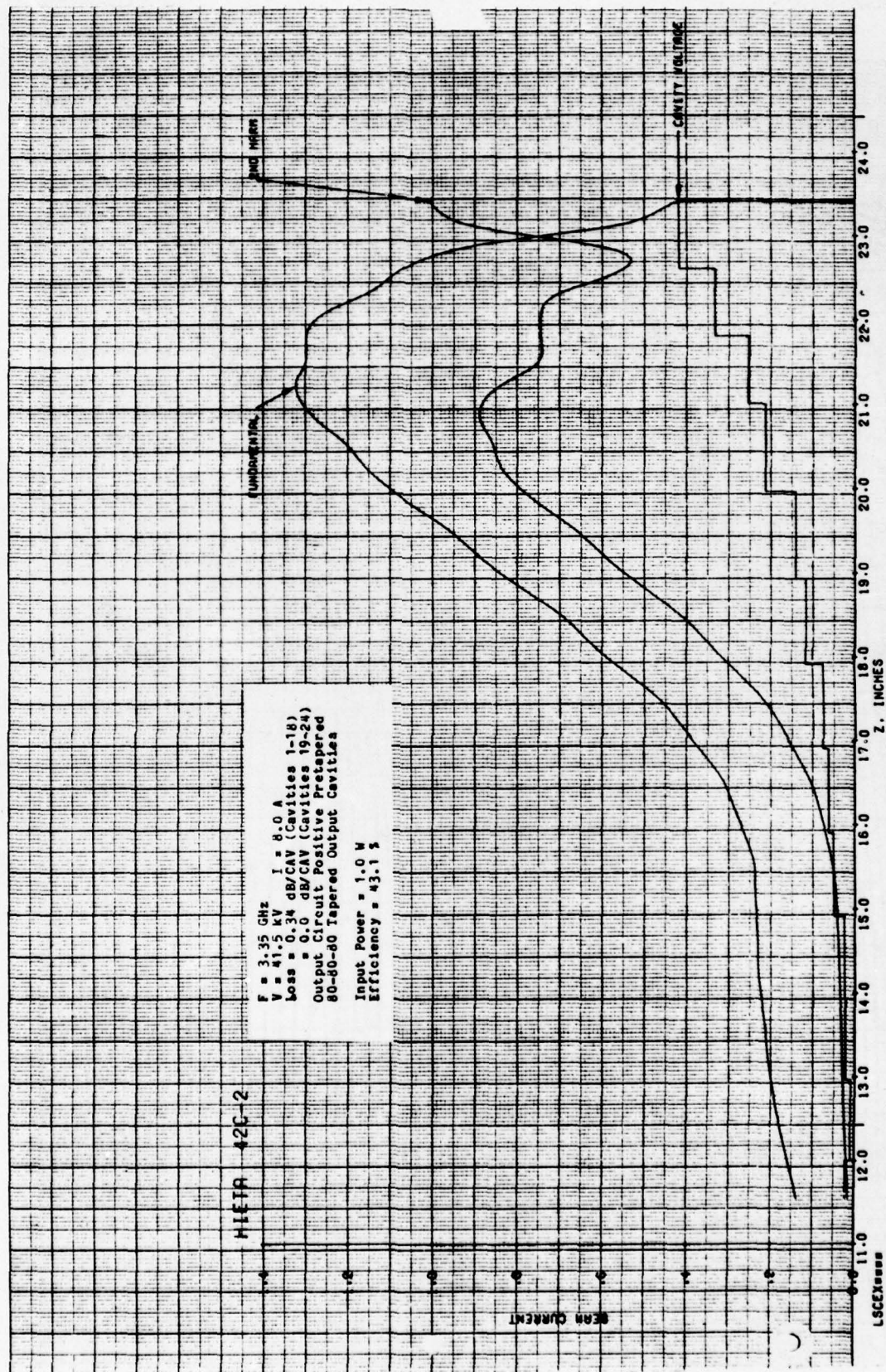


FIGURE 6.70 COMPUTED RF BEAM CURRENTS AND GAP VOLTAGES VS DISTANCE IN SIMULATED COUPLED-CAVITY TWT WITH SIX LOSSLESS OUTPUT CAVITIES, POSITIVE PRETAPERED OUTPUT CIRCUIT, AND FINAL THREE CAVITIES WITH DECREASED PERIODS

HIETA 42C-2

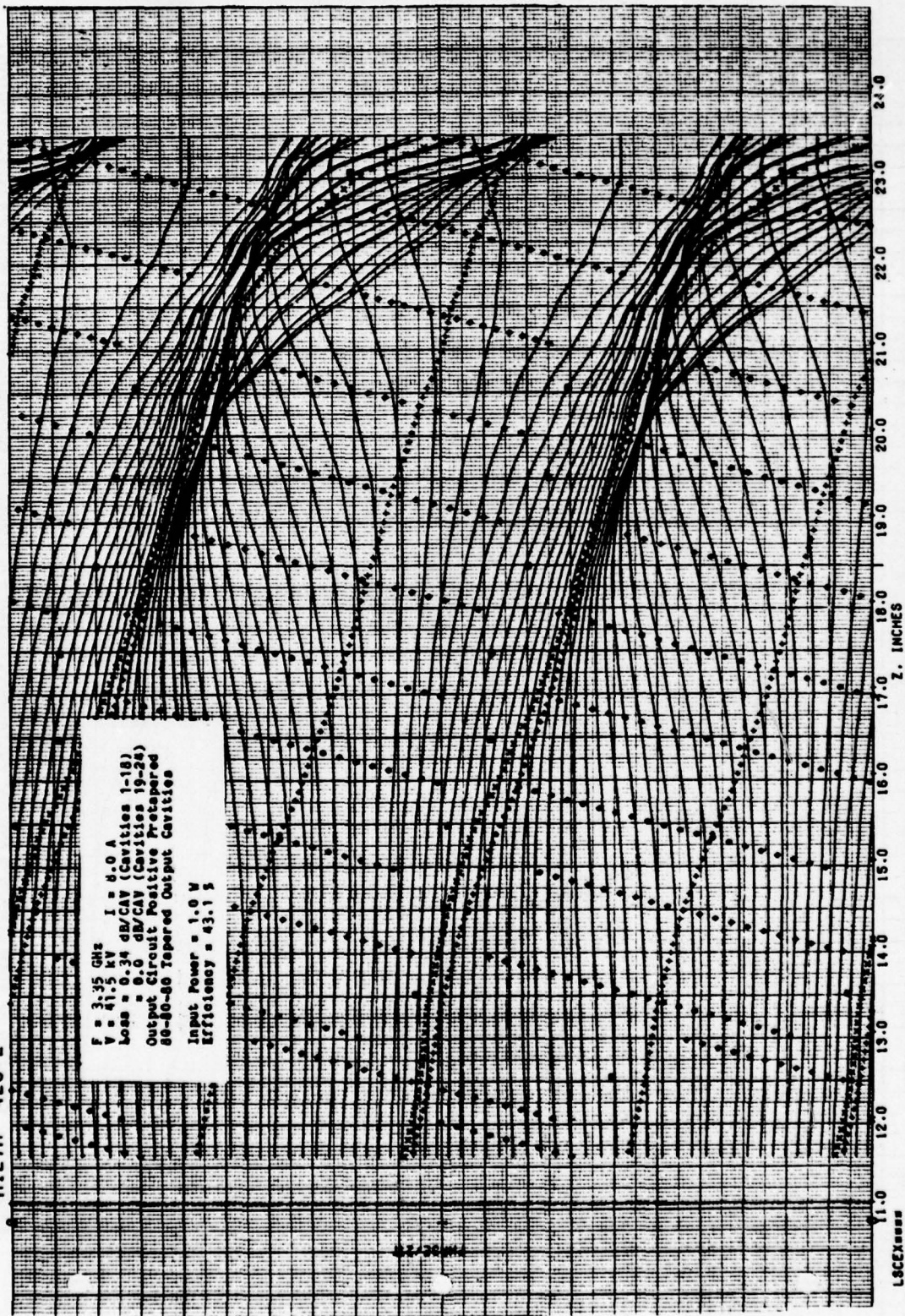


FIGURE 5.71 COMPUTED RELATIVE PHASES OF ELECTRON DISKS VS DISTANCE IN SIMULATED COUPLED-CAVITY TWT WITH SIX LOSSLESS OUTPUT CAVITIES, POSITIVE PRE-TAPERED OUTPUT CIRCUIT, AND FINAL THREE CAVITIES WITH DECREASED PERIODS

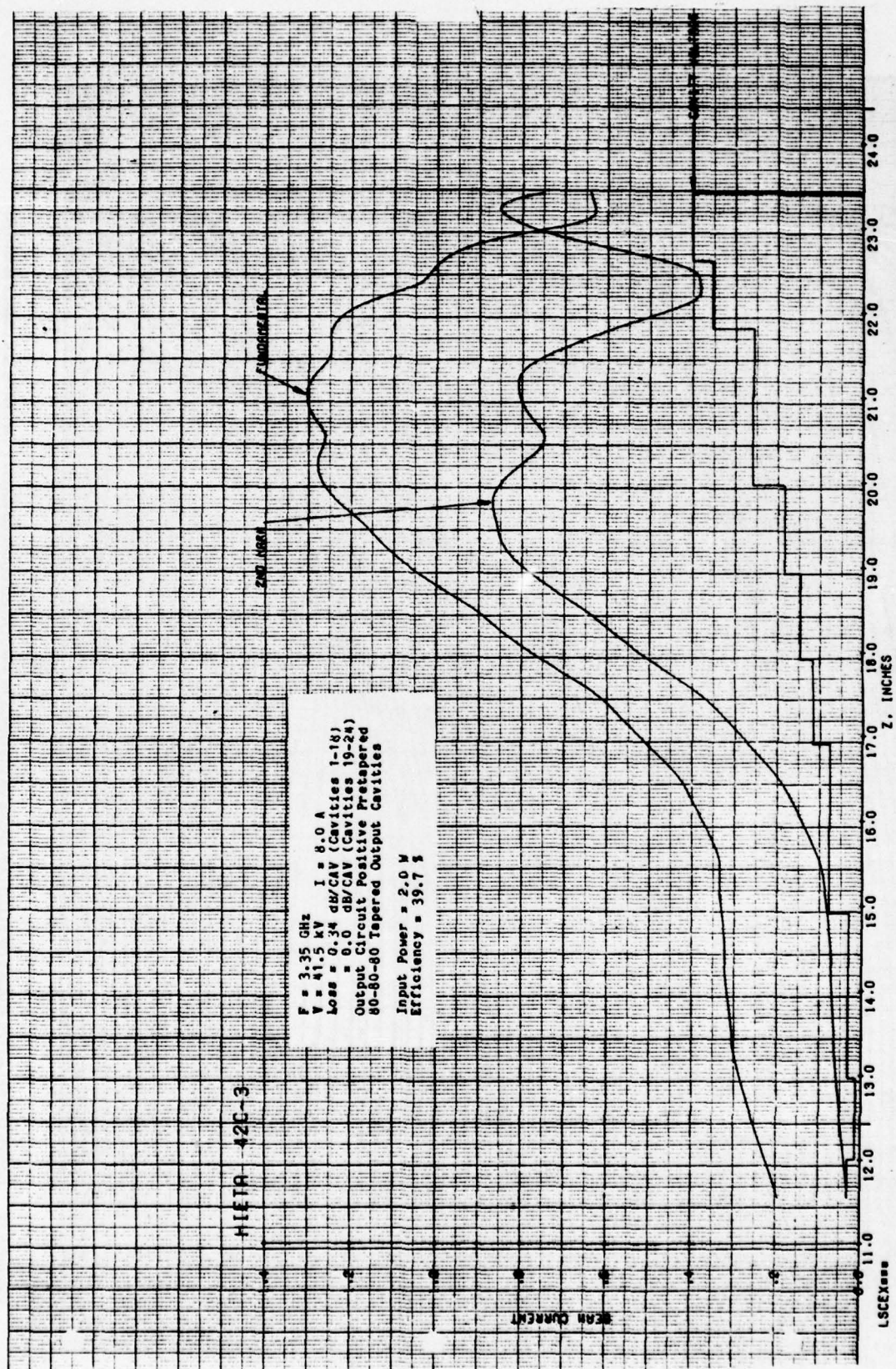


FIGURE 5.72 COMPUTED RF BEAM CURRENTS AND GAP VOLTAGES VS DISTANCE IN SIMULATED COUPLED-CAVITY TWT WITH SIX LOSSLESS OUTPUT CAVITIES, POSITIVE PRETAPERED OUTPUT CIRCUIT, AND FINAL THREE CAVITIES WITH DECREASED PERIODS

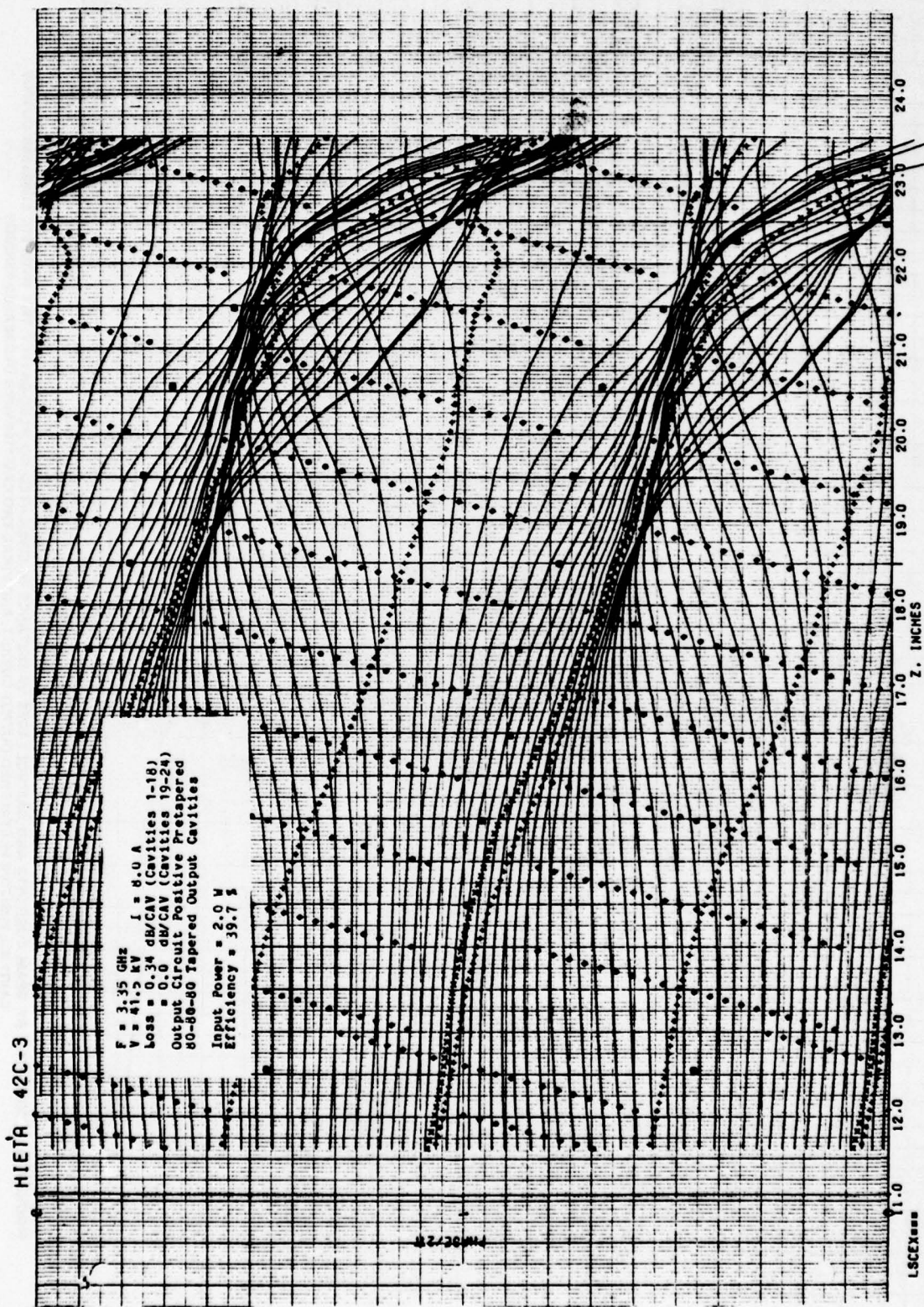


FIGURE 5.73 COMPUTED RELATIVE PHASES OF ELECTRON DISKS VS DISTANCE IN SIMULATED COUPLED-CAVITY TWT WITH SIX LOSSLESS OUTPUT CAVITIES, POSITIVE PRETAPERED OUTPUT CIRCUIT, AND FINAL THREE CAVITIES WITH DECREASED PERIODS

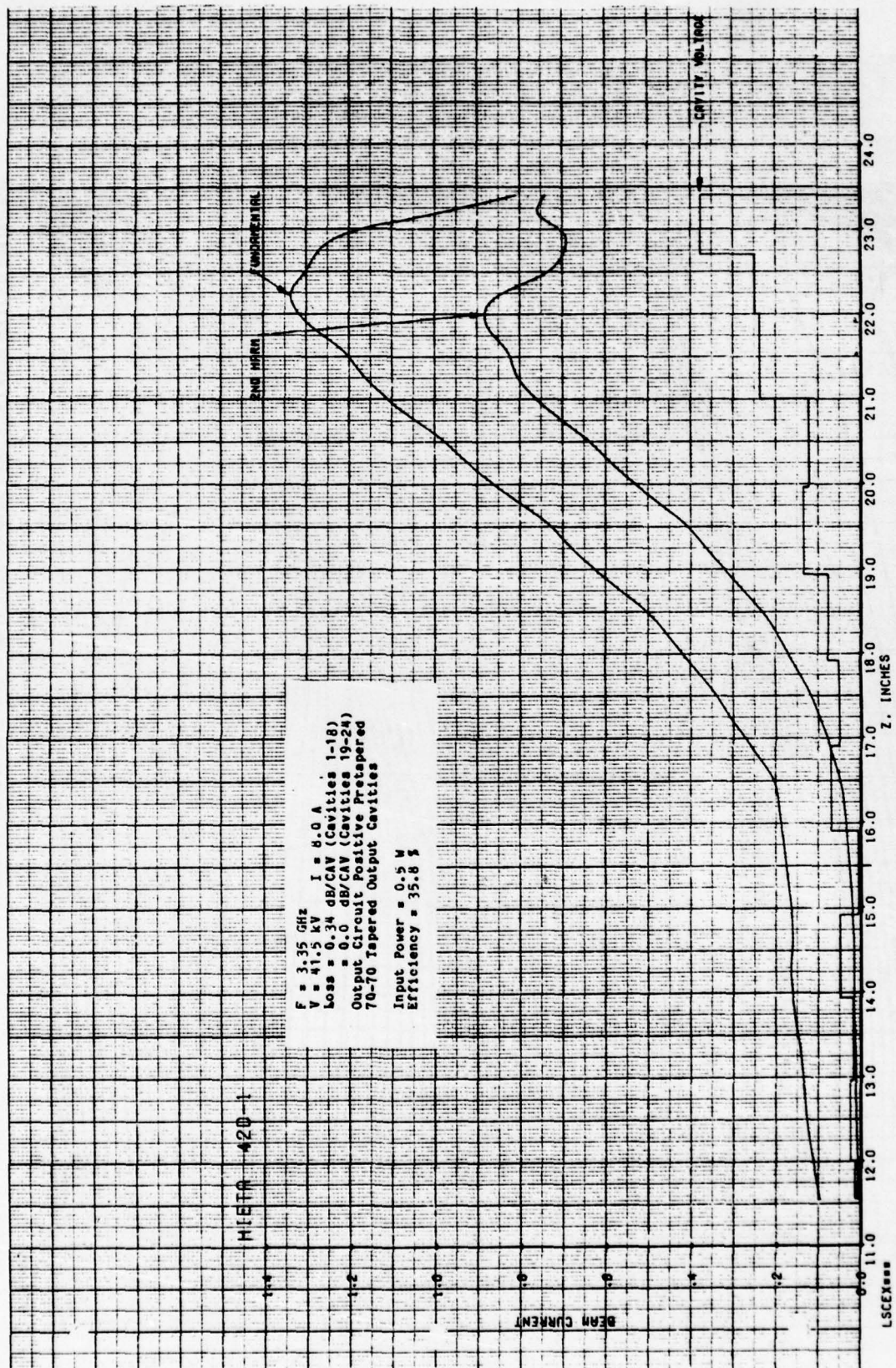


FIGURE 5.74 COMPUTED RF BEAM CURRENTS AND GAP VOLTAGES VS DISTANCE IN SIMULATED COUPLED-CAVITY TWT WITH SIX LOSSLESS OUTPUT CAVITIES, POSITIVE PRETAPERED OUTPUT CIRCUIT, AND FINAL TWO CAVITIES WITH DECREASED PERIODS

HIETA 420-1

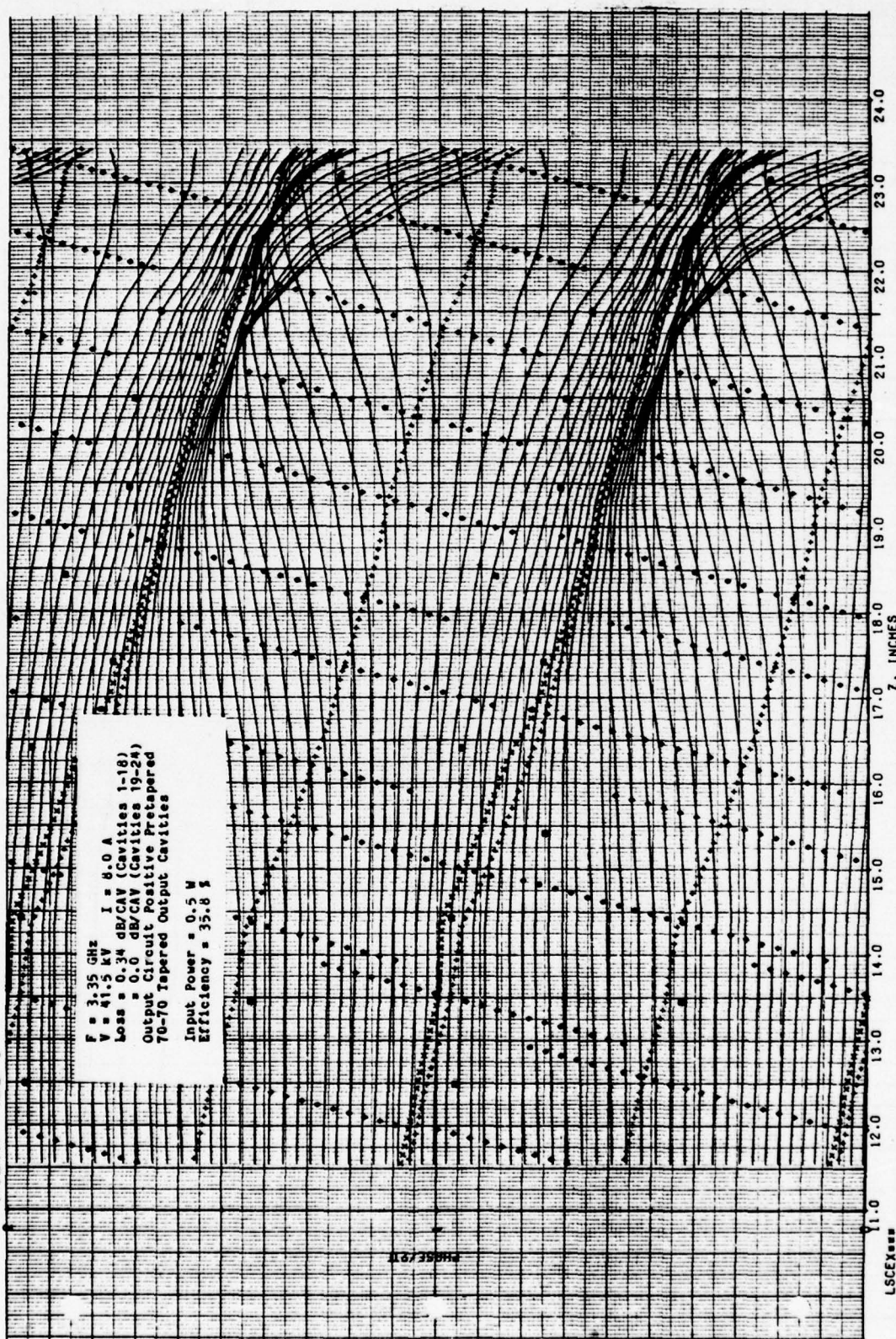


FIGURE 5.75 COMPUTED RELATIVE PHASES OF ELECTRON DISKS VS DISTANCE IN SIMULATED COUPLED-CAVITY TWT WITH SIX LOSSLESS OUTPUT CAVITIES, POSITIVE PRETAPERED OUTPUT CIRCUIT, AND FINAL TWO CAVITIES WITH DECREASED PERIODS

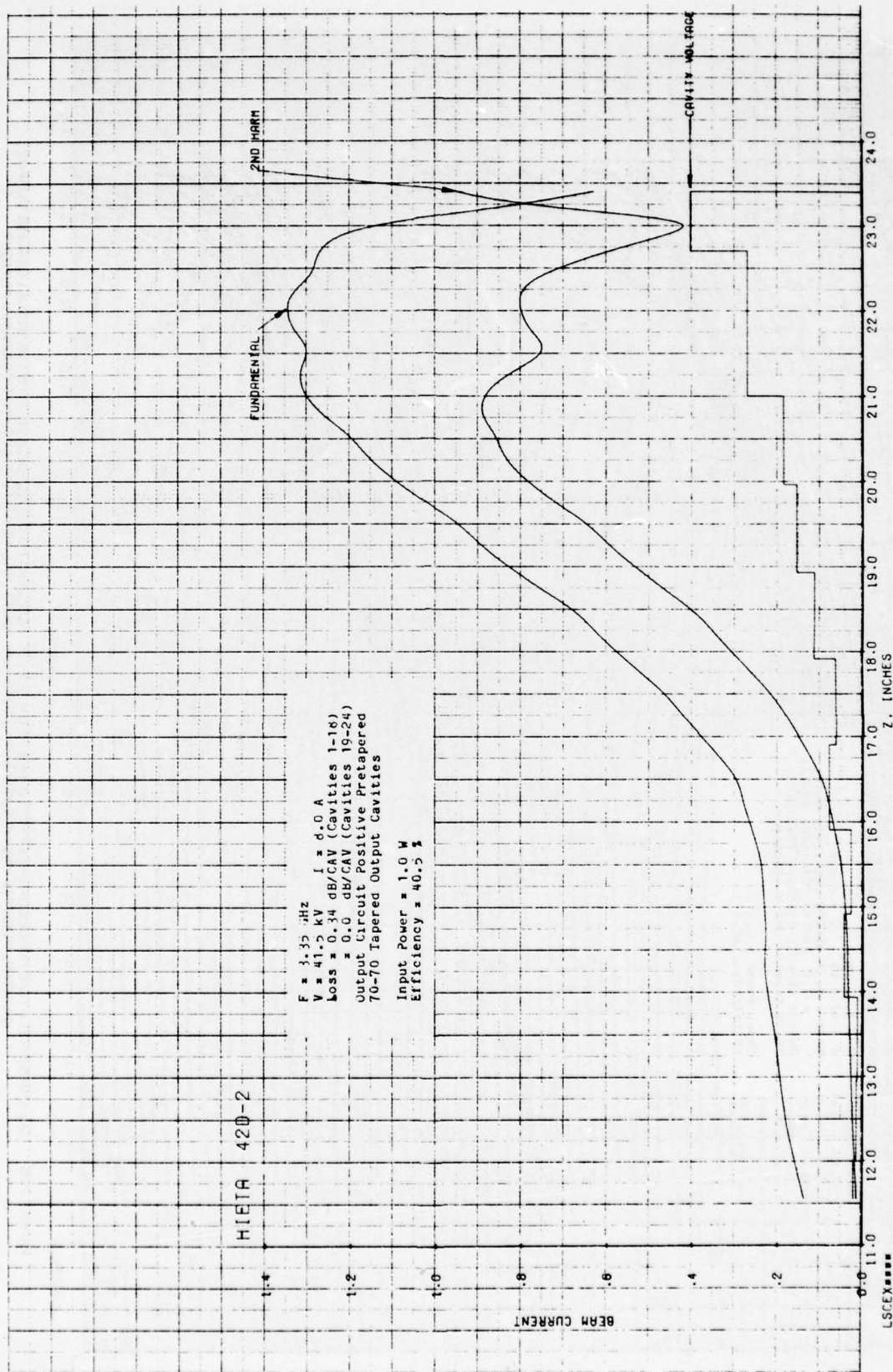


FIGURE 5.76 COMPUTED RF BEAM CURRENTS AND GAP VOLTAGES VS DISTANCE IN SIMULATED COUPLED-CAVITY TWT WITH SIX LOSSLESS OUTPUT CAVITIES, POSITIVE PRETAPERED OUTPUT CIRCUIT, AND FINAL TWO CAVITIES WITH DECREASED PERIODS

HIETA 420-2

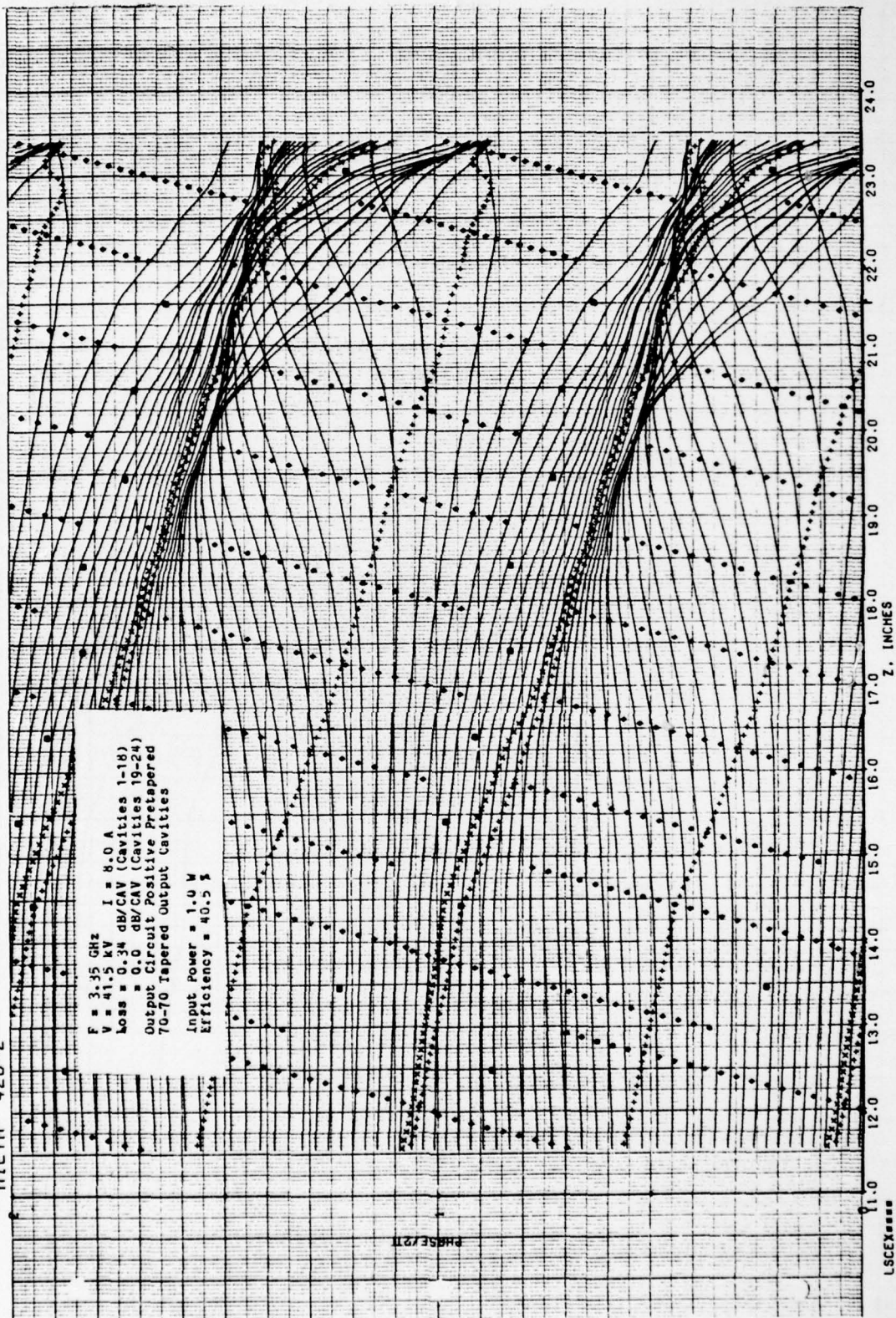


FIGURE 5.77 COMPUTED RELATIVE PHASES OF ELECTRON DISKS VS DISTANCE IN SIMULATED COUPLED-CAVITY TWT WITH SIX LOSSLESS OUTPUT CAVITIES, POSITIVE PRETAPERED OUTPUT CIRCUIT, AND FINAL TWO CAVITIES WITH DECREASED PERIODS

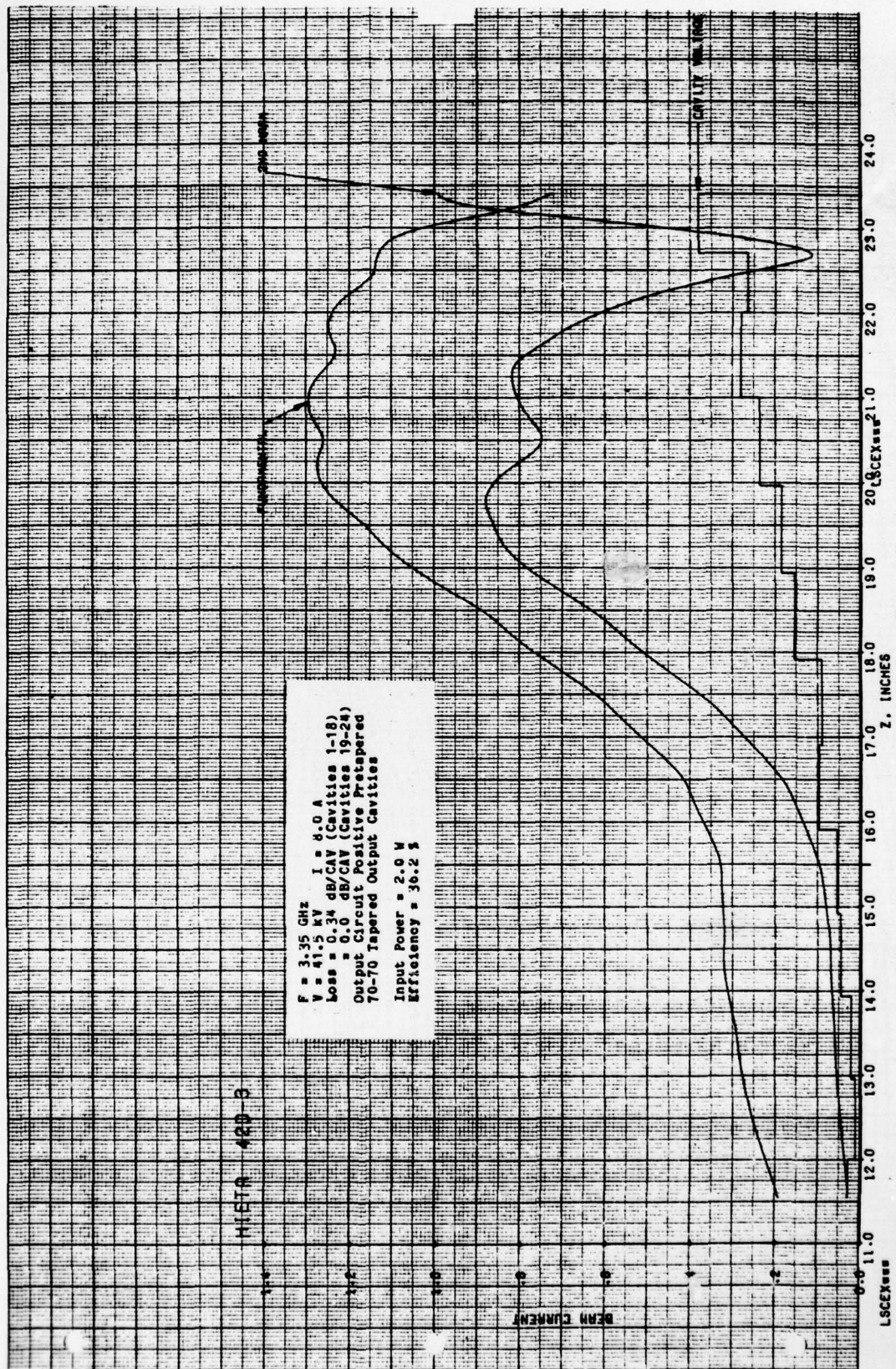


FIGURE 5.78 COMPUTED RF BEAM CURRENTS AND GAP VOLTAGES VS DISTANCE IN SIMULATED COUPLED-CAVITY TWT WITH SIX LOSSLESS OUTPUT CAVITIES, POSITIVE PRETAPERED OUTPUT CIRCUIT, AND FINAL TWO CAVITIES WITH DECREASED PERIODS

HIETA 42D-3

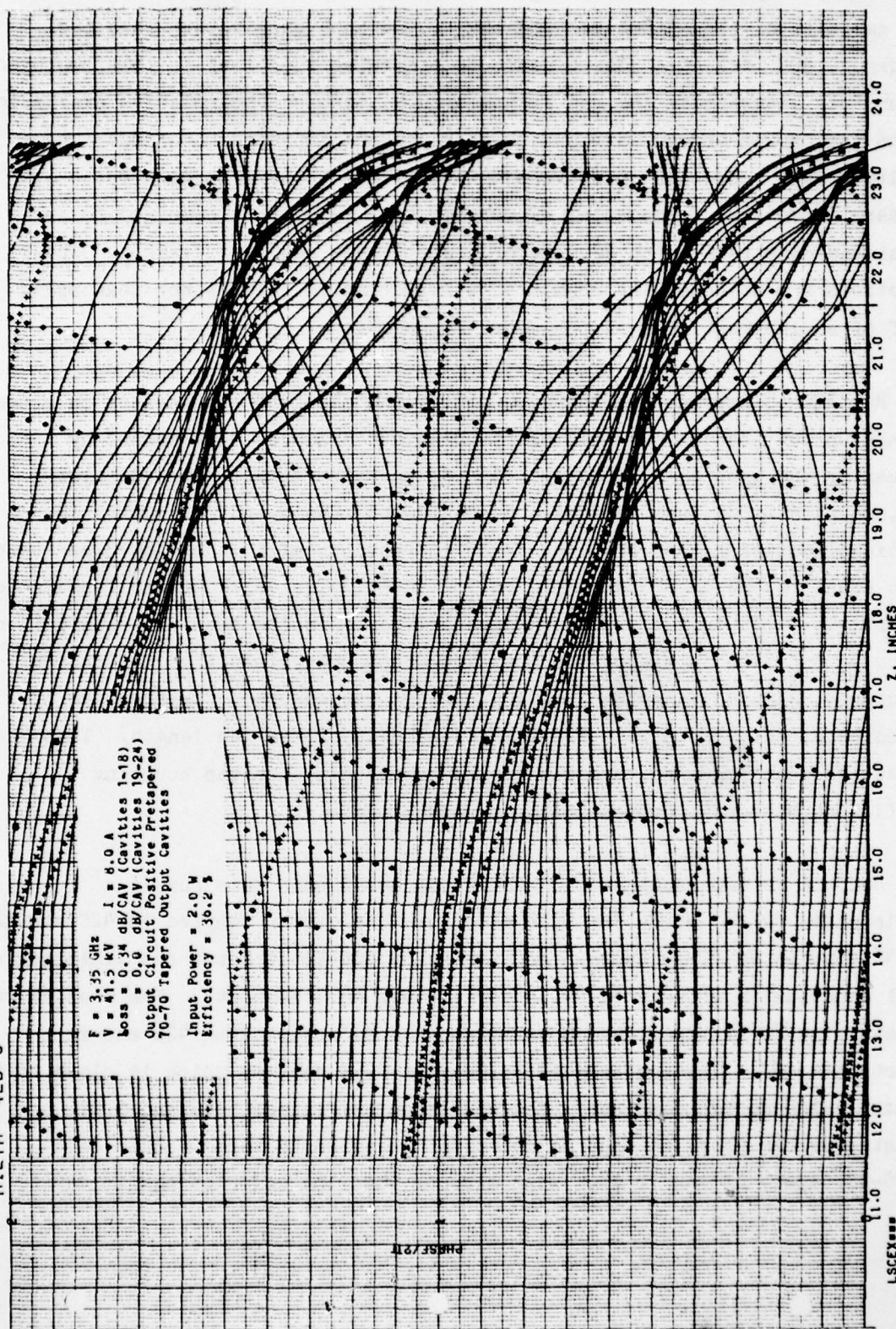


FIGURE 5.79 COMPUTED RELATIVE PHASES OF ELECTRON DISKS VS DISTANCE IN SIMULATED COUPLED-CAVITY TWT WITH SIX LOSSLESS OUTPUT CAVITIES, POSITIVE TAPERED OUTPUT CIRCUIT, AND FINAL TWO CAVITIES WITH DECREASED PERIODS

Run 43A is represented by Figures 5.80 and 5.81. In this run the first nine cavities of the output section have 0.500 inch gaps rather than the standard 0.300 inch gap. The circuit is otherwise identical to that employed in Run 40A. Increasing the gap length should increase the relative excitation of the fast space-charge wave and thereby produce improved bunching. The results show a reduction in conversion efficiency to 39.2 percent but a decrease in maximum fundamental rf current to $I_1 = 1.14 I_0$ compared to the normal gap case (40A) with 42.9 percent efficiency and $I_1 = 1.29 I_0$. These reductions are no doubt the result of a reduction in gain rather than being proof of an inherent flaw in the above argument.

Run 43D is represented by Figures 5.82 and 5.83 and represented an attempt to make up for the loss in gain of the previous example (43A) caused by increasing the gaps to 0.500 inch. In the present example, two additional cavities with 0.500 inch gaps have been added to the output circuit. The additional cavities have resulted in an increase in efficiency to 43 per cent; about equal to the standard configuration (40A). The value of the fundamental current, $I = 1.15$ is virtually unchanged. These results show that the gain of the output section is one of the most important determinants of conversion efficiency. In modeling the long gap case it was assumed, for the sake of convenience, that the cavity R/Q was independent of the gap length. This assumption penalizes the long gap cavity by reducing the gap coupling coefficient without a compensating increase in R/Q.

Run 45A is represented by Figures 5.84 and 5.85. This run is a continuation of the effort to find a better final taper started in 42C and 42D. Run 42C had an 80-80-80 taper. Run 42D had a 100-70-70 taper and exhibited a small decrease in efficiency (40.5 percent vs. 43.1 percent). The present run employs a 90-80-70 taper, which is somewhat less abrupt than 42D and more abrupt than 42C. The computed efficiency is 42.9 percent which is close to the maximum value so far computed. Run 45B shown in Figures 5.86 and 5.87 illustrates the final attempt to optimize the velocity taper. This is a 70-80-90 taper, chosen to show what happens when the major change in cavity

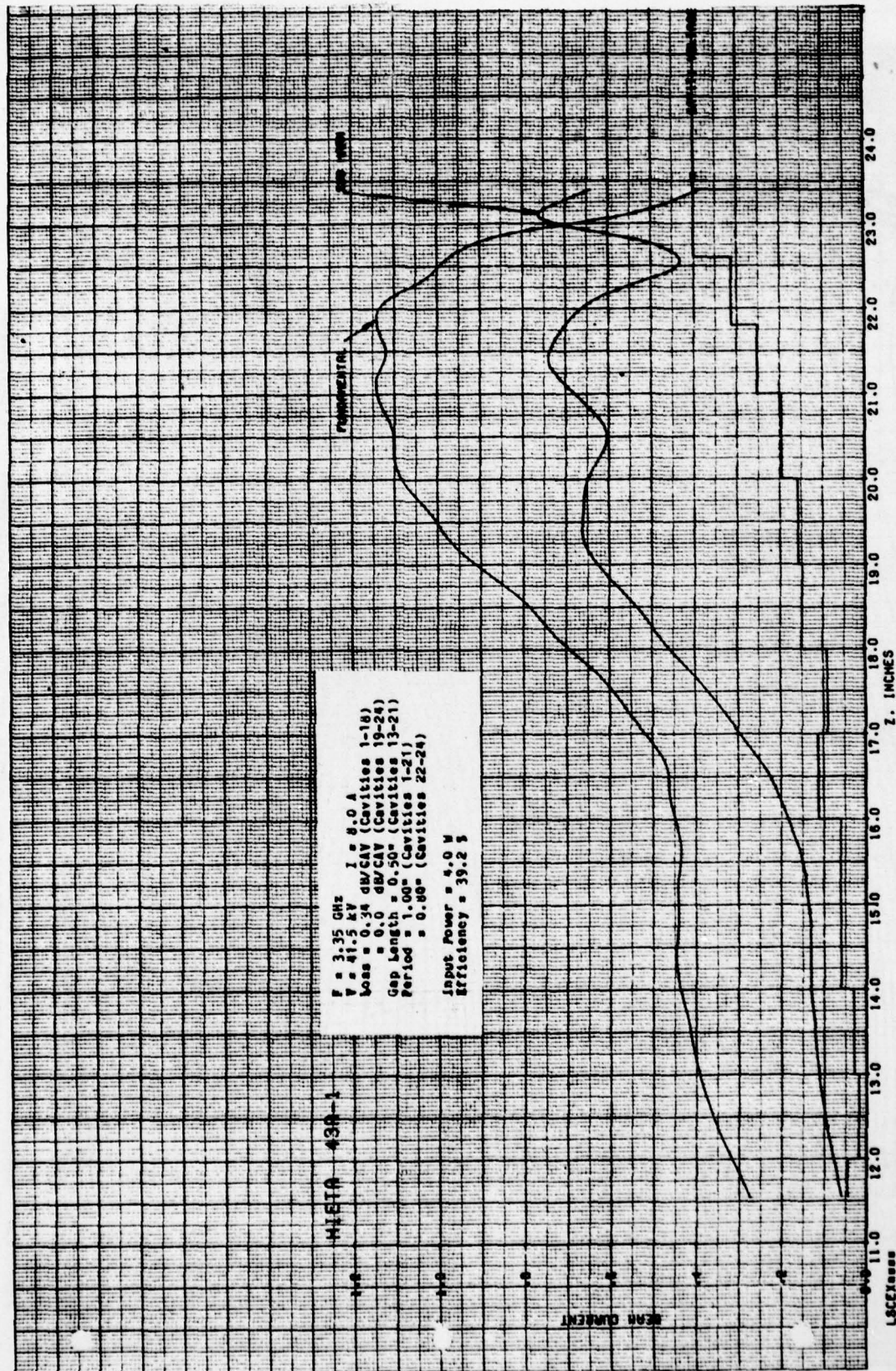


FIGURE 5.90 COMPUTED RF BEAM CURRENTS AND GAP VOLTAGES VS DISTANCE IN SIMULATED COUPLED-CAVITY TWT WITH SIX LOSSLESS OUTPUT CAVITIES, LARGE GAPS IN OUTPUT SECTION, AND FINAL THREE CAVITIES WITH DECREASED PERIODS

MIETA 43R-1

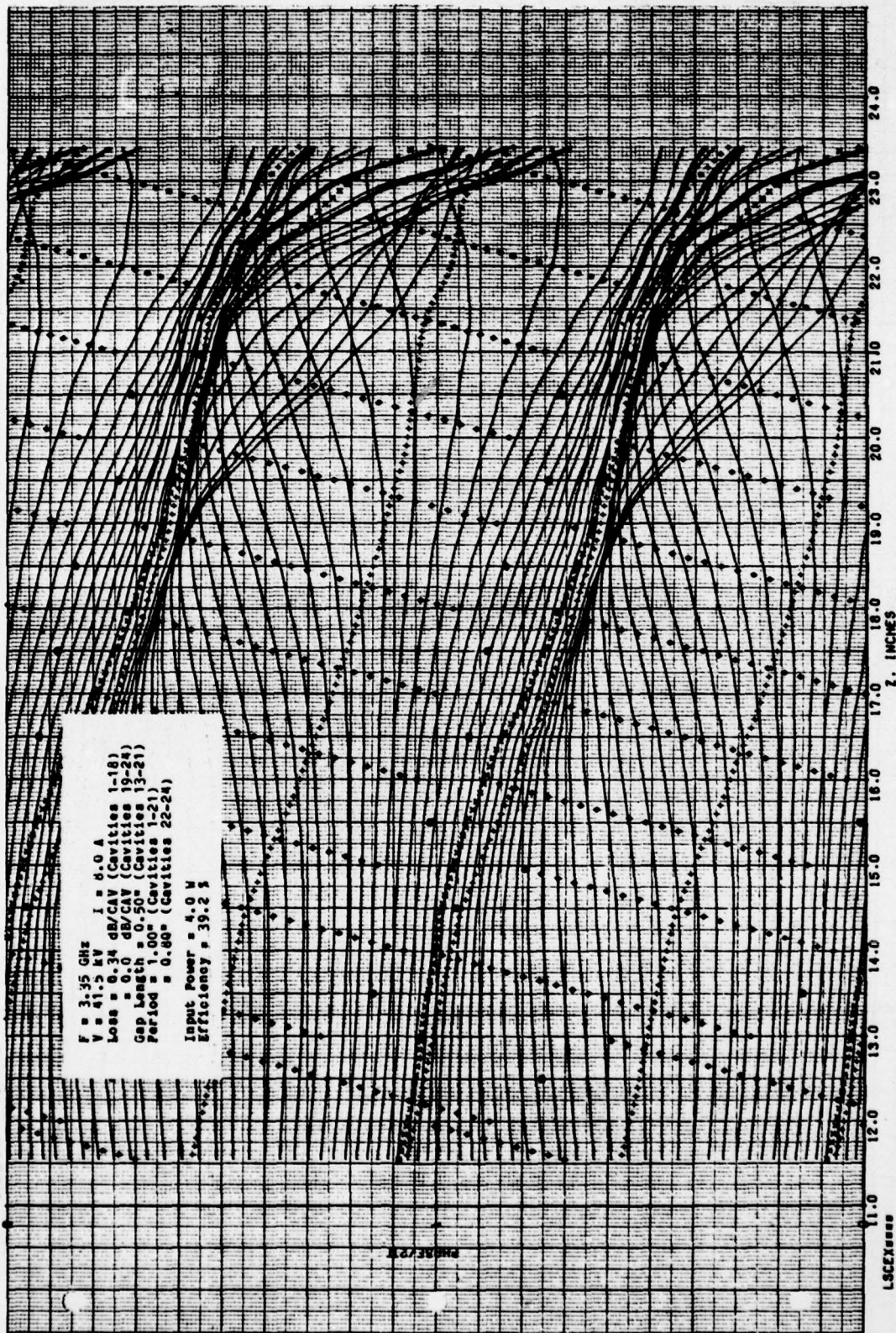
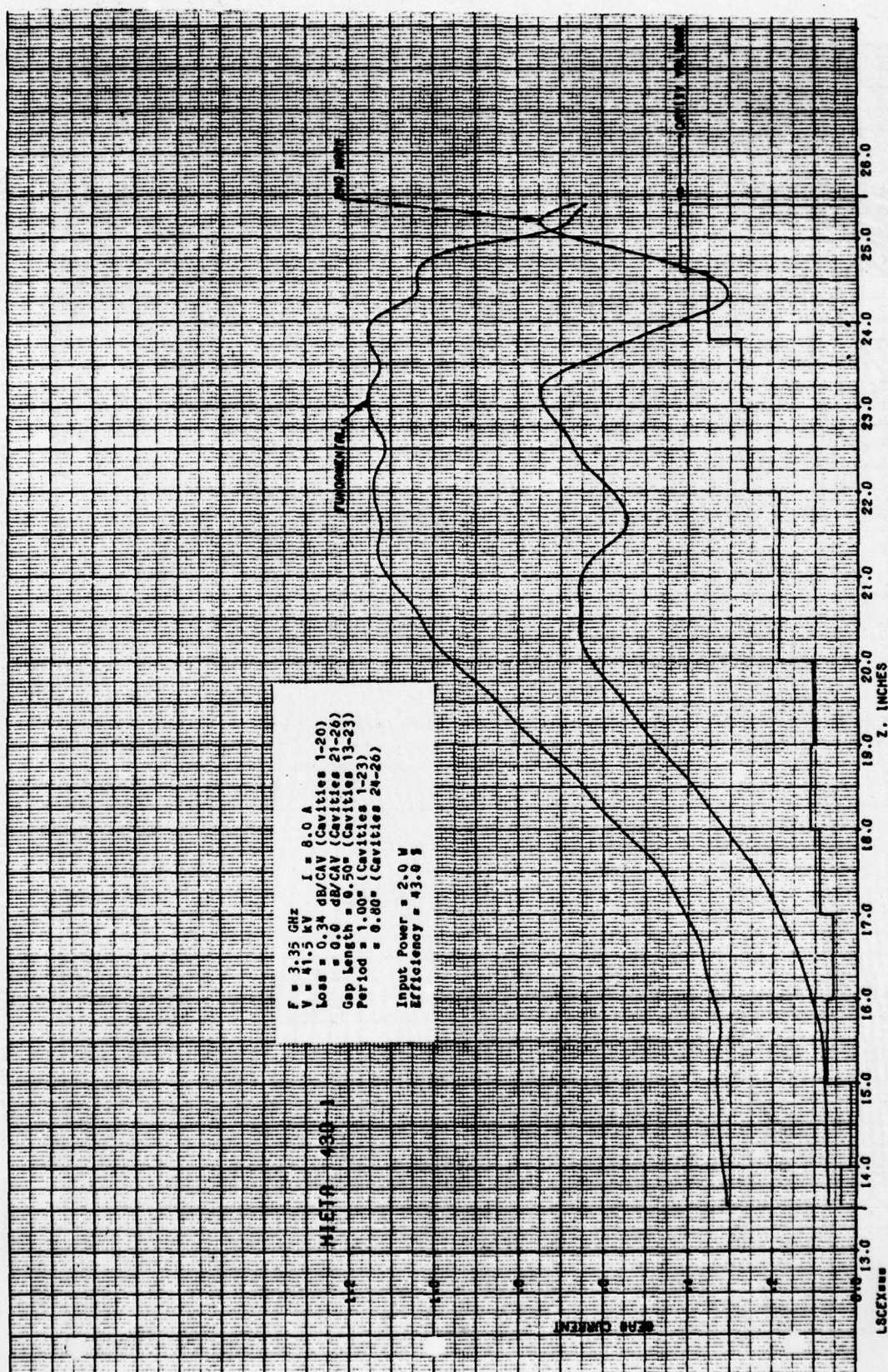


FIGURE 5.81 COMPUTED RELATIVE PHASES OF ELECTRON DISKS VS DISTANCE IN SIMULATED COUPLED-CAVITY TWT WITH SIX LOSSLESS OUTPUT CAVITIES, LARGE GAPS IN OUTPUT SECTION, AND FINAL THREE CAVITIES WITH DECREASED PERIODS



HIETA 430-1

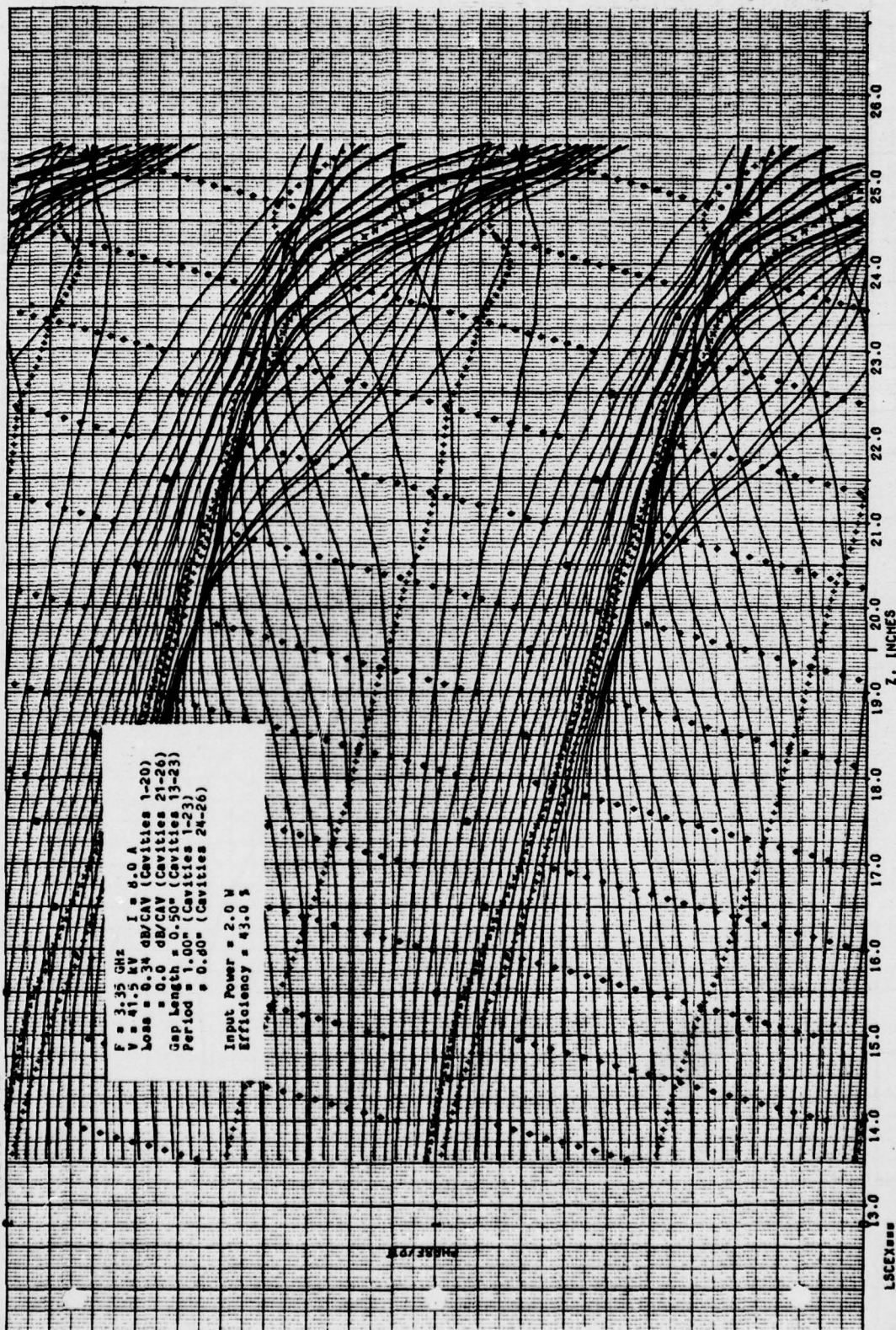


FIGURE 5.23 COMPUTED RELATIVE PHASES OF ELECTRON DISKS VS DISTANCE IN SIMULATED COUPLED-CAVITY TWT WITH SIX LOSSLESS OUTPUT CAVITIES, LARGE GAPS IN OUTPUT SECTION, AND FINAL THREE CAVITIES WITH DECREASED PERIODS

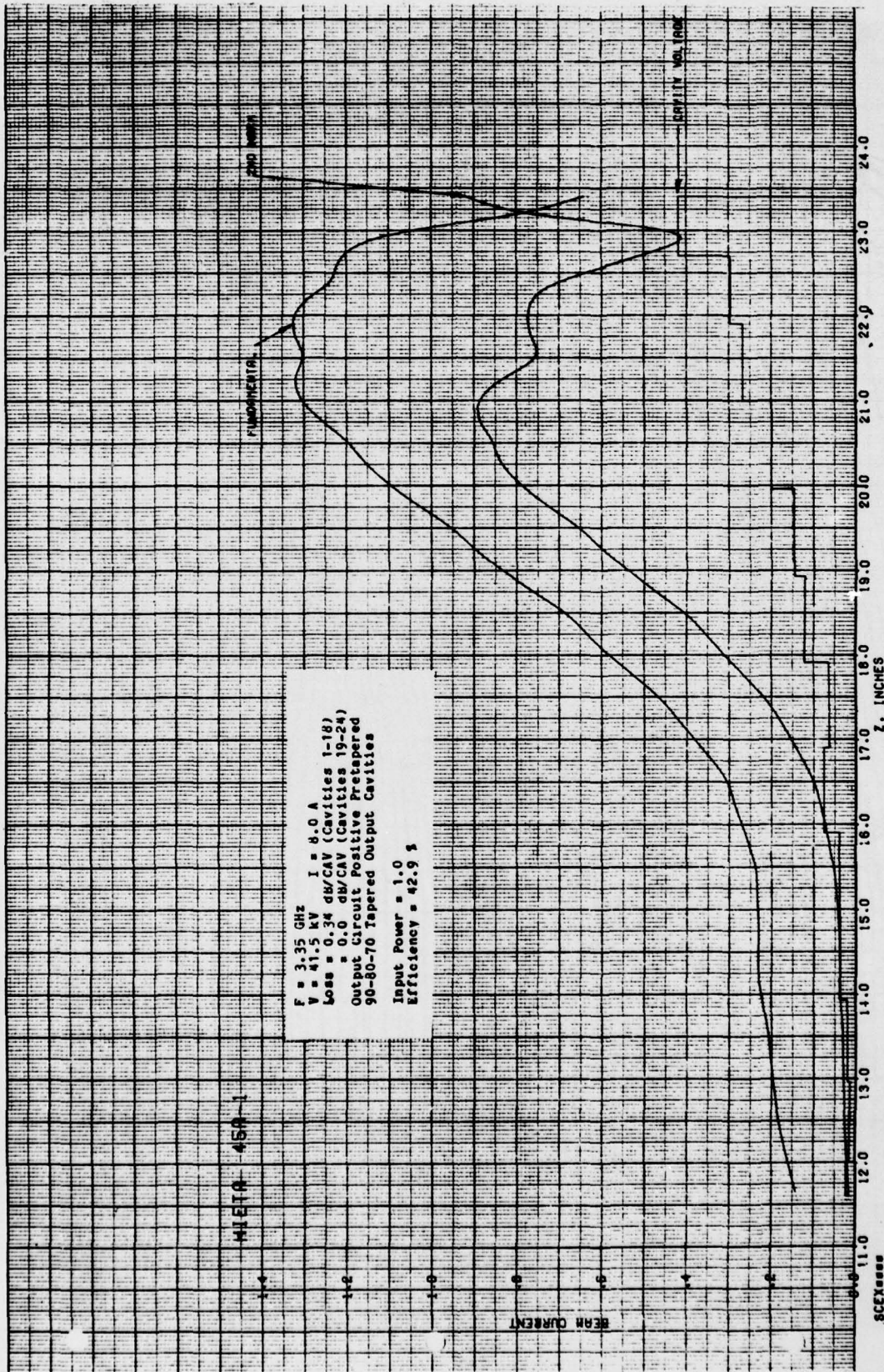


FIGURE 5.84 COMPUTED RF BEAM CURRENTS AND GAP VOLTAGES VS DISTANCE IN SIMULATED COUPLED-CAVITY TWT WITH SIX LOSSLESS OUTPUT CAVITIES, POSITIVE TAPERED OUTPUT CIRCUIT, AND FINAL THREE CAVITIES WITH DECREASED PERIODS

HIETA 45A-1

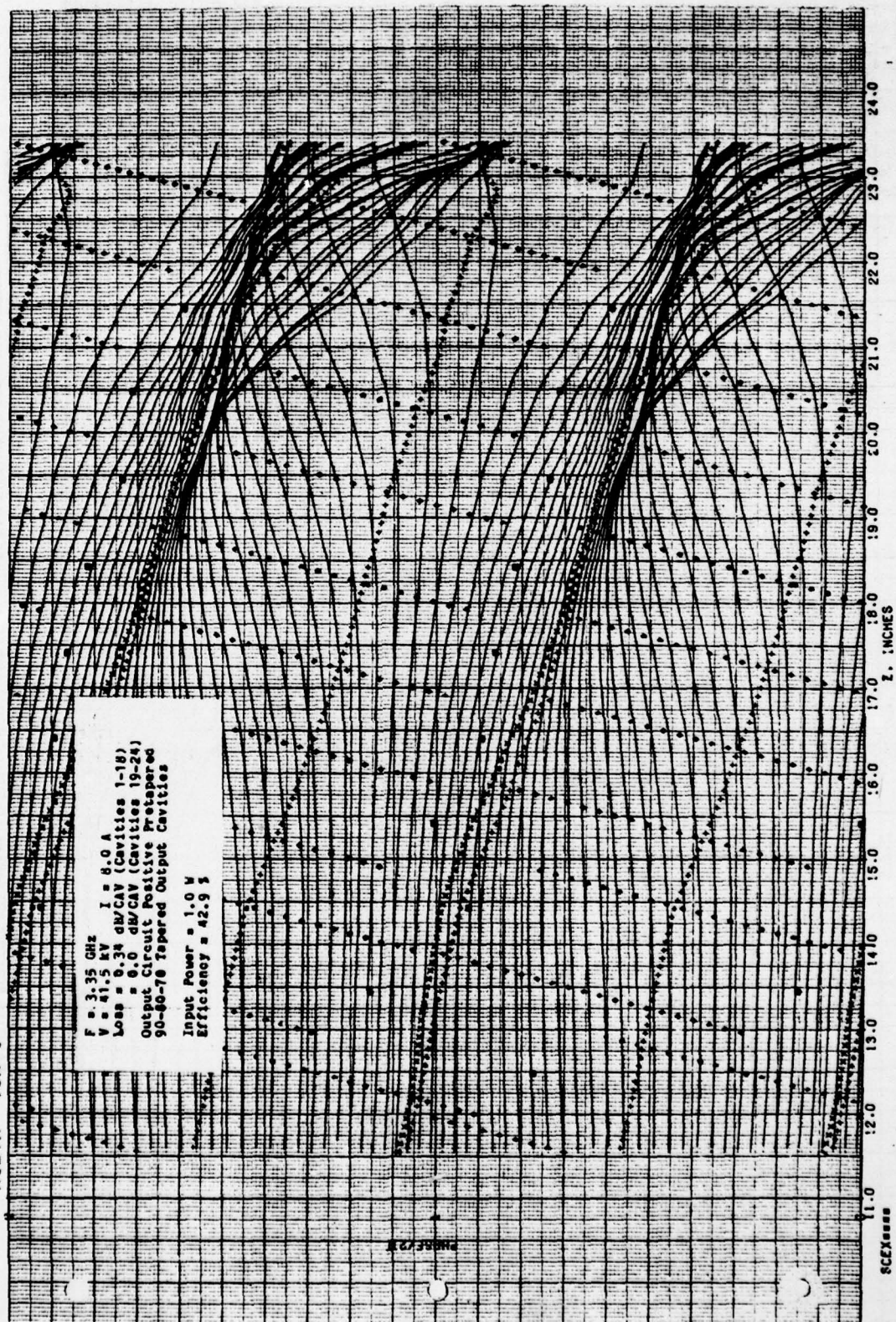


FIGURE 5.85 COMPUTED RELATIVE PHASES OF ELECTRON DISKS VS DISTANCE IN SIMULATED COUPLED-CAVITY TWT WITH SIX LOSSLESS OUTPUT CAVITIES, POSITIVE PRETAPERED OUTPUT CIRCUIT, AND FINAL THREE CAVITIES WITH DECREASED PERIODS

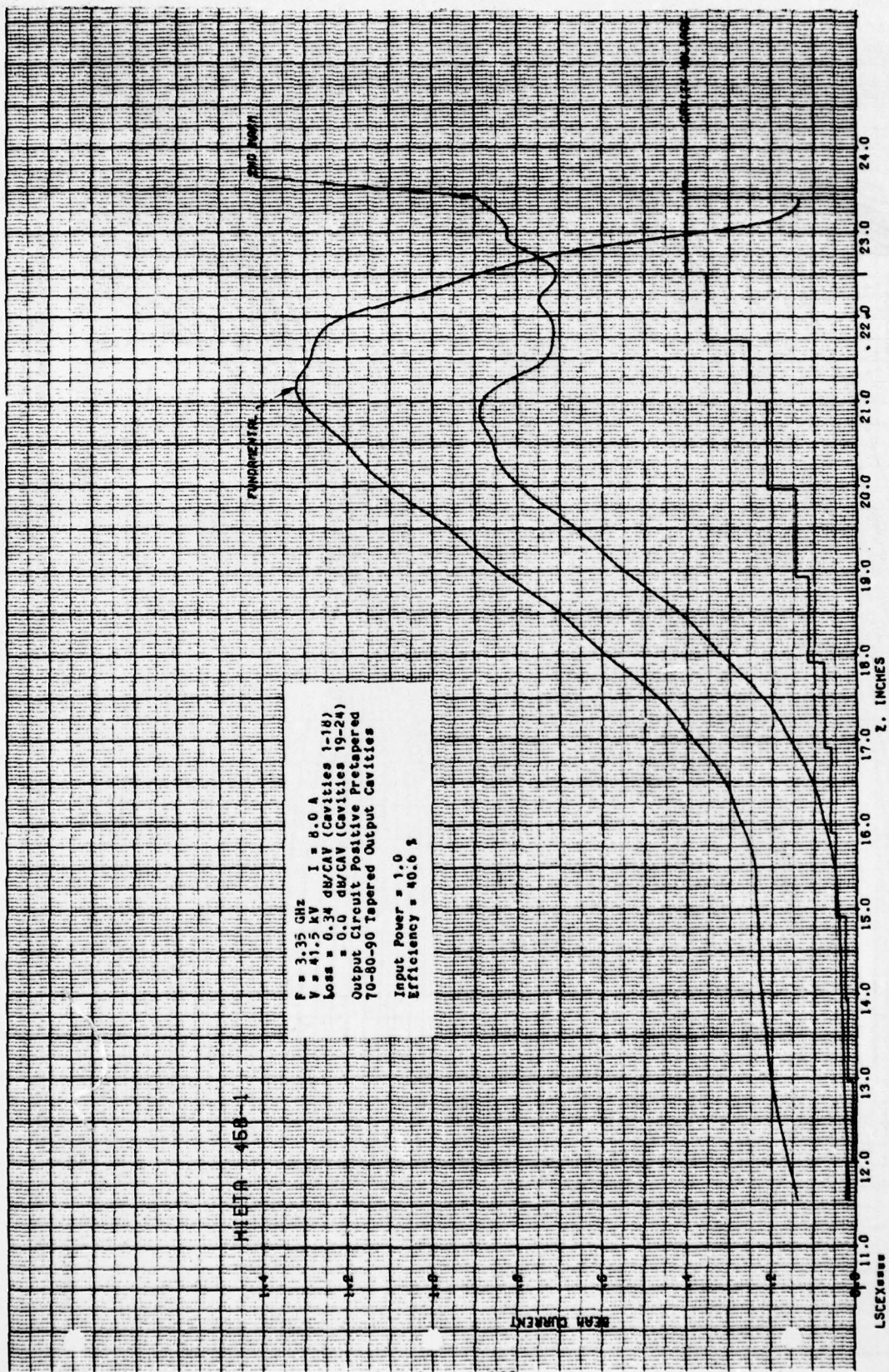


FIGURE 5.96 COMPUTED RF BEAM CURRENTS AND GAP VOLTAGES VS DISTANCE IN SIMULATED COUPLED-CAVITY TWT WITH SIX LOSSLESS OUTPUT CAVITIES, POSITIVE PRE-TAPERED OUTPUT CIRCUIT, AND FINAL THREE CAVITIES WITH DECREASED PERIODS

HIETA 45B-1

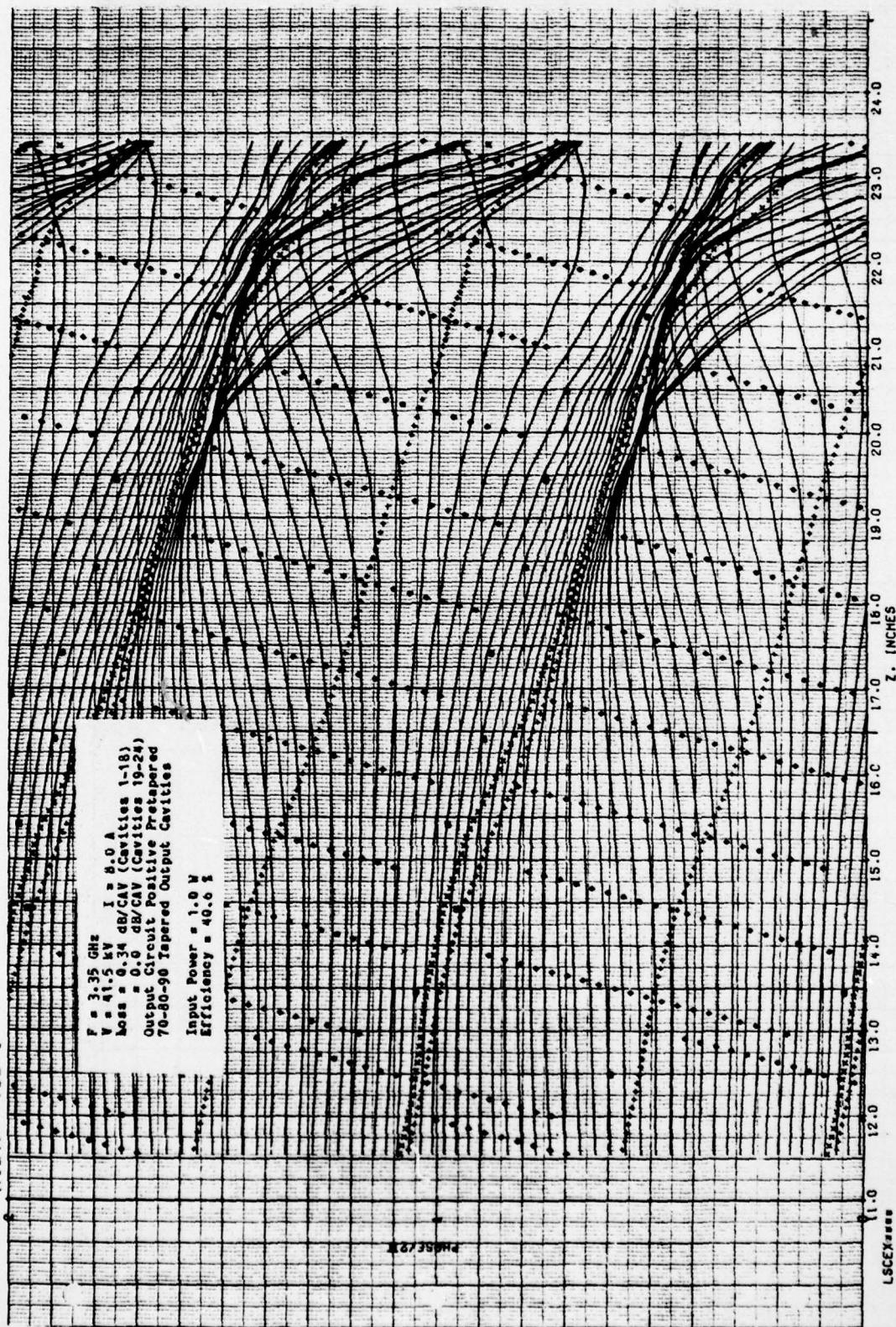
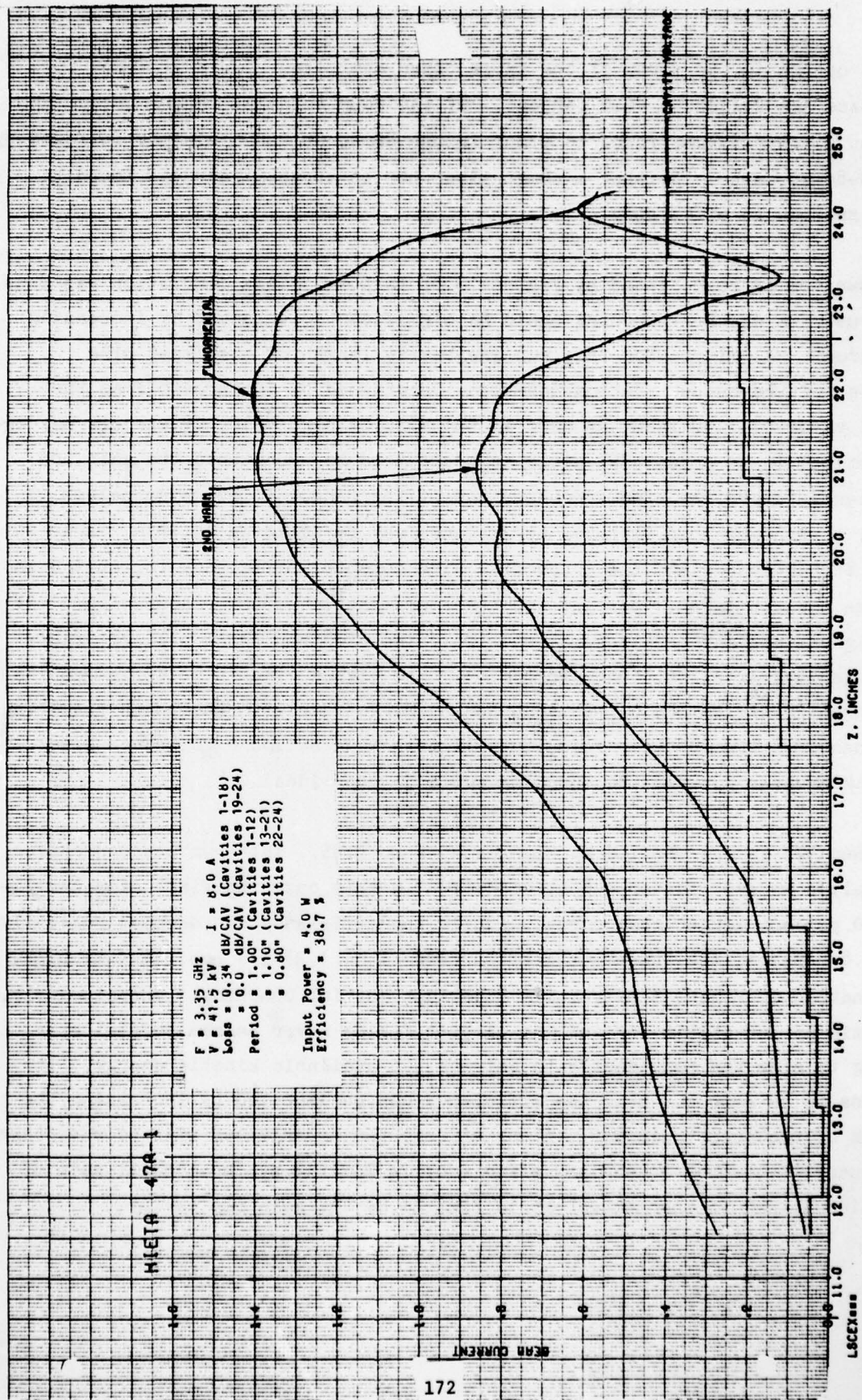


FIGURE 5.37 COMPUTED RELATIVE PHASES OF ELECTRON DISKS VS DISTANCE IN SIMULATED COUPLED-CAVITY TWT WITH SIX LOSSLESS OUTPUT CAVITIES, POSITIVE PRETAPERED OUTPUT CIRCUIT, AND FINAL THREE CAVITIES WITH DECREASED PERIODS

length occurs in the first of the three taper cavities. The efficiency for this case has fallen to 40.6 percent. Of the four velocity tapers tried, the highest efficiency was found to occur in the 80-80-80 taper closely followed by the 90-80-70 taper. Neither a short taper nor an abrupt taper was found to yield as high an efficiency.

Run 47A is represented by Figures 5.88 to 5.91. This simulation was done to illustrate whether bunching could be significantly enhanced by increasing the circuit velocity. For this run the cavity length of the first nine cavities of the output section have been lengthened by 10 percent from the normal value of 1.00 inch, as used in Run 40A. A high velocity circuit may be impractical in an actual TWT since it would tend to accentuate the gain and efficiency toward the high frequency end of the band. It is nevertheless useful to know whether improved performance may be achieved in this manner so as to better understand the tradeoffs. The computed efficiency for this high voltage circuit is 42.7 percent and the fundamental current reaches $I_1 = 1.42 I_0$, higher than any previous calculation. The electron phase plot of Figure 5.89 displays excellent bunch formation. The higher circuit velocity results in a greater excitation of the fast space-charge wave with the bunch traveling more nearly at the DC beam velocity. If means can be found to reduce electron overtaking near $Z = 20$ " the bunching would be near ideal.

Run 47B is represented by Figures 5.92 to 5.95. This run was undertaken to analyze an even faster output circuit. In this case the first nine cavities are 20 percent longer than normal. While the efficiency has dropped radically to 29.8 percent, the fundamental rf current ($I_1 = 1.37 I_0$) has remained high. Examination of Figure 5.94 reveals excellent initial bunching. Unfortunately, the gain per cavity is low and the circuit fields never become sufficiently strong to slow the beam enough to extract the available kinetic energy. It remains to be seen how much the efficiency can be improved by increasing the length of the output circuit. A set of computer experiments will be undertaken to determine to what extent the efficiency is limited by the overall gain of the circuit and to what extent it is limited by the gain per cavity.



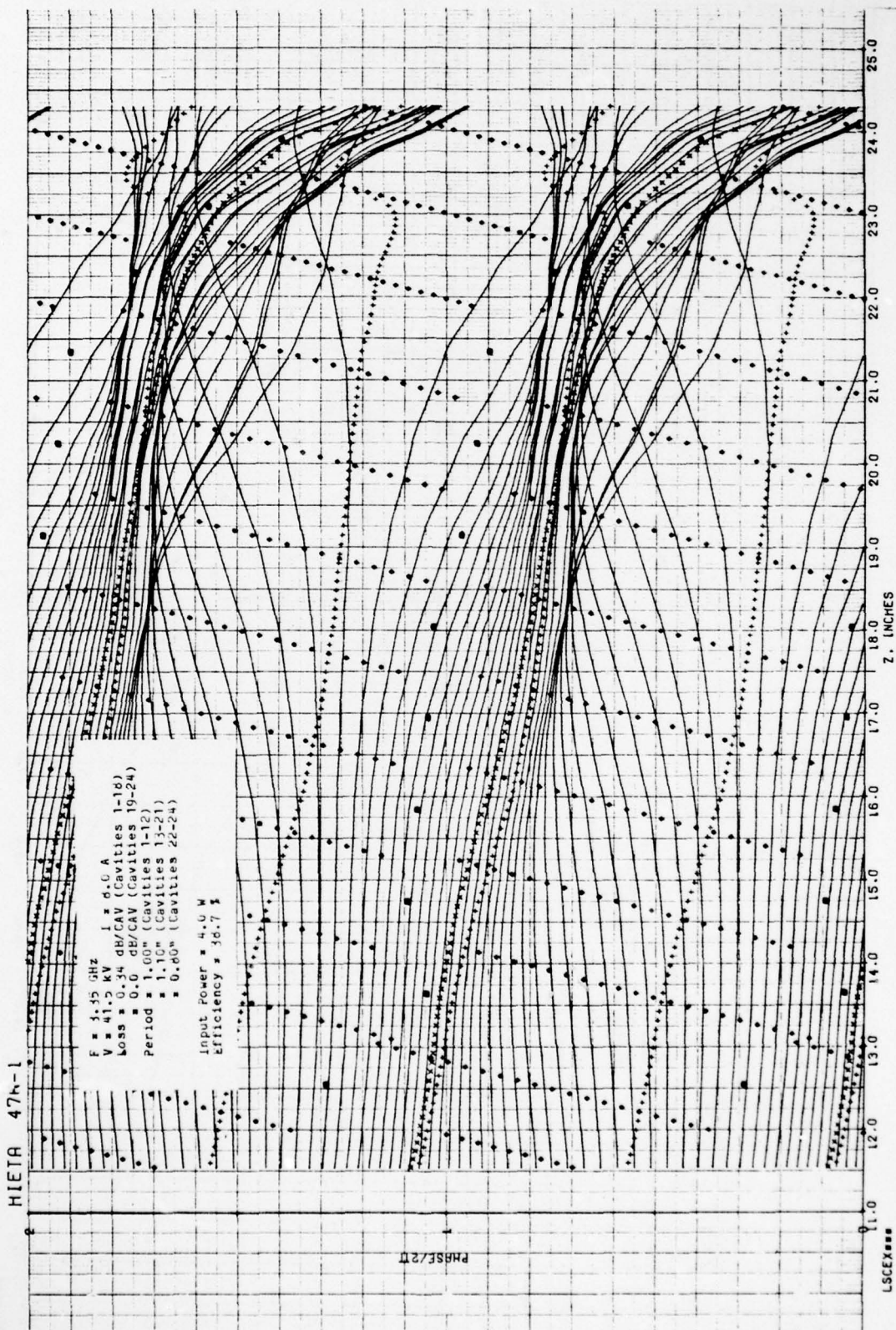


FIGURE 5.89 COMPUTED RELATIVE PHASES OF ELECTRON DISKS VS DISTANCE IN SIMULATED COUPLED-CAVITY TWT WITH SIX LOSSLESS OUTPUT CAVITIES, FASTER VELOCITY OUTPUT CIRCUIT AND FINAL THREE CAVITIES WITH DECREASED PERIODS

AD-A080 961

VARIAN ASSOCIATES INC PALO ALTO CA PALO ALTO MICROWAVE--ETC F/G 9/1
EFFICIENCY IMPROVEMENTS IN COUPLED CAVITY TRAVELING WAVE TUBES.(U)
OCT 79 W R AYERS, F R WALKER F30602-78-C-0117

UNCLASSIFIED

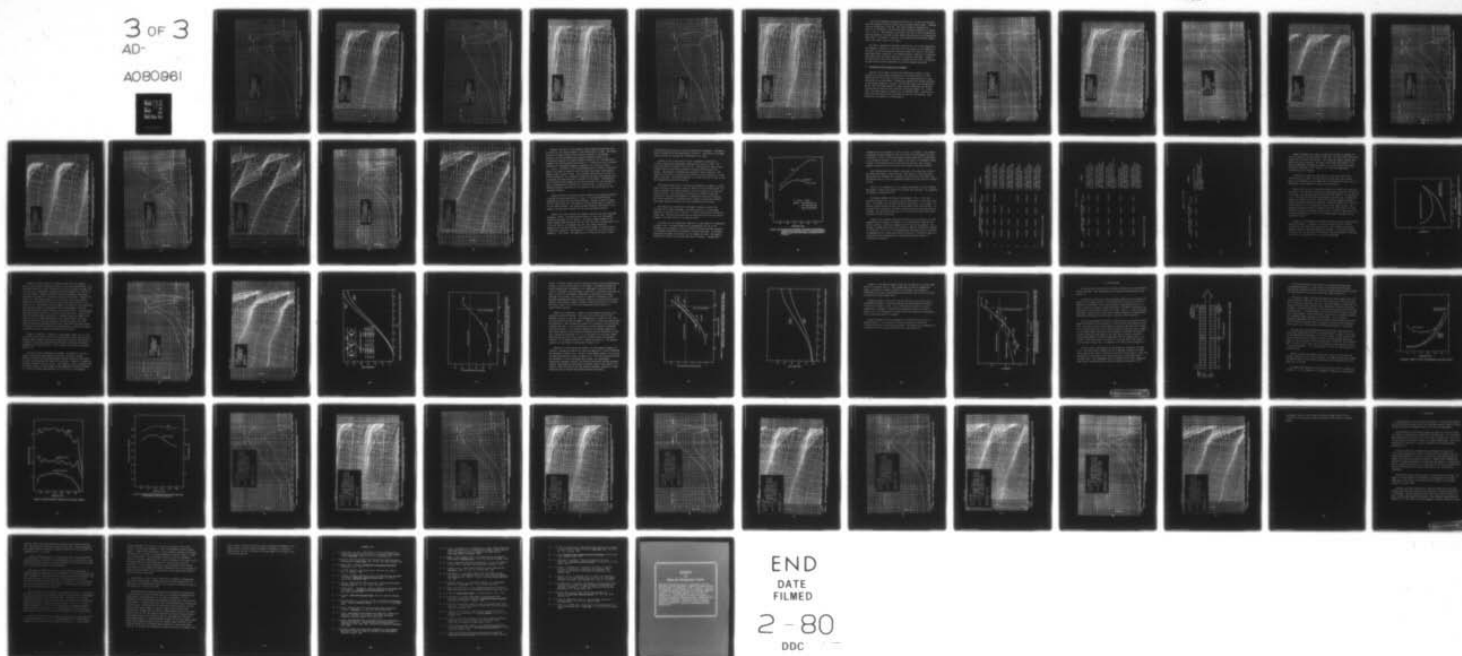
RADC-TR-79-264

NL

3 OF 3

AD-

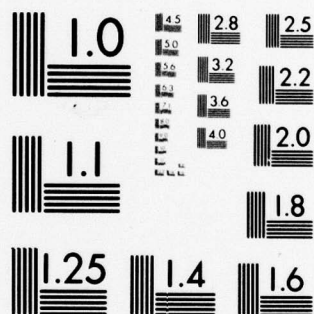
A080961



END
DATE
FILMED

2-80

DDC



MICROCOPY RESOLUTION TEST CHART
NATIONAL BUREAU OF STANDARDS-1963-A

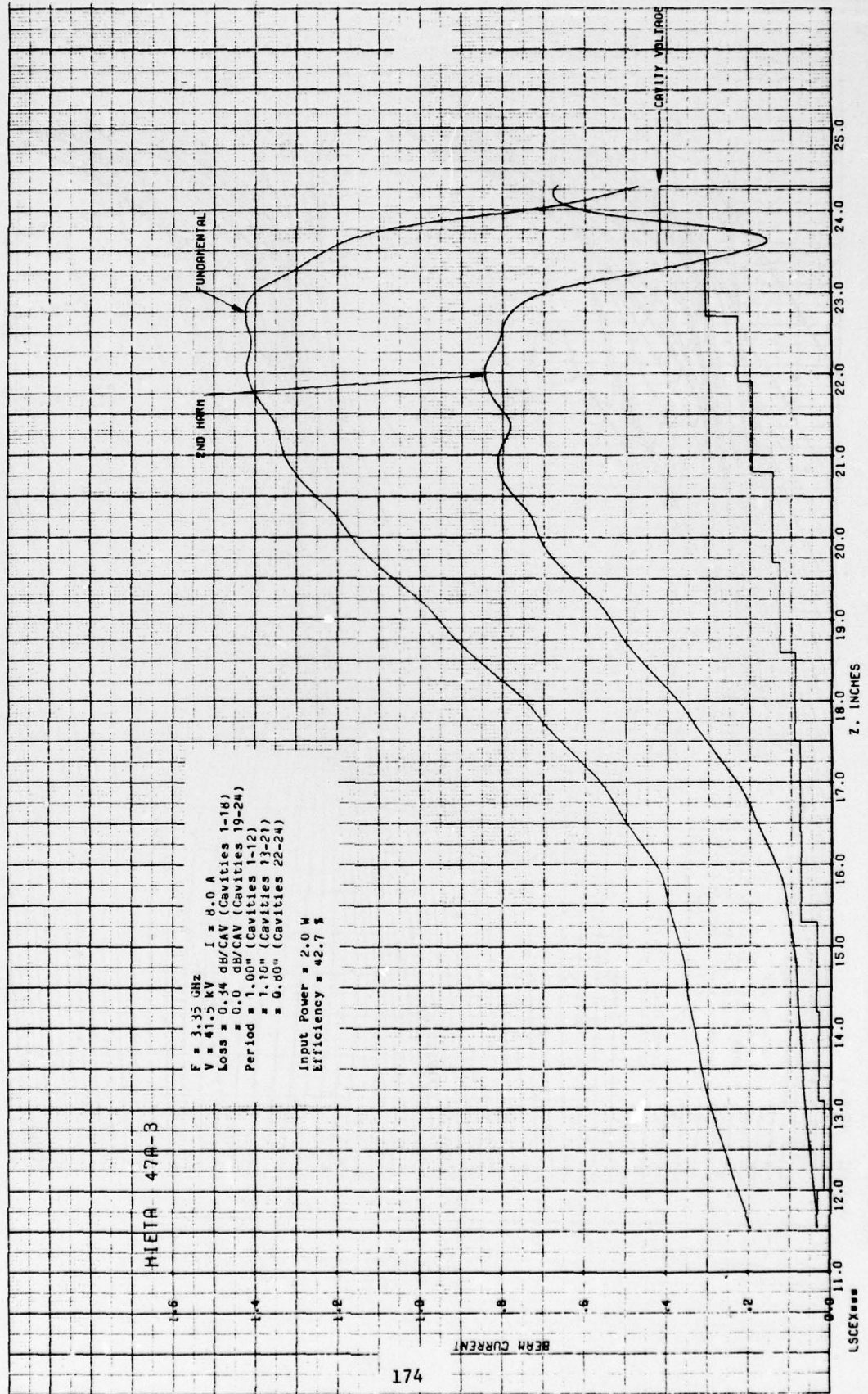


FIGURE 5.90 COMPUTED RF BEAM CURRENTS AND GAP VOLTAGES VS DISTANCE IN SIMULATED COUPLED-CAVITY TWT WITH SIX LOSSLESS OUTPUT CAVITIES, FASTER VELOCITY OUTPUT CIRCUIT AND FINAL THREE CAVITIES WITH DECREASED PERIODS

HIETA 47A-3

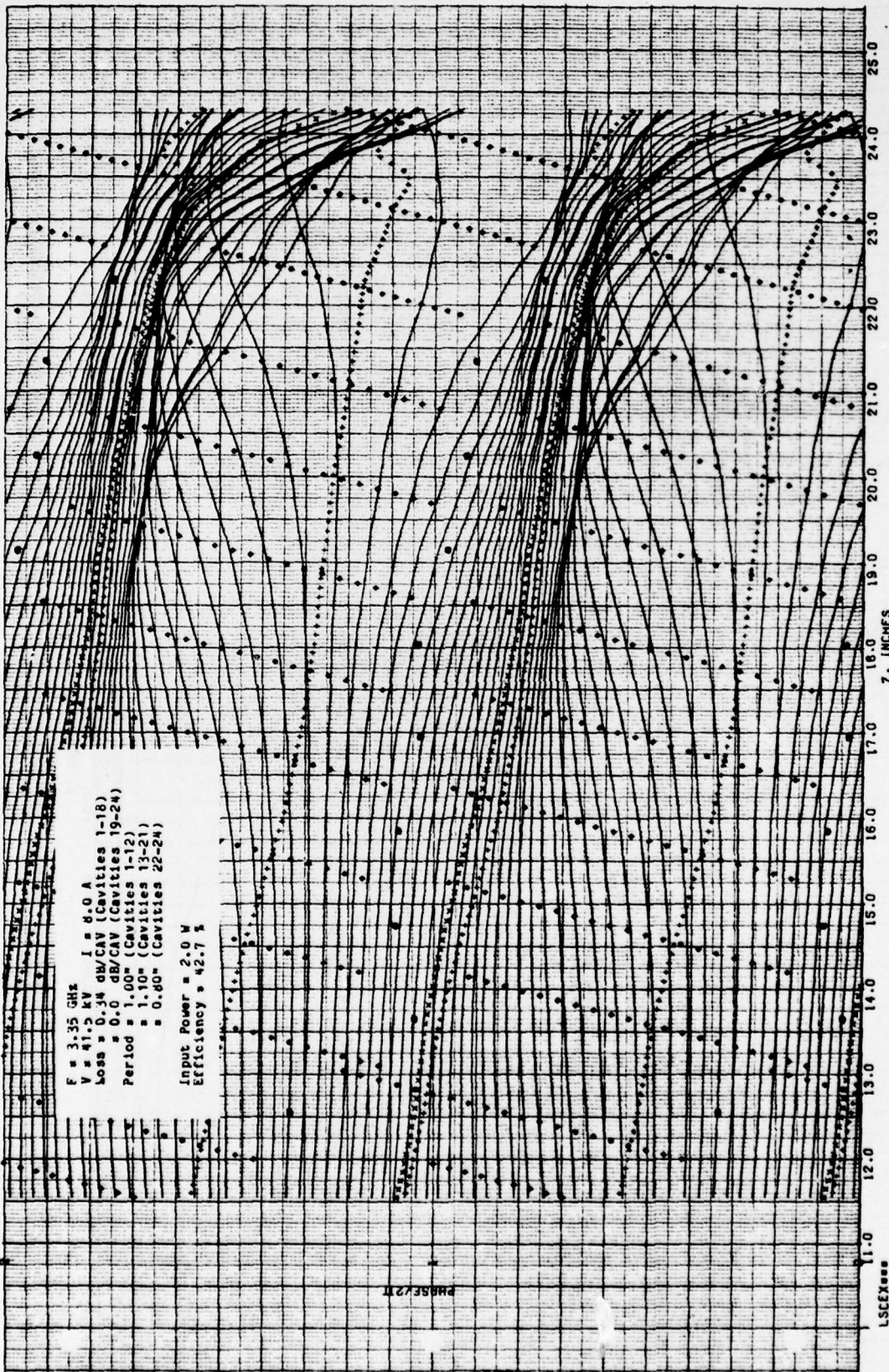


FIGURE 5.91 COMPUTED RELATIVE PHASES OF ELECTRON DISKS VS DISTANCE IN SIMULATED COUPLED-CAVITY TWT WITH SIX LOSSLESS OUTPUT CAVITIES, FASTER VELOCITY OUTPUT CIRCUIT AND FINAL THREE CAVITIES WITH DECREASED PERIODS

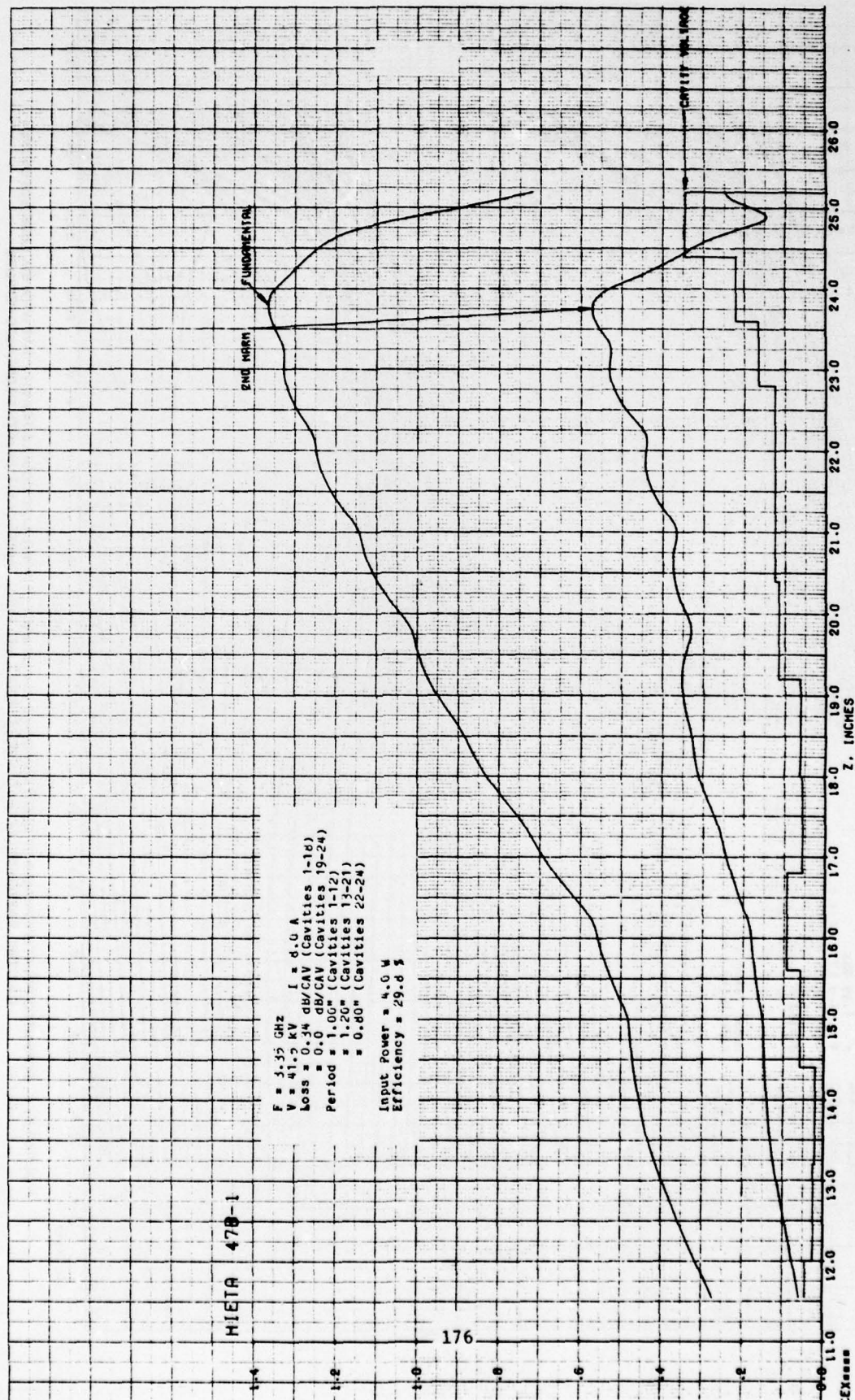


FIGURE 5.92 COMPUTED RF BEAM CURRENTS AND GAP VOLTAGES VS DISTANCE IN SIMULATED COUPLED-CAVITY TWT WITH SIX LOSSLESS OUTPUT CAVITIES. FASTER VELOCITY OUTPUT CIRCUIT AND FINAL THREE CAVITIES WITH DECREASED PERIODS

HIEIR 478-1

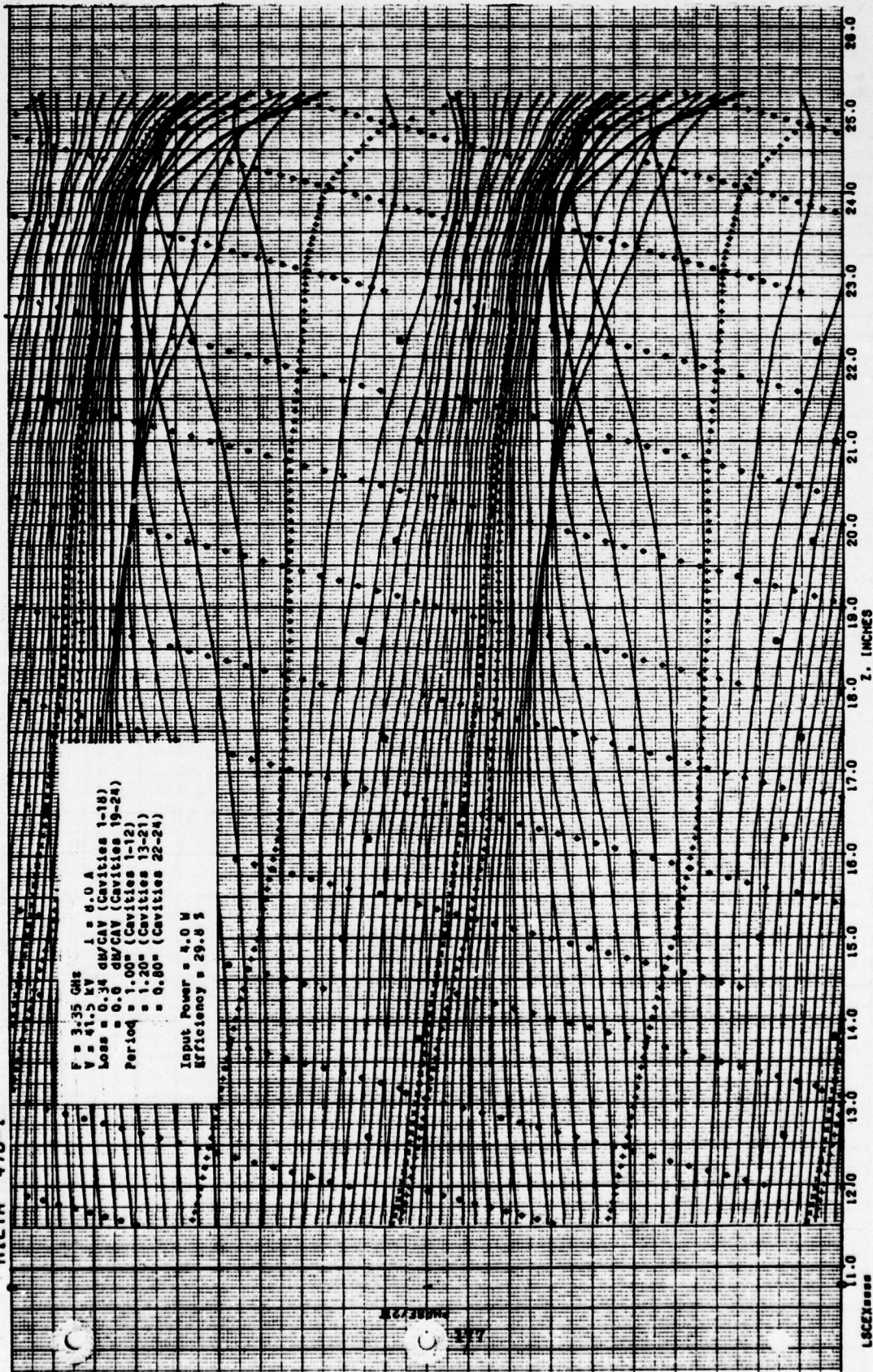


FIGURE 5.03 COMPUTED RELATIVE PHASES OF ELECTRON DISKS VS DISTANCE IN SIMULATED COUPLED-CAVITY TWT WITH SIX LOSSLESS OUTPUT CAVITIES, FASTER VELOCITY OUTPUT CIRCUIT AND FINAL THREE CAVITIES WITH DECREASED PERIODS

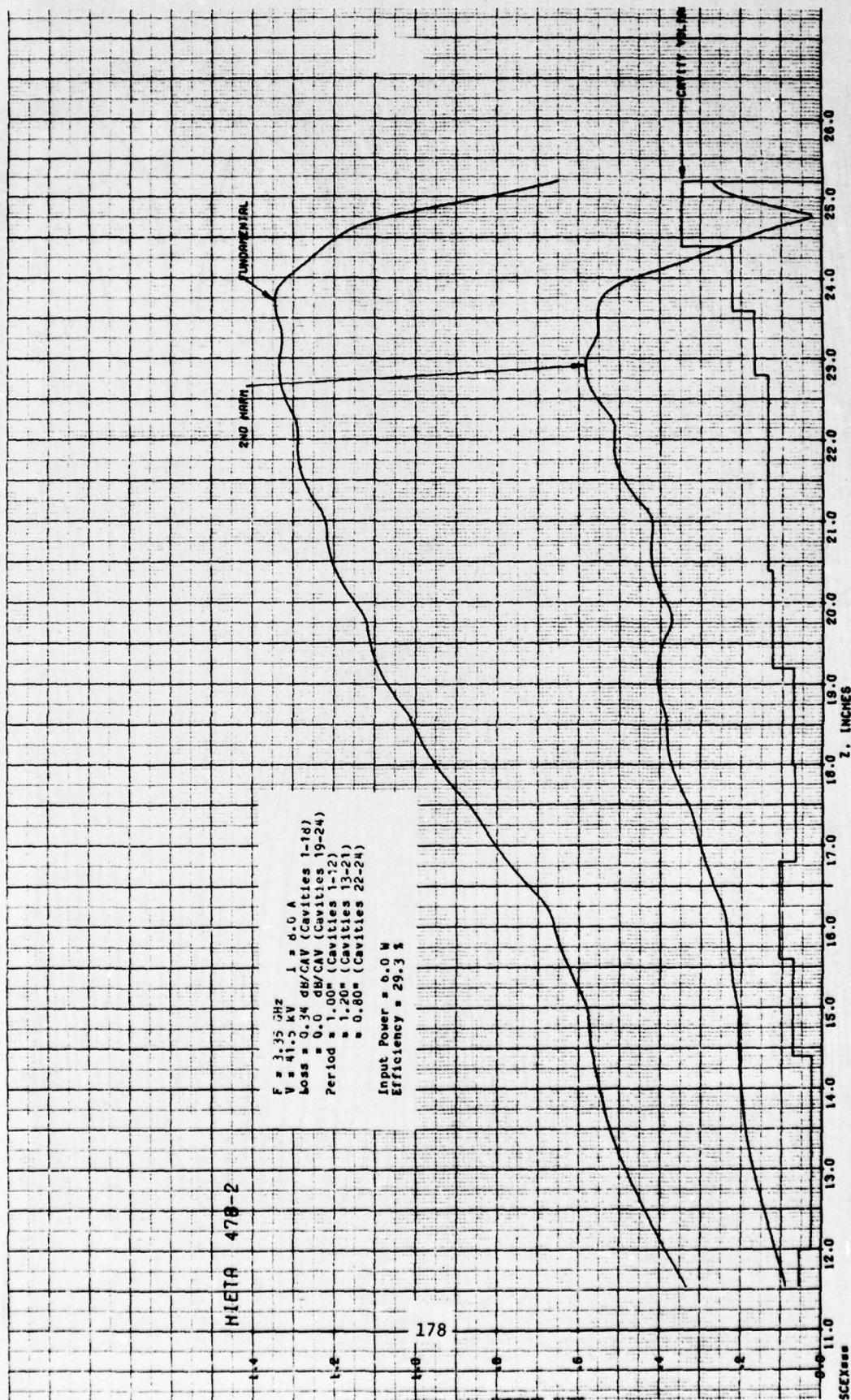


FIGURE 5.94 COMPUTED RF BEAM CURRENTS AND GAP VOLTAGES VS DISTANCE IN SIMULATED COUPLED-CAVITY TWT WITH SIX LOSSLESS OUTPUT CAVITIES, FASTER VELOCITY OUTPUT CIRCUIT AND FINAL THREE CAVITIES WITH DECREASED PERIODS

HIETA 478-2

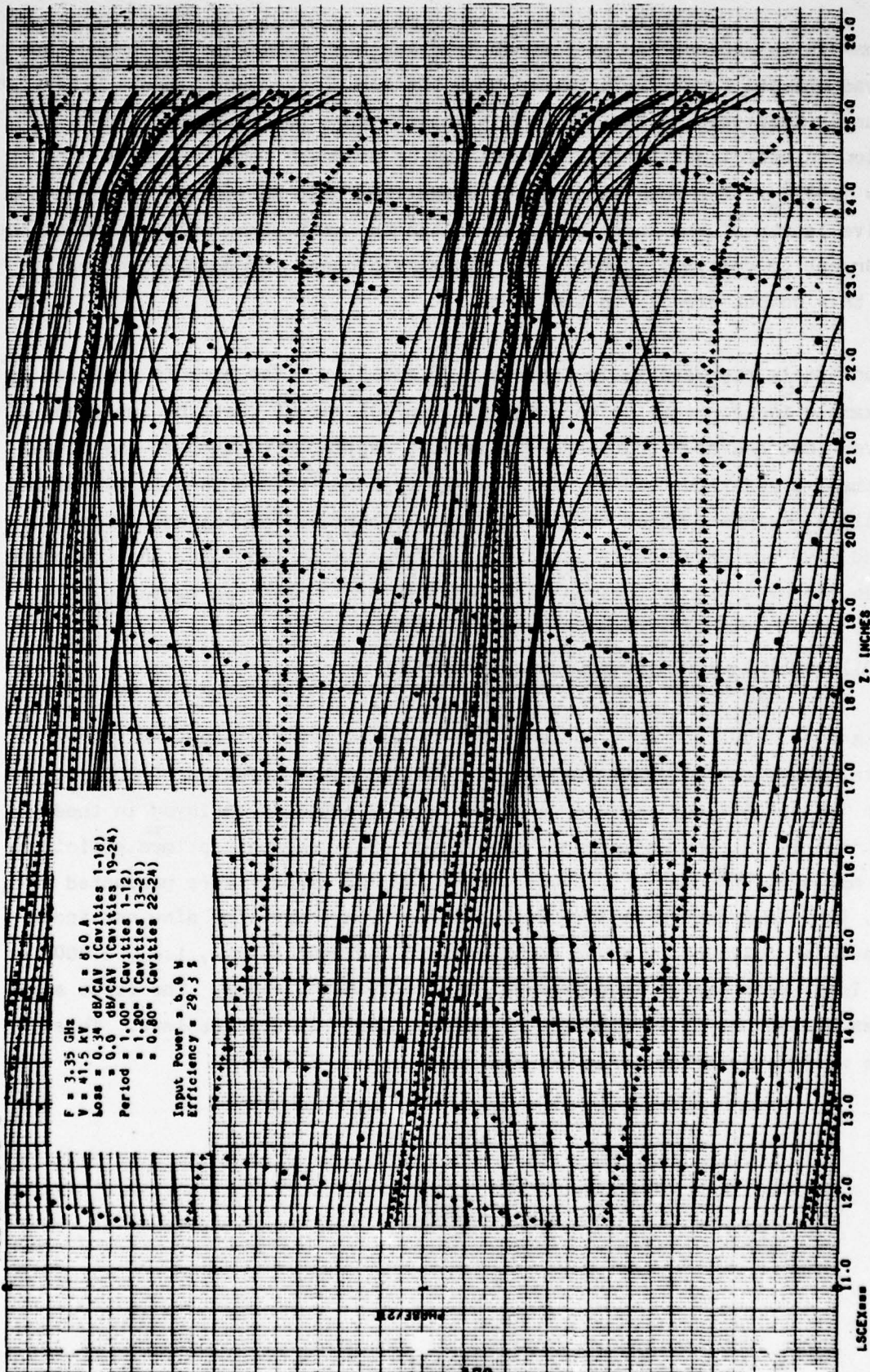


FIGURE 5.95 COMPUTED RELATIVE PHASES OF ELECTRON DISKS VS DISTANCE IN SIMULATED COUPLED-CAVITY TWT WITH SIX LOSSLESS OUTPUT CAVITIES, FASTER VELOCITY OUTPUT CIRCUIT AND FINAL THREE CAVITIES WITH DECREASED PERIODS

Run 47E is represented by Figures 5.96 and 5.97. In this run the output taper was changed to 90-70-75 rather than the normal 80-80-80 taper. Otherwise this run is identical to Run 47A. This taper change has resulted in a reduction in efficiency to 40.2 percent and an increase fundamental rf current to $I_1 = 1.44 I_0$. The conclusion to be drawn from this is that by reducing the effective length of the taper we have reduced the efficiency while allowing the beam current to continue to build up. This reinforces the conclusion reached above; this output circuit is too short.

Run 48A is represented in Figures 5.98 and 5.99. The circuit employed in this example is identical to that used in Run 40A except that the impedance of the sever load has been adjusted to provide a perfect hot match at the output under small-signal conditions. This design feature is important in minimizing small-signal gain and phase ripple due to an imperfect load match. Figures 5.98 and 5.99 are very nearly identical to Figure 5.56 and 5.58. Hot matching has been achieved without degradation in other performance parameters.

5.7 Optimization with Frequency as a Parameter

Figures 5.100 through 5.105 show the computed gap voltages, rf beam currents, and electron phase trajectories in the output section of a two-section TWT with 12 cavities in each section. The design employed in these simulations is the most simple of those which provided near optimum efficiency at the mid-band frequency, 3.35 GHz. The 3.35 GHz results were presented as Run No. 40A. This design employs an output section comprising nine one-inch-long cavities followed by three cavities of 80 percent length, i.e., 0.800 inch. This taper design is referred to as an 80-80-80 taper. The first six cavities of the output section are lossy, the last six are lossless. This vehicle will be referred to as TWT Design A.

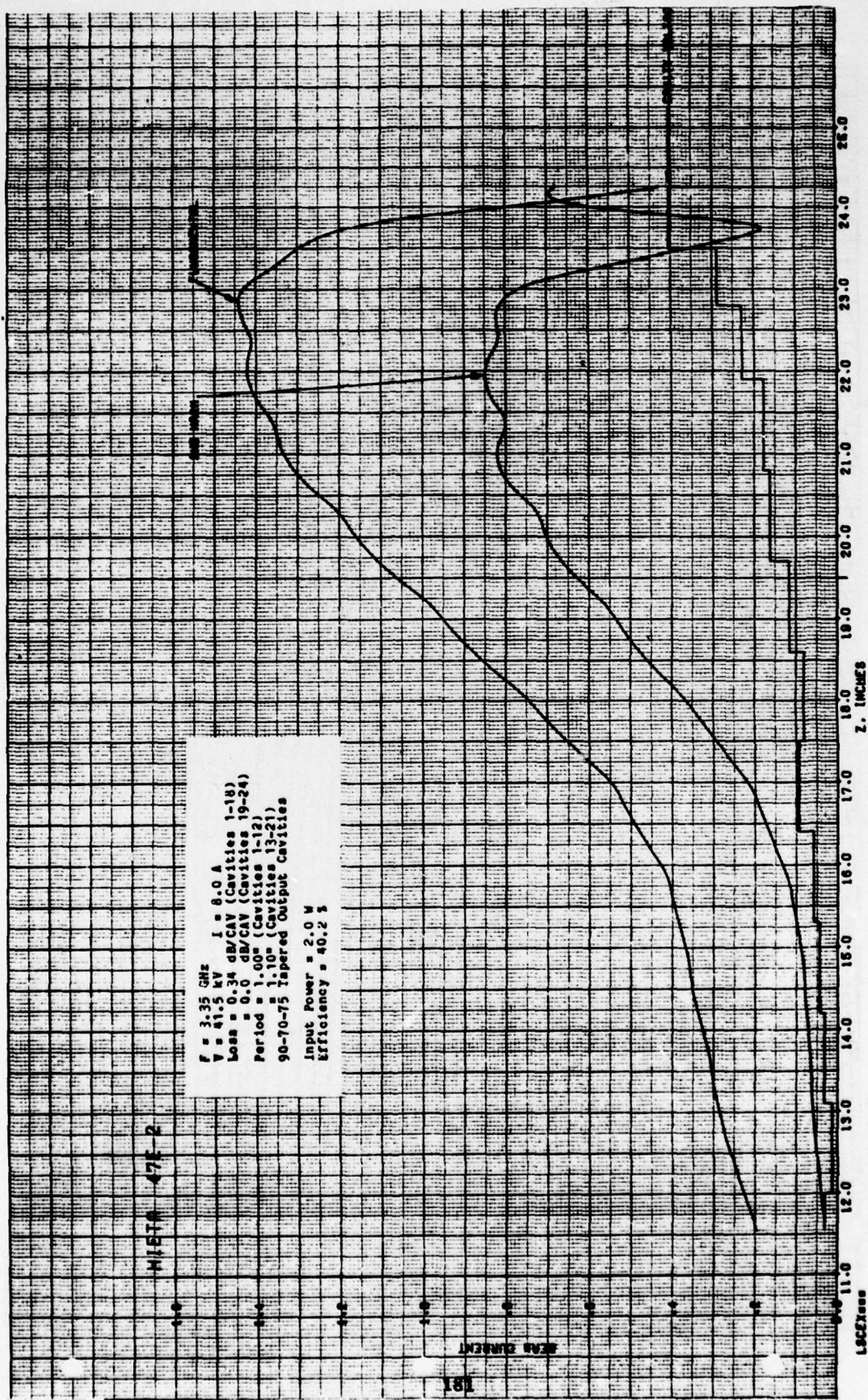


FIGURE 6.96 COMPUTED RF BEAM CURRENTS AND GAP VOLTAGES VS DISTANCE IN SIMULATED COUPLED-CAVITY TWT WITH SIX LOSSLESS OUTPUT CAVITIES, FASTER VELOCITY OUTPUT CIRCUIT AND FINAL THREE CAVITIES WITH DECREASED PERIODS

HIETA 47E-2

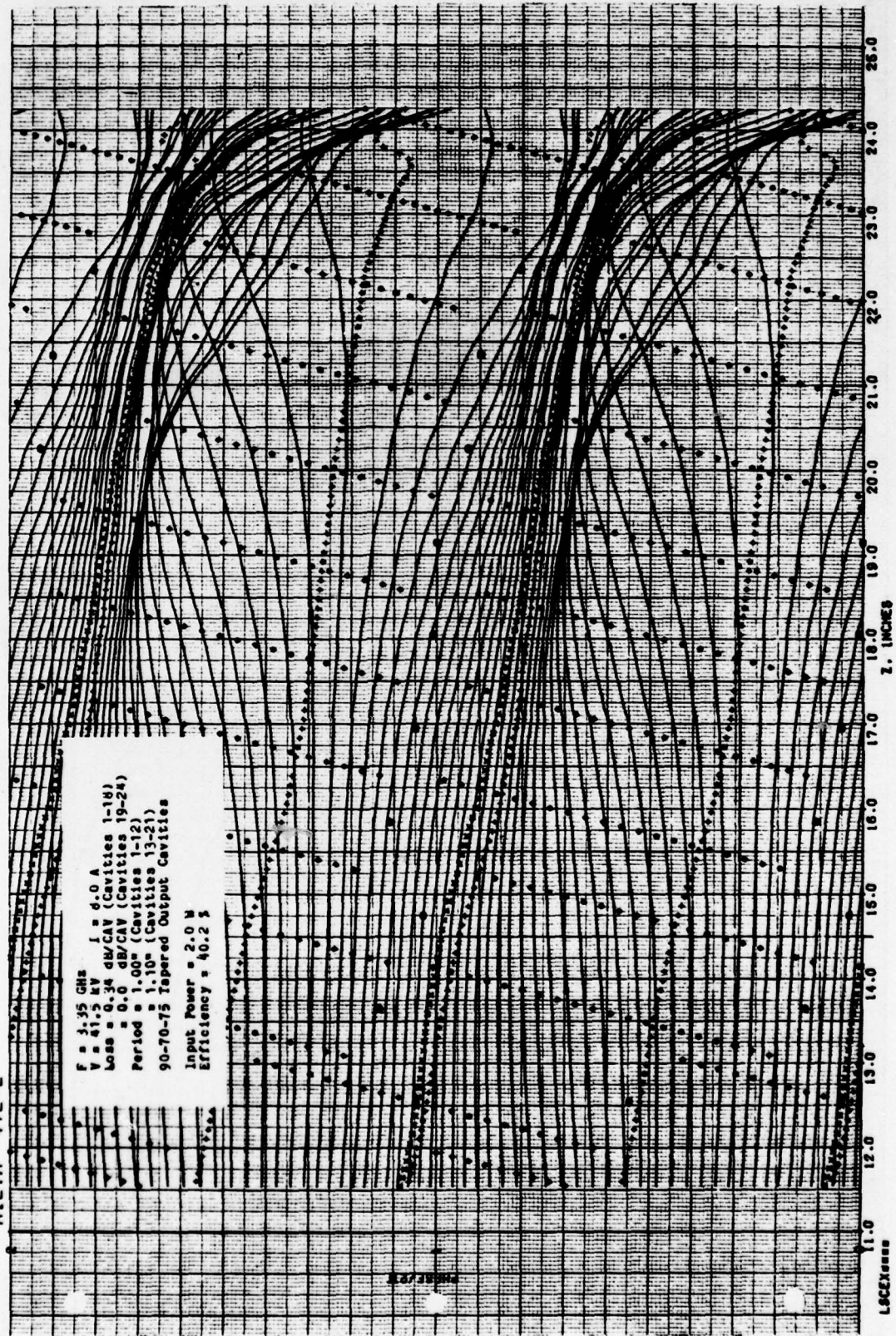


FIGURE 5.97 COMPUTED RELATIVE PHASES OF ELECTRON DISKS VS DISTANCE IN SIMULATED COUPLED-CAVITY TWT WITH SIX LOSSLESS OUTPUT CAVITIES, FASTER VELOCITY OUTPUT CIRCUIT AND FINAL THREE CAVITIES WITH DECREASED PERIODS

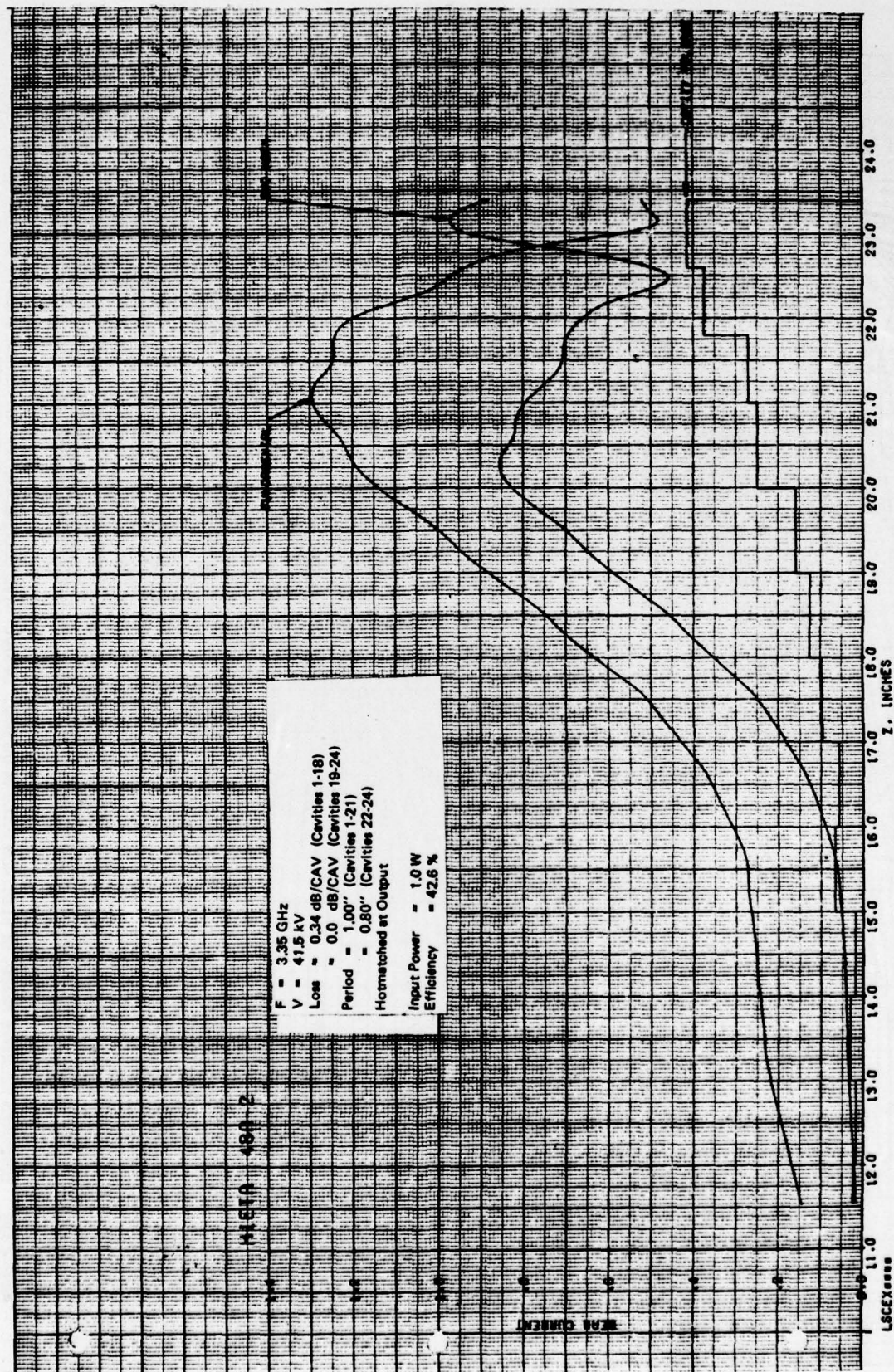


FIGURE 5.98 COMPUTED RF BEAM CURRENTS AND GAP VOLTAGES VS DISTANCE IN SIMULATED COUPLED-CAVITY TWT HOTMATCHED AT OUTPUT, WITH SIX LOSSLESS OUTPUT CAVITIES, AND FINAL THREE CAVITIES WITH DECREASED PERIODS

HIETA 48A-2

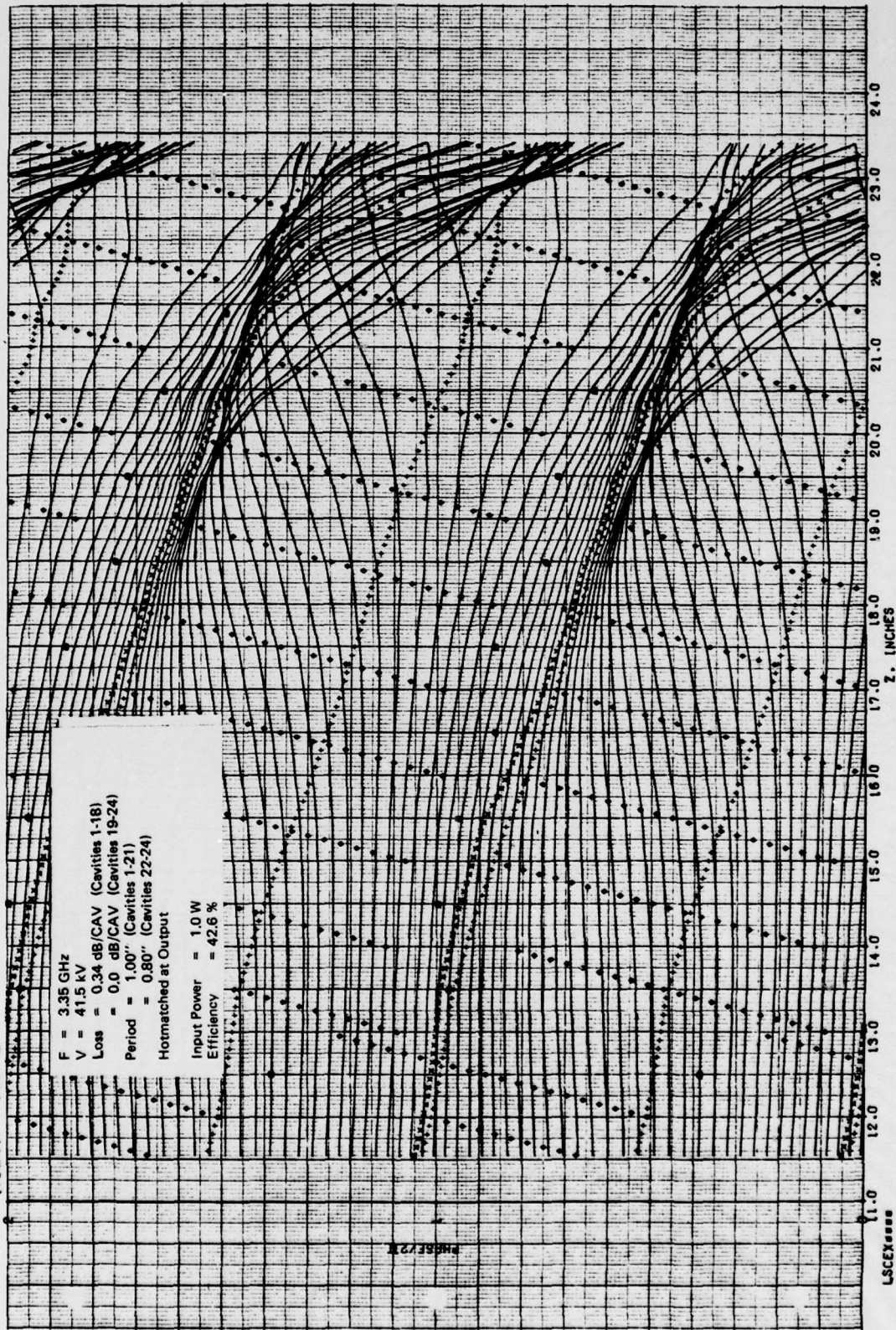


FIGURE 5.96 COMPUTED RELATIVE PHASES OF ELECTRON DISKS VS DISTANCE IN SIMULATED COUPLED-CAVITY TWT HOTMATCHED AT OUTPUT WITH SIX LOSSLESS OUTPUT CAVITIES, AND FINAL THREE CAVITIES WITH DECREASED PERIODS

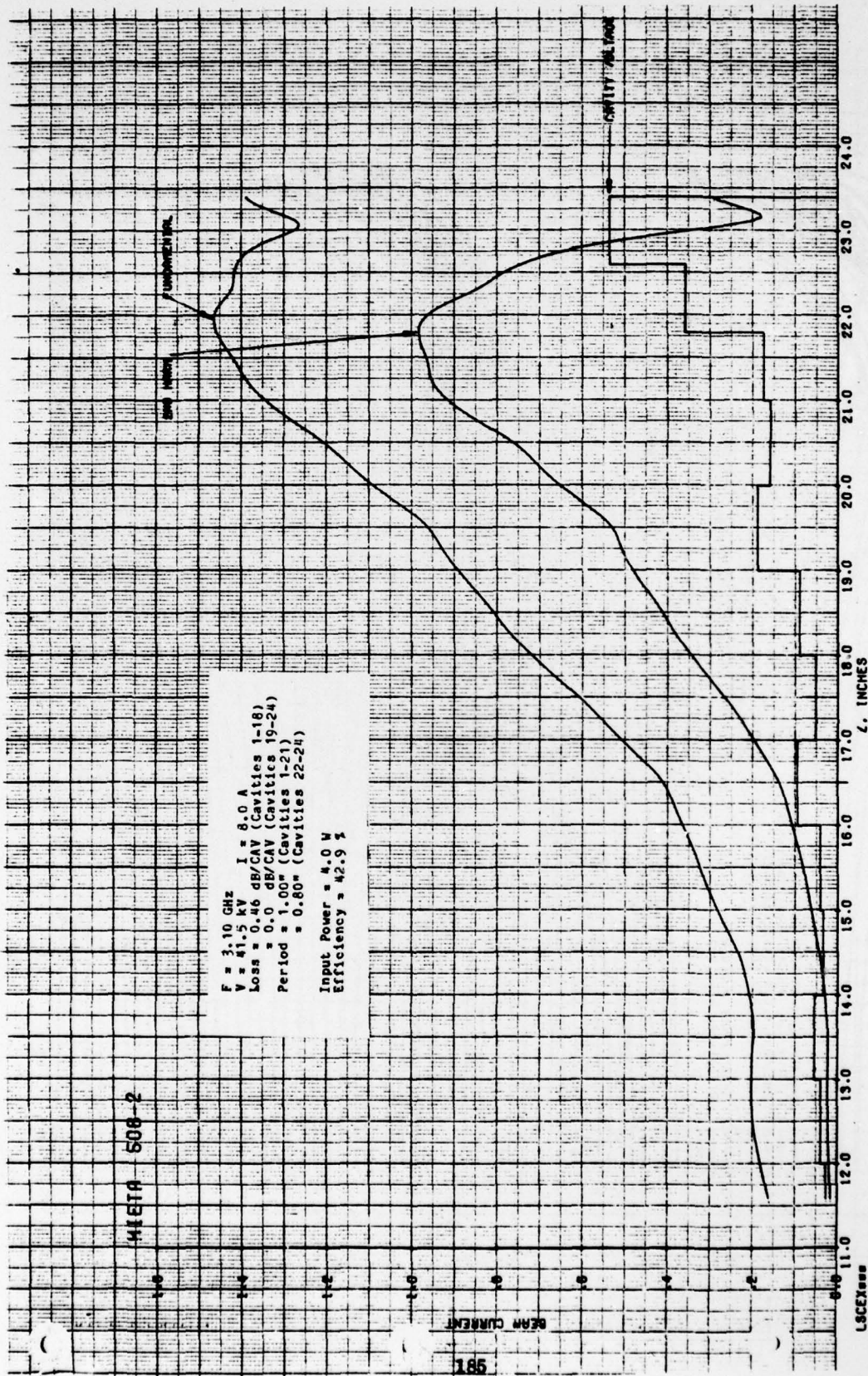


FIGURE 6.100 COMPUTED RF BEAM CURRENTS AND GAP VOLTAGES VS DISTANCE IN SIMULATED COUPLED-CAVITY TWT WITH TWELVE CAVITY OUTPUT SECTION AND SIX LOSSLESS OUTPUT CAVITIES AT A FREQUENCY OF 3.1 GHz

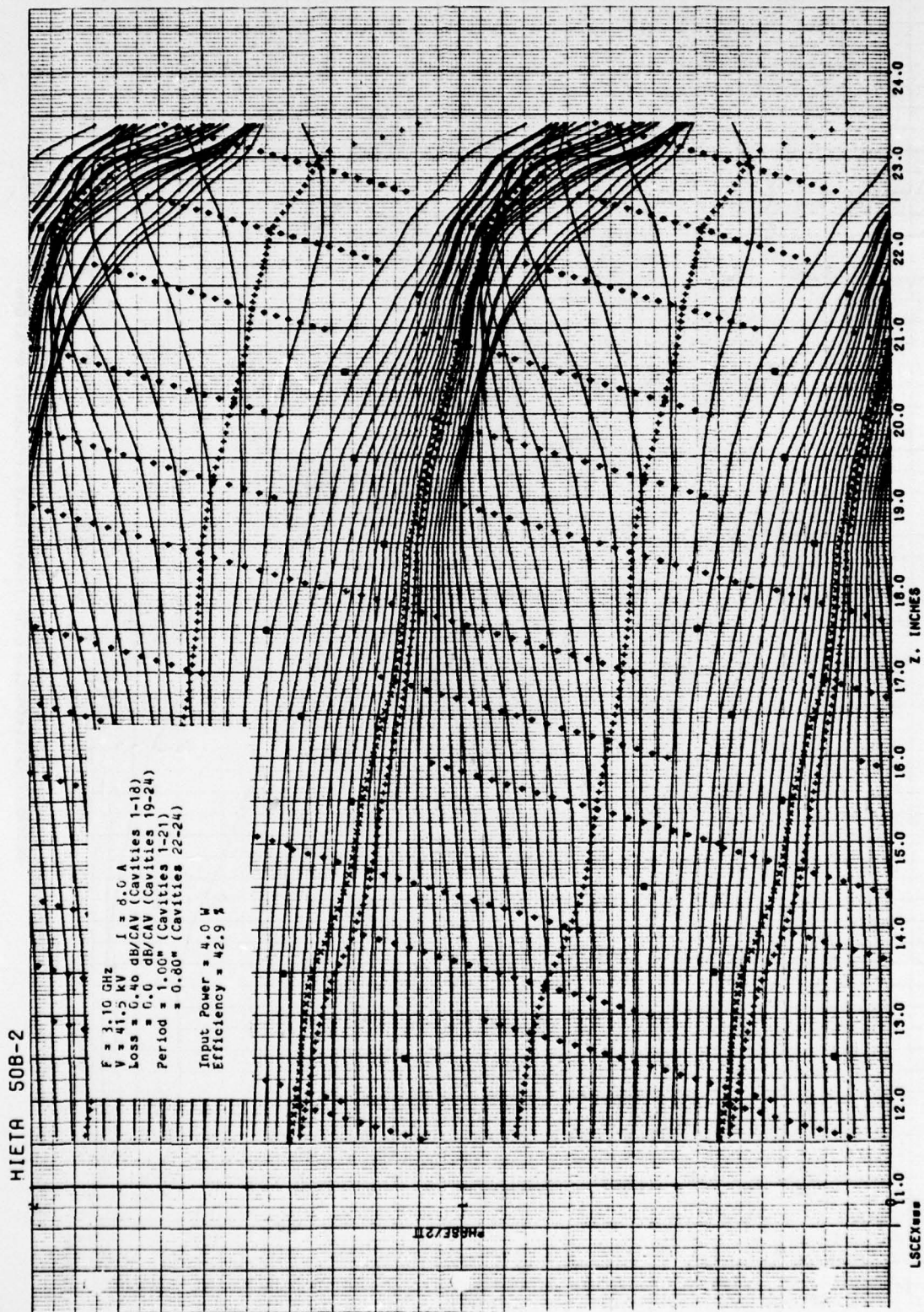
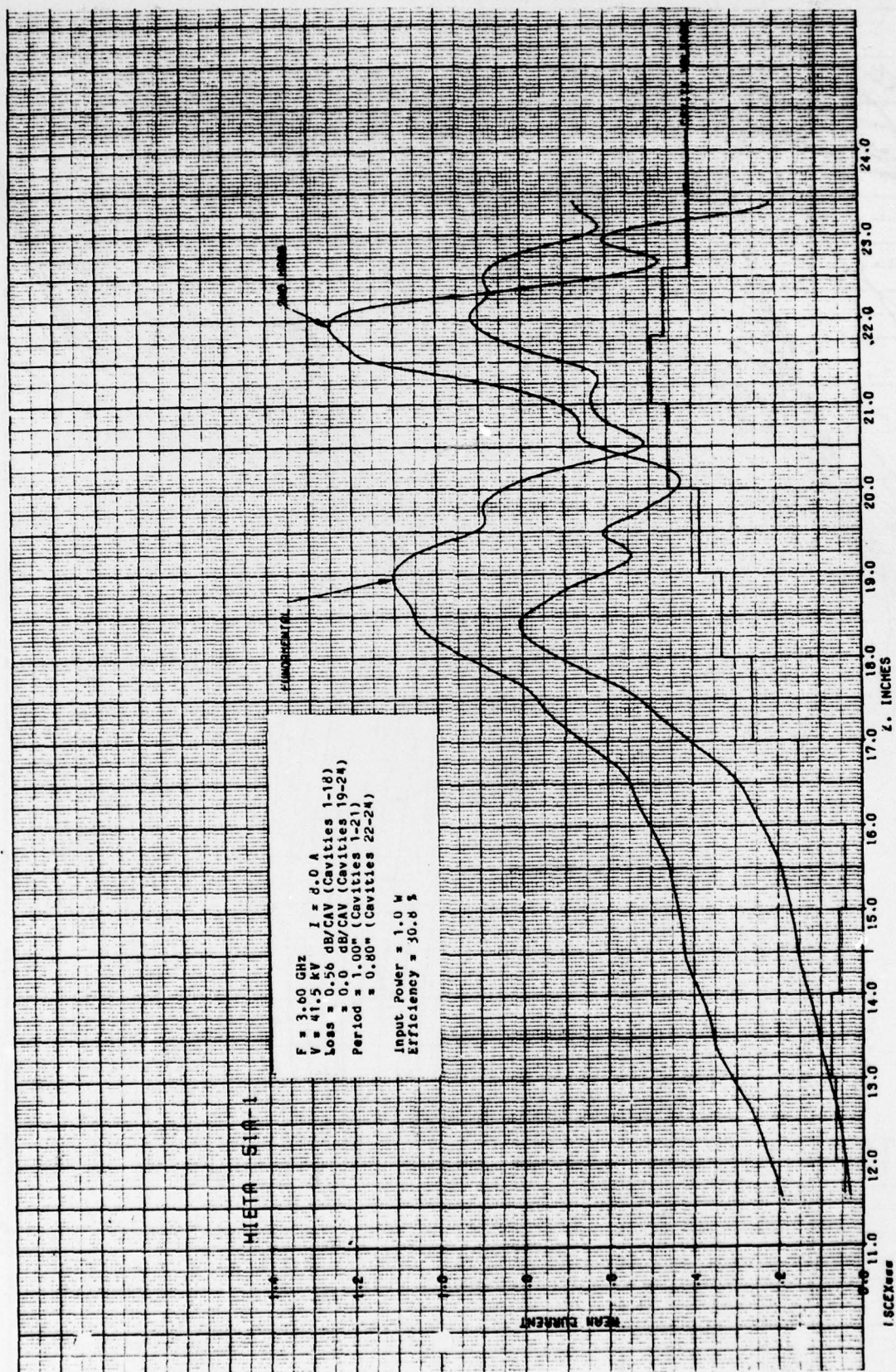


FIGURE 5.101 COMPUTED RELATIVE PHASES OF ELECTRON DISKS VS DISTANCE IN SIMULATED COUPLED-CAVITY TWT WITH TWELVE CAVITY OUTPUT SECTION AND SIX LOSSLESS OUTPUT CAVITIES AT A FREQUENCY OF 3.1 GHz



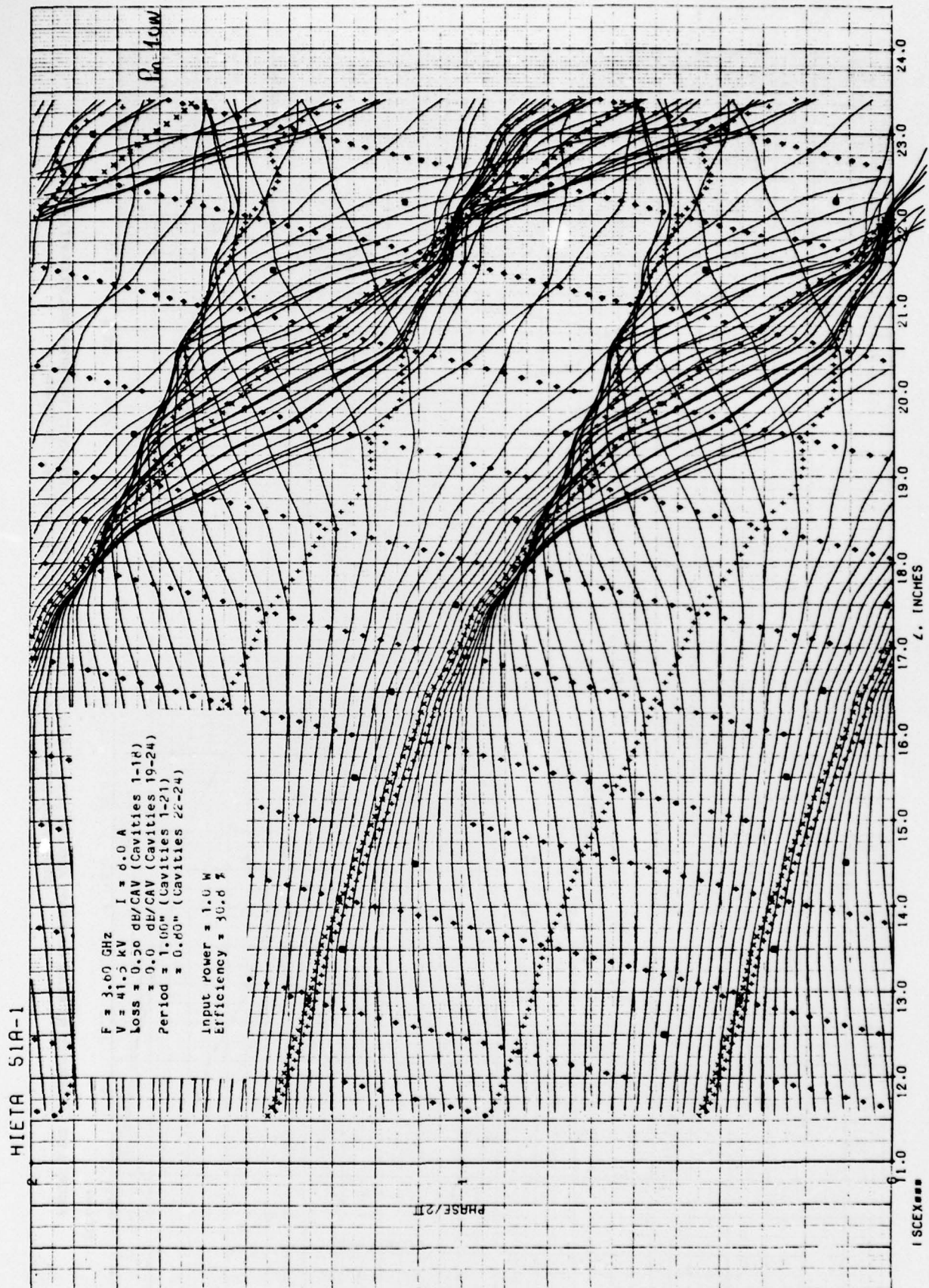


FIGURE 5.103 COMPUTED RELATIVE PHASES OF ELECTRON DISKS VS DISTANCE IN SIMULATED COUPLED-CAVITY TWT WITH TWELVE CAVITY OUTPUT SECTION AND LOSSLESS OUTPUT CAVITIES AT A FREQUENCY OF 3.6 GHz

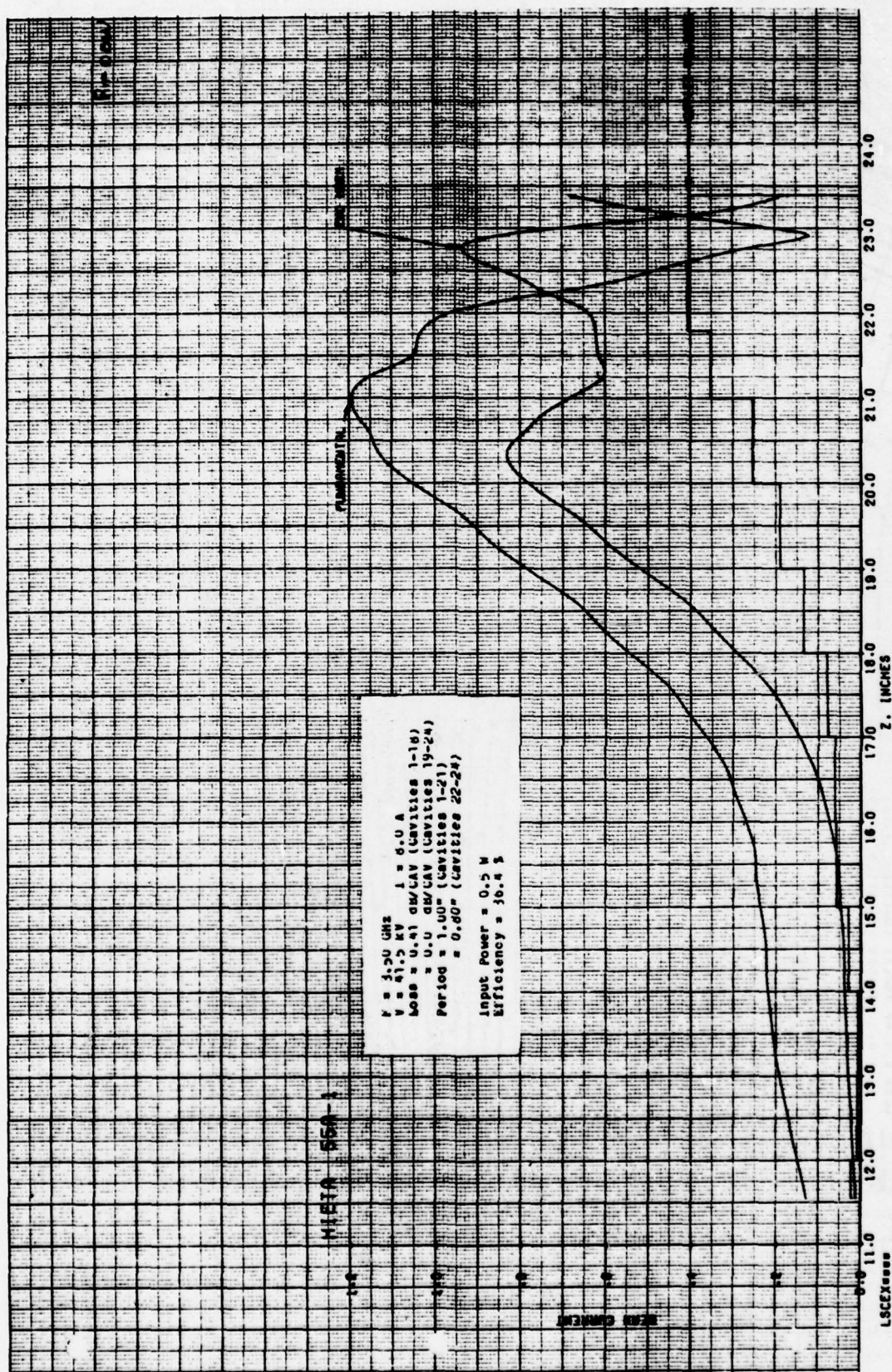


FIGURE 6.104 COMPUTED RF BEAM CURRENTS AND GAP VOLTAGES VS DISTANCE IN SIMULATED COUPLED-CAVITY TWT WITH TWELVE CAVITY OUTPUT SECTION AND SIX LOSSLESS OUTPUT CAVITIES AT A FREQUENCY OF 3.5 GHz

HIETA 55A-1

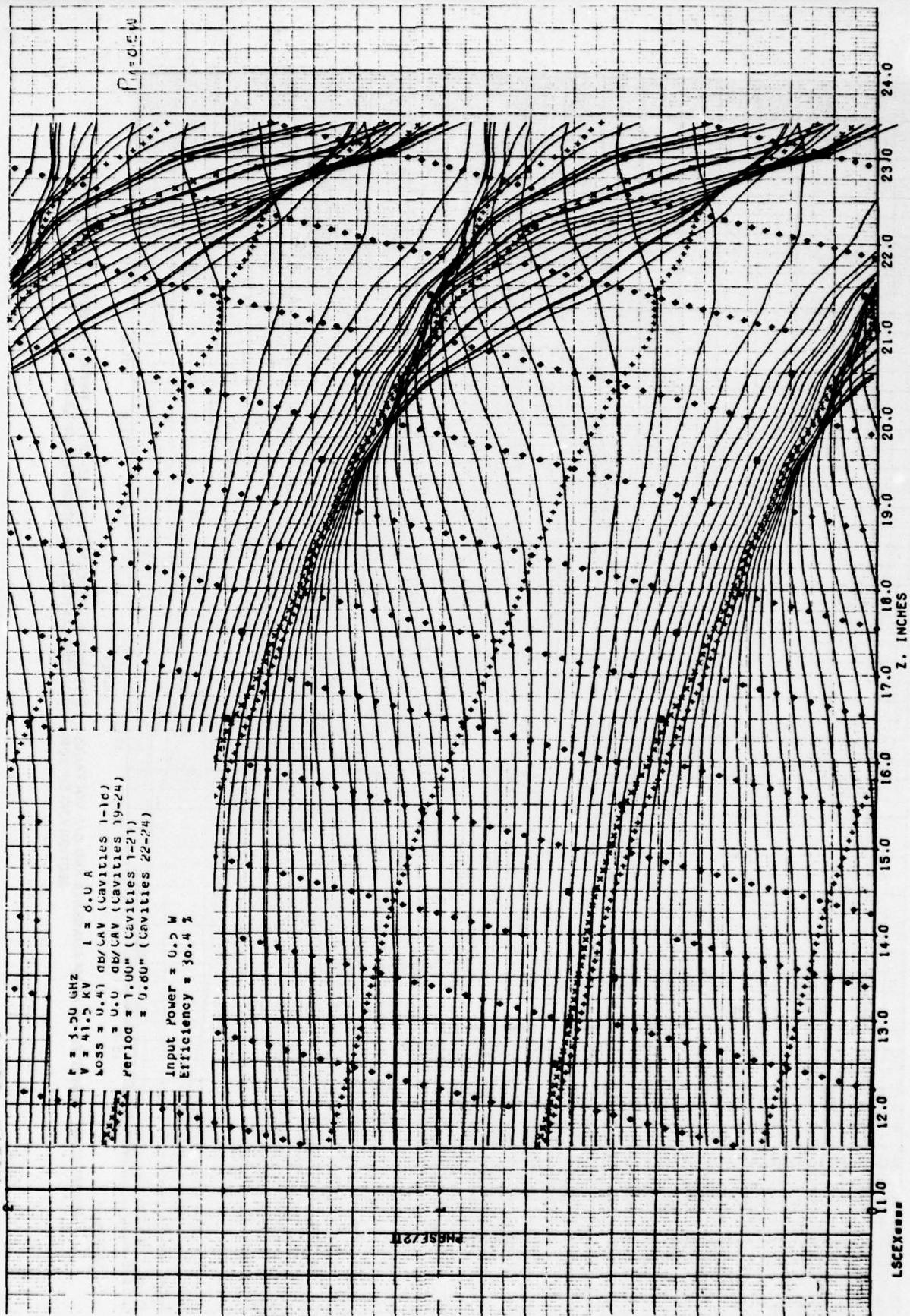


FIGURE 5.105 COMPUTED RELATIVE PHASES OF ELECTRON DISKS VS DISTANCE IN SIMULATED COUPLED-CAVITY TWT WITH TWELVE CAVITY OUTPUT SECTION AND SIX LOSSLESS OUTPUT CAVITIES AT A FREQUENCY OF 3.5 GHz

Figures 5.100 and 5.101 show computed results employing saturated drive (4.0 watts) at the lowest frequency in the desired band (3.1 GHz). The results shown here strongly resemble those previously computed at the midband frequency. The strong backward-wave component manifests itself in the non-monotonic behavior of the gap voltages in Figure 5.100. The high-circuit impedance and sub-synchronous beam velocity ($b = -0.835$) give rise to excellent bunching, with a maximum fundamental component of rf convection current $I_1 = 1.46 I_0$. The effect of the strong backward-wave is further illustrated in Figure 5.101 where the phases of the cavity gap fields (small dark squares) appear grouped in sets of three. The conversion efficiency could likely be further optimized at this frequency by modifying the gap-to-gap spacings so as to minimize the phase excursions illustrated in this figure. Unfortunately, such a procedure would damage the conversion efficiency at other frequencies where the backward-wave interferes in a different way. In any case, the computed conversion efficiency of 42.9 percent is quite acceptable for the band-edge frequency.

Figures 5.56 and 5.57 show the results computed at the midband frequency (3.35 GHz) with a saturated drive of 1 watt. At the midband frequency, backward-wave effects are much less pronounced. The gap voltages of Figure 5.56 are almost monotonic. The phases of the gap fields shown in Figure 5.57 are very nearly uniform. The computed midband conversion efficiency is 42.9 percent, the same value predicted for the lower band-edge frequency.

Figures 5.102 and 5.103 show the computed results at the upper band edge frequency, 3.6 GHz. The saturated drive power is 1 watt and the computed conversion efficiency is 30.8 percent. The double peaked fundamental and second harmonic beam currents and the fact that the cavity voltage peaks in the third last cavity, would suggest that the tube is being overdriven. Examination of the electron phase trajectories in Figure 5.103 would tend to confirm this conclusion. Nevertheless, it is found that the output power is maximum at 1 watt drive. The computation at 3.6 GHz is the first of those

presented here which failed to achieve backward-wave convergence. Convergence was not achieved after six backward-wave iterations. This failure to converge should be taken as a warning that the TWT may not be stable.

Because of the low efficiency and poor convergence encountered at 3.6 GHz, an additional large-signal computation was done at 3.5 GHz. The results are shown in Figures 5.104 and 5.105. Saturated drive power at this frequency was 0.5 watts and the computed conversion efficiency was 36.4 percent. Backward-wave convergence was achieved in three iterations. The figures do not exhibit the features which made the results computed at 3.6 GHz appear overdriven. The computed behavior at 3.5 GHz is similar to that at 3.35 GHz, backward-wave effects are minimal.

TWT Design A comes close to the desired performance but exhibits a rather drastic fall-off in efficiency toward the upper end of the frequency band. To improve bunching at the upper band-edge it will be necessary to increase the circuit velocity. This increase can be expected to reduce the gain and efficiency at the bottom band-edge and to degrade the electronic stability. The latter problem will be addressed after a design is found which displays more nearly balanced efficiency over the frequency band of interest.

TWT Design B is a modification of Design A intended to correct low efficiency at the upper band-edge. The output circuit in the new design comprises 13 cavities, with 10 cavities 1.1 inches long and three cavities 0.8 inches long. The first seven cavities are lossy and the last six cavities are lossless. The input section is the same as before.

The results of the large-signal computation on TWT Design B are summarized in Figure 5.106. The small-signal gain is maximum near the top of the frequency band, as expected, and the conversion efficiency has been increased at the higher frequencies and decreased at the lower band-edge. The midband conversion efficiency, 44.2 percent, is the largest yet found. The computed efficiency is flatter over the band than that for Design A. Backward-wave

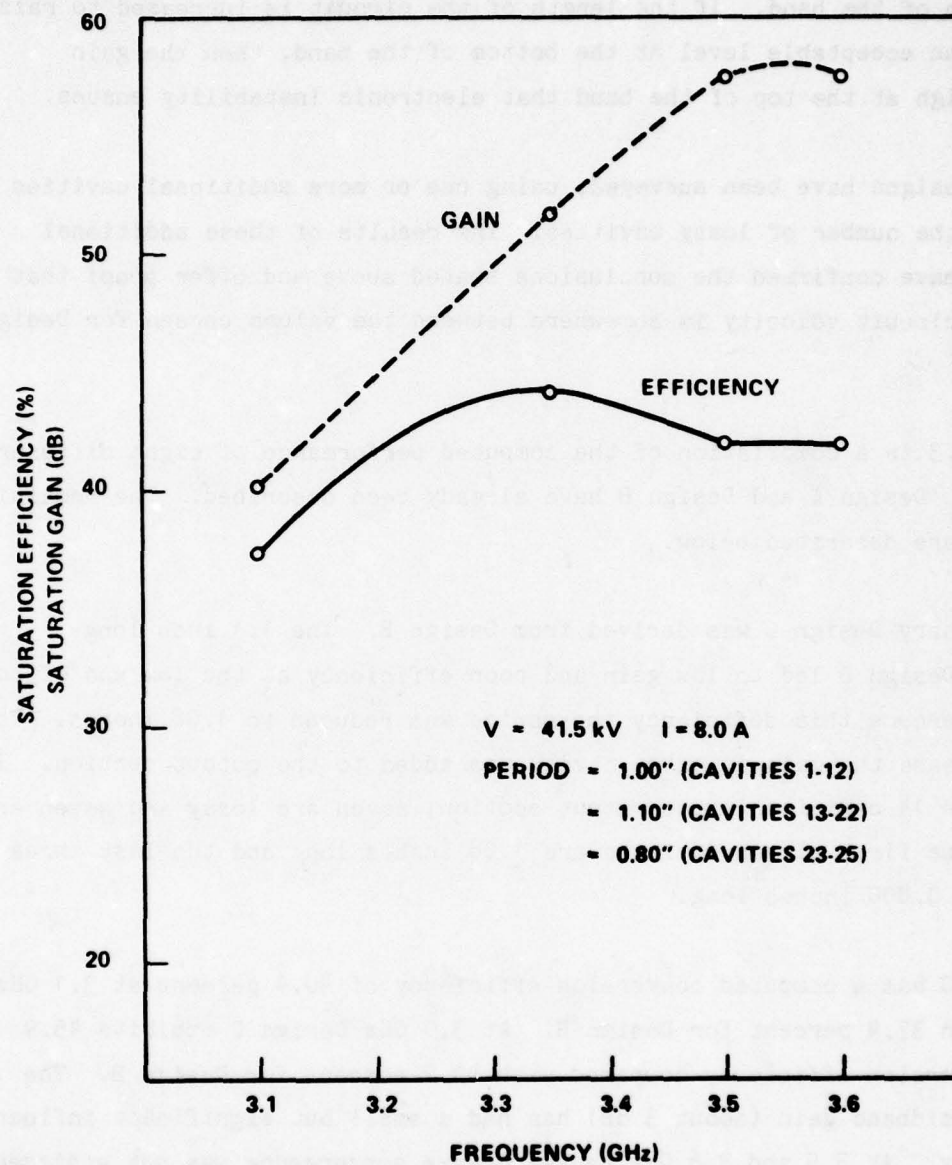


**FIGURE 5.106 SATURATION GAIN AND EFFICIENCY VS FREQUENCY
IN SIMULATED COUPLED CAVITY TWT WITH THIRTEEN
CAVITY OUTPUT SECTION AND SIX LOSSLESS OUTPUT
CAVITIES**

convergence was not achieved at 3.6 GHz, nor was it in Design A. The problem illuminated by these findings is that the circuit velocity required for good efficiency at the top of the band produces low gain, and hence low efficiency at the bottom of the band. If the length of the circuit is increased to raise the gain to an acceptable level at the bottom of the band, then the gain becomes so high at the top of the band that electronic instability ensues.

Other designs have been surveyed, using one or more additional cavities and varying the number of lossy cavities. The results of these additional simulations have confirmed the conclusions stated above and offer proof that the optimum circuit velocity is somewhere between the values chosen for Designs A and B.

Table 5.3 is a compilation of the computed performance of eight different TWT designs. Design A and Design B have already been described. The remaining six designs are described below.

Preliminary Design C was derived from Design B. The 1.1 inch long cavities of Design B led to low gain and poor efficiency at the low end of the band. To overcome this deficiency the period was reduced to 1.08 inches. To further increase the gain an extra cavity was added to the output section. In all there are 14 cavities in the output section; seven are lossy and seven are lossless. The first eleven cavities are 1.08 inches long and the last three cavities are 0.800 inches long.

Design C has a computed conversion efficiency of 40.4 percent at 3.1 GHz compared with 37.4 percent for Design B. At 3.5 GHz Design C exhibits 45.9 percent conversion efficiency compared with 44.2 percent for Design B. The increase in midband gain (about 3 dB) has had a small but significant influence on efficiency. At 3.5 and 3.6 GHz backward-wave convergence was not achieved; the message here is to check for electronic stability. A stability check of a lower gain circuit reported below is convincing proof that Design C is electronically unstable.

TABLE 5.3

Comparison of Computed TWT Characteristics

DESIGN	SATURATION DRIVE (W)/EFFICIENCY (%)			COMMENTS
	3.10 GHz	3.35 GHz	3.50 GHz	3.60 GHz
A	4.0/42.9	1.0/42.9	0.5/36.4	1.0/30.8* 12 cavity output section 6 lossless output cavities 1.00" period (cavities 1-21)
B	12.0/37.4	1.0/44.2	0.25/42.0*	0.25/42.2* 13 cavity output section 6 lossless output cavities 1.10" period (cavities 13-22)
C	8.0/40.4	0.5/45.9	0.06/38.1*	--- 14 cavity output section 7 lossless output cavities 1.08" period (cavities 13-23)
D	0.125/41.3	1.0/45.5	1.0/40.1	--- 14 cavity output section 7 lossless output cavities 0.90" period (cavities 1-12) 1.08" period (cavities 13-23)
E	8.0/37.5	2.0/43.5	---	1.0/39.7* 14 output cavity section 6 lossless output cavities 1.08" period (cavities 13-23) 4 times standard loss
F	4.0/39.8	2.0/44.5	1.0/40.4	1.0/43.0* 13 cavity output section 6 lossless output cavities 1.08" period (cavities 13-22) Loss tapered with frequency
G	8.0/42.0	2.0/44.0	2.0/38.3	2.0/36.7* 12 cavity output section 6 lossless output cavities 1.05" period (cavities 13-21) Loss tapered with frequency

*Computed solution did not converge

TABLE 5.3 (Continued)

DESIGN	SATURATION DRIVE (W)/EFFICIENCY (%)			COMMENTS	
	3.10 GHz	3.55 GHz	3.60 GHz		
H	12.0/42.6	4.0/42.3	4.0/37.5	1.0/29.3	12 cavity output section 5 lossless output cavities 1.05" period (cavities 13-21) Loss tapered with frequency
I	12.0/39.5	4.0/41.6	2.0/36.1	2.0/34.6	12 cavity output section 5 lossless output cavities 1.05" periods (cavities 13-21) Loss tapered with frequency Last 2 cavities high frequency
J	16.0/36.5	2.0/40.5	4.0/36.7	2.0/43.6*	12 cavity output section 5 lossless output cavities 1.08" periods (cavities 13-21) Loss tapered with frequency High frequency circuit (cavities 13, 14, 23, 24)
K	24.0/30.7	4.0/37.5	4.0/37.1	1.0/31.4	12 cavity output section 5 loss output cavities 1.08" periods (cavities 13-21) Loss tapered with frequency Ultra high frequency circuit (cavities 13, 14, 23, 24)
L	8.0/32.0	2.0/38.7	1.0/36.9	0.5/31.7	13 cavity output section 5 lossless output cavities 1.08" periods (cavities 13-22) Loss tapered with frequency Ultra high frequency circuit (cavities 13, 14, 24, 25)

*Computed solution did not converge

TABLE 5.3 (Continued)

DESIGN	SATURATION DRIVE (W)/EFFICIENCY (%)		COMMENTS
	3.10 GHz	3.35 GHz	
M	12.0/39.7	2.0/41.7	12 cavity output section
		3.0/36.0	5 lossless 1.05" periods (cavities 13-21) Loss tapered with frequency High frequency circuit (cavities 13, 14, 23, 24)
		2.0/33.5	
		3.60 GHz	

#Computed solution did not converge

Design D represents an attempt to adjust gain flatness by changing the circuit velocity in the input section of the TWT. The input circuit period was reduced from 1.00 inch to 0.900 inch. This change was somewhat greater than required for gain flattening. The output circuit which was computed to be almost backward-wave convergent in Design C at 3.5 GHz achieved convergence yielding an efficiency of 40.1 percent. At 3.6 GHz the large-signal calculation did not converge.

In Design E the number of lossy cavities in the output section was increased by one to eight. The loss factor was made four times as great. Despite the increased loss this design was not noticeably more stable than its predecessor and was computed to provide lower efficiency.

Design F was contrived to improve on Design E by increasing the gain and efficiency at the low end of the band while decreasing the gain at the high end of the band. The gain was reduced by decreasing the number of cavities from 14 to 13. The seven lossy cavities have frequency selective loss. A comparison between the loss per cavity for a constant loss factor (Design E) and for a linearly increasing loss factor (Design F) is shown in Figure 5.107. The loss factor referred to is the reciprocal Q factor of the lossy cavities. The computed conversion efficiency of Design F runs from 39.8 percent at 3.1 GHz through 44.5 percent at midband to 43.0 percent at 3.6 GHz. These results are very encouraging except for the fact that backward-wave convergence was not achieved at 3.6 GHz.

Design G is a modification of Design F intended to further reduce gain and improve convergence. It employs a 12 cavity output with nine 1.05 inch cavities and three 0.800 inch taper cavities. The six lossy cavities have frequency selective loss as was employed in Design F. This design has good efficiency over the lower half of the band but less than 40 percent efficiency at the top of the band where it still remains unconverged.

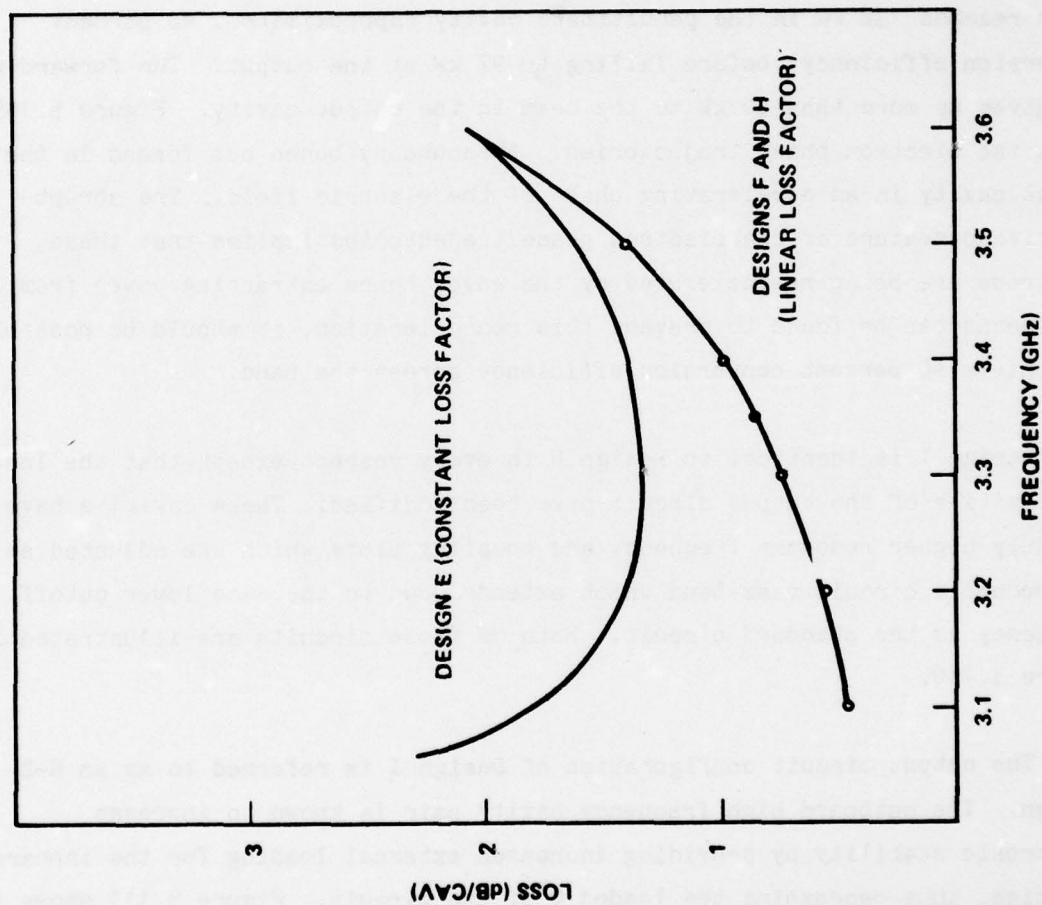


FIGURE 5.107 LOSS PER CAVITY VS FREQUENCY FOR COUPLED CAVITY DESIGNS E, F AND H

Design H is almost identical to Design G except that the frequency selective loss is more accentuated toward the top of the frequency band. This change has resulted in lower efficiency at the top of the band, although, for the first time, backward-wave convergence has been achieved at 3.6 GHz (not at all drive levels). Figures 5.108 and 5.109 show the computed large-signal performance of Design H at 3.6 GHz with 2 watts of drive power. Figure 5.108 shows the rf beam current peaking in the third last cavity then dropping abruptly at the beginning of the output cavity then rising steeply in the output cavity. The printout from this computer run shows that the forward-wave power reaches 132 kW in the penultimate cavity (approximately 40 percent conversion efficiency) before falling to 97 kW at the output. The forward-wave has given up more than 30 kW to the beam in the output cavity. Figure 5.109 shows the electron phase trajectories. A secondary bunch has formed in the output cavity in an accelerating phase of the electric field. The abrupt positive curvature of the electron phase trajectories implies that these electrons are being reaccelerated by the wave, hence extracting power from it. If a means can be found to prevent this reacceleration, it should be possible to achieve 40 percent conversion efficiency across the band.

Design I is identical to Design H in every respect except that the last two cavities of the output circuit have been modified. These cavities have a slightly higher resonant frequency and coupling slots which are adjusted so as to produce a circuit pass-band which extends down to the same lower cutoff frequency as the standard circuit. Both of these circuits are illustrated in Figure 5.110.

The output circuit configuration of Design I is referred to as an N-2 design. The outboard high frequency cavity pair is known to increase electronic stability by providing increased external loading for the inboard cavities, thus decreasing the loaded Q of the circuit. Figure 5.111 shows the electronic stability for this circuit. This figure is a plot of computed start oscillation current vs beam voltage with the frequency of oscillation marked in. Since the nominal operating point is 8 A at 41.5 kV, this design is

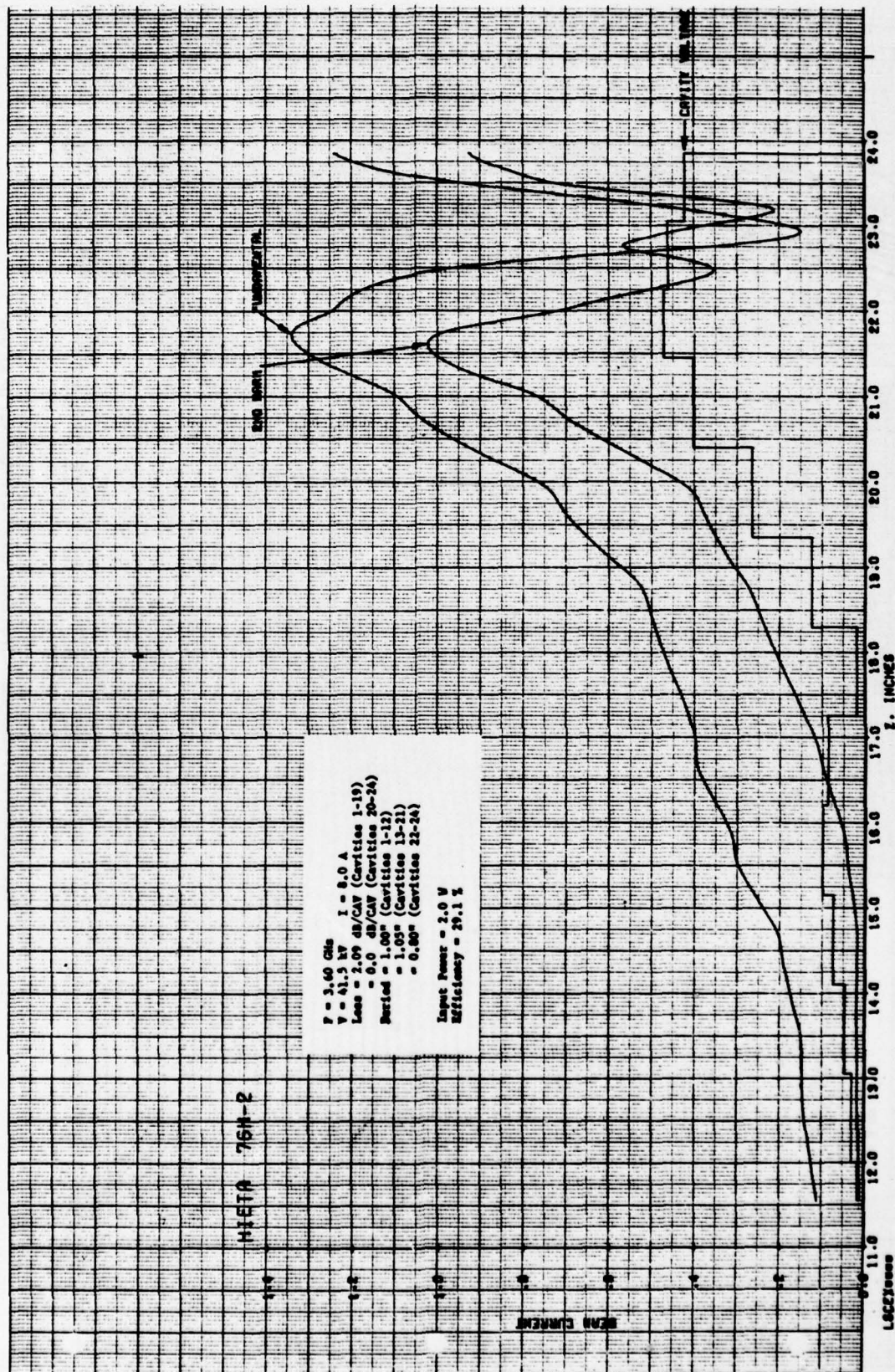


FIGURE 5.108 COMPUTED RF BEAM CURRENTS AND GAP VOLTAGES VS DISTANCE IN SIMULATED COUPLED-CAVITY TWT WITH TWELVE CAVITY OUTPUT SECTION AND FIVE LOSSLESS OUTPUT CAVITIES AT A FREQUENCY OF 3.6 GHz

MIETA 76H-2

$F = 3.60 \text{ GHz}$
 $V = 41.5 \text{ kV}$
 $I = 9.0 \text{ A}$
 $\text{Loss} = 2.09 \text{ dB/Cav}$ (Cavities 1-19)
 $= 0.0 \text{ dB/Cav}$ (Cavities 20-24)
 $\text{Period} = 1.00^\circ$ (Cavities 1-12)
 $= 1.05^\circ$ (Cavities 13-21)
 $= 0.80^\circ$ (Cavities 22-24)

$\text{Input Power} = 2.0 \text{ W}$
 $\text{Efficiency} = 25.1 \%$

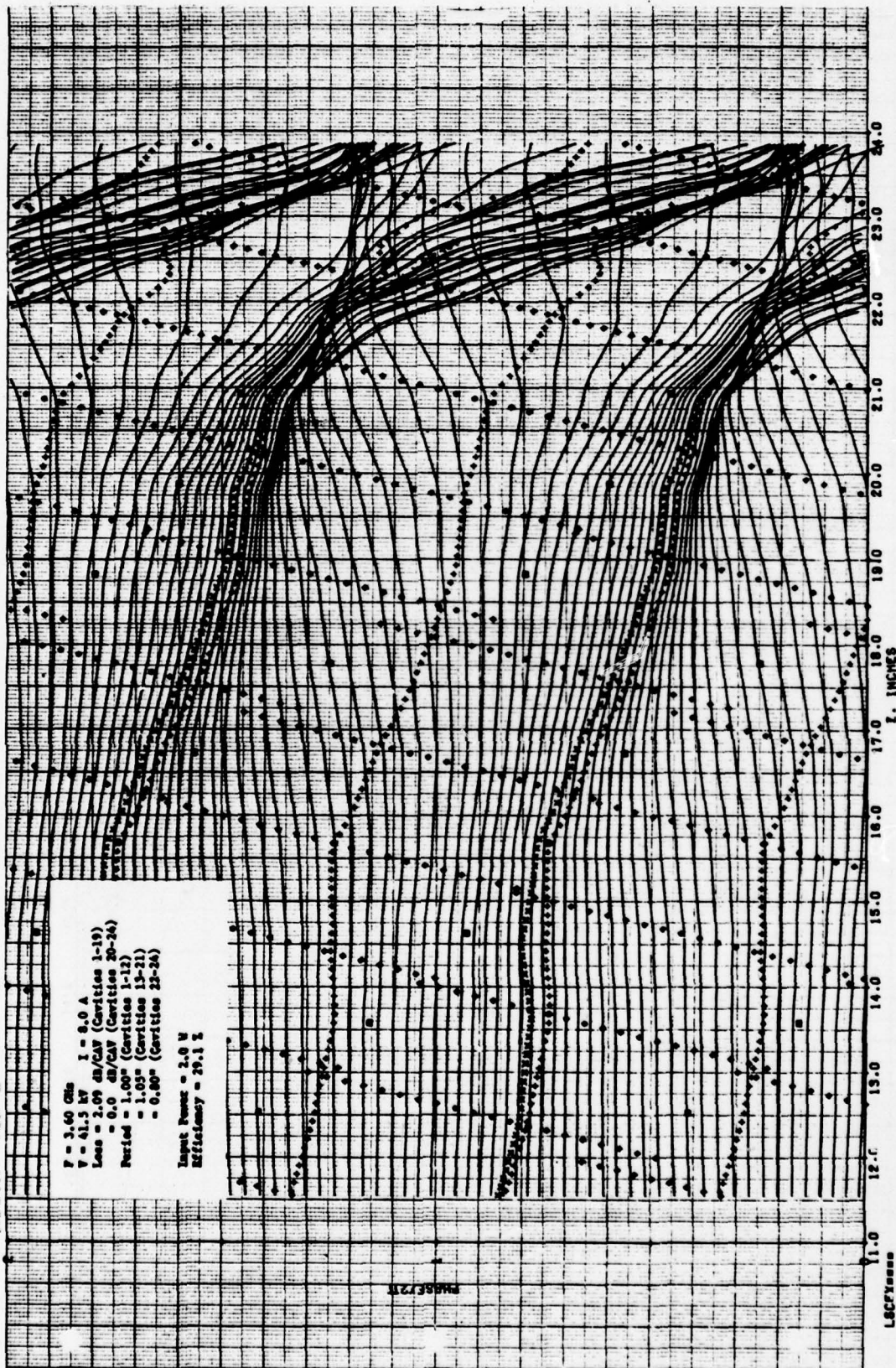


FIGURE 5.108 COMPUTED RELATIVE PHASES OF ELECTRON DISKS VS DISTANCE IN SIMULATED COUPLED-CAVITY TWT WITH TWELVE CAVITY OUTPUT SECTION AND FIVE LOSSLESS OUTPUT CAVITIES AT A FREQUENCY OF 3.6 GHz

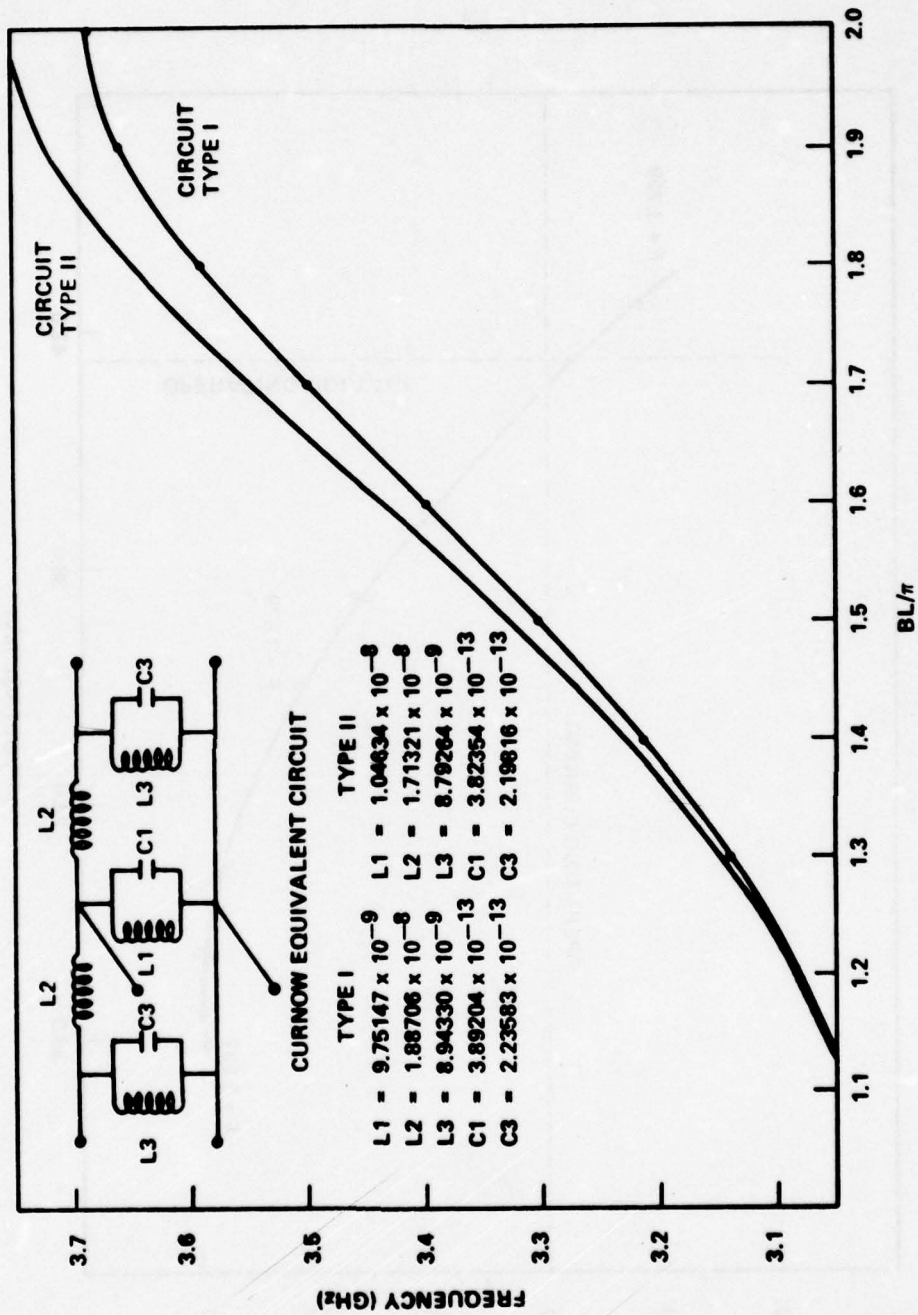


FIGURE 5.110 BRILLOUIN DIAGRAM FOR VTS-5753 AND HIGH FREQUENCY CIRCUIT

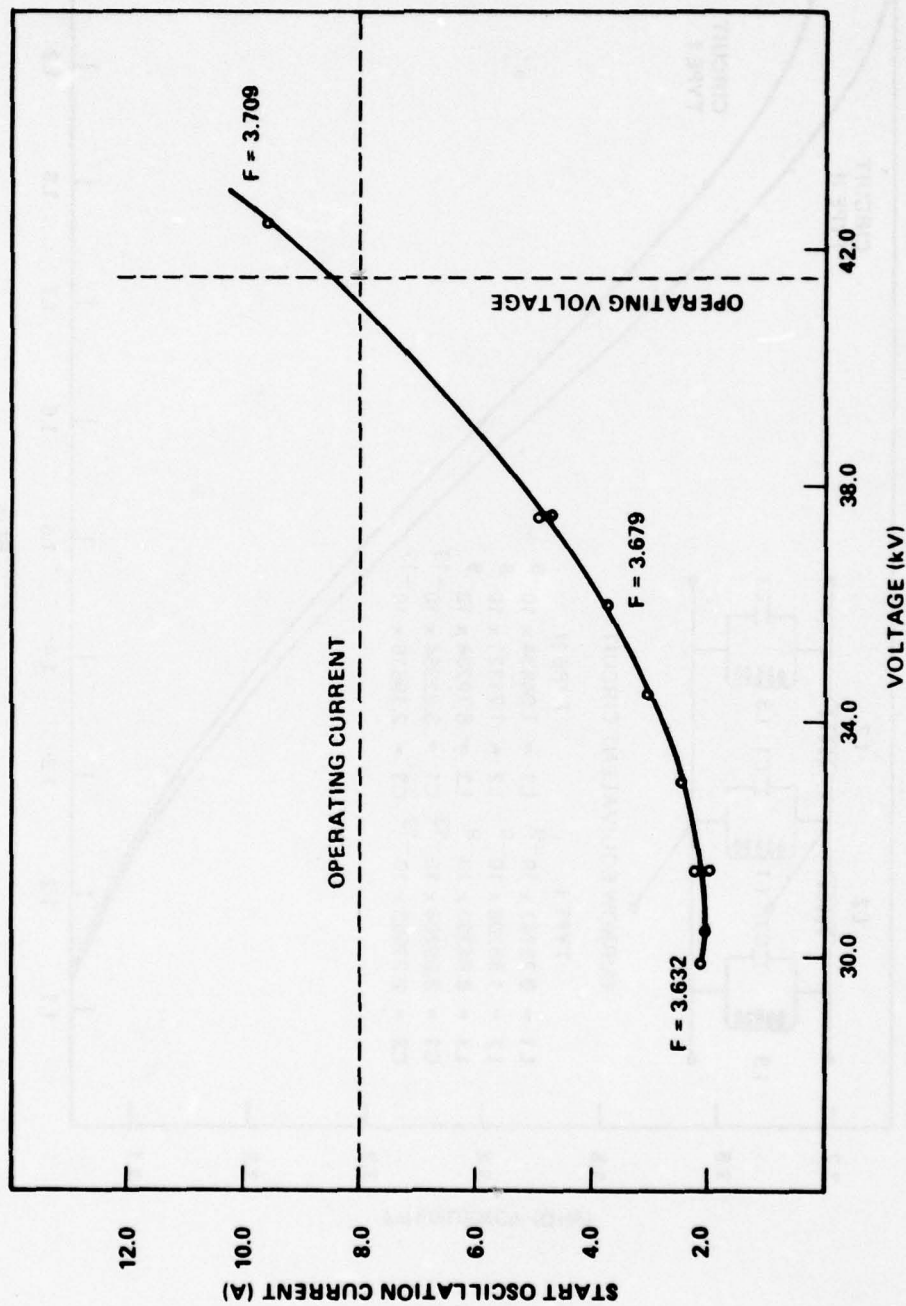


FIGURE 5.111 COMPUTED START OSCILLATION CURRENT VS BEAM VOLTAGE FOR SIMULATED N-2 DESIGN COUPLED-CAVITY TWT WITH TWELVE CAVITY OUTPUT SECTION AND FIVE LOSSLESS OUTPUT CAVITIES

stable. A further increase in start oscillation current would nevertheless be desirable to provide extra margin in the design. This improved design has yielded backward-wave convergence in all large-signal calculations but the stability of Design I has been bought at some cost to conversion efficiency, as shown in Table 5.3. The apparent improvement in efficiency at the upper band-edge, 34.6 percent vs 29.3 percent, is mainly a consequence of the strangely depressed efficiency of Design H which is not electronically stable. Design F, also unstable, showed 43 percent conversion efficiency at 3.6 GHz. This latter result is of little value because the output section is electronically unstable.

Design J was undertaken to attempt to further improve stability and to increase conversion efficiency. The output circuit has a pair of high frequency cavities at each end. This configuration is referred to as 2-N-2. The cavity period has been increased to 1.08 inch to increase the high end gain and efficiency. These changes have reduced the efficiency at the low end and increased the efficiency at the high end of the band, however the excellent high end efficiency of 43.6 percent represents an unconverged computation. This result implies that 43.6 percent efficiency could be achieved at 3.6 GHz with a reflection coefficient of 0.113 on the output (in the correct phase). Unfortunately, with this output condition the TWT would be electronically unstable. It is important therefore to improve the stability. The marginal stability of this design is illustrated in Figure 5.112.

Design K is a 2-N-2 design like Design J but with higher frequency end cavities. The cavities used are the same ones employed in a Varian S-band TWT and described in Figure 5.113. The use of these higher frequency end cavities has improved stability as shown in Figure 5.112. The start oscillation current has increased to 10 A at the design beam voltage. All large-signal computations converged; however, the conversion efficiency has been adversely effected, particularly at the bottom of the band, where it has fallen to 30.7 percent. While this circuit has the requisite electronic stability it lacks sufficient gain to achieve the required conversion efficiency.

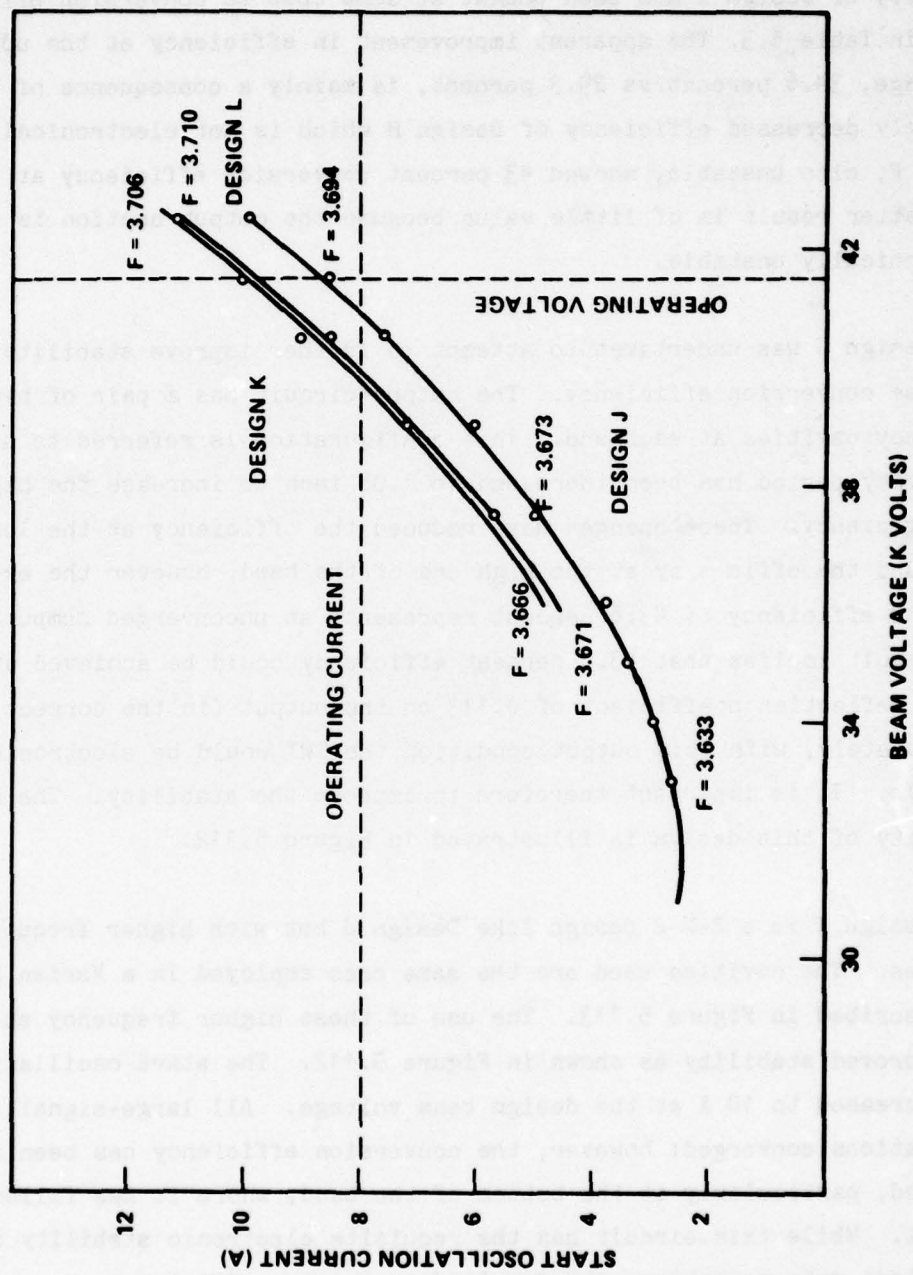


FIGURE 5.112 COMPUTED START OSCILLATION CURRENT VS BEAM VOLTAGE IN SIMULATED 2-N-2 DESIGN COUPLED-CAVITY TWT WITH 1.08" PERIODS

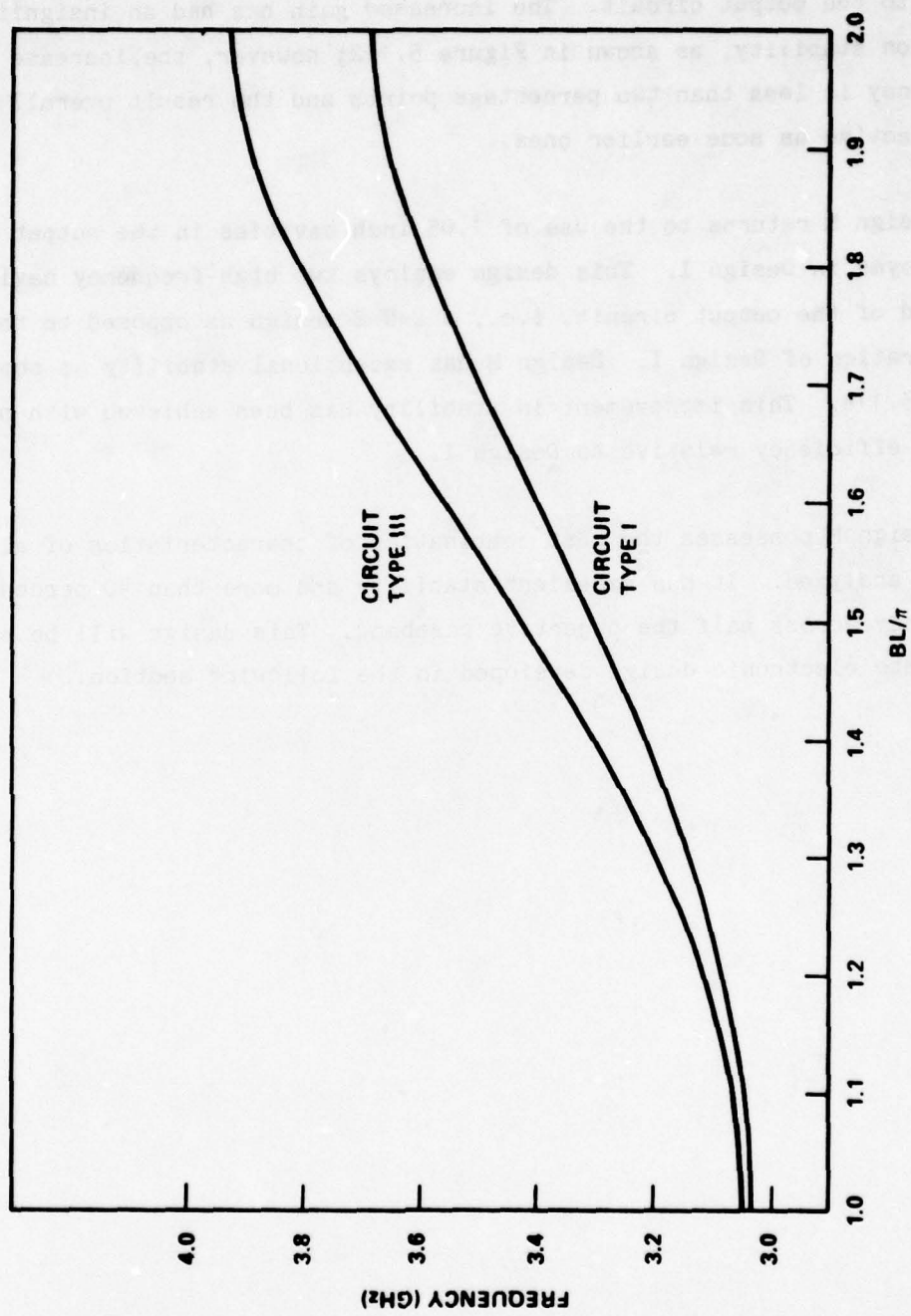


FIGURE 5.113 BRILLOUIN DIAGRAM FOR VTS-5753 AND ULTRA-HIGH FREQUENCY CIRCUIT

Design L is the same as Design K except for the addition of one more lossy cavity to the output circuit. The increased gain has had an insignificant effect on stability, as shown in Figure 5.112; however, the increase in efficiency is less than two percentage points and the result overall not nearly so attractive as some earlier ones.

Design M returns to the use of 1.05 inch cavities in the output circuit, as employed in Design I. This design employs two high-frequency cavities at each end of the output circuit, i.e., a 2-N-2 design as opposed to the N-2 configuration of Design I. Design M has exceptional stability as shown in Figure 5.114. This improvement in stability has been achieved with negligible loss in efficiency relative to Design I.

Design M possesses the best combination of characteristics of all the designs analyzed. It has excellent stability and more than 40 percent efficiency across half the objective passband. This design will be employed in a complete electronic design developed in the following section.

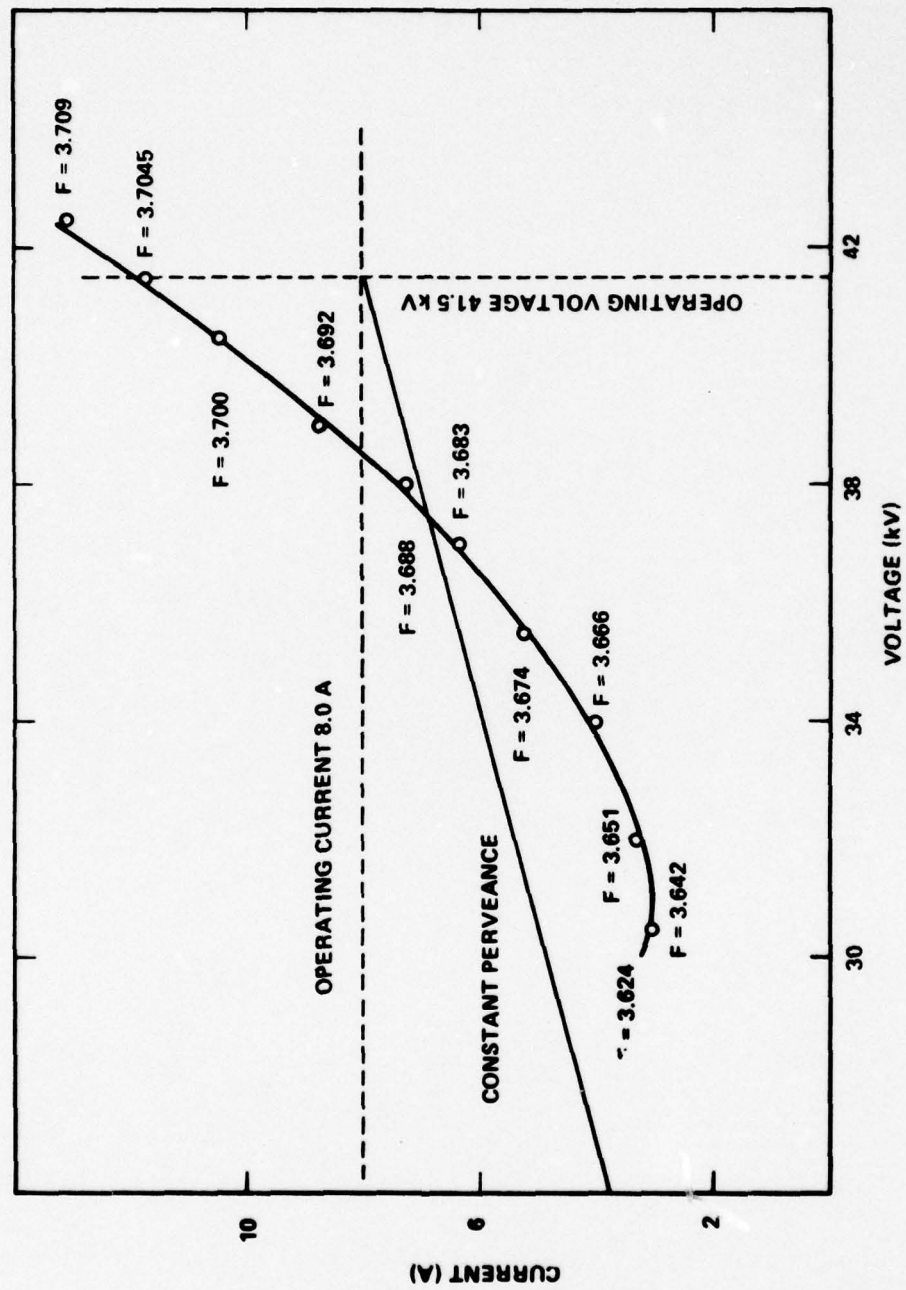


FIGURE 5.114 COMPUTED START OSCILLATION CURRENT VS BEAM VOLTAGE IN SIMULATED 2-N-2 DESIGN COUPLED-CAVITY TWT WITH TWELVE CAVITY OUTPUT SECTION AND FIVE LOSSLESS OUTPUT CAVITIES

6.0 FINAL DESIGN

In this section a final electronic design is derived for a high efficiency 100 KW S-band TWT. This design makes use of the most promising results from Section 5.

In Section 5, the choice of operating beam voltage and beam perveance was found not to be highly critical. An existing circuit type with the correct bandwidth was available. This circuit operates at approximately 40 kV. In order to assure the required 100 KW output power at 40 percent efficiency with some margin it was decided to employ a 8 A beam (1 μ perv). A lower voltage TWT operating at higher current would almost certainly exacerbate the space-charge debunching problem which has been shown to seriously limit efficiency.

The cavities employed are similar to cavities used in the Varian VTS-5753. These cavities have a tunnel diameter of 0.443 inch and a gap spacing of 0.300 inch. The output circuit section employs 12 cavities, the first nine of which are 1.05 inches long and the last three of which are 0.80 inch long. A number of trial small-signal calculations were performed to determine the length of the input section and the length of the input section cavities required to provide approximately 50 dB small-signal gain over the frequency band 3.1 to 3.6 GHz. These trials lead to the choice of an eleven cavity input circuit with cavities 0.98 inch long. A schematic of the TWT is shown in Figure 6.1.

The two circuit types employed in the design are illustrated in Figure 5.110. The lower cavity frequency circuit is employed throughout the input section and in the central 8 cavities of the output circuit section. The first and last pair of cavities in the output section are of the higher cutoff frequency type. This arrangement, which is referred to as a 2-N-2 design has been found to possess excellent electronic stability (see Figure 5.114).

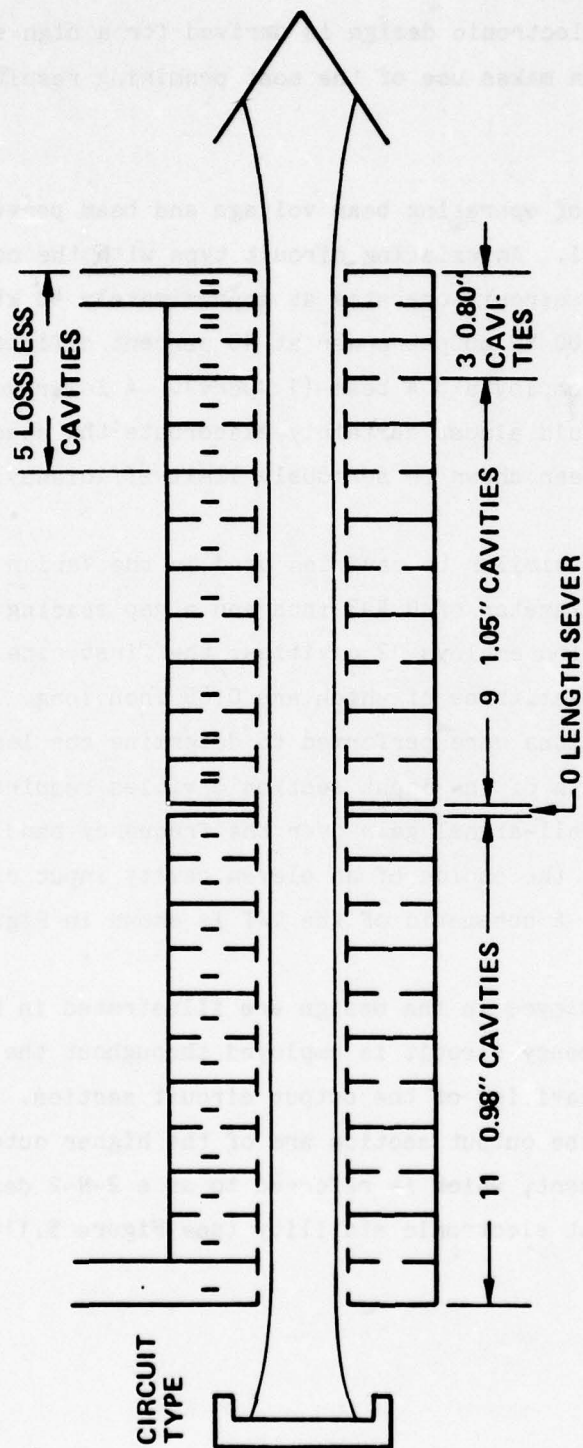


FIGURE 6.1 SCHEMATIC FOR 100 kW S-BAND COUPLED-CAVITY TWT (FINAL DESIGN)

The loss in the input circuit section is uniformly distributed and non-frequency-selective. In the output circuit section the first seven cavities have frequency selective loss and the remaining cavities are lossless. The characteristics of the lossy cavities are shown in Figure 6.2.

The velocity taper is achieved by reducing the cavity length of the last three cavities to 0.800 inch. The first nine cavities are 1.050 inches long with a 0.250 inch inter-cavity web, i.e., the cavity height is 0.800 inch. The thick web is well chosen in case a future implementation should require PPM focusing. The taper cavities have a 0.700 inch cavity height with a 0.100 inch intercavity web. In a PPM embodiment the last three cavities would be focused with a single magnet, thereby allowing all cavity parts to be made of copper so as to minimize thermal degradation of performance. In the presently recommended embodiment this TWT would be solenoid focused, using the brillouin field in order to optimally check the computer prediction without obscuring these results due to the unpredictable focusing performance of a PPM stack.

The input and output matching sections and the sever loads would be of conventional design such as used on the Varian VTS-5753. Figure 6.3 is a plot of the computed small-signal gain of the final design. Further tuning of the sever load design could be expected to improve the small-signal gain ripple. Normally, one would expect to find three sections in a TWT with 40 dB saturated gain. In this tube the output section is required to have high gain in order to optimize efficiency. It is thus possible to achieve the required gain in a two-section TWT.

Figure 6.4 shows the computed output power and gain at saturated drive. The gain exceeds 40 dB over the entire band. The computed output power exceeds the required 100 kW. The conversion efficiency is below expectations in the upper part of the band.

The large-signal behavior of the output section is plotted in Figures 6.5 through 6.14. At all frequencies the fundamental component of rf beam current

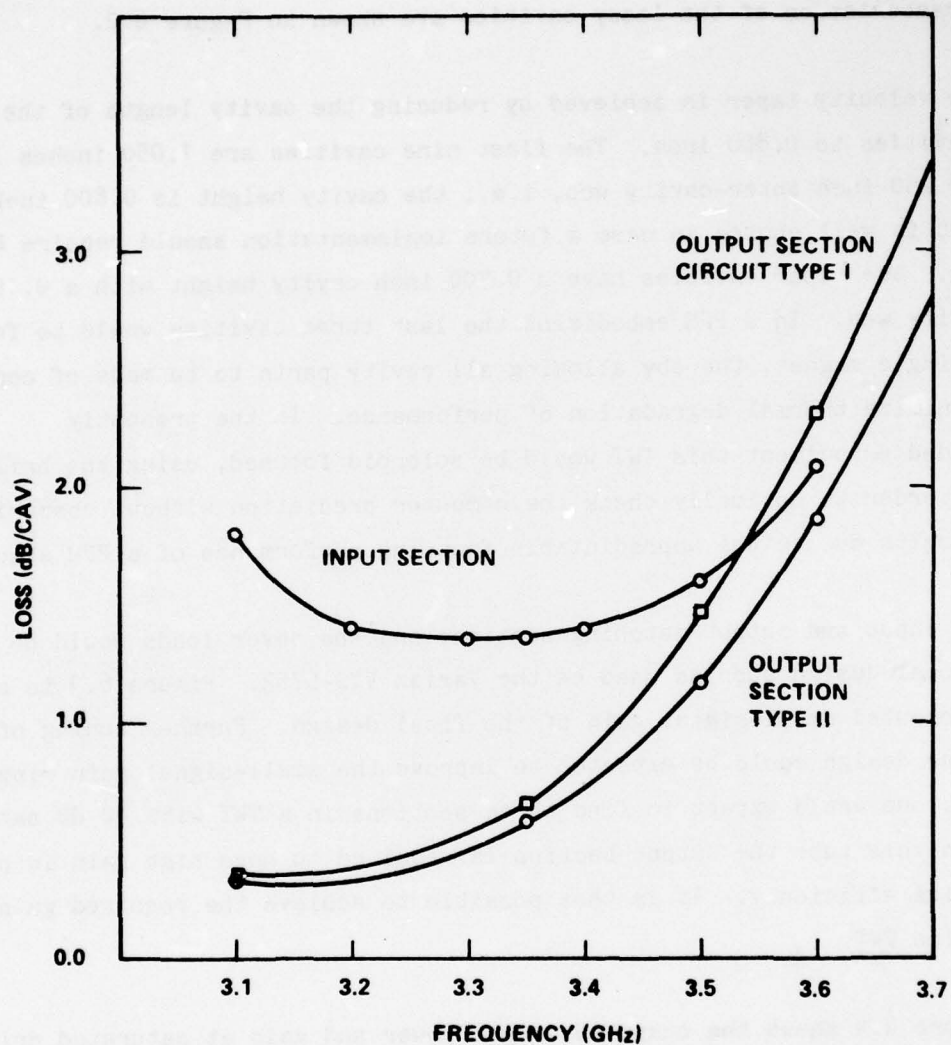


FIGURE 6.2 LOSS PER CAVITY VS FREQUENCY FOR FINAL DESIGN

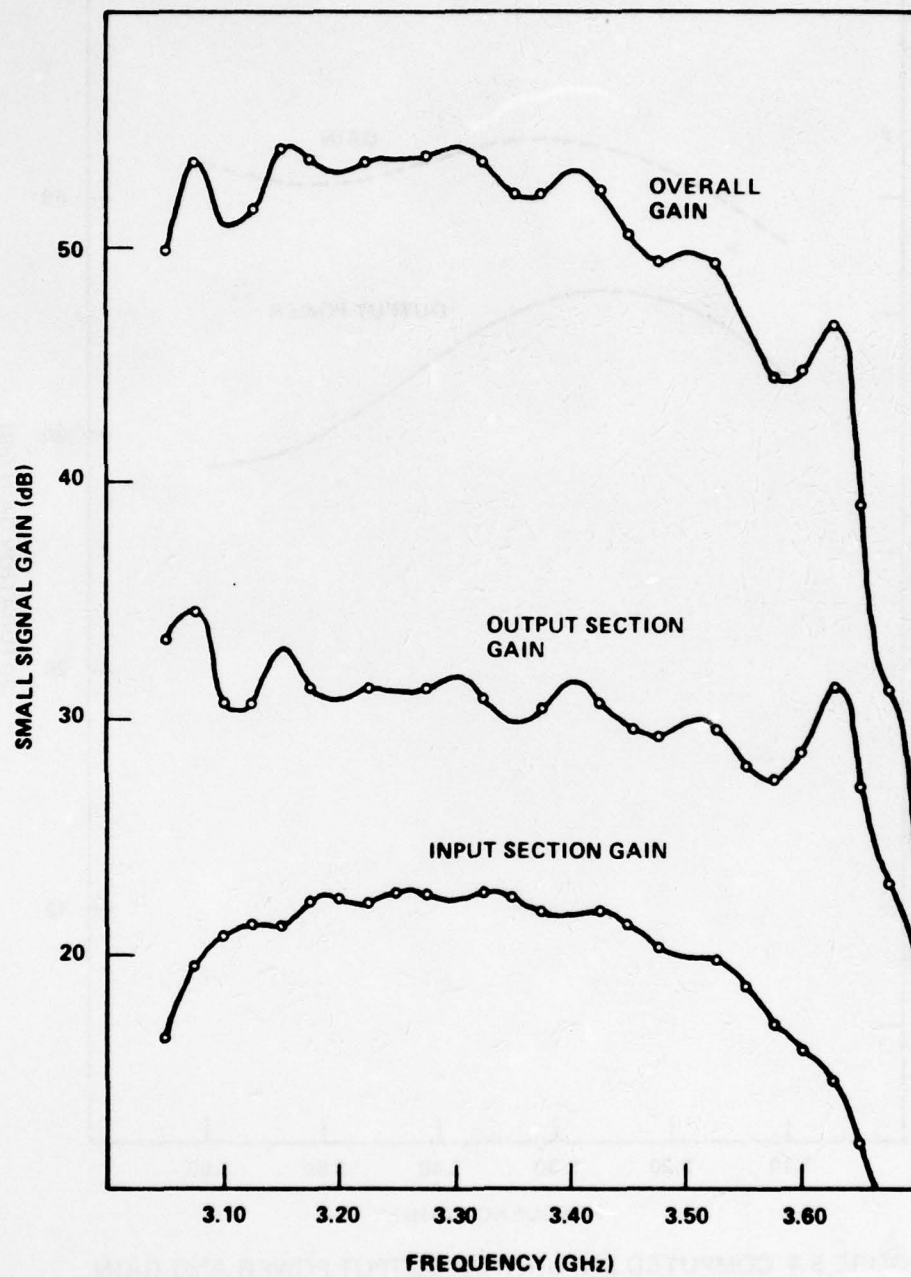


FIGURE 6.3 COMPUTED SMALL SIGNAL GAIN FOR FINAL DESIGN

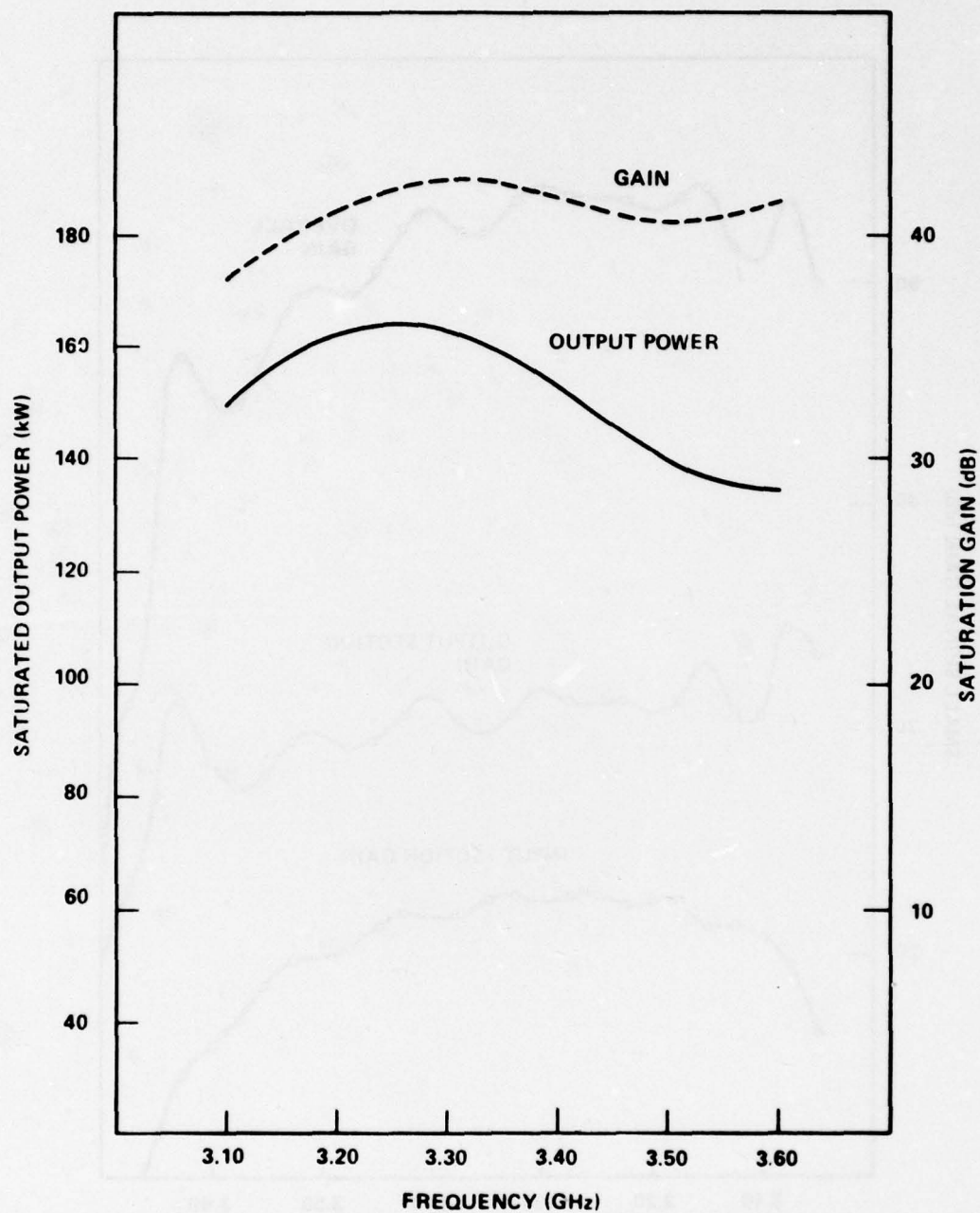


FIGURE 6.4 COMPUTED SATURATED OUTPUT POWER AND GAIN VS FREQUENCY FOR FINAL DESIGN

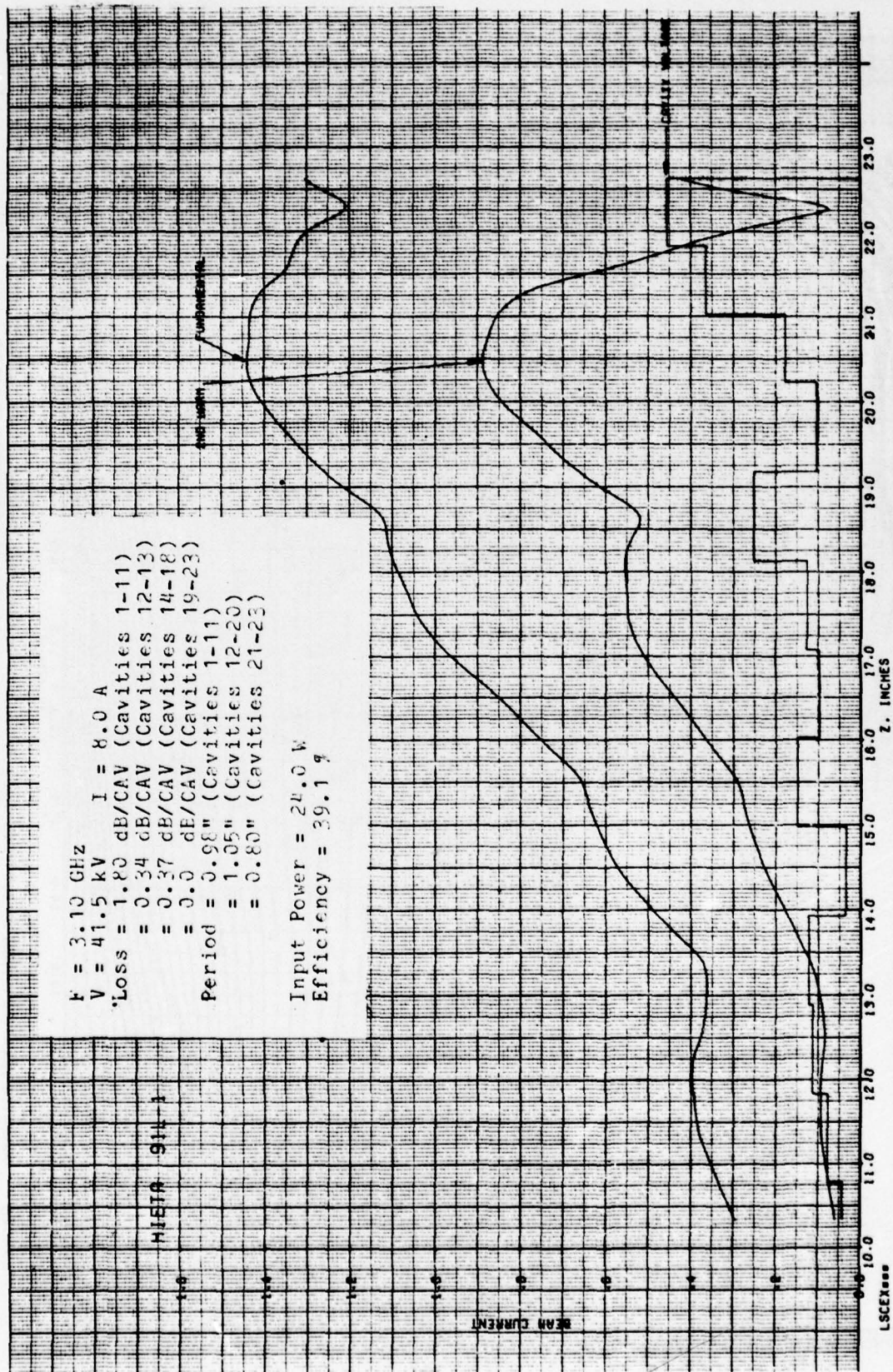


FIGURE 6.5 COMPUTED RF BEAM CURRENTS AND GAP VOLTAGES VS DISTANCE IN SIMULATED COUPLED-CAVITY TWT WITH TWELVE CAVITY OUTPUT SECTION AND FIVE LOSSLESS OUTPUT CAVITIES AT A FREQUENCY OF 3.10 GHz

HIETA 91L-1

$F = 3.10 \text{ GHz}$
 $V = 41.5 \text{ kV}$
 $I = 8.0 \text{ A}$
 $\text{Loss} = 1.80 \text{ dB/CAV (Cavities 1-11)}$
 $= 0.34 \text{ dB/CAV (Cavities 12-13)}$
 $= 0.37 \text{ dB/CAV (Cavities 14-18)}$
 $= 0.0 \text{ dB/CAV (Cavities 19-23)}$
 $\text{Period} = 0.98'' \text{ (Cavities 1-11)}$
 $= 1.05'' \text{ (Cavities 12-20)}$
 $= 0.80'' \text{ (Cavities 21-23)}$

$\text{Input Power} = 24.0 \text{ W}$
 $\text{Efficiency} = 39.1 \%$

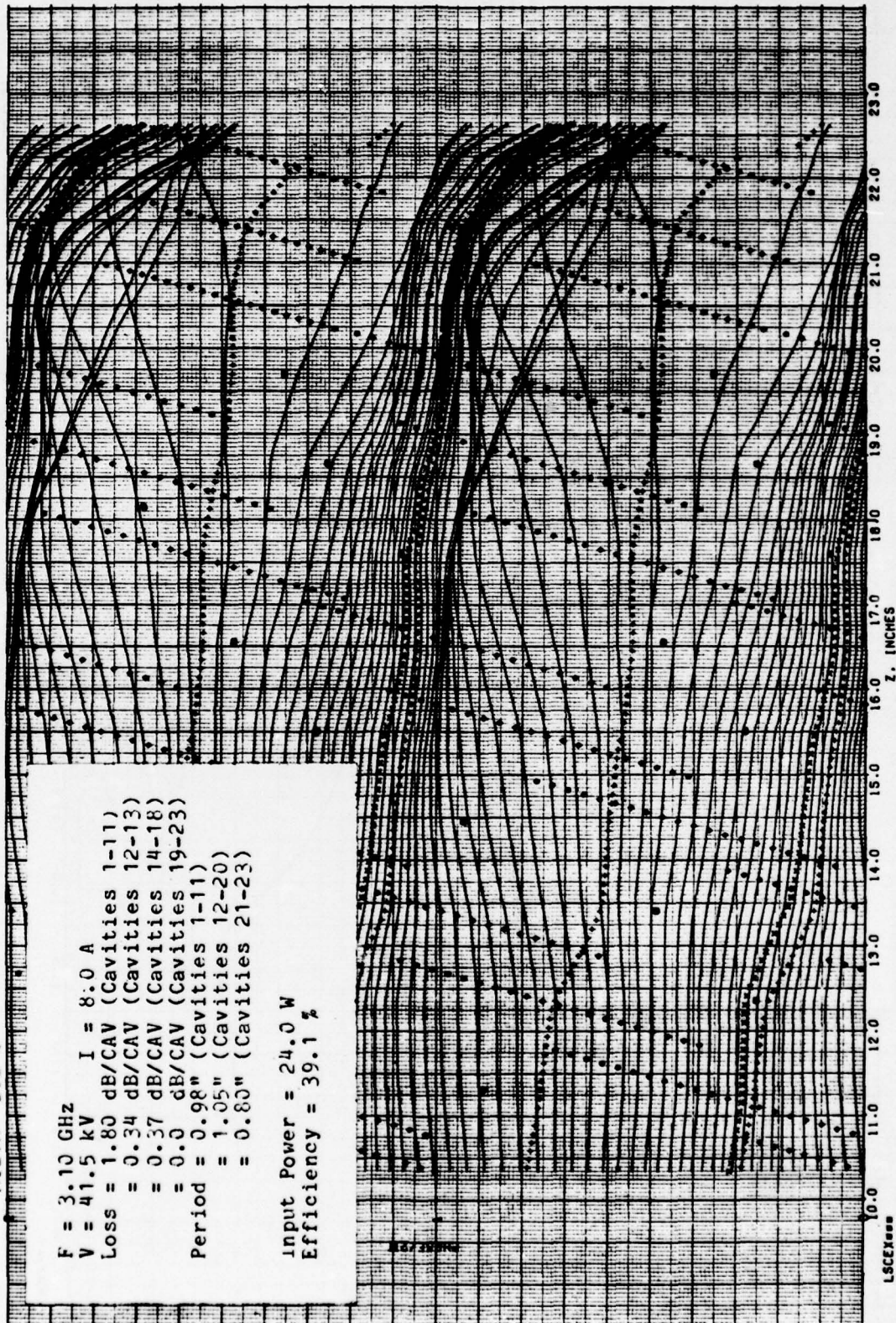


FIGURE 6.8 COMPUTED RELATIVE PHASES OF ELECTRON DISKS VS DISTANCE IN SIMULATED COUPLED-CAVITY TWT WITH TWELVE CAVITY OUTPUT SECTION AND FIVE LOSSLESS OUTPUT CAVITIES AT A FREQUENCY OF 3.10 GHz

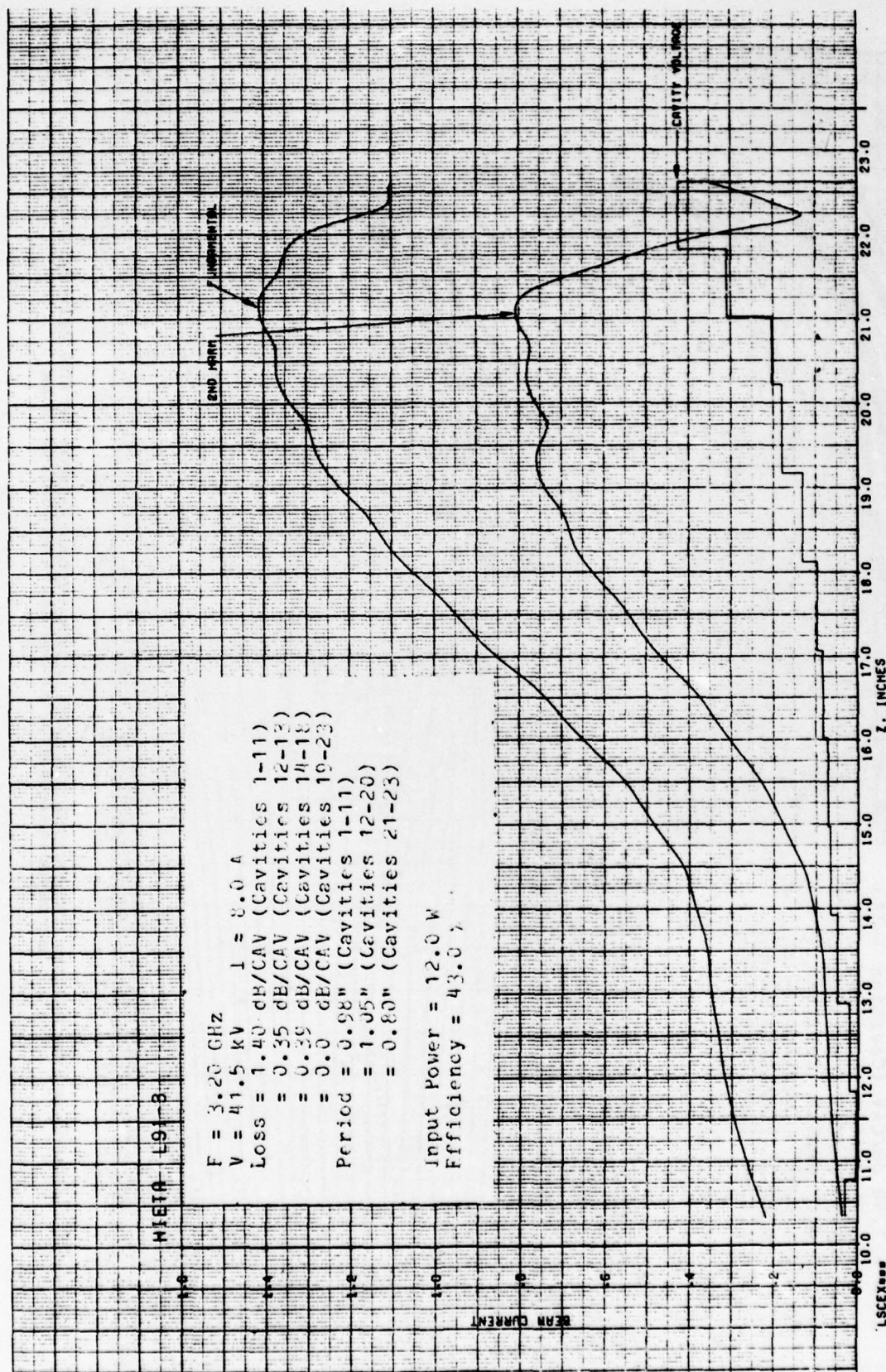


FIGURE 6.7 COMPUTED RF BEAM CURRENTS AND GAP VOLTAGES VS DISTANCE IN SIMULATED COUPLED-CAVITY TWT WITH TWELVE CAVITY OUTPUT SECTION AND FIVE LOSSLESS OUTPUT CAVITIES AT A FREQUENCY OF 3.20 GHz

HIETA L91-3

$F = 3.20 \text{ GHz}$
 $V = 41.5 \text{ kV}$
 $I = 8.0 \text{ A}$
 $\text{Loss} = 1.40 \text{ dB/CAV (Cavities 1-11)}$
 $= 0.35 \text{ dB/CAV (Cavities 12-13)}$
 $= 0.39 \text{ dB/CAV (Cavities 14-18)}$
 $= 0.0 \text{ dB/CAV (Cavities 19-23)}$
 $\text{Period} = 0.98'' \text{ (Cavities 1-11)}$
 $= 1.05'' \text{ (Cavities 12-20)}$
 $= 0.80'' \text{ (Cavities 21-23)}$

$\text{Input Power} = 12.0 \text{ W}$
 $\text{Efficiency} = 43.0 \%$

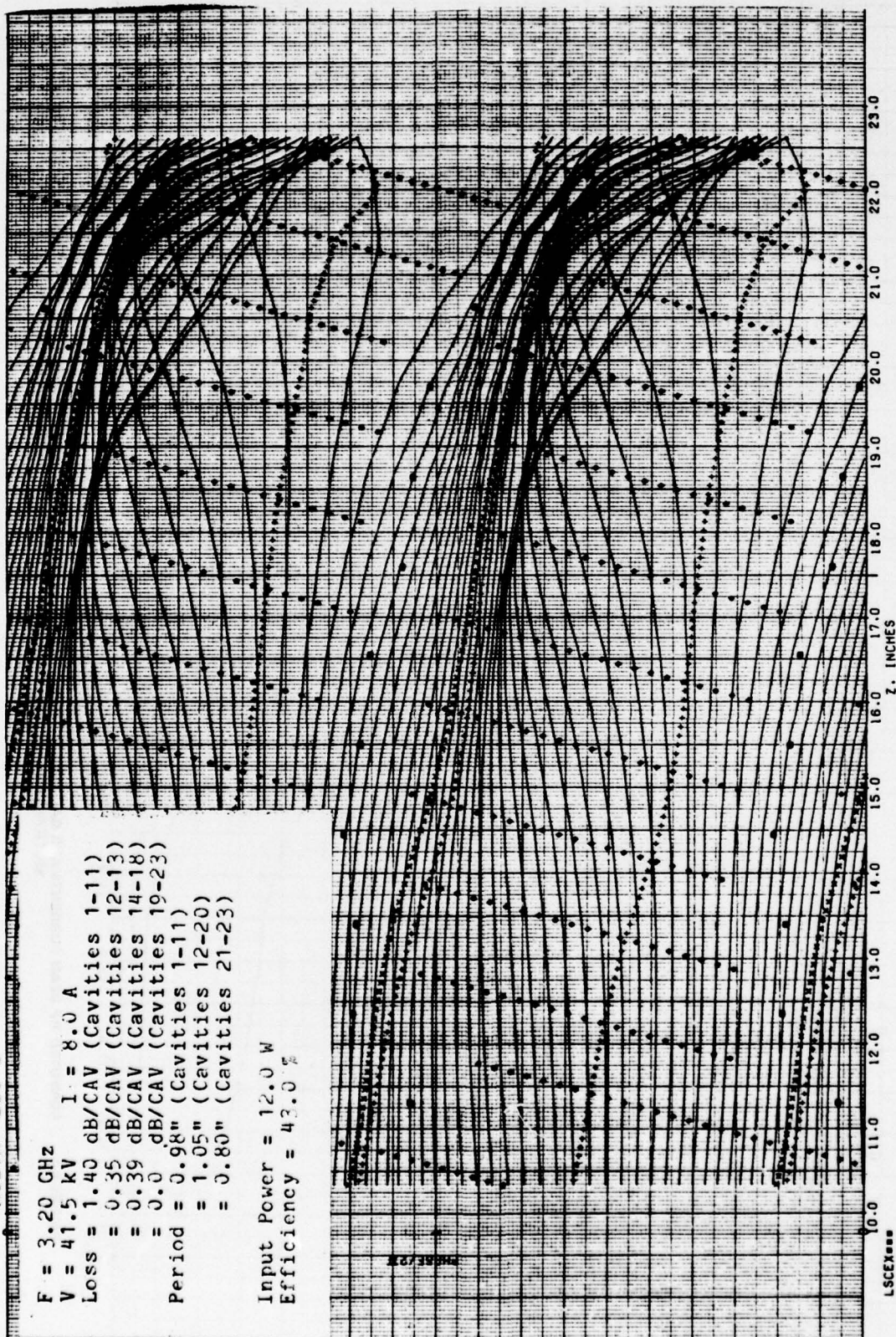


FIGURE 9.3 COMPUTED RELATIVE PHASES OF ELECTRON DISKS VS DISTANCE IN SIMULATED COUPLED-CAVITY TWT WITH TWELVE CAVITY OUTPUT SECTION AND FIVE LOSSLESS OUTPUT CAVITIES AT A FREQUENCY OF 3.20 GHz

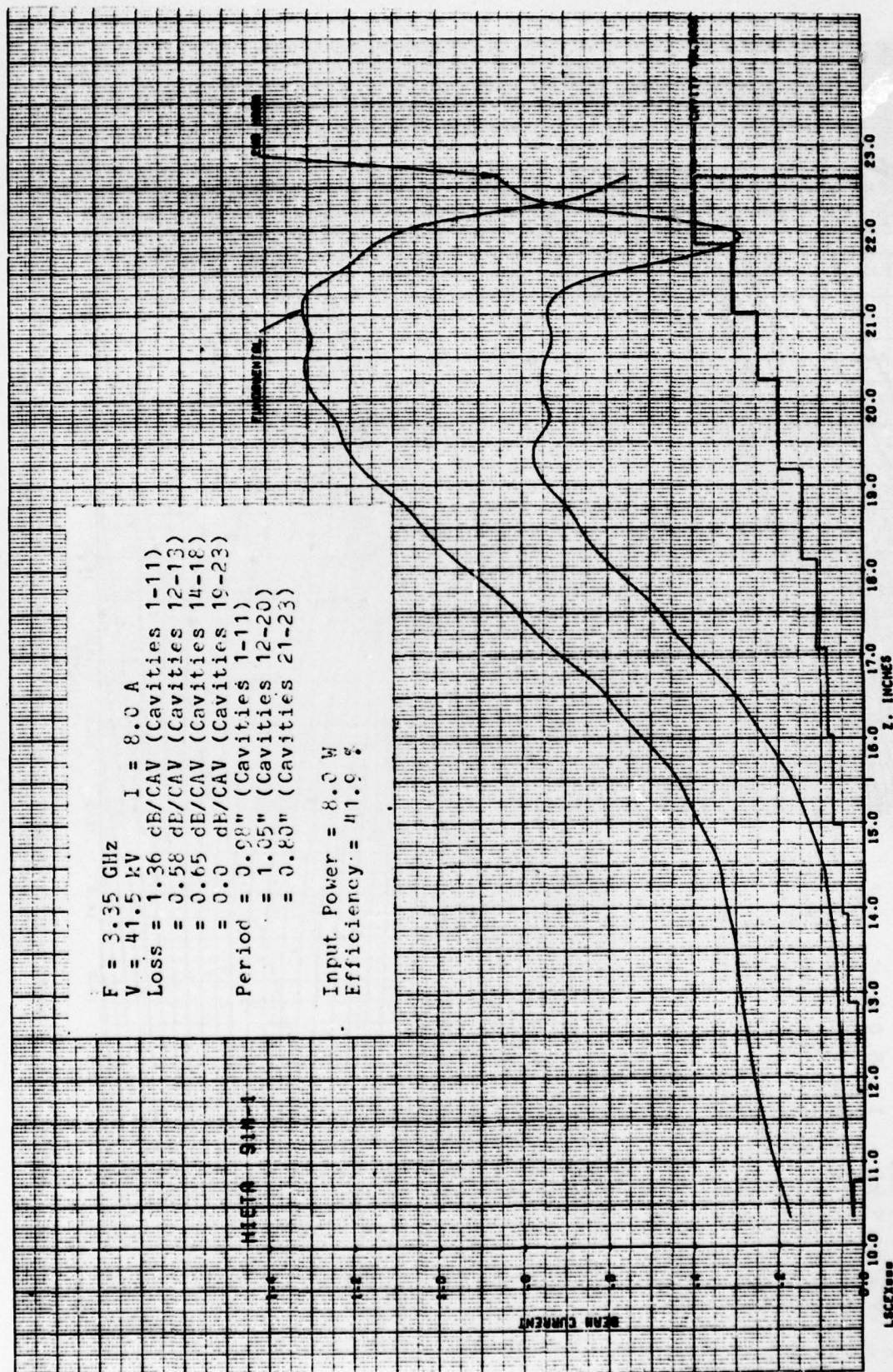


FIGURE 6.9 COMPUTED RF BEAM CURRENTS AND GAP VOLTAGES VS DISTANCE IN SIMULATED COUPLED-CAVITY TWT WITH TWELVE CAVITY OUTPUT SECTION AND FIVE LOSSLESS OUTPUT CAVITIES AT A FREQUENCY OF 3.35 GHz

NIETA 91M-1

$F = 3.35 \text{ GHz}$
 $V = 41.5 \text{ kV}$
 $I = 8.0 \text{ A}$
 $\text{Loss} = 1.36 \text{ dB/CAV (Cavities 1-11)}$
 $= 0.58 \text{ dB/CAV (Cavities 12-13)}$
 $= 0.65 \text{ dB/CAV (Cavities 14-18)}$
 $= 0.0 \text{ dB/CAV (Cavities 19-23)}$
 $\text{Period} = 0.98'' \text{ (Cavities 1-11)}$
 $= 1.05'' \text{ (Cavities 12-20)}$
 $= 0.80'' \text{ (Cavities 21-23)}$

$\text{Input Power} = 8.0 \text{ W}$
 $\text{Efficiency} = 41.9 \%$

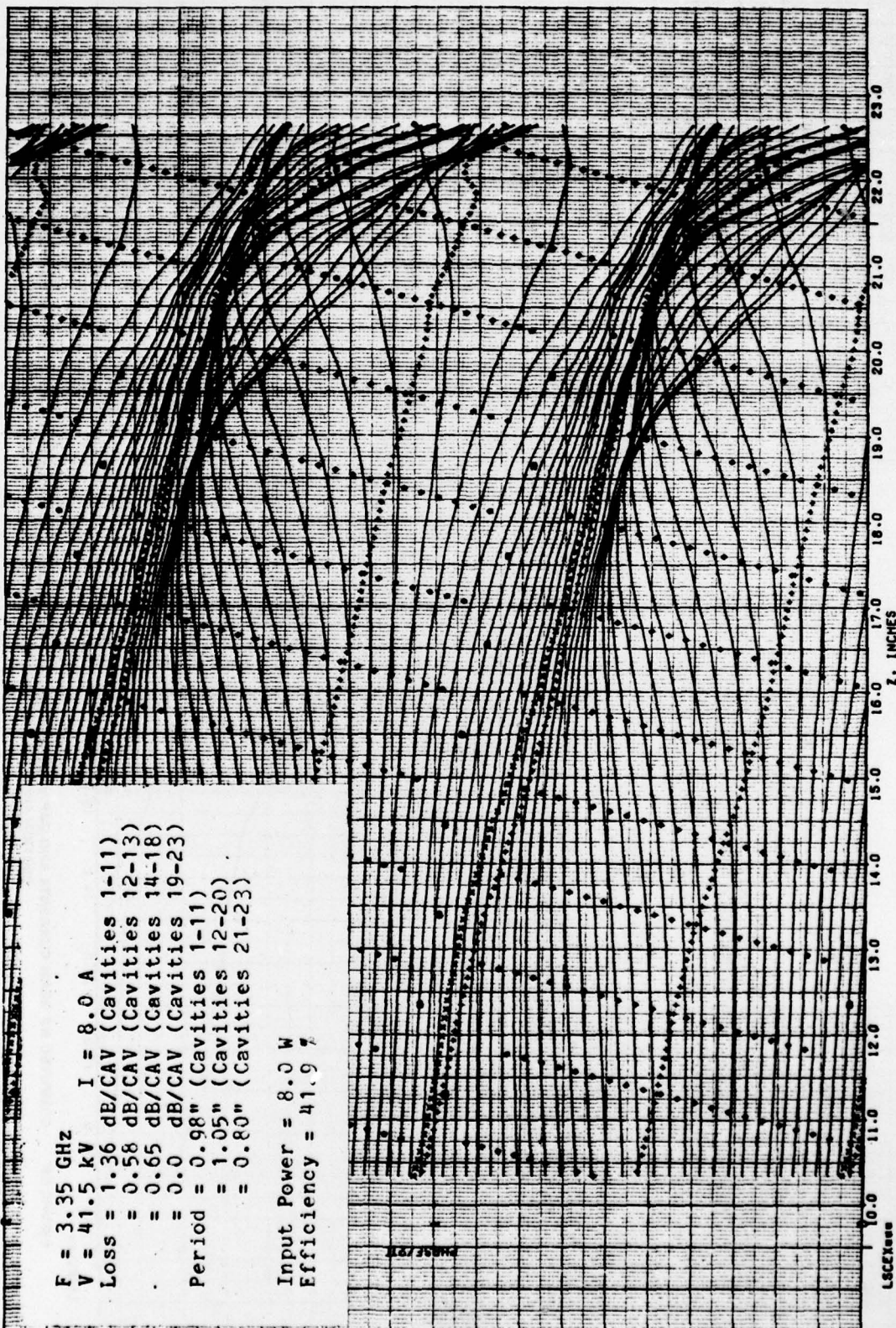


FIGURE 6.10 COMPUTED RELATIVE PHASES OF ELECTRON DISKS VS DISTANCE IN SIMULATED COUPLED-CAVITY TWT WITH TWELVE CAVITY OUTPUT SECTION AND FIVE LOSSLESS OUTPUT CAVITIES AT A FREQUENCY OF 3.35 GHz

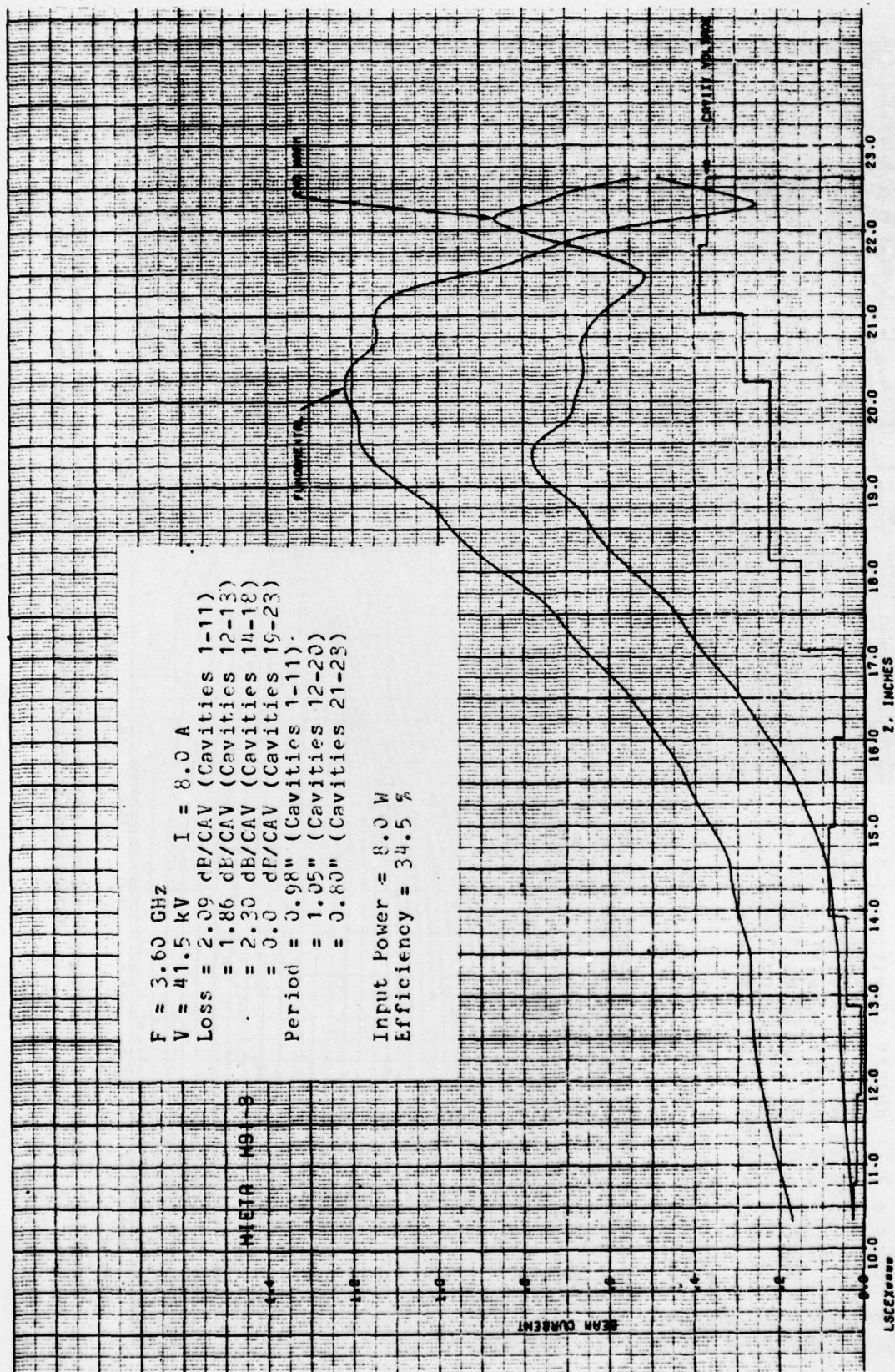


FIGURE 6.11 COMPUTED RF BEAM CURRENTS AND GAP VOLTAGES VS DISTANCE IN SIMULATED COUPLED-CAVITY TWT WITH TWELVE CAVITY OUTPUT SECTION AND FIVE LOSSLESS OUTPUT CAVITIES AT A FREQUENCY OF 3.60 GHz

HIETA H91-3

$F = 3.60 \text{ GHz}$
 $V = 41.5 \text{ kV}$
 $I = 8.0 \text{ A}$
 $\text{Loss} = 2.09 \text{ dB/CAV (Cavities 1-11)}$
 $= 1.86 \text{ dB/CAV (Cavities 12-13)}$
 $= 2.30 \text{ dB/CAV (Cavities 14-18)}$
 $= 0.0 \text{ dB/CAV (Cavities 19-23)}$
 $\text{Period} = 0.98'' \text{ (Cavities 1-11)}$
 $= 1.05'' \text{ (Cavities 12-20)}$
 $= 0.80'' \text{ (Cavities 21-23)}$
 $\text{Input Power} = 8.0 \text{ W}$
 $\text{Efficiency} = 34.5 \%$

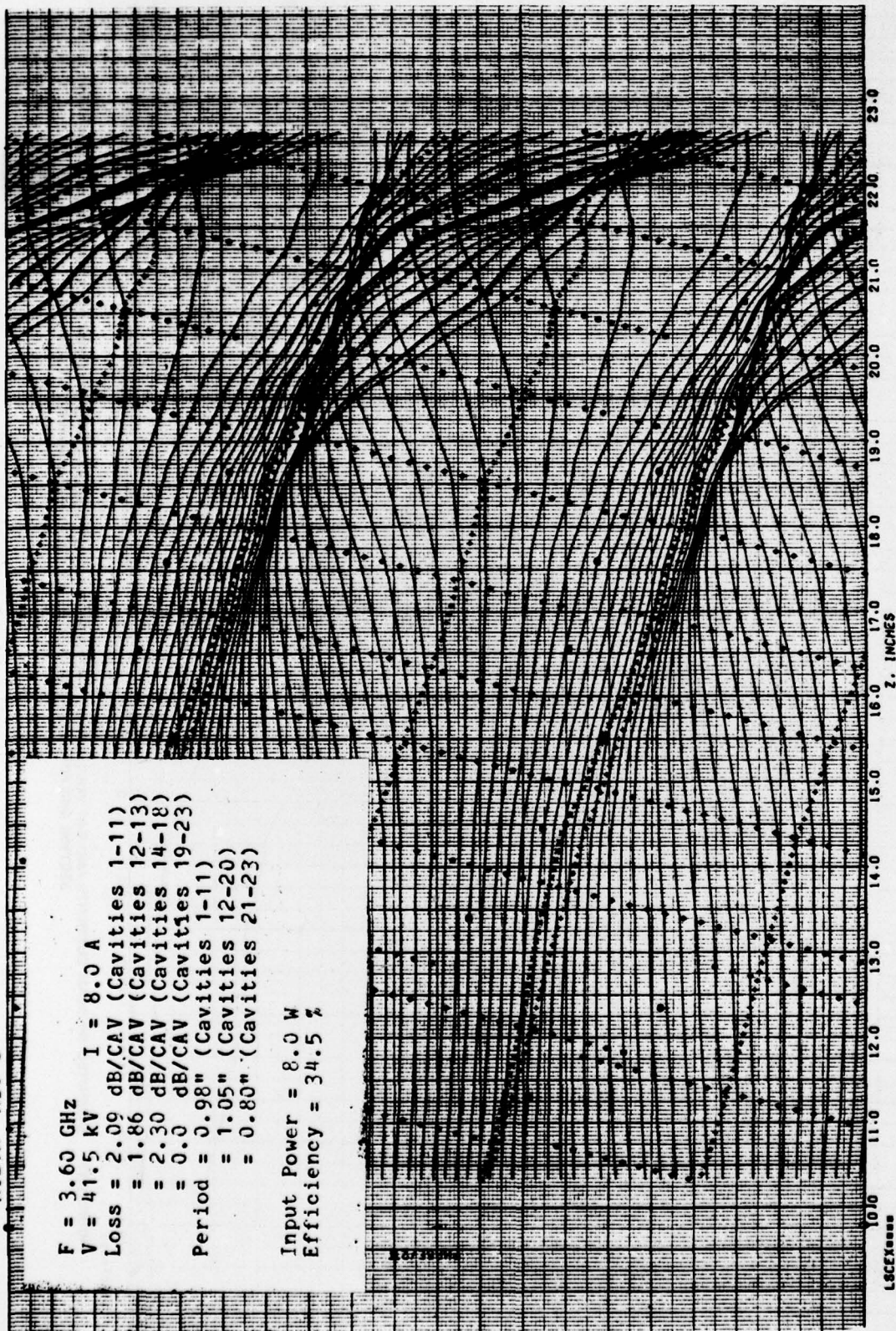


FIGURE 6.12 COMPUTED RELATIVE PHASES OF ELECTRON DISKS VS DISTANCE IN SIMULATED COUPLED-CAVITY TWT WITH TWELVE CAVITY OUTPUT SECTION AND FIVE LOSSLESS OUTPUT CAVITIES AT A FREQUENCY OF 3.60 GHz

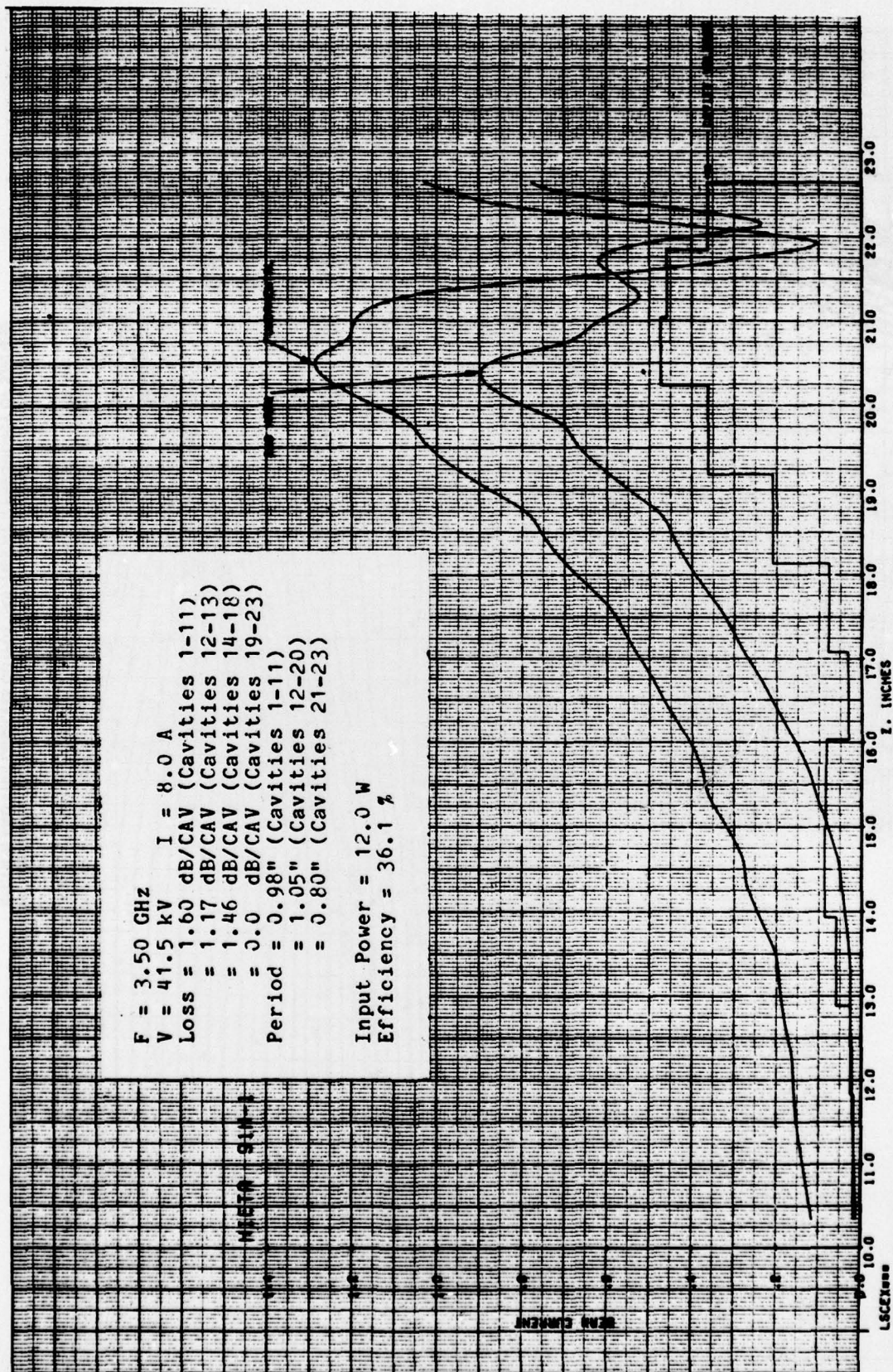


FIGURE 6.13 COMPUTED RF BEAM CURRENTS AND GAP VOLTAGES VS DISTANCE IN SIMULATED COUPLED-CAVITY TWT WITH TWELVE CAVITY OUTPUT SECTION AND FIVE LOSSLESS OUTPUT CAVITIES AT A FREQUENCY OF 3.5 GHz

HIETA 9IH-1

$F = 3.50 \text{ GHz}$
 $V = 41.5 \text{ kV}$ $I = 8.0 \text{ A}$
 $\text{Loss} = 1.60 \text{ dB/CAV (Cavities 1-11)}$
 $\quad = 1.17 \text{ dB/CAV (Cavities 12-13)}$
 $\quad = 1.46 \text{ dB/CAV (Cavities 14-18)}$
 $\quad = 0.0 \text{ dB/CAV (Cavities 19-23)}$
 $\text{Period} = 0.98'' \text{ (Cavities 1-11)}$
 $\quad = 1.05'' \text{ (Cavities 12-20)}$
 $\quad = 0.80'' \text{ (Cavities 21-23)}$

$\text{Input Power} = 12.0 \text{ W}$
 $\text{Efficiency} = 36.1 \%$

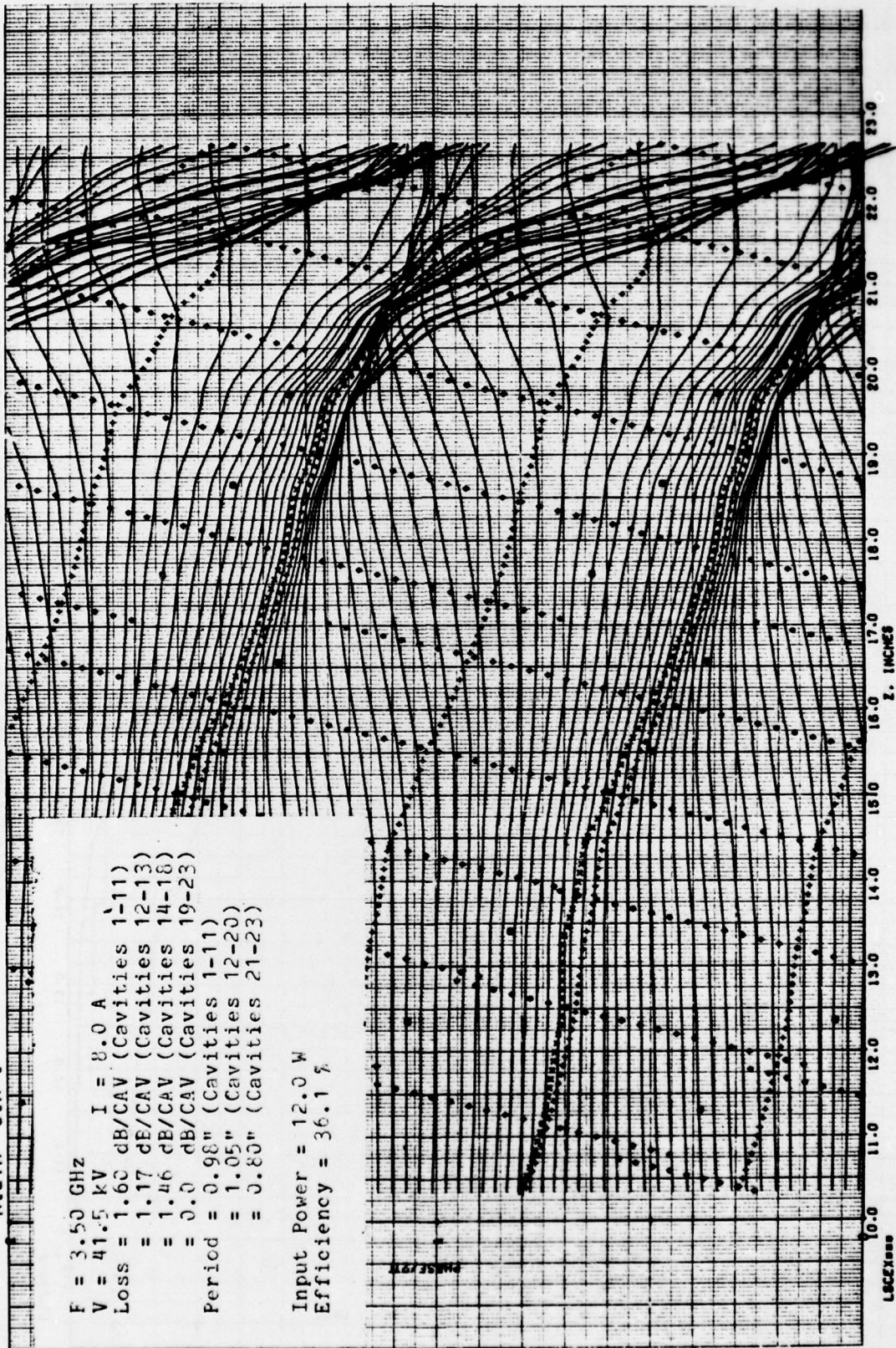


FIGURE 6.14 COMPUTED RELATIVE PHASES OF ELECTRON DISKS VS DISTANCE IN SIMULATED COUPLED-CAVITY TWT WITH TWELVE CAVITY OUTPUT SECTION AND FIVE LOSSLESS OUTPUT CAVITIES AT A FREQUENCY OF 3.50 GHz

be necessary either to form a bunch containing a larger fraction of the electrons or to extract more energy from those electrons which are properly phased.

7.0 CONCLUSION

The optimization of the conversion efficiency of a 100 kW S-band coupled-cavity TWT has been studied by means of large-signal computer emulation using a slow-wave circuit with parameters derived from cold-test measurement.

The examination of the bunching process has shown that the best bunches are formed in a buncher which is operated sub-synchronously, i.e., with the dc beam traveling more slowly than the circuit wave. The best choice of circuit to beam velocity ratio tends to result in an upward ramping gain. This can be neutralized, to some extent, by using a prebuncher with compensating gain characteristics.

A study of the effect of magnetic beam confinement has shown that brillouin focusing provides the best conditions for bunch formation and the highest small-signal gain. There is no question but that weak focusing can enhance the theoretical conversion efficiency. Whether weak confinement can satisfy the thermal requirements of a high power TWT design is a problem which must be resolved empirically, as is the question of the effect on efficiency of the loss of electrons in the velocity taper section due to insufficient confinement.

The optimum velocity taper was found to be relatively non-critical. The length of the taper needs to be equivalent to approximately 6 dB of small-signal gain. The velocity of the taper needs to be equal to the terminal velocity of the main bunch.

One major difficulty encountered in this work stems from the fact that efficiency and electronic stability seen inevitably to stand in contradiction of one another. Without high gain in the output circuit section there is no hope to achieve high conversion efficiency. With high gain comes electronic instability. In this work it was found possible to moderate instability using

a special circuit matching technique in conjunction with frequency selective loss. The results are impressive though they fall short of the design goals. The computed conversion efficiency exceeds 40 percent over more than half the frequency band 3.1 to 3.6 GHz.

Another problem encountered is the substantial gain ripple generated by the backward-wave. The effect of the backward-wave can be neutralized to some extent by the careful design of the sever impedance. The efficiency was shown not to be greatly effected by the backward-wave.

This report contains the results of a large number of large-signal computer simulations demonstrating the consequence of choosing various beam and circuit parameters. The computer results have been exhibited in graphical form and analyzed; stressing those characteristics which might be expected to improve or diminish conversion efficiency. The computer results are presented in a form which should permit other workers to infer important results which may have been overlooked by the authors.

While not explicitly investigated in this work, the effect of relativistic beam velocities should not be forgotten when one considers means for maximizing conversion efficiency in very high power TWTs. The possibility for phase focusing using highly relativistic beams is very attractive and has never been adequately exploited. Slowing a beam from 200 kV to 100 kV, a 2:1 ratio in energy, corresponds to a 1.26:1 ratio in velocities. Developing effective phase focusing for such small velocity changes would be relatively simple, particularly so because of the relativistic reduction in space-charge forces.

Proof of the validity of the concepts developed in this investigation will require the construction and test of an experimental TWT. This TWT should incorporate the design features described in Section 6.0. A special effort

reaches a maximum in the vicinity of the third last cavity (first taper cavity). At the lowest frequency, 3.1 GHz, the fundamental current reaches almost 1.5 times the dc beam current. As the frequency increases the bunching declines until at 3.6 GHz, the maximum fundamental current is about 1.3 times the dc beam current. The second harmonic current mimics the fundamental current at the lower frequencies with a sharp low minimum in the output cavity. This would imply that the rf beam current in the output gap is nearly sinusoidal. At the mid-band frequency the second harmonic current minimum occurs sooner and at progressively higher frequencies there are more maxima and minima of second harmonic current attesting to a more complex phase pattern with more electron overtaking.

The buildup in cavity voltage is monotonic at midband but progressively less nearer the band edges. Nothing else could so clearly demonstrate the importance of the backward-wave and the vital necessity to include this wave in the analysis of a coupled cavity TWT.

The electron phase diagrams illustrate how the phases of the gap fields are non-uniform for exactly the same reason that the gap field amplitudes are non-monotonic; the backward-wave is, of course, the offender. At low frequencies few of the electrons are significantly slowed until they reach the taper section. At midband significant electron overtaking occurs five cavities from the output. Many electrons are slowed early and continue thru the tube without further major change in velocity. Many of these electrons are accelerated in the gaps then decelerated by space-charge forces in the tunnels. The net result is that they leave the interaction structure slowed well below the DC beam velocity but not nearly so much as they might be if they were better phase focused. At high frequencies one group of electrons forms a bunch which is well phased for power extraction; however, about one-third of the electrons end up in the interbunch space traveling at or near the DC beam velocity. To increase the conversion efficiency at the top of the band it will

should be made to provide a flexible system for magnetic confinement of the beam in order to test the effects of magnetic confinement on conversion efficiency and in order to determine an optimum magnetic field shape in the velocity taper section.

REFERENCE LIST

1. D. J. Bates and A. W. Scott, "The Effects of Circuit Tapering on the Efficiency, Bandwidth Characteristics of Dispersive Traveling-Wave Tubes," IRE Trans., PGED, Vol. ED-10, p. 89, March 1963.
2. L. Brillouin, "The Traveling-Wave Tube (Discussion of Waves for Large Amplitudes)," J. Appl. Phys., Vol. 20, pp. 1196-1206, December 1946.
3. M. Chodorow and C. Susskind, Fundamentals of Microwave Electronics, McGraw-Hill, Inc., 1964.
4. G. M. Clarke, "Tapered Traveling-Wave Tube," Ferranti (Ed), Report No. 117, November, 1960.
5. H. J. Curnow, "A General Equivalent Circuit for Coupled-Cavity Slow-Wave Structures," IEEE Trans. Microwave Theory Tech., Vol. MTT-13, pp. 671-675, September, 1965.
6. C. C. Cutler, "The Nature of Power Saturation in Traveling-Wave Tubes," Bell Sys. Tech. J., Vol. 35, p. 847, July 1956.
7. C. C. Cutler and D. J. Brangaccio, "Factors Affecting Traveling-Wave Tube Power Capacity," IRE Trans. on Electron Devices, Vol. ED-9, pp. 35-40, January, 1962.
8. J. F. Gittens, Power Traveling Wave Tubes, New York: American Elsevier, 1965.
9. J. F. Gittens and A. B. J. Sullivan, "On Electron Bunching by Traveling Waves," S.E.R.L. Technical Journal, Vol. 5, No. 4, p. 127, December, 1955.
10. R. W. Gould, "Characteristics of Traveling-Wave Tubes with Periodic Circuits," IRE Trans., Vol ED-5, pp. 186-195, July 1958.
11. R. L. Hess, "Large-Signal Traveling-Wave Tube Operation: Concepts and Analysis," University of California Electronics Technology Laboratory, ASD Tech. Report 61-15, July, 1961.
12. R. L. Hess, "Traveling-Wave Tube Large Signal Theory with Application to Amplifiers Having D.C. Voltage Tapered with Distance," Ph.D. Dissertation, Elec. Engr. Dept., University of California, Berkeley, July, 1960.
13. A. Kiel and P. Parzen, "Non-Linear Wave Propagation in Traveling-Wave Amplifiers," TR/AF-13, Radiation Laboratory, The Johns Hopkins University, March, 1955.

14. G. S. Kino, Y. Hiramatsu, W. A. Harman and J. A. Ruetz, "Small-Signal and Large-Signal Theories for the Coupled-Cavity TWT," in Proc. 6th Int. Conf. on Microwave and Optical Generation and Amplification (Cambridge, England, September, 1966).
15. R. Kompfner, "Traveling-Wave Valve -- New Amplifiers for Centrimetric Wave-lengths," Wireless World, Vol. 52, pp. 369-372, November, 1946.
16. E. L. Lien, "High Efficiency Klystron Amplifiers, in conv. Rec. MOGA 70 (8th Int. Conf., Amsterdam, The Netherlands, September, 1970).
17. J. G. Meeker and J. E. Rowe, "Phase Focusing in Linear Beam Devices," IRE Trans., PGED, Vol. ED-9, pp. 257-266, May, 1962.
18. K. B. Niclas and R. W. Gershberg, "New Concepts for Achieving High Efficiency in Traveling-Wave Tubes," U.S. Army Electronics Command, Fort Monmouth, N.J., Repts. 2, 3 and 6, Contract DA28-043-AMC-00076 (E), 1965.
19. A. Nordsieck, "Theory of the Large-Signal Behavior of Traveling-Wave Amplifiers," Proc. IRE, Vol. 41, pp. 630-637, May, 1953.
20. P. Parzen, "Nonlinear Effects in Traveling-Wave Amplifiers," TR/AF-4, Radiation Laboratory, The Johns Hopkins University, April 27, 1954.
21. J. R. Pierce, Traveling-Wave Tubes, D. Van Nostrand Co., N.Y., 1950.
22. N. H. Pond and R. J. Twigg, "Improvement of Traveling-Wave Tube Efficiency Through Period Tapering," IEEE Trans. Electron Devices, Vol. ED-13, pp. 956-961, December, 1966.
23. H. C. Poulter, "Large Signal Theory of the Traveling-Wave Tube," Tech. Report No. 73, Electronics Research Laboratory, Stanford University, California, January, 1954.
24. O. T. Purl, H. M. von Foerster, "Velocity Spectrograph of Electron Dynamics in a Traveling Field," J. Appl. Physics, Vol. 26, p. 351, October, 1953.
25. J. E. Rowe, "A Large Signal Analysis of the Traveling-Wave Amplifier," Tech. Rep. No. 19, Electron Tube Lab., Elect. Engr. Dept., University of Michigan, Ann Arbor, April, 1955.
26. J. E. Rowe, "A Large Signal Analysis of the Traveling-Wave Amplifier: Theory and General Results," IRE Trans. Electron Devices, Vol. ED-3, pp. 39-57, January, 1956.
27. J. E. Rowe, "N-Beam Nonlinear Traveling-Wave Amplifier Analysis," IRE Trans. on Electron Devices, Vol. ED-8, pp. 279-284, July 1961.

28. J. E. Rowe, "One Dimensional Traveling-Wave Tube Analysis and the Effect of Radial Electric Field Variations," Trans. IRE, PGED, Vol. ED-7, pp. 16-21, January, 1960.
29. J. E. Rowe, Nonlinear Electron-Wave Interaction Phenomena, New York and London Academic Press, 1965.
30. J. E. Rowe and C. A. Brackett, "Velocity Tapering in Microwave Amplifiers," IEEE Trans. Electron Devices, Vol. ED-12, pp. 441-447, August, 1965.
31. J. A. Ruetz, D. Robinson and J. Pavkovich, "The Effect of Tapered Circuits on Efficiency for High-Power Traveling-Wave Tubes," presented at IRE Electron Devices Meeting, Washington, D.C., October, 1960.
32. J. A. Ruetz, G. Kino, Y. Hiramatsu, and D. J. Bates, "A Large Signal Analysis for 'O' Type Microwave Amplifiers," in Proc. High-Power Microwave Tubes Symp. (Fort Monmouth, N.J., May 19 - 20, 1965).
33. O. G. Sauseng and M. N. Ernstoff, "Advancements in Traveling-Wave Tube Efficiency with Combined Voltage Jump Tapers and Enhanced Beam Bunching," presented at the IEEE Int. Electron Devices Meeting, Washington, D.C., October 26-28, 1966.
34. A. W. Scott, "Why a Circuit Sever Affects Traveling-Wave Tube Efficiency," IRE Trans. Electron Devices, Vol. ED-9, pp. 35-40, January, 1962.
35. P. K. Tien, "A Large-Signal Theory of Traveling-Wave Amplifiers," Bell Sys. Tech. J., Vol. 35, pp. 349-374, 1956.
36. P. K. Tien, L. R. Walker and V. M. Wolontis, "A Large-Signal Theory of Traveling-Wave Amplifiers," Proc. IRE, Vol. 43, pp. 260-277, March, 1955.

A decorative border with a repeating scroll-like pattern surrounds the central text.

MISSION of Rome Air Development Center

RADC plans and executes research, development, test and selected acquisition programs in support of Command, Control Communications and Intelligence (C³I) activities. Technical and engineering support within areas of technical competence is provided to ESD Program Offices (POs) and other ESD elements. The principal technical mission areas are communications, electromagnetic guidance and control, surveillance of ground and aerospace objects, intelligence data collection and handling, information system technology, ionospheric propagation, solid state sciences, microwave physics and electronic reliability, maintainability and compatibility.